

Studies of the ionospheric E-F layer transition

by

JOHN WILLIAM SYDNEY HART

being the dissertation submitted to the Faculty of Science,
University of Leicester, in candidature for the
Degree of Philosophiae Doctor.

Department of Physics,
University of Leicester.
October 1970.

UMI Number: U632534

All rights reserved

INFORMATION TO ALL USERS

The quality of this reproduction is dependent upon the quality of the copy submitted.

In the unlikely event that the author did not send a complete manuscript and there are missing pages, these will be noted. Also, if material had to be removed, a note will indicate the deletion.



UMI U632534

Published by ProQuest LLC 2015. Copyright in the Dissertation held by the Author.
Microform Edition © ProQuest LLC.

All rights reserved. This work is protected against
unauthorized copying under Title 17, United States Code.



ProQuest LLC
789 East Eisenhower Parkway
P.O. Box 1346
Ann Arbor, MI 48106-1346

x753044462

Studies of the isoelectric A-V layer transition

by

THESIS

JOHN WILLIAM BENDALL FARR

395914

1971

Being the dissertation submitted to the Faculty of Science,
University of Leicester, in candidature for the
Degree of Philosophy Doctor.

Department of Physics,
University of Leicester,
Leicester LE1 7RH.

Acknowledgements

Firstly, I would like to thank Professor E.A. Stewardson and Professor J.E. Enderby for the opportunity of working in the Physics Department of the University of Leicester.

I am particularly grateful to the G.C.H.Q, Cheltenham for sponsoring this project and for the receipt of a research assistantship for 3 years. I would also like to thank Dr. N. Taylor for unpublished data, Mr. T.J. Sherlock and Mr. N. Spendlove for assistance in the construction and maintenance of apparatus, and my wife for her unfailing help and encouragement.

Finally, I would like to thank Dr. T.B. Jones for originally suggesting the present investigation and for his constant guidance and helpful advice throughout the progress of the work.

Table of Contents

		<u>Page</u>
Chapter 1	Introduction	1
1.1	Historical	1
1.2	Formation of the Ionosphere	3
1.3	Variations in the Quiet Ionosphere	5
1.3.1	D Region	5
1.3.2	E Region	7
1.3.3	F Region	9
1.4	Study of the Ionosphere	11
1.4.1	Theoretical	11
1.4.2	Experimental	13
1.5	Proposed Investigation	16
Chapter 2	Applications of the Ray Theory	18
2.1	Ray Theory	18
2.2	Calculation of True Height	18
2.3	Correction of Real Height profiles	23
2.4	Calculation of Absorption	25
2.5	Phase Integral Method	27
2.6	Collisional Frequency	27
Chapter 3	Theoretical Studies	30
3.1	Magneto-Ionic Theory	30
3.2	Calculation of Collisional Frequency	32
3.3	The Calculation of Absorption and Virtual Height by the Phase Integral Method	36

	<u>Page</u>
3.4 Reduction of Ionograms by the Polynomial Method	41
3.5 The Validity of the Polynomial Reduction Technique	43
3.5.1 Sensitivity to Geomagnetic Variation	43
3.5.2 The Scaling Interval in Frequency	44
3.5.3 Comparison with Analytic Profiles	46
3.5.4 Comparison with Lamination Method	47
 Chapter 4	
Previous Experimental Studies of Absorption and Virtual Height	49
4.1 Pulse Techniques	49
(a) Pulse Sounding	50
(b) Measurement of Absorption	51
4.2 The Experimental Studies of the Regular Features of the Ionosphere	52
4.3 Irregular Ionospheric Features in the E-F Transition Region	53
 Chapter 5	
Pulse Measurements in the Ionosphere	58
5.1 Absorption	58
5.1.1 Principle of measurements	58
5.1.2 Experimental Techniques	59
5.1.3 Non-Dissipative Attenuation	61
5.1.4 Sampling	63

	<u>Page</u>
5.2 Virtual Height	64
5.2.1 Principle of measurements	64
5.2.2 Distortion	65
5.2.3 Lyon and Moorat Correction	65
Chapter 6 Experimental Studies	67
6.1 Equipment	67
6.1.1 Radio Ionosonde	67
6.1.2 A1 Absorption Equipment	68
6.2 Observations	72
6.2.1 Ionospheric Soundings	72
6.2.2 Absorption Measurements	73
6.2.3 Virtual Height	73
Chapter 7 The Post-Sunrise Changes in the Virtual Height-Frequency Variation	76
7.1 Introduction	76
7.2 Occurrence of Fine Structure on Ionograms	77
7.3 Correlation of Cusp Activity with Magnetic and Solar Indices	82
7.4 Interpretation of Model Cusp Structures in terms of Disturbances in the Electron Density Profile	84
7.5 Cusp Development Following Sunrise	88
7.5.1 Theoretical Profiles	88
7.5.2 Direct Observations of Virtual Height at Leicester	90
7.5.3 Electron Densities Observed by Thomson Scatter	91

	<u>Page</u>
7.6 Comparison of the Virtual Height Profiles for the Post Sunrise Period	93
7.7 Comparison of the True Height Profiles for the Post Sunrise Period	97
 Chapter 8	
The Variation of Absorption and Virtual Height of a fixed frequency following sunrise	100
8.1 Introduction	100
8.2 Simultaneous Observations of Absorption and Virtual Height of a Fixed Frequency	101
8.2.1 Variation of Virtual Height with time	101
8.2.2 Variation of Absorption with time	103
8.3 Computed variations of Absorption and Virtual Height at a Fixed Frequency	105
8.3.1 Collisional Frequency in the height range 110-120 km	105
8.3.2 Calculation of Absorption and Virtual Height variations with time in the early morning	107
8.4 The Influence of the Electron Density Distribution below 100 km on Absorption in the early morning	110
8.5 Comparison of computed time variations of Virtual Height and Absorption with observed values	112
 Chapter 9	
Summary and Conclusions	116
General Conclusions	120
Suggestions for future investigation	121

	<u>Page</u>
Appendix I Vertical Incidence $A(f)$ sounding	123
Appendix II Circuit Components	126
Bibliography	129

A list of symbols and abbreviations used in the text

A	Total Absorption, or a constant
c	velocity of light in vacuo
E	electric component of wave field
f	wave frequency
f_N	plasma frequency
f_H	gyrofrequency $eB/2\pi m$
h	true height
h'	virtual height
k	absorption coefficient, Boltzman's constant, or $2\pi f/c$
L	absorption
N	electron density
n	complex phase refractive index, or number density
P	phase height
R	polarization, or reflection coefficient
s	path length
t	time
T_e	electron temperature
X	f_N^2/f^2
Y	f_H/f
Y_L	$Y \sin \theta$
Y_T	$Y \cos \theta$
Z	v/ω
z	true height
θ	Dip angle
μ	real part phase refractive index
μ'	real part group refractive index

- ν collisional frequency
 τ time
 χ Zenith angle
 ω $2\pi f$
 ω_H $2\pi f_H$
E.U.V. extreme ultra-violet
H horizontal component of the earth's magnetic field
H.F. High frequency
M.F. Medium frequency
Rz Zurich sunspot number
I.G.Y. International Geophysical Year

Abstract

The region of the ionosphere situated above the E layer peak and below the F layer is difficult to investigate using conventional ground based techniques, consequently our knowledge of this region is limited. The existence of a re-entrant feature in the electron density-height profile, the so called 'valley', has been postulated, but direct ground based observations of the region are rare since the form of the ionization distribution makes such observations difficult by virtue of the large absorption and group retardation produced. An attempt has been made in this study to construct representative electron density distributions from a consideration of the fine structure observed on ionospheric sounding records and of the variation of the absorption and virtual height of a fixed frequency during the growth of the ionosphere below 200 km following the sunrise.

A computer programme based upon the polynomial reduction method is described for the computation of monotonic electron density distributions from vertical sounding observations of virtual height. The phase integral technique was adopted in the development of a second computer programme for the calculation of absorption and virtual height of frequencies reflected throughout the electron density distribution. Special reference was made to the results obtained for frequencies reflected near the E layer peak and the validity of this analysis in this region of high deviative absorption and group retardation is discussed. Attention is drawn to the large variation in published values of the collisional frequency

above 120 km and an attempt has been made to construct a suitable height variation of this parameter for use in the calculation of absorption.

Routine ionospheric soundings were made hourly over an extended period and augmented with continuous soundings on a number of selected days between February and June 1969. Also on 42 days during this period, measurements of absorption and virtual height were carried out on a fixed frequency for several hours following the sunrise.

The variations of absorption with time and virtual height with time and frequency were computed from the electron density profiles obtained from 3 independent sources

- (a) Theoretical post sunrise profiles constructed by Bourne, Setty and Smith.
- (b) Monotonic profiles computed from Leicester Ionograms
- (c) Profiles observed by a Thomson Scatter technique at R.R.E. Malvern.

The results of these calculations are compared directly with the experimental observations and computations of the variation of absorption with frequency are also discussed.

From a synoptic study of the cusp features observed on ionospheric soundings it is found that complex cusp structure around $f E$ is a regular phenomenon at Leicester occurring throughout the day but showing some decrease in occurrence frequency towards noon. The development of this structure can be represented by an expression of the form

$$f_{\text{cusp}} = A \cos^n \alpha$$

where different cusp features take differing values of the constant A.

The comparisons made in this study indicate that the polynomial reduction technique produces monotonic electron density profiles which satisfactorily represent conditions when only the virtual height is considered but are not capable of producing calculated absorption values to the same degree of accuracy. The virtual height and absorption values computed from the Thomson Scatter profiles are in good agreement with experimental observations of these parameters at Leicester. These profiles are therefore considered to accurately represent the structure of the electron density distribution. The existence of the small undulations, as evident in these profiles, is shown to account for the multi-cusp phenomenon and various observations concerning the variability and extent of such structures are described. In addition, these comparisons have indicated some inadequacy in the growth theory employed in the derivation of the Bourne, Setty and Smith profiles.

As a result of comparing the variation with frequency of both the virtual height and absorption it has been shown experimentally and supported theoretically that

$$\frac{\Delta A}{A} > \frac{\Delta h'}{h'}$$

indicating that absorption especially in the deviative region may be a more sensitive parameter to profile fine structure. It is anticipated therefore that sweep frequency absorption sounding may indicate more clearly short term perturbations in

the electron density profile. In Appendix I a preliminary feasibility study of this technique is reported and a new method for absorption sounding is briefly outlined.

Chapter 1

Introduction

1.1 Historical

The first postulation of the existence of an ionized layer in the upper atmosphere, later called the 'ionosphere' by Watson-Watt, is attributed to Balfour Stewart (1878), who invoked such a layer to explain the diurnal variations of the earth's magnetic field. It has been suggested, however, that Faraday (1832), Gauss (1839), and Lord Kelvin (1860), independently made similar postulations at much earlier dates (Kaiser 1962; Chalmers 1962). The concept of an ionized layer in the upper atmosphere was not utilized in connection with the propagation of radio waves until Kennelly (1902), and Heaviside (1902), suggested such a phenomenon to explain the necessary bending of radio waves transmitted by Marconi between England and the United States of America in 1901. Heaviside further suggested that the layer contained positive and negative ions produced by the ionizing action of solar radiation upon the constituents of the ionosphere around 80 km. This theory was not readily accepted by many principal physicists of the time, who favoured a diffraction theory expounded by Watson in 1919. In particular, Sommerfeld carried out extensive calculations of signal strength which were later shown experimentally to be too low for each case considered.

The actual manner in which the charged particles affect the propagation of radio waves through an ionized medium was first investigated by Eccles (1912), who assumed that the medium acted as a conductor and that the effective charges were those carried by ions of atomic mass. Larmor (1924), modified this theory by replacing the concept of a sharp conducting reflector by a dielectric medium which returned rays to the earth by gradual refraction. This work laid the foundation on which Appleton and Barnett (1925), Nichols and Schellang (1925), and Lassen (1927), worked to apply the principles of ray theory as set down by Drude (1902), and Lorentz (1909). The culmination of this effort was the formulation of the magneto-ionic theory of radio wave propagation which was first outlined by Appleton (1927), and later presented in detail by Hartree (1931), and Appleton (1932).

The early theoretical considerations remained without experimental support until, in 1924, Appleton and Barnett (1925), obtained conclusive evidence of the existence of an ionosphere from a wave interference experiment. This was quickly followed by the experiments of Breit and Tuve (1925), which introduced the technique of pulse sounding.

The study of the physical and chemical properties of the ionosphere was started in 1931, by Chapman. He was the first author to consider the formation of the ionized layers in the upper atmosphere, and showed that by taking a particular atmospheric constituent and irradiating it with monochromatic ionizing radiation, the ionizing rate was a maximum at a specific altitude. The formulation of the Chapman theory provided a basis for later theoretical modelling of the ionosphere.

Thus, with the development of the Appleton-Hartree and the Chapman theories, and with the experimentation of Breit and Tuve, the foundations were laid for the further detailed study of the ionosphere.

1.2. Formation of the Ionosphere

The formation of ionization in the upper atmosphere is a direct result of the irradiation of the atmospheric constituents by solar radiation. It is therefore necessary to consider both the relative concentrations of the atoms and molecules present in the region and their reactions to various wavelengths in the solar spectrum. It has been shown by Chapman that the incidence of monochromatic ionizing radiation on a single constituent exponential atmosphere will produce an ion distribution which has a characteristic shape, showing a single maximum, figure 1.1. The extension of this treatment to an atmosphere having many constituents, irradiated by many different wavelengths, gives rise to a complex ion distribution which may exhibit many maxima.

The neutral atmosphere at ground level consists chiefly of a mixture of eight gases, of which only two are in proportions which warrant consideration; these are molecular oxygen and molecular nitrogen. From the lower boundary of the ionosphere, usually taken as 50 km, up to 100 km a state of thorough mixing is assumed throughout, and while pressure decreases steadily from ground level the atmospheric composition of four parts molecular nitrogen to one part molecular oxygen remains unchanged. Minor constituents can play a part in the ionization reactions in this region, and Nicolet (1949),

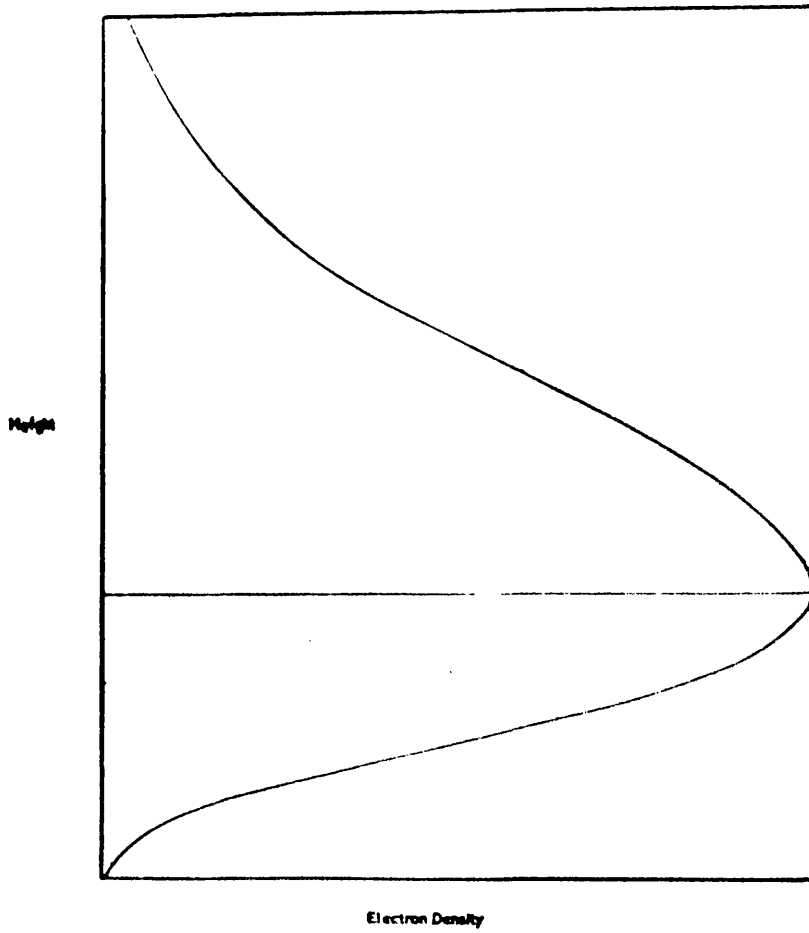


FIG. 1.1 The Chapman layer.

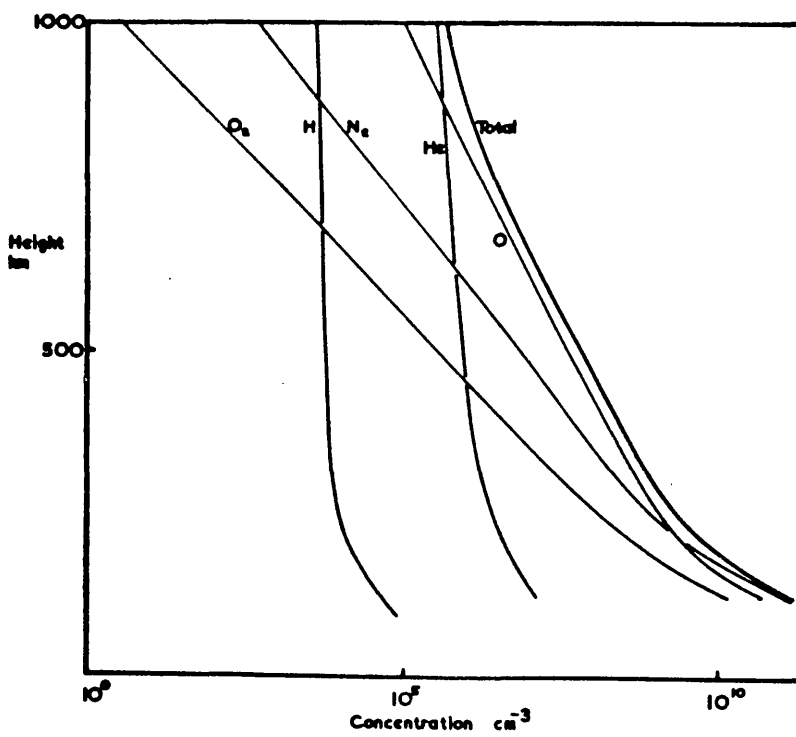


FIG. 1.2 Neutral atmospheric constituents above 100 km.

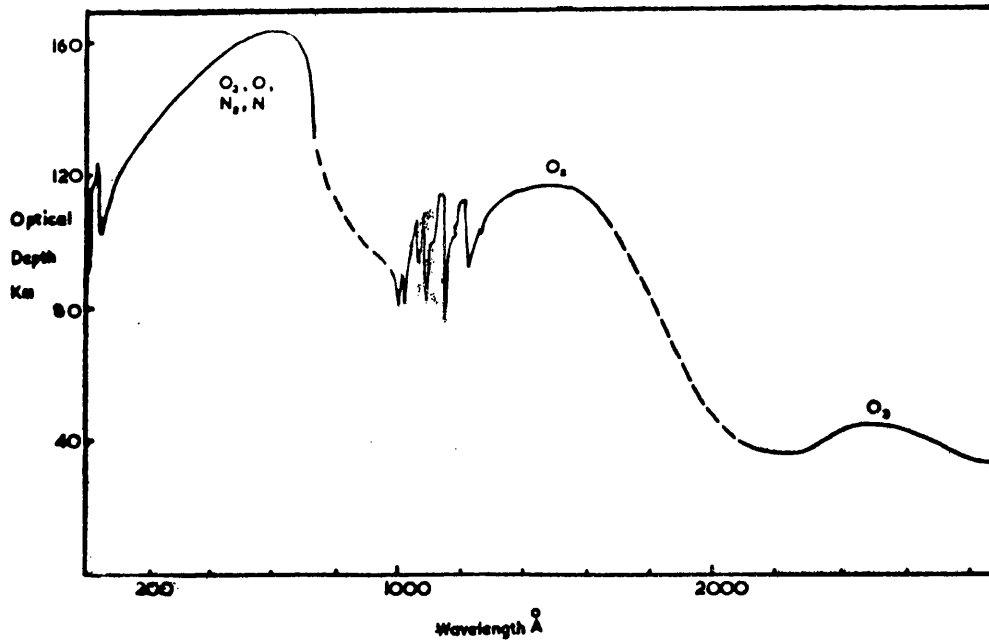


FIG. 1.3 The optical depth of radiation vertically incident on the atmosphere.

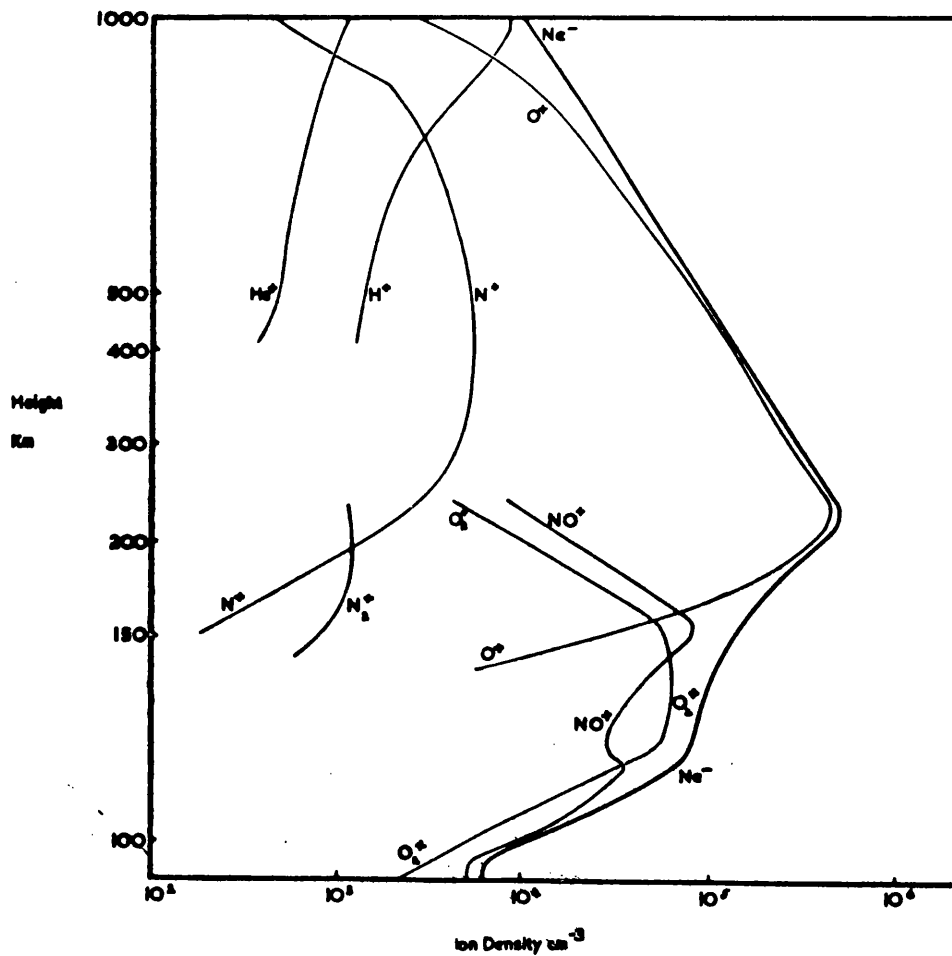


FIG. 1.4 Rocket measurements of the ion content of the ionosphere above 100 km.

has discussed the role of nitric oxide in the absorption of Lyman α radiation below 100 km. Above 100 km the assumed state of thorough mixing no longer applies, and atomic oxygen becomes more important, as indicated in figure 1.2.

The solar spectrum is represented in terms of the height at which a particular radiation is absorbed by a factor $1/e$, plotted against wavelength, in figure 1.3. The constituents ionized by various regions of this spectrum are also shown in the figure.

In the upper regions of the ionosphere, above 120 km, the primary ions are O^+ and N_2^+ which, by charge exchange, lead to a state in which O^+ , O_2^+ and NO^+ ions predominate, giving rise to the highest ion density in the ionosphere. This broad maximum and the surrounding region, from approximately 140 to 1,000 km, is referred to as the F region. The combination of the various ion distributions shown in figure 1.4. may give rise to a subsidiary maximum or inflection in the total ion distribution; this is called the F_1 layer, while the higher maximum is designated F_2 .

The E region, between 90 and 120 km, closely follows the predictions of the Chapman theory, and is produced by the action of X-rays in the range 10 to 200 \AA , and the E.U.V. in the range 1,000 to 1,500 \AA , upon molecular oxygen and nitrogen, with atomic oxygen becoming important higher in the region. The predominant ions produced are O_2^+ , NO^+ and O^+ although mass spectroscopic study has shown the presence of many minor ions, which are believed to play an important part in the anomalous phenomena observed in the region.

The remaining height range, 50 to 90 km, is referred to as the D region, and has been shown, by Deeks (1966), to have a complex structure often exhibiting two maxima. This complexity is a result of combined effects of short X-rays, Lyman α and cosmic rays, in this region of high particle density.

The concentration of positive ions can be taken as a direct indication of the electron density in the two upper regions of the ionosphere. However, in the high neutral density of the D region, the loss of electrons to form negative ions is considerable. The complex interactions of electrons and ions has been treated in detail by Donahue (1966), while Nicolet and Aiken (1960), considered the ionization of the principal constituents by solar radiation of various wavelengths.

1.3. Variations in the Quiet Ionosphere

The effects of solar radiation in forming ionized layers in the ionosphere have been discussed and it is now necessary to consider the changes which are observed in these layers as the density of ionizing radiation varies with the diurnal, seasonal and sunspot cycles. These variations are widely different from layer to layer, so that it is convenient to consider each one separately.

1.3.1. D Region

Since the D region is the lowest part of the ionized atmosphere the neutral gas density has its greatest value, exceeding the electron density by a factor of 10^{12} . Con-

sequently, the reactions of the region are strongly influenced by the presence of neutral atoms and molecules. In particular, the very high frequency of electron collisions with these neutral particles produces excessive absorption of medium frequency radio waves, thus making direct sounding very difficult. Alternative indirect methods of observation have been developed and widely used, but this still remains the least well defined region of the ionosphere.

Observations of the phase variation of low frequency radio waves transmitted over paths of varying lengths have indicated that the D region should be further subdivided to give a lower C layer. This region is due to cosmic radiation which would remain reasonably constant throughout the whole day, giving rise to the constant phase difference shown in figure 1.5(a). It has also been suggested that the attachment of electrons to neutral atoms produces a rapid fall in electron density at sunset, and that photodetachment at sunrise results in the swift rise in electron density.

Decreasing the path length of the low frequency transmissions increases the apparent height of reflection and the diurnal phase variation indicates a smooth zenith angle variation of electron density throughout the sunlit hours. This type of variation, as predicted for a Chapman layer predominates through the upper D and E regions. The sunspot cycle variation in the D region is more complex since it is produced by the interplay of two mechanisms. Firstly, Lyman α radiation varies very little over the sunspot cycle, and thus gives an almost constant source of ionization throughout the cycle. Superimposed upon this is the variation in X-ray

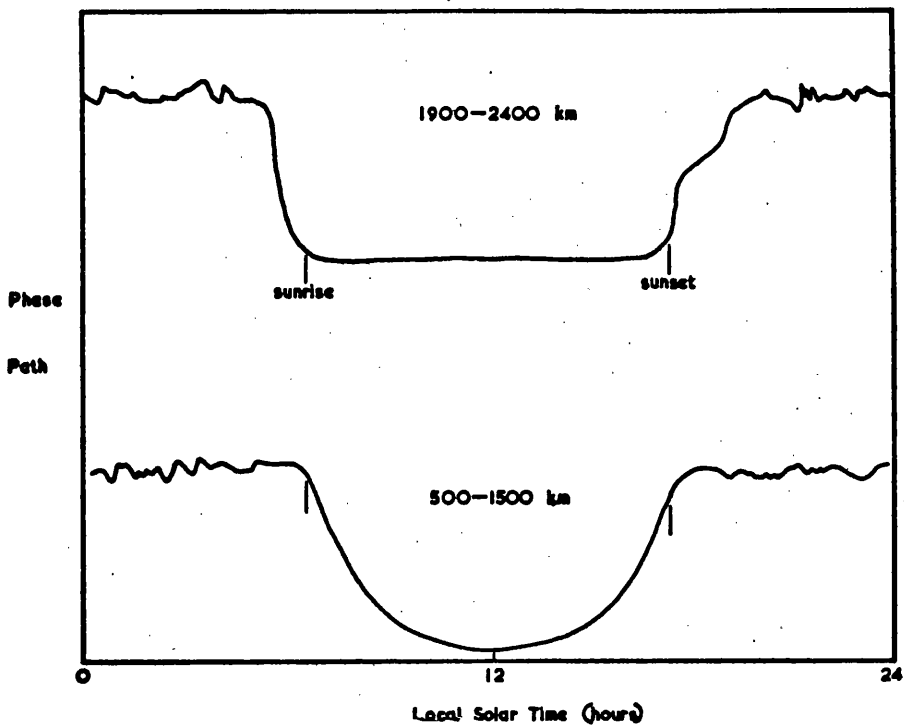


FIG.1.5 Diurnal variation of phase path for low frequencies near 80 kHz propagated at medium latitudes to the distances shown.

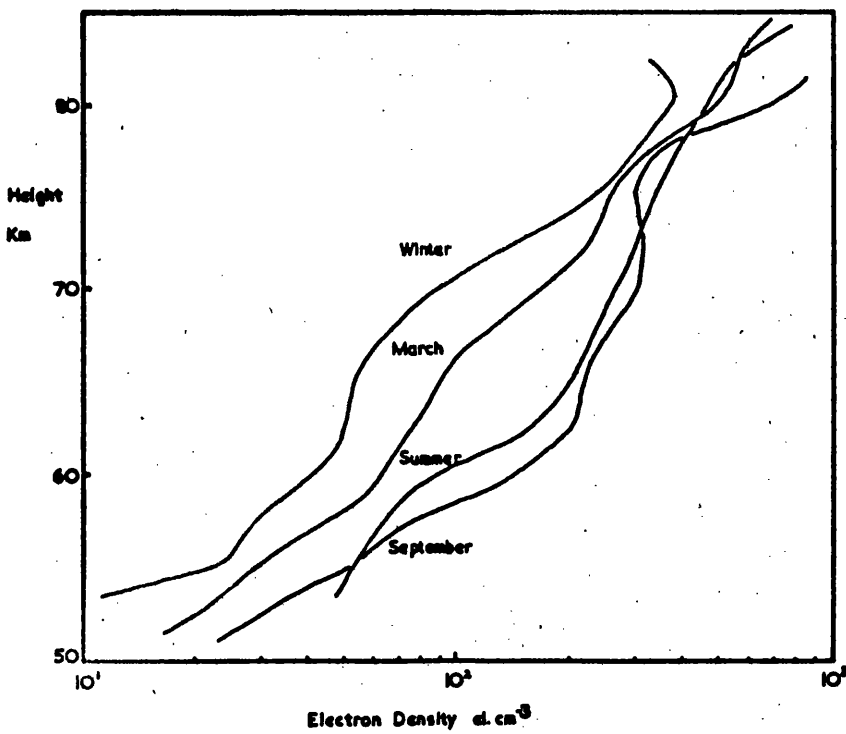


FIG.1.6 Seasonal changes in D region electron density (after Belrose 1965).

flux which may change by two or more orders of magnitude during the sunspot cycle.

The seasonal variation of the region also shows marked differences from that expected from a Chapman-like layer. Typical seasonal profiles are shown in figure 1.6. These show a marked variation, particularly around 65 km, in which the electron density increases normally until midsummer, but then remains roughly constant until the equinox, when a rapid change takes place leading to minimum conditions in November. This anomalous behaviour has been called the 'November effect' and has, as yet, no satisfactory explanation. The solutions to this anomaly and to the winter anomaly are expected to come from studies of the interaction of meteorological effects in the stratosphere and the lower D region.

1.3.2. E Region

The E region is the most 'well behaved' part of the ionosphere, and it is possible to predict its basic variations fairly accurately from Chapman theory. However, superimposed upon these trends are observed several minor irregularities. Among these the appearance of thin, highly dense layers, collectively called Sporadic E layers, has received most attention (Whitehead 1970). These layers play an important part in observations of the E layer, and, as yet, defy prediction and have no complete explanation. The most recent theory of their production is the Wind Shear theory, by which an accumulation of electrons is thought to be produced in a region where two opposing wind systems come into contact (Axford and Cunnold 1966). Rocket profiles show another of

these minor phenomena, the existence of a large number of minor maxima at the layer peak. The largest of these maxima are often observed on the records of ground based sounding equipment as multiple cusp structures. A detailed study of both the diurnal and seasonal variations of this fine structure has been undertaken, and is discussed fully in Chapter 7.

The basic variations of the E region are usually observed and illustrated in terms of the highest frequency reflected from the E layer, the critical frequency, f_oE . Diurnal plots of this parameter show a dependence on the zenith angle

$$f_oE = A \cos^n \chi .$$

The exponent for a true Chapman layer would be $\frac{1}{2}$, and departures from this value are attributed to the height variation of scale height and recombination coefficient. These diurnal plots further show the growth and decay of the E layer to be almost symmetrical about noon, with a slight offset of about twenty minutes after noon, indicating a rapid recombination rate for electrons in the region. The extent of solar control and the high rate of recombination are further illustrated in figure 1.7, where f_oE is plotted for the partial eclipse day of the 20th May, 1966. The observations taken in Leicester show clearly the symmetrical decay in f_oE during the partial eclipse. At night the electron density in the E region falls below that detectable by most ground based radio sounding equipment designed for E region observation. However, rocket measurements at night have detected a residual E layer with an electron density of the order of 10^3 electrons/c.c. Thus

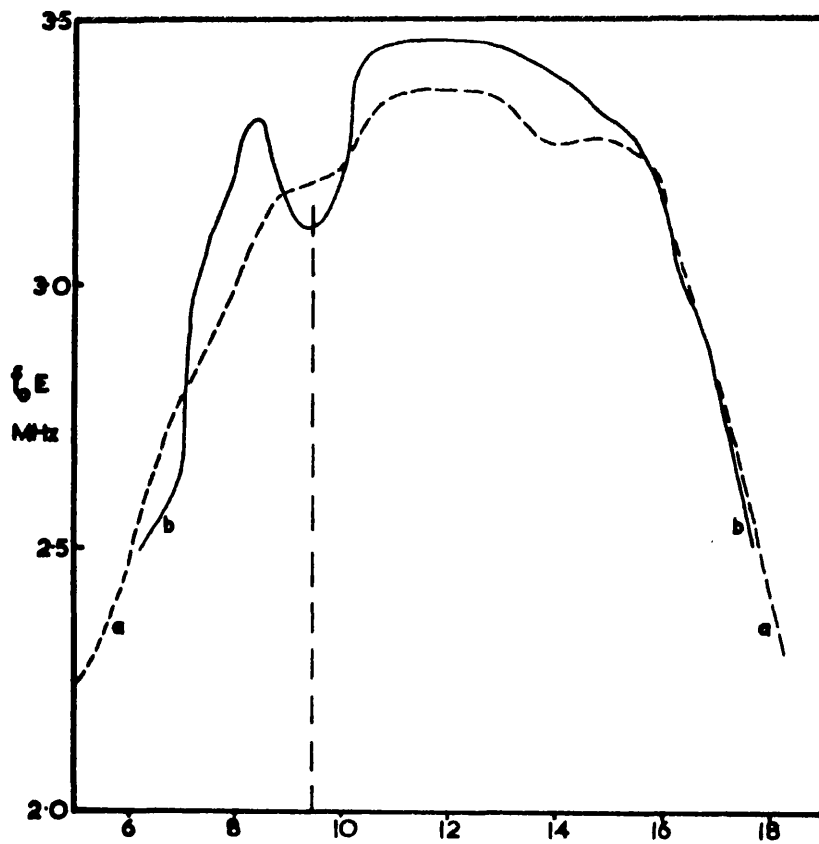


FIG. 1.7 Diurnal variation of f_oE

- (a) Mean of 5 normal days
- (b) Partial eclipse day, 20th May 1966
(maximum phase 0930)

the critical frequency falls from around 3.5 MHz at noon, to approximately 0.3 MHz at midnight.

The seasonal and solar cycle variations further underline the importance of solar control in this region; the seasonal variation showing, in temperate latitudes, a change in f_oE from approximately 4.0 MHz in summer, to approximately 3.0 MHz in winter. A comprehensive study of this region and its variations was published by Robinson (1960), and his work and some recent theories will be discussed later.

1.3.3. F Region

This region of the ionosphere includes all ionization above about 140 km, although the arbitrary upper limit of 1,000 km is often imposed. The electron density rises to the overall ionization maximum of the ionosphere situated between 250 and 500 km, and then decays exponentially with increasing height. Between 140 km and this maximum a subsidiary maximum or inflection is often observed which is designated the F_1 layer, and which it is convenient to consider separately.

The F_1 layer, like the E layer below it, exhibits strong solar control and Chapman - like diurnal and seasonal variations. Attempts to derive a $\cos^{\frac{1}{n}} \chi$ law for the layer exhibit a difference between the two layers in that the value of n for the F_1 layer varies with season and latitude, and has a numerical value greater than four. These departures from Chapman-like behaviour are due to the influence of the far more variable F_2 layer above. The F_1 layer is only

observed when the F_2 maximum is small and at the top of its height range. For example, at night when the F_2 layer diminishes and loses height, the F_1 layer is absorbed into it to form a single nocturnal F layer. This influence is further illustrated by the seasonal and sunspot variations of the layer. At temperate latitudes during solar minimum conditions $f_o F_1$ has a maximum around 3.7 MHz in winter, increasing to 4.1 MHz in summer, while the diurnal variation exhibits reasonable symmetry around noon. However, at sunspot maximum, when the F layer is much enhanced, $f_o F_1$ shows diurnal asymmetry, (maximum one hour after noon), and an increase from 5.1 MHz in summer to a value in the region of 6.0 MHz in winter. This last figure is based on a very few observations since a separate F_1 layer is rarely observed in winter at solar maximum.

The F_2 layer, to which the anomalies in F_1 layer are attributed, is more complex and no simple model can be employed to predict its behaviour. The diurnal variation shows a regular pattern during daylight hours, having a maximum just after noon in temperate latitudes. However, at night, two minima in critical frequency can often be detected. The complexity is more marked when considering the seasonal variation. This depends strongly upon the epoch of the solar cycle, giving an almost invariant mean daily maximum of around 5 MHz at sunspot minimum, while at sunspot maximum the variation is from around 8.0 MHz in summer to 12.0 MHz in winter.

The day to day fluctuations in the value of $f_o F_2$ are also considerable during solar maximum, suggesting the

existence of highly energetic movements within the F region. Such movements have received extensive study, as have the many anomalies in F region behaviour, but as yet no single theory can explain all aspects of F region morphology.

1.4. Study of the Ionosphere

1.4.1. Theoretical

Theoretical studies of the ionosphere can be divided into two main categories. The first sets out to derive models of the ionosphere by considering the interaction of ionizing particles and radiations with the neutral atmosphere. The study of radio wave propagation through the ionized layers constitutes the second category.

The Chapman theory forms a basis for a large number of modelling techniques, namely, those which attempt to represent the electron distribution with height in terms of the solar radiation and ion chemistry. Observations of the solar spectrum under quiet and disturbed conditions and direct sampling of the atmospheric composition have enabled many workers to derive models of the electron distribution under a variety of different conditions. This work has been discussed in detail by Nicolet and Aiken (1960), and Donelley (1967). The distribution of electron collisional frequency with height has also been modelled by considering the atmospheric composition and the gas, ion and electron temperatures in the ionosphere (Thrane and Piggott 1966). This second group of modelling techniques is discussed in Chapters 2 and 3. In addition to these two main groups many problems involving

irregular phenomena have been treated by the introduction of specialised models, an example of which is the Wind Shear theory of the Sporadic E layer.

The theoretical study of radio wave propagation through the ionosphere is based upon two types of development from the electro-magnetic theory, as formulated in Maxwell's equations, and the constitutive relations of a dielectric medium situated in a magnetic field. The first approach, the ray theory, attempts to describe the characteristics of a wave in terms of its refractive index, wave polarization and absorption index. The two characteristic waves which are propagated, the ordinary and extraordinary rays, are further assumed to travel independently through the medium with no interchange of energy between them. Inherent in this theory is the assumption that the properties of the medium are constant or vary very little in the space of one wavelength.

Thus, at low frequencies, or in regions where the medium varies very rapidly, the ray theory breaks down and the more complete wave theory must be applied. This second approach requires that Maxwell's equations be employed and solutions for the wave fields found at each point in space. At medium and high frequencies the wave theory has the major disadvantage that the computations become exceedingly long as many wavelengths are involved in the propagation path.

The wave theory has been described in detail by Pitteway (1965), and its application to the propagation of very low frequency radio waves in the earth-ionosphere waveguide has been extensively discussed by Wait (1962). In the work which follows the ray theory will be employed and its applications

to propagation problems is discussed in Chapters 2 and 3.

1.4.2. Experimental

The experimental study of the ionosphere can be conveniently treated in two sections differentiating between ground based experiments and direct sampling experiments carried out by rockets and satellites.

(a) Ground Based Experiments

The most common experiment carried out on a routine basis is the sounding of the ionosphere by means of repetitive pulses of radio energy of continuously varying frequency in the range 1 to 20 MHz. This technique gives an indication, through the variation of the retardation of the reflected pulses with frequency, of the distribution of electron density above about 100 km. A similar technique employing fixed frequency M.F. and H.F. pulses has been widely used in the study of radio wave absorption and phase path in the ionosphere. The use of pulses in the measurement of absorption and virtual height is discussed in detail in later Chapters.

Regions below 100 km have comparatively small electron densities and high molecular densities and although pulse sounding at frequencies below 1 MHz have been carried out it requires very high power transmitters to obtain workable echo amplitudes at these low frequencies. However, two techniques involving medium frequency pulse transmissions have been developed for observations of the D region. These are the cross modulation experiment described by Fejer (1955), and

the partial reflection experiment due to Gardner and Pawsey (1953), which gives estimates of both the electron density and the collisional frequency at heights below 100 km

The techniques mentioned so far are concerned with vertical incidence propagation or the interaction of two signals in a very restricted region and give results which are relevant to a fairly well defined point in the ionosphere. However, the prediction of the performance of high frequency communication circuits is studied more satisfactorily by observations taken along the path of the proposed circuit. Thus the sounding technique has been extended to give oblique incidence ionograms which give a direct observation of the lowest and highest usable frequency as well as the mode structure on a particular communications circuit. A further development in oblique sounding is the Chirp system described by Fenwick and Barry (1965). Here, a continuous wave, which is continuously varying in frequency, is transmitted, and the delay time is measured by comparing the frequency of the returned wave with that of the transmitted wave. As well as these sounding techniques the monitoring of fixed frequency continuous wave transmissions can give estimates of the fluctuations in height of a particular electron density value at a remote point in the ionosphere. Similar monitoring of levels in the D region can be undertaken by observing the diurnal variation of the phase and amplitude of very low frequency transmissions which are reflected from this region of the ionosphere.

The technique of back scatter sounding (Shearman 1956) differs from the systems outlined above in that although it

observes reflections from an oblique path both the transmitter and receiver are situated at the same point. By this technique a high energy radar pulse can be used to study the behaviour of the Sporadic E layer within the radius of about 1,000 km by virtue of the energy returned along the original path by back scatter from the ground. A further application of high energy radar technique was described by Gordon (1958), to detect the incoherent scattering of radio waves by free electrons in the ionosphere. Some observations made by this technique at R.R.E., Malvern, have been employed in the discussion incorporated in Chapters 7 and 8, and the technique is therefore discussed in some detail below.

A single free electron scatters some of the energy associated with an incident radio wave, and the effect can be described in terms of a scattering coefficient or cross-section. Thus, each electron in an ionized medium containing many electrons scatters some of the energy associated with a radio wave propagated through the medium. The scattered waves will have coherence, limited coherence or incoherence depending on conditions of wavelength and geometry. Coherent scattering is the case of refraction of a radio wave by the ionosphere and limited coherence, where the scattered waves are coherent from limited volumes only, corresponds to the phenomena of ionospheric back and forward scatter. When complete incoherence occurs the effect is usually referred to as "Thomson scatter" since scattering from a single electron was first predicted by Thomson early this century.

In the ionosphere the electrons have thermal velocities, consequently the frequencies of the scattered waves differ from that of the incident wave due to Doppler effects. The width of the frequency spectrum of the scattered signals essentially provides a measure of the ion temperature. Incoherent scatter of radio waves from the ionosphere may be used to determine the electron density and temperature as a function of height well above the F-region peak, which is the upper limit for conventional ground based sounding.

The mechanism of scattering has been extensively discussed in the literature (Fejer, 1961; Dougherty and Farley, 1960; Waldteufel, 1965) and it is sufficient here to quote a simplified equation giving the received signal-to-noise power ratio, η , for a vertically looking radar system:

$$\eta = K \frac{P_T A N_e \sigma \tau}{R^2 T B} \quad 1.2$$

Here P_T is the peak transmitted power, A is the effective area of the receiving aerial, N_e is the electron concentration, R is the range (the same as the height, h , in this case), T is the system noise temperature, B is the receiver bandwidth, τ is the pulse duration, σ is the scattering cross-section per electron and K is a constant. For the normal mode of scattering, in which the signal spectrum is broadened by an amount characteristic of the thermal velocities of the ions,

$$\sigma = \sigma_e / \left(1 + \frac{T_e}{T_i} \right) \quad 1.3$$

where σ_e is the Thomson electron scattering cross-section and T_e , T_i are the electron and ion temperatures respectively.

Equation 1.3 holds true (Buneman, 1962) as long as

$$\lambda_0 \gg 4\pi \lambda_D \quad 1.4$$

where λ is the radar wavelength and λ_D is the Debye length in the plasma, proportional to $(T_e/N_e)^{\frac{1}{2}}$. When $\lambda \gtrsim 4\pi \lambda_D$, a significant proportion of the scattered power originates from the classical Thomson process, with a spectral spread corresponding to the thermal velocities of the electrons rather than the ions. Although in this case $\sigma = \sigma_e$ rather than as in equation 1.3, the signal to noise ratio is degraded because of the broader bandwidth. This situation, which occurs both at low heights

in the D-region, and at great heights around 2000 km, determines the region of the ionosphere from which it is possible to get useful information by the incoherent scattering technique for a given λ_0 . It is assumed that the occurrence of collisions between electrons and heavy particles has no effect on σ .

The form of the spectrum depends primarily upon the ratio T_e/T_i , although Evans (1969) has indicated that other ionospheric parameters such as ion composition, vertical drift and the frequency of collisions can be deduced from the spectrum shape. The spectrum half width for $\lambda > 25\lambda_D$ is a function of the ion temperature which, in conjunction with the temperature ratio, yields a value for the electron temperature and also the mean scattering cross section for the medium.

One further consideration of the form of the scattering medium introduces an upper limit to the range of useful wavelengths. Local fluctuations in electron density and hence dielectric constant will lead to a further coherent component in the scattered signal. This will be undetectable if the incident wavelength is less than $L/10$, where L is the scale size for weak irregularities. Thus an upper limit is set upon the wavelength of approximately one meter.

The data employed in this study was recorded at Malvern (J.S. Hey et al., 1968) by means of a ten megawatt pulsed radar, operating at a frequency of 400 MHz. The spectral analysis of the scattered signal at various intervals in time following the initial pulse gives a series of Doppler spectra from which the variation of electron and ion temperatures and mean scattering cross section with height can be deduced by comparison with spectrum shapes computed from model plasmas. A relative electron distribution with height may then be computed from the total received signal in each spectrum and the scattering cross section. Independent observations of the F layer penetration

frequency provide an absolute measurement of the electron density to which the relative distribution may be fitted. Thus routine observations of the temperature and electron density distributions in the ionosphere between 100 and 1,000 km can be made. Several similar methods for the observations of so-called "Thomson scatter" are reviewed by Evans (1969).

A further group of experiments which use either natural sources of radio energy or sources outside the ionosphere give a measure of the total electron content of the ionosphere. The monitoring of atmospheric whistlers, cosmic radio noise and the rotation of the plane of polarization, Faraday rotation, of transmissions from satellites may be included in this group.

(b) Direct Sampling

The development of sophisticated rocket and satellite techniques in the last twenty-five years has enabled a larger number of direct sampling experiments to be undertaken. Apart from the measurement of pressure and temperature variations with height, such parameters as the conductivity of the plasma have been measured (Booker and Smith, 1970). The measurement of electron density and ion composition have been extensively carried in rockets by means of the Langmuir probe and Mass Spectroscopy techniques. Further -

more, many ground based experiments have been modified and carried out in artificial satellites giving, among other measurements, soundings of the ionosphere from above and continuous monitoring of solar activity (Eccles and King, 1970).

1.5. Proposed Investigation

The physical properties of the normal E and F layers and their effects on radio wave propagation have been extensively studied; however the transition region between these layers, 110 to 170 km, has received little attention. The presence of low electron density gradients or reentrant features in the electron density distribution produce high absorption and group retardation, thus rendering ground based experimental investigation difficult and complicating the analysis of the observations. Furthermore in these so called 'cusp' regions the simple approximations to the magneto-ionic theory break down and a more elaborate analysis becomes necessary. In this study a detailed investigation of the absorption and virtual height of reflection of radio wave pulses reflected in this region of large group retardation has been undertaken in order to determine the electron density distribution at these heights, and to investigate the behaviour of radio waves in such a region.

Experimental observations of vertical incidence absorption and virtual height are made on a fixed frequency which is reflected from the F region shortly after sunrise and from the E region later in the morning. Thus it is possible, using a single frequency, to measure these parameters as the radio wave reflection level traverses the transition region. These observations are augmented by

ionospheric sounding in the frequency range 1.5 to 7.0 MHz both on an hourly routine basis and at three minute intervals on selected days.

The analysis of the experimental results has necessitated the use of computer methods for the reduction of ionogram data to electron density profiles. The profiles thus derived are compared with those obtained from other sources and the growth of the transition region after sunrise is discussed in terms of these distributions.

Recent advances in the application of the magneto-ionic theory and computer techniques have enabled calculations of the absorption and virtual height of radio waves, reflected in a region of high group retardation, to be undertaken. The 'phase integral' analysis is adopted for the computation of these parameters from the various ionospheric models described and by comparison with the experimental observations an estimate of the validity of these results is obtained.

Chapter 2

Applications of the Ray Theory

2.1. Ray Theory

The theoretical work which follows is based upon the principles of the magneto-ionic ray theory summarized by the Appleton-Hartree formula

$$n^2 = 1 - \frac{X}{1 - iZ - \frac{Y_T^2}{2(1-X-iZ)} \pm \left[\frac{Y_T^4}{4(1-X-iZ)^2} + Y_L^2 \right]^{1/2}} \quad 2.1.1$$

$$R = \frac{i}{Y_L} \left[-\frac{Y_T^2}{2(1-X-iZ)} \pm \left\{ \frac{Y_T^4}{4(1-X-iZ)^2} + Y_L^2 \right\}^{1/2} \right]$$

in which the positive sign refers to the ordinary wave and the negative sign to the extraordinary wave. The developments from this formula to suit the needs of various theoretical studies are discussed in the following sections and in Chapter 3.

2.2. Calculation of True Height

A representative model of the electron density distribution with height is a fundamental requirement of many theoretical studies of the ionosphere. In many cases the use of a simple model, such as that described by Chapman (1931) is sufficient to indicate the usefulness of a theoretical approach, but in others a more quantitative description of the distribution existing at a particular time becomes necessary. Regular vertical incidence pulse sounding of the

ionosphere at many locations throughout the world provides a ready source of virtual height data from which highly localised electron density-height distributions can be obtained.

The virtual height of reflection of a radio wave incident normally upon the ionosphere is a double valued function of the sounding frequency; the two values representing an ordinary and an extraordinary ray. The real and virtual heights are related by the integral equation

$$h'(f) = \int_0^{h_r(f)} \mu'(f, f_N, f_H, \theta, \nu) dh \quad 2.2.1.$$

in which the group refractive index, μ' , may be considered a function of the sounding frequency, f , and the plasma frequency, f_N , while the gyro frequency, f_H , and the dip angle, θ , can be considered constant and the effect of the collision frequency, ν , can be neglected (Titheridge, 1961b). The inversion of this equation to give electron density as a function of height from the ionogram data has been investigated by many workers and the various analyses which have been evolved will be discussed briefly in this section.

The first technique for the analysis of virtual height data was an indirect comparison method described by Ratcliffe (1951). This widely followed system requires the matching of virtual height profiles derived from a series of model electron distributions to the observed profile. The first direct analysis of virtual height data was described by Kelso (1952), and this was later modified by Shinn (1953), to allow for the effect of the earth's magnetic field. These authors described a manual method by which the real height of reflection at a frequency, f_o , could be expressed as the mean

of a fixed number of virtual heights scaled at a series of frequencies, f_i . The Shinn-Kelso coefficients define the scaling points in terms of the ratios f_i/f_0 , five or ten terms being used depending on the accuracy required in the electron density profile.

The 'five point' and 'ten point' manual methods give an indication of the height of the maximum and of the thickness of the observed layer, but very little structural detail. Consideration of this point led Wright and Smith (1967), to suggest a classification of reduction methods into two groups, those techniques which give a distribution representing only part of the complete profile, and those more sophisticated analyses which attempt to give a distribution satisfying the whole range of the vertical sounding data. The first group of analyses, in which Wright and Smith included the original manual methods, has the major advantage that from a limited amount of scaling the gross features of the layers can be calculated. With the growth of interest in the ionosphere throughout the world, the output of virtual height data has reached such a level that only a small proportion can be fully analysed by the more complex methods of the second group. This has encouraged Schmerling (1967) and Titheridge (1967b), to develop rapid manual methods for routine use in deriving the height of the peaks of different layers, the scale height at the peak, and the total number of electrons below the peak.

The first analysis in the second group to be generally accepted as giving a practical solution to equation 2.2.1, was that described by Budden (1955), and developed as a

computer analysis by Thomas, Haselgrove and Robbins (1958). This method, which was presented together with computing details by Thomas and Vickers (1959), represents the ionosphere in terms of a series of horizontal lamina, and leads to a series of so-called 'lamination methods' which constitute the majority of the complete analyses in use today.

The lamination methods first assume that the virtual height at any point in the ionosphere can be expressed as the sum of the individual effects of many horizontal lamina below this point. The coefficients in such a sum will depend upon the plasma frequency in each lamina, and upon the exploring frequency, as well as upon the geomagnetic parameters at the particular location in the ionosphere. These coefficients are conveniently expressed in matrix form, and by inversion of this matrix a value for the real height may be represented in terms of wave retardation experienced in each lamina. In calculating the matrix terms a distribution of electron density within the lamina must be assumed, and this is the point at which modern developments have deviated from Budden's original analysis.

The choice of an analytic distribution which closely resembles that of the electrons in the lamina will either result in a more accurate analysis or in the use of fewer lamina and hence fewer scaling points to obtain a required accuracy. The distribution can be expressed as a differential equation of any order (Paul 1960),

$$\frac{d^n h}{d\phi^n} = \text{constant} \quad 2.2.2.$$

where ϕ is any single valued differentiable function of the electron density.

Budden's method assumes n equal to one, and is thus a first order method, in which the function $\phi = N^{1/2}$. Other first order methods have been described by King (1960), and by Fitzenreiter and Blumle (1964), both employing the function

$$\phi = \log f_N^2$$

Wright and Smith (1967) have concluded that although the function $\phi = N^2$ gives the best analytical fit at the peak of a layer, the most satisfactory function throughout the profile is $\phi = N$.

In considering higher order methods Paul (1960), and Paul and Wright (1963), concluded that a second order assumption is optimum for the analysis, since it not only overcomes the excess weighting produced by the upper part of the lamina by giving an independent value to

$$\frac{dh}{d\phi}$$

at reflection, but also

produces a better approximation to the true distribution regardless of the local curvature of the profile. The major disadvantages of such methods are that they demand a free choice of scaling interval and two sets of coefficients, and are thus only of use where large, high speed computers are available.

An alternative to the lamination method was that described by Titheridge (1959a), in which the real height profile was represented by a polynomial whose coefficients could be determined by the solution of several simultaneous equations formed from equation 2.2.1. This approach was later modified by Titheridge (1961a), so that only a segment

of the profile was described by any particular polynomial, thus overcoming the complexity and inaccuracy involved in finding a single polynomial representing the whole profile. This procedure has been adopted in the present study since its scaling and computing requirements suited those available and it is described in more detail in Chapter 3.

2.3. Correction of Real Height Profiles

The analyses discussed above all depend upon the inversion of equation 2.2.1 and hence the assumption that the function, μ' , is single valued which in turn requires a monotonic solution to the electron density distribution. It has, however, been suggested that the ionogram cusp formed at the critical frequency of the E layer may be indicative of a distinct maximum in the distribution above which a reentrant region may exist. Such a feature has come to be called the 'valley' and several workers (Davies and Saha 1962, Paul and Wright 1963) have followed an approach described by Titheridge (1959), by which the extraordinary ionogram trace can be used to adjust the profile shape in this 'valley' region. Davies and Saha (1962) have gone further in adopting a technique described by Manning (1949) and have represented the valley structure by an equivalent single valued distribution producing identical group retardation curves. The electron density profiles obtained by this method were later shown not to be unique (Saha 1964) but to fall into a family of such curves representing the same virtual height data. This ambiguity has been discussed further by Paul (1966), who has attempted, by the use of phase height data, to obtain a unique 'valley' profile. However, he concludes

that although this approach gives a lower limit to the valley width it cannot define exactly the electron distribution in the region.

An associated problem is that concerned with the effect of ionization existing below the reflection level of the minimum observed frequency, f_{\min} , on the ionograms. This ionization which is unobserved by the medium frequency ionosonde can again be accounted for by the extraordinary ray analysis. Long (1962) has compensated for this ionization by introducing a slab of constant electron density below the f_{\min} reflection height, while Sanatani and Shirke (1966) used a computer to extrapolate the electron density profile below f_{\min} . These correction procedures have been employed to estimate the extent of the nocturnal E layer since both the ordinary and extraordinary waves are strongly reflected by the F layer at night. However the extraordinary E region trace is heavily attenuated during the day thus rendering this type of analysis impracticable in many cases.

The correction analyses discussed above require that the ordinary and extraordinary traces can be reconstructed from the adjusted electron density height profile. This reconstruction can be made directly from equation 2.2.1, and provision for it has been made in many ionogram reduction methods (Titheridge 1959b). In the present study the phase integral analysis outlined by Altman (1965) is used and is discussed in detail in Chapter 3.

The region above the E layer maximum has been referred to as the valley, and the work of the authors mentioned has

entailed the representation of the electron distribution in this region by a single well defined minimum. However, vertical incidence ionograms very rarely show a simple structure in this region and the existence of rapid gradient changes are indicated by direct rocket observations (Smith 1966). Since it is common to observe several cusps on ionograms representing multiple minima or inflections in this region it will be referred to in this study as the E-F transition region, and some observations of its fine structure will be discussed in detail in Chapter 7.

2.4. Calculation of Absorption

The magneto-ionic theory defines the attenuation of a radio wave in terms of the absorption index k which is related to the refractive index in the following equation:-

$$n = \mu - i \frac{kc}{\omega} \quad 2.4.1.$$

Many workers have investigated the properties of the Appleton-Hartree formula with a view to calculating the total absorption of the ray along its path to a reflection level. The work of Appleton (1937), and later that of Jaeger (1947), is outstanding, since it formulated the concept of Deviative and Non-deviative absorption. Their work, incorporating the quasi-longitudinal and quasi-transverse magnetic field approximations suggested by Booker (1935), was based on the assumption that the total absorption could be considered as a combination of the contributions from two special cases. Firstly, the contribution from that region of the path where the refractive index could be considered equal to unity, non-

deviative absorption, and secondly, that from the region near reflection where the refractive index is sufficiently small for its variation with frequency to significantly affect the absorption index, deviative absorption. This technique has been used by many workers in their investigations of ionospheric absorption (Piggott 1953, Piggott, Beynon and Brown 1957). Two problems encountered by this approach, the validity of the Booker approximations to longitudinal or transverse propagation in the earth's magnetic field and the infinite value of the absorption index at the reflection level, have been studied by several workers (Whitehead 1952, 1956; Hibberd 1962), and many modifications have been made to the original Appleton formulation.

A direct numerical method of calculation was given by Bailey and Somerville (1938), and more recently, Titheridge (1961b, 1967b) has proposed a method by which the absorption index might be effectively integrated, for the deviative condition, to a complex reflection point which more nearly represents the propagation conditions when electron collisions are included. By this new approach an expression for an equivalent absorption index k_0 , for the case where the collision frequency is zero, is obtained and integrated to the corresponding real reflection height. Titheridge has shown that, for a sharp linear layer, the additional absorption produced by integration of the equivalent absorption index is equal to that produced by integrating the index k into the complex height plane, to a high degree of accuracy.

The application of the phase integral technique by Budden (1961) and Cooper (1964), leads to a direct calculation

of the reflection coefficient of the ionosphere by comparison of the amplitudes of upgoing and downcoming waves. This method is discussed separately in the next section.

2.5. Phase Integral Method

The application of the phase integral method to the solution of the problem of radio propagation in the ionosphere was first suggested by Eckersley (1931, 1932a, b). This suggestion was taken up by Budden (1961), who described fully the use of the method to determine reflection parameters in ionized layers. Following upon this work Cooper (1961) applied the technique directly to a number of layer models and showed, by assuming a constant collisional frequency throughout the layer, that meaningful propagation parameters could be obtained. This work was further extended by Budden and Cooper (1962), who showed, by comparison with full wave results, that the use of the phase integral method gave accurate results provided that the ionospheric profile contained no gradient discontinuities. Further generalisation of the method to account for the variation of collisional frequency with height was made by Cooper (1964), and a complete analysis was presented with some computing details by Altman (1965). This later work and the mathematical treatment will be discussed in Chapter 3.

2.6. Collisional Frequency

The propagation of a radio wave in a magneto-ionic medium results in the electrons and ions assuming an ordered,

oscillatory motion in addition to their random thermal motion. Appleton and Chapman (1932) have discussed the effect of collisions between the constituent particles of the medium upon this motion, and have shown the attenuation of the wave, and the refractive index of the medium to be functions of the collisional frequency of these particles. These authors have also shown that only the electron collisions are significant in E and F regions. The dependence of propagation parameters upon the collision frequency is embodied in the Appleton-Hartree equation (2.1) and was accounted for in terms of a retarding force $m\gamma v$, proportional to the electron velocity v and an effective collision frequency γ . This effective collision frequency was assumed to be constant for all electrons, until the work of Phelps and Pack (1959) showed its dependence upon the electron velocity. The modification of the magneto-ionic theory to include this dependence and the distribution of electron velocity was undertaken by Sen and Wyller (1960). Their results, which have been derived by Budden (1965), by a less complex mathematical approach, demand the use of a modified collisional frequency in the original Appleton-Hartree formula.

A second problem involved in establishing a collisional frequency profile for use in ionospheric calculations is that direct measurement of this parameter is difficult and observed values differ widely, Fig. 8.3.1. Several workers have therefore formulated collisional frequency profiles from the known parameters of the ionosphere. Thus, using the analysis developed by Chapman and Cowling (1939), and Cowling (1945), Nicolet (1953, 1959) derived expressions for electron

collisions with both neutral molecules and charged particles. Thrane and Piggott (1966), have summarized these theoretical studies and, neglecting the collisions with charged particles, have derived from the U.S. Standard Atmosphere (Sissenwine et al. 1962) a profile for collisions in the D and E regions which agrees well with experimental observations. These calculations and the importance of charged particles collisions above the E layer maximum will be discussed in Chapter 3.

Chapter 3

Theoretical Studies

The application of the magneto-ionic theory, as described by the Appleton-Hartree formula, to radio wave propagation in the earth's ionosphere has been discussed in detail by Ratcliffe (1959) and Budden (1961). In this chapter the calculation of the real height of reflection of a wave and the ionospheric absorption loss are discussed in detail. In addition, the computation of electron collision frequency from kinetic considerations of the atmospheric conditions is discussed as a preliminary to the calculation of the absorption.

3.1. Magneto-ionic Theory

The Appleton-Hartree equation (equation 2.1.1) may be used to derive expressions for both the total absorption and the virtual height of reflection of a pulse of radio waves. If the complex refractive index defined by equation 2.1.1 is expressed as the sum of a real and an imaginary part

$$n = \mu - i\chi$$

a wave incident on the medium of the form

$$E = E_0 \exp \left[i\omega \left(t - \frac{nz}{c} \right) \right]$$

can be expressed by substitution as

$$E = E_0 \exp \left[- \frac{\omega \chi z}{c} \right] \cdot \exp \left[i\omega \left(t - \frac{\mu z}{c} \right) \right]$$

The exponent of the attenuation term may be written in the form

$$-\frac{\omega \chi z}{c} = -kz$$

where k is the absorption coefficient which can thus be equated

$$\frac{\omega \chi}{c} = k$$

and the refractive index expressed as

$$n = \mu - \frac{ikc}{\omega}$$

Hence by separation of real and imaginary parts the absorption coefficient of the wave may be written in terms of the Appleton-Hartree equation. Many forms of this equation have been described for conditions under which the quantities Y_T or Y_L can be considered zero and the approximate cases where the real part of the refractive index is considered unity or very much less than one. These cases have been treated by Ratcliffe (1959) and the published forms of the expressions have been reviewed and compared by Murty (1964).

The second parameter with which this study is concerned is the group retardation of the wave along its path to reflection. It has been shown by Budden (1961) that the group refractive index of a pulse of radio waves may be related to the phase refractive index by the relationship

$$\mu' = \frac{\partial}{\partial f}(\mu f) \quad 3.1.1.$$

and the field of the reflected wave reaching the ground having been reflected at a height $z_0(f)$ is

$$E(t) = \int_{-\infty}^{+\infty} F(f) \exp \left[2\pi i f \left(t - \frac{2}{c} \int_0^{z_0(f)} \mu dz \right) \right] df$$

where $F(f)$ is the Fourier transform of the pulse. If now the condition that the exponent, or phase term, shall not vary with frequency is imposed, then the equation

$$\left[\frac{\partial}{\partial f} \left[f \left(\tau - \frac{2}{c} \int_0^{z_0} \mu dz \right) \right] \right]_{f=f_1} = 0 \quad 3.1.2.$$

is obtained for the predominant frequency f_1 . The quantity τ is the time taken for the pulse to travel to its reflection height and back to the ground, and an equivalent or virtual height may thus be defined as

$$h'(f) = \frac{1}{2} c \tau(f) \quad 3.1.3.$$

Further from equation 3.1.2.

$$c \tau = 2 \int_0^{z_0} \left[\frac{\partial}{\partial f} f \mu \right]_{f=f_1} dz + 2 f_1 \mu(z_0) \left[\frac{\partial z_0}{\partial f} \right]_{f=f_1} \quad 3.1.4.$$

and since $\mu(z_0)$ is zero and $\partial z_0 / \partial f$ is finite except when the frequency is close to the penetration frequency of a layer, the expression

$$h'(f) = \int_0^{z_0(f)} \mu' dz \quad 3.1.5.$$

can be obtained by substitution of expressions 3.1.1. and 3.1.4. in 3.1.3. Thus the virtual height of reflection of a pulse can be expressed in terms of the parameters of the Appleton-Hartree equation, 2.1.1.

3.2. Calculation of Collisional Frequency

The application of the Appleton-Hartree expression to

the calculation of absorption and virtual height has been discussed briefly above in its general form containing the parameter Z and hence the effect of the frequency of collisions between electrons and the other particles which form the ionosphere. Furthermore the absorption of a wave has been shown to depend directly upon the imaginary part of the refractive index and thus very strongly upon the collisional frequency.

Following sunrise, the reflection of frequencies in the range 1.5 to 2.5 MHz may take place at heights above 150 km and it is therefore necessary to consider a region of the ionosphere where not only collisions with molecular oxygen and nitrogen are experienced (Thrane and Piggott 1966) but also those with atomic oxygen and positive ions. Thrane and Piggott have derived the expression

$$\nu_M = \left[1.11 \cdot 10^{-7} n(N_2) + 7 \cdot 10^{-8} n(O_2) \right] k T_e \quad 3.2.1.$$

for the collisional

frequency of electrons with energy kT from the observations of Pack and Phelps (1961) and Phelps (1960) and following the theoretical approach described by Nicolet (1959). The addition of a term for electron-ion collisions has been discussed by Thrane and Piggott and has the form

$$\nu_i = \left[a + b \ln T_e \left(\frac{T_i}{N_i} \right)^{1/2} \right] N_i T_e^{-3/2}$$

The constants a and b have been computed by fitting this formula to the laboratory results obtained by Anderson and Goldstein (1955) and may be further simplified assuming the slowly varying logarithmic term to be constant giving

$$\nu_i = 38 \cdot N_i T_e^{-3/2} \quad 3.2.2.$$

The collision rate with atomic oxygen has been considered by Klein and Brueckner (1958) and their results have been adopted by Shkarofsky (1961) to obtain the expression

$$\gamma_o = 3.7 \cdot 10^{-6} n(0) k T_e^{1/2} \quad 3.2.3.$$

The dependence of the collisional frequency with atomic oxygen, γ_o , upon the square root of the absolute temperature, T , is derived from an observation made by Klein and Brueckner that the collision cross section of atomic oxygen was independent of the electron velocity which in turn depends on $(T)^{1/2}$.

Thus by following the practice of previous workers an expression for the total monoenergetic collision frequency was obtained. It has however been pointed out by many authors (Sen and Wyller 1960, Shkarofsky 1961, Budden 1965) that care must be taken in the substitution of theoretically derived values of collisional frequency into the Appleton-Hartree equation. By allowing the electrons to have a Maxwellian distribution of velocity, Sen and Wyller (1960) have described a generalised form of the Appleton-Hartree equation in which an effective collisional frequency is adopted in place of the monoenergetic frequency given by the expressions above. They further related the two quantities by the formula

$$\gamma_{\text{eff}} = 2.5 \gamma_M$$

for conditions where $\gamma_M \ll \omega$ or ω_H

In the present study the collisional frequency profile has been computed for each electron density distribution in turn from the expressions 3.2.1, 3.2.2 and 3.2.3. The

neutral atmospheric data has been taken from the Cospar International Reference Atmosphere 1965. The mean solar 10.7 cm radio wave flux for January to May 1969 was $156 \times 10^{-22} \text{ W/m}^2 \cdot \text{Hz}$ and the model for solar activity represented by a flux of $175 \times 10^{-22} \text{ W/m}^2 \cdot \text{Hz}$ was adopted. This model provided the constituent densities and the neutral gas temperature which was increased by a factor of 1.37 to give an estimated electron temperature. This factor was derived from the observations of Spence and Brace (1965) who have published both neutral gas and electron temperature variations with height. It has however been pointed out by many workers (Bauer et al. 1964, Sagalyn and Smiddy 1964, Oya and Aso 1968) that the electron temperature in the upper E region and above may vary appreciably from day to day and since no measure of these changes could be made during the study it was accepted that an appreciable error might exist in the final estimation of the collisional frequencies above 100 km.

The effect of the addition of the atomic oxygen and ion collision components is illustrated by the collisional frequency-height profiles represented in figure 3.2.1. These profiles have been derived from a theoretical electron density distribution described by Bourne Setty and Smith (1964) for conditions in the E-F transition region, 110-170 km, one hour after sunrise. The three curves represent (a) molecular collisions only, (b) molecular and atomic collisions, and (c) the total collisional frequency including the electron-ion collisions. These marked differences in the collisional frequency have been compared with the values given by other workers in section 8.3.1, which also includes a discussion of their

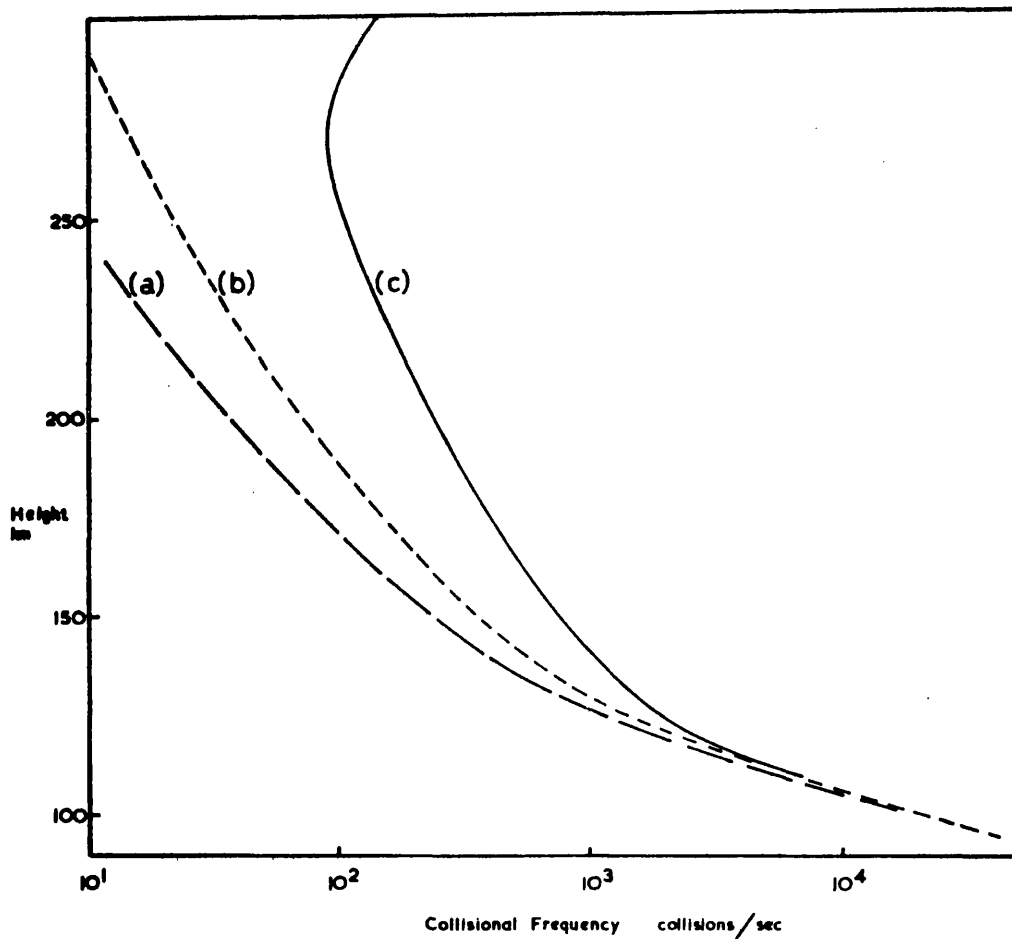


FIG.3.2.1 Collisional frequency-height profiles incorporating
 (a) molecular collisions,
 (b) all neutral particle collisions,
 and (c) all collisions including ionic collisions.

effect upon the absorption and virtual height of reflection of a radio wave pulse.

3.3. The Calculation of Absorption and Virtual Height by the Phase Integral method

The absorption coefficient, k , can be expressed in terms of the imaginary part of the complex refractive index defined by equation 2.1.1. (section 3.1). Thus, if the variation of the parameters X , Y and Z are known with respect to height the total absorption suffered by the pulse can be written as

$$L = 2 \int_0^{h_0} k ds$$

where h_0 is the reflection height and ds is an element of the ray path. However two difficulties arise; firstly, k tends to infinity as the reflection point is approached and secondly, the reflection height, i.e. the level at which the refractive index becomes zero, may not lie on the real height axis since the refractive index is a complex quantity. In simple ray theory the reflection height is considered real and the path into the complex plane neglected. This necessitates approximations to the integral of k in the last element of the path to reflection, commonly called the last 'slab'. The approximation near the reflection level has been investigated by many workers and many forms of the simple ray theory have been described and are reviewed by Murty (1964).

In order to account completely for the path of the ray into the imaginary height plane near the reflection point, Budden (1961) has applied the phase integral method to the region of the ionosphere where the physical conditions

undergo little change in the space of one wavelength of the propagating wave. Budden has discussed in detail how the W.K.B. approximate solutions of the wave equation

$$\frac{\partial^2 E}{\partial s^2} + k^2 E = 0 \quad 3.3.1.$$

can be used to give an expression for the reflection coefficient measured at the ground

$$R = i \exp \left[-2ik \int_0^{z_0} n dz \right] \quad 3.3.2.$$

in which the exponent without the unit vector i is the phase integral. The evaluation of the phase integral requires the integration of the complex refractive index to its zero in the complex plane defined by the complex reflection height z_0 . Since the refractive index is multivalued there will be several points at which it becomes zero and the first requirement of the phase integral analysis is the location of these so called branch points. By inspection of equation 2.1.1. these reflection branch points occur when

$$X = 1 - iZ \quad 3.3.3.$$

for the ordinary ray and

$$X = 1 \pm Y - iZ \quad 3.3.4.$$

for the extraordinary ray. Further coupling branch points are located at the height in the complex plane where the ordinary and extraordinary refractive indices are equal. These points are located where the square root term in equation 2.1.1.

$$\left[\frac{1}{4} Y^4 \sin^2 \Theta + Y^2 \cos^2 \Theta (1 - X - iZ)^2 \right]^{1/2} \quad 3.3.5.$$

becomes zero.

Introducing the critical value $Z_c = \frac{Y \sin^2 \theta}{2 \cos \theta}$

this expression becomes

$$Z_c^2 + (1 - X - iZ)^2 = 0 \quad 3.3.6.$$

which is satisfied when

$$X = 1 + i(\pm Z_c - Z) \quad 3.3.7.$$

thus defining two coupling points.

The one incorporating the minus sign is ignored as it lies further from the real axis and hence has less physical significance. In this coupling region interchange may take place between the ordinary and extraordinary modes, giving rise to an 'initial ordinary' ray which will be reflected at the upper extraordinary reflection height. For the radio waves reflected in the E region Z_c is generally more than $70 \times Z$ so that the three contours represented in figure 3.3.1 are considered to be physically significant.

Following the technique described by Altman (1965) the branch points were located by assuming that the X and Z height profiles have the form

$$\begin{aligned} X &= X_0 e^{az} \\ Z &= Z_0 e^{-bz} \end{aligned} \quad 3.3.8.$$

in the proximity of the branch points. The values of X_0 , Z_0 , a and b were obtained at the points $X = 1$ or $X = 1 \pm Y$ by linear interpolation between the data points of the log X and log Z profiles. Substitution of the expressions 3.3.8 into equations 3.3.3, 3.3.4 and 3.3.7, for the branch points, give the coordinates of the reflection points as

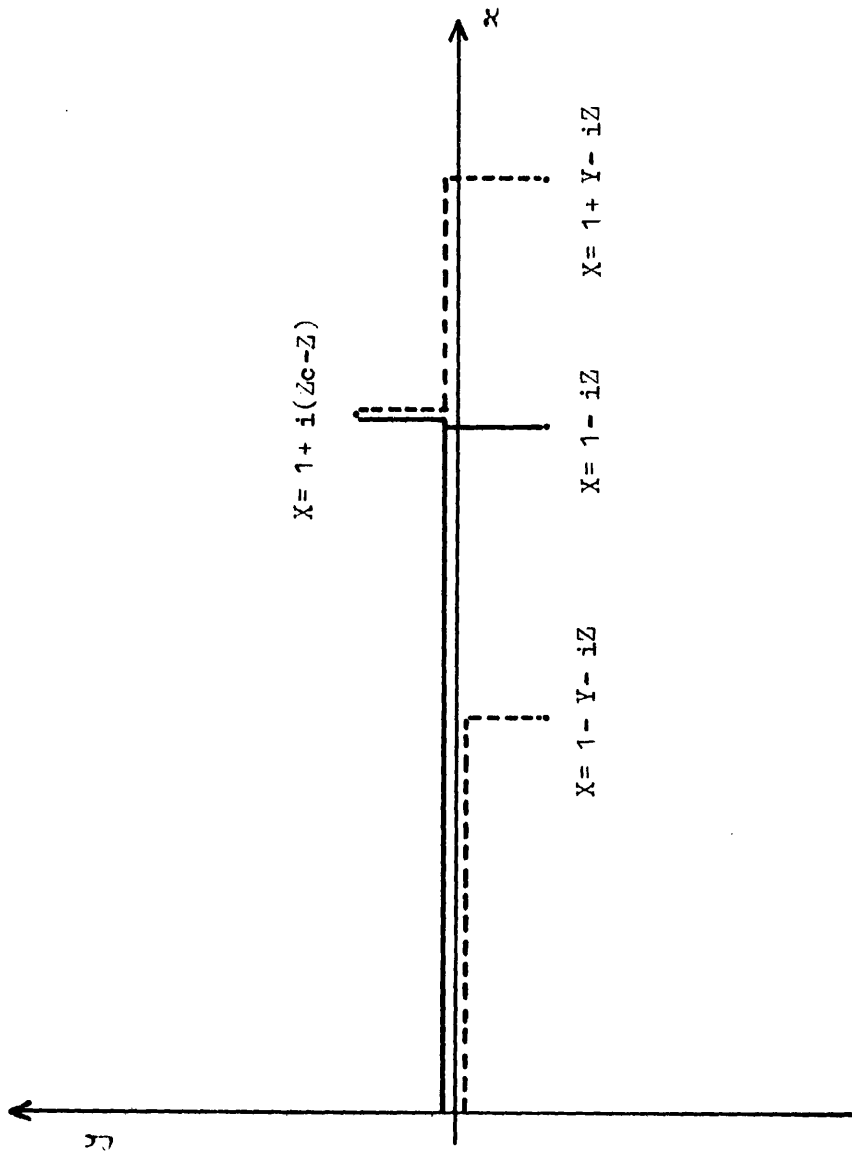


FIG. 3.3.1 Schematic representation of the main integration paths in the complex height plane.
 ——— ordinary wave, - - - extraordinary wave

$$x_r = \frac{1}{a} \log \left[\frac{\cos by_r}{\cos(a+b)y_r} \right] = \frac{1}{b} \log \left[\frac{Z_o \cos(a+b)y_r}{-X_o \sin ay_r} \right] \quad 3.3.9.$$

and the coupling point as

$$x_c = \frac{1}{a} \log \left[\frac{\cos by_c - Z_c \sin by_c}{\cos(a+b)y_c} \right] = \frac{1}{b} \log \left[\frac{Z_o \cos(a+b)y_c}{Z_c \cos ay_c - \sin ay_c} \right] \quad 3.3.10.$$

where X_o and Z_o are given values appropriate to the various branch points. Z_o for the coupling point is taken as the value of Z at the level $X = 1$. The trigonometrical functions in equations 3.3.9. are taken to be in the first quadrant so that y_r takes the necessary negative value. In this study Z_c is always greater than Z and y_c is assumed positive in equations 3.3.10. The y coordinates in equations 3.3.9 and 3.3.10 have been located by finding the zeros of the expressions involving y only. This has been done by stepping y_r away from the real axis in fixed steps until the function

$$F = \frac{1}{a} \log \left[\frac{\cos by_r}{\cos(a+b)y_r} \right] - \frac{1}{b} \log \left[\frac{Z_o \cos(a+b)y_r}{-X_o \sin ay_r} \right] \quad 3.3.11$$

changes sign and the zero was then located within a given step in y_r by step halving. Further accuracy of location was obtained by Newton's method, in which the tolerance was set at 10^{-10} km. Coordinates x_r and y_r were computed and stored along with the coupling coordinates obtained from equation 3.3.10 by the same iteration method.

A phase integral expression for the total absorption of a radio wave can be obtained directly from equation 3.3.2 as

$$L = -2k \int \left(\int_c^{z_o} n dz \right) \quad 3.3.12.$$

in which z_0 is one of the reflection points defined by coordinates x_r, y_r . The integration was carried out along the real axis to the value x_r and then perpendicularly into the complex plane to z_0 . In all calculations the initial step from the base of the ionosphere was taken as 1 km and this was progressively decreased to a lower limit of 1 meter in the real direction and $1/10$ meter in the imaginary direction. Within each step a 3 point Simpson's rule was used to evaluate the integral. A similar analysis was carried out to obtain the virtual height from the expression

$$h' = \frac{d}{df} \Re \left[f \int_0^{z_0} n dz \right] \quad 3.3.13.$$

The gradient was determined between two adjacent frequencies, f and $f + \Delta f$, where Δf was set at 300 Hz.

The accuracy of the computer programme in satisfying the reflection conditions 3.3.3 and 3.3.4 was found to be high, these being satisfied to 9 decimal places. As a further test of the programme a comparison was made between the results obtained by this analysis and those from a similar programme developed by Thomas (1968). For the ordinary ray (table 3.3.1) the agreement is to within 4.4% and this error was considered to be due mainly to the large fixed integration step length (2 km) adopted by Thomas. Some further absorption values calculated by the Leicester programme for a range of fixed integration step lengths are presented in table 3.3.2 and these illustrate the large errors which can arise if the integration is carried out over coarse steps throughout the analysis. It has been shown by Cooper (1961) that the absorption values computed for an exponential distribution of

Frequency MHz	Virtual Height km			Absorption nepers		
	a	b	c	a	b	c
2.0	105.56618	105.64836	105.43	2.9852377	3.0094086	3.137
2.4	108.57615	108.53880	108.31	2.6268376	2.7201192	2.705
4.0	142.71625	143.67296	-	1.3764977	1.3819695	1.389
4.3	141.17943	141.13148	-	1.2212962	1.2483671	1.110

Table 3.3.1 Comparison of computations made by 3 analyses
(a) Leicester Phase Integral program, with decreasing step length.
(b) " " " " , 0.25km step length.
(c) Thomas(1968) Phase Integral program, with 2km step length.

Frequency MHz	Absorption nepers						
	a	b	c	d	e	f	g
2.0	0.56404645	0.26409325	0.26269883	0.21283589	0.1943780	0.19195579	0.1720210
3.4	1.95620940	1.65903450	1.57067700	1.56536130	1.5627910	1.56145000	1.1607750
3.5	4.83314230	4.83023510	4.65479950	4.56636090	4.5465212	4.53991840	3.7535759
4.0	1.92430910	1.55512090	1.55349210	1.49835190	1.4957822	1.47912260	1.9089663

Table 3.3.2 Computations of Absorption in a Parabolic Model (122 fig.7.4.11) with constant Collisional Frequency by the analyses:

(a) Phase Integral program with step length 1.0km

(b) 0.5km

(c) 0.25km

(d) 0.1km

(e) 0.05km

(f) progressively decreasing

(g) Analytic calculation on a parabolic layer.

Frequency MHz	Absorption nepers	Deviation
2.0	0.6016	0.002
2.5	0.6008	0.0028
3.0	0.6003	0.0033
3.5	0.6022	0.0014
4.0	0.6038	0.0002
4.5	0.6071	0.0035
5.0	0.6094	0.0058
Mean	0.6036	0.0027

Table 3.3.3 Absorption in an Exponential layer.

electron density with constant collision frequency should be independent of the wave frequency. This observation is borne out by the values computed by the Leicester programme and presented in table 3.3.3 to better than 1%.

3.4 Reduction of ionograms by the Polynomial Method

The methods available for the reduction of virtual height data to electron density-height profiles have been discussed in section 2.2. In this study the polynomial method, as described initially by Titheridge (1959a), has been employed since it offers the same degree of accuracy as the lamination methods with fewer scaling points and hence smaller tabulated matrices. This factor has enabled a higher degree of accuracy to be obtained with the limited computer capacity available. Titheridge (1961a) has further modified the analysis by limiting the extent of the region represented by any particular polynomial. Details of the analysis are discussed below.

In order to compute the real height of the reflection h_i of a frequency f_i a polynomial of degree four is required to represent the real height profile at heights h_{i-2} , and h_{i-1} and to reproduce the observed virtual heights, h'_{i-1} , h'_i and h'_{i+1} through equation 2.2.1. Thus, by assuming that the virtual height and the real height are identical at the lowest frequency observed on the ionogram and that the real height of reflection has not changed in the frequency interval below this, successive real heights may be calculated by step by step method along the frequency scale.

In considering the calculation of h_i it is assumed that h_{i-2} and h_{i-1} are known and that the real height profile between plasma frequencies

$f_N = f_{i-2}$ and $f_N = f_{i+1}$ can be represented by the polynomial

$$h = (\alpha_0)_i + (\alpha_1)_i f_N + (\alpha_2)_i f_N^2 + (\alpha_3)_i f_N^3 + (\alpha_4)_i f_N^4 \quad 3.4.1$$

Thus h_{i-2} and h_{i-1} may be represented as

$$h_{i-2} = (\alpha_0)_i + (\alpha_1)_i f_{i-2} + (\alpha_2)_i f_{i-2}^2 + (\alpha_3)_i f_{i-2}^3 + (\alpha_4)_i f_{i-2}^4$$

and

$$h_{i-1} = (\alpha_0)_i + (\alpha_1)_i f_{i-1} + (\alpha_2)_i f_{i-1}^2 + (\alpha_3)_i f_{i-1}^3 + (\alpha_4)_i f_{i-1}^4$$

Furthermore, if the quantity $H'_{i-1;i-2}$ is defined as the virtual height resulting from the passage of a radio wave of frequency f_{i-1} through ionisation above the level h_{i-2} , so that

$$H'_{i-1,i-2} = \int_{h_{i-2}}^{h_{i+1}} \mu'(f_{i-1}, f_N) dh \quad 3.4.2.$$

then from equation 3.4.1

$$H'_{i-1,i-2} = (\alpha_1)_i \int_{f_{i-2}}^{f_{i-1}} \mu' df_N + 2(\alpha_2)_i \int_{f_{i-2}}^{f_{i-1}} \mu' f_N df_N + 3(\alpha_3)_i \int_{f_{i-2}}^{f_{i-1}} \mu' f_N^2 df_N + 4(\alpha_4)_i \int_{f_{i-2}}^{f_{i-1}} \mu' f_N^3 df_N$$

If the "partial" virtual heights $H'_{i,i-2}$ and $H'_{i+1,i-2}$ for frequencies f_i and f_{i+1} are also expressed in this form five simultaneous equations are produced which may be represented in the matrix form -

h_{i-2}	1	f_{i-2}	f_{i-2}^2	f_{i-2}^3	f_{i-2}^4	$(\alpha_0)_i$
h_{i-1}	1	f_{i-1}	f_{i-1}^2	f_{i-1}^3	f_{i-1}^4	$(\alpha_1)_i$
$H'_{i-1,i-2}$	0	$\int_{f_{i-2}}^{f_{i-1}} \mu' df_N$	$2 \int_{f_{i-2}}^{f_{i-1}} \mu' f_N df_N$	$3 \int_{f_{i-2}}^{f_{i-1}} \mu' f_N^2 df_N$	$4 \int_{f_{i-2}}^{f_{i-1}} \mu' f_N^3 df_N$	$(\alpha_2)_i$
$H'_{i,i-2}$	0	$\int_{f_{i-2}}^{f_i} \mu' df_N$	$2 \int_{f_{i-2}}^{f_i} \mu' f_N df_N$	$3 \int_{f_{i-2}}^{f_i} \mu' f_N^2 df_N$	$4 \int_{f_{i-2}}^{f_i} \mu' f_N^3 df_N$	$(\alpha_3)_i$
$H'_{i+1,i-2}$	0	$\int_{f_{i-2}}^{f_{i+1}} \mu' df_N$	$2 \int_{f_{i-2}}^{f_{i+1}} \mu' f_N df_N$	$3 \int_{f_{i-2}}^{f_{i+1}} \mu' f_N^2 df_N$	$4 \int_{f_{i-2}}^{f_{i+1}} \mu' f_N^3 df_N$	$(\alpha_4)_i$

which may be further abbreviated to

$$H_i = G_i \alpha_i \quad 3.4.3$$

Furthermore, the equation on 3.4.1 gives the expression

$$h_i = (\alpha_0)_i + (\alpha_1)_i f_i + (\alpha_2)_i f_i^2 + (\alpha_3)_i f_i^3 + (\alpha_4)_i f_i^4$$

for the real height of reflection of a frequency f_i .

This may be expressed in the matrix form

$$h_i = F_i \cdot \alpha_i \quad 3.4.4$$

in which F_i is the row matrix $(1, f_i, f_i^2, f_i^3, f_i^4)$

Thus, by combining equations 3.4.3 and 3.4.4

$$h_i = [F_i G_i^{-1}] \alpha_i \quad 3.4.5$$

from which the real height h_i can be computed from the

quantities h_{i-1} , h_{i-2} and the partial virtual heights at frequencies f_{i-1} , f_i and f_{i+1} . The partial virtual heights defined by the equation 3.4.2 can be expressed in the form

$$H'_{i-1, i-2} = h'_{i-1} - \left[h_0 + \sum_{j=2}^{i-2} \mu'_{i,j} (h_j - h_{j-1}) \right] \quad 3.4.6$$

by employing a lamination method to evaluate the

integral. The height h_0 is the real height at which the analysis is begun and is assumed equal to the observed virtual height of the lowest observed frequency on the ionogram. The mean phase refractive index in each lamina defined by the subject j can be expressed in the form

$$\bar{\mu}'_{i,j} = \frac{1}{f_j - f_{j-1}} \int_{f_{j-1}}^{f_j} \mu'(f_i, f_N) df_N \quad 3.4.7$$

and this expression has been further simplified to

$$\bar{\mu}'_{ij} = \frac{1}{2} (\mu'_{ij} + \mu'_{i,j-1})$$

for the calculation of values up to $j = i - 2$.

However, for the case where $j = i - 1$, the integral is evaluated by a three point Simpson's rule technique. The integrals involved in the matrix G_i have been determined by the application of 10 point Gauss Quadrature formula described by Lowan, Davids and Levenson (1942). The values of $\bar{\mu}'_{ij}$ and the row matrix $F_i G_i^{-1}$ have been calculated for Leicester adopting the geomagnetic parameters in table 3.4.1. and a frequency range of 1.4 to 10.0 MHz in 0.2 MHz steps in f_i and f_w and were stored in matrix form for routine ionogram reduction.

3.5. The validity of the polynomial reduction technique

3.5.1. Sensitivity to Geomagnetic variation

The geomagnetic parameters listed in table 3.4.1 have been interpolated from values for Slough and Inverness taken at ground level. These parameters are known to vary with time and also with height above the ground. In order to ascertain the sensitivity of the tabulated values of $\bar{\mu}'_{ij}$ and $F_i G_i^{-1}$ with changes in these parameters the matrices were calculated for several values of the gyrofrequency, 1.2, 1.25 and 1.3 MHz and of the dip angles, 67.5° , 67° and 66.5° . The resulting nine pairs of matrices were used in the reduction of the test virtual height curves A, B and C of figure 3.5.1. The deviation between the resulting electron density profiles for various combinations of the gyro-

Geographic Latitude	52° 37' N
" Longitude	1° 6' W
Gyro-frequency	1.28 MHz
Dip Angle	66° 44'

Table 3.4.1 Geomagnetic and Geographic parameters of Leicester.

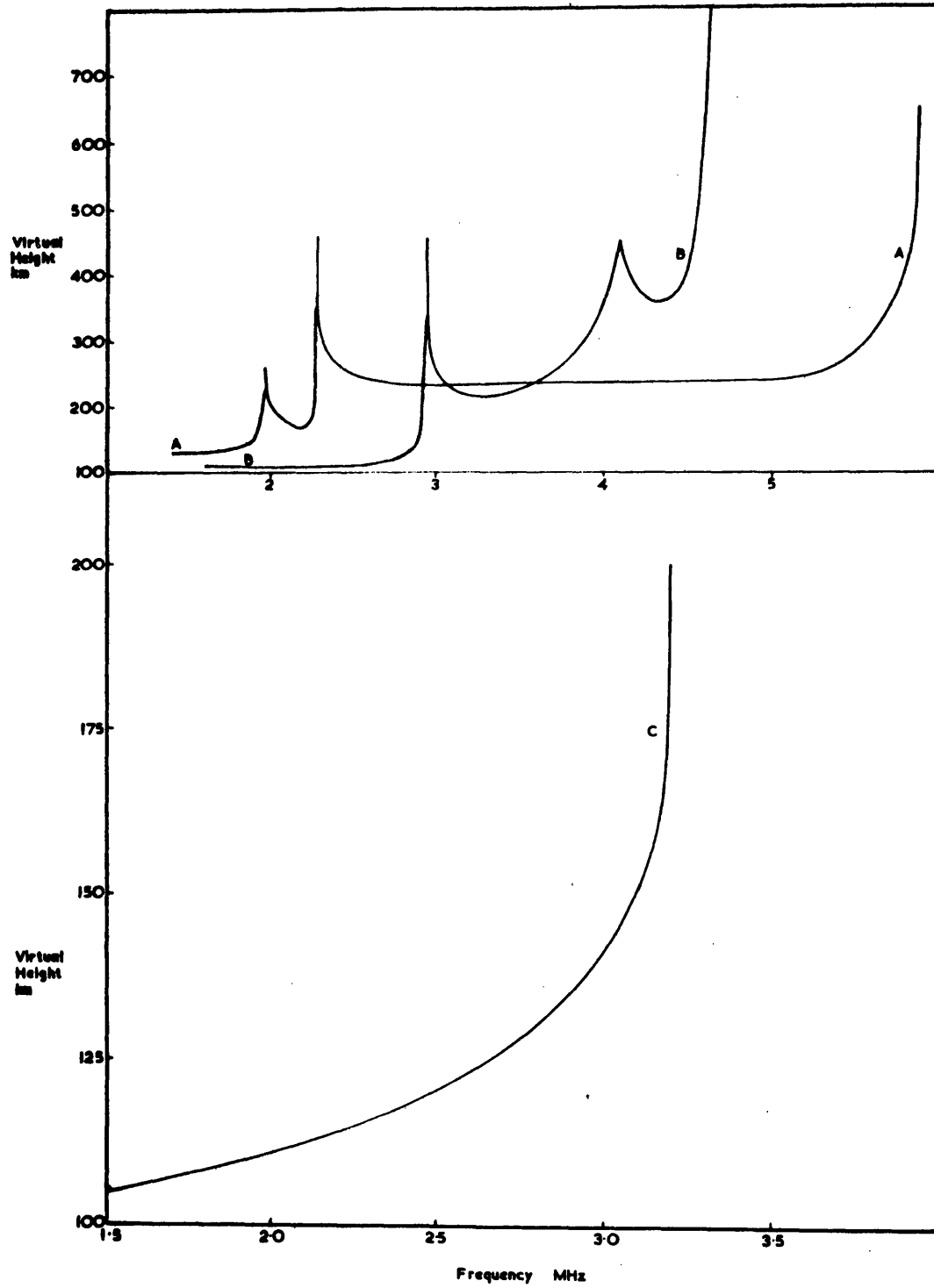


FIG.3.5.1 Virtual height-frequency test curves for the polynomial analysis.

frequency and dip angle was never more than 0.25% while the changes in the two parameters were 7.7% and 1.5% respectively. Thus the sensitivity of the analysis to fluctuations in the geomagnetic parameters is small and the error induced into the analysis by inaccuracies in the estimation of these parameters can be considered negligible when compared with the errors involved in the scaling of the virtual height data which will be discussed in Chapter 5.

3.5.2. The scaling interval in frequency

This study is concerned with the disturbed region around the peak of the E layer as indicated by the fine structure recorded on ionograms. The size of the scaling interval is therefore of particular importance in respect of the ability of the reduction analysis to account for these fine structures. In section 3.4 the scaling interval used was 0.2 MHz following the recommendation of Titheridge (1961a). However figure 3.5.3 illustrates the variation which was produced in the electron density profile when the test curve D, figure 3.5.2, was moved along the frequency scale between the two extremities shown in the figure. The virtual height curve was arranged so that the cusp occurred at 1.9, 1.95, 2.0, 2.05 and 2.1 MHz and the reduction analysis was carried out for each case. The results indicate that when the cusp was positioned at the scaling frequency or below it, the computed real heights lay on or within two kilometers of the dashed profile. The lower dotted profile was the result of taking the cusp to a frequency above the scaling point. Thus the position of the cusp had little effect upon the resulting profile unless its position was changed from one side of the scaling point to the other, in which case the profile was greatly

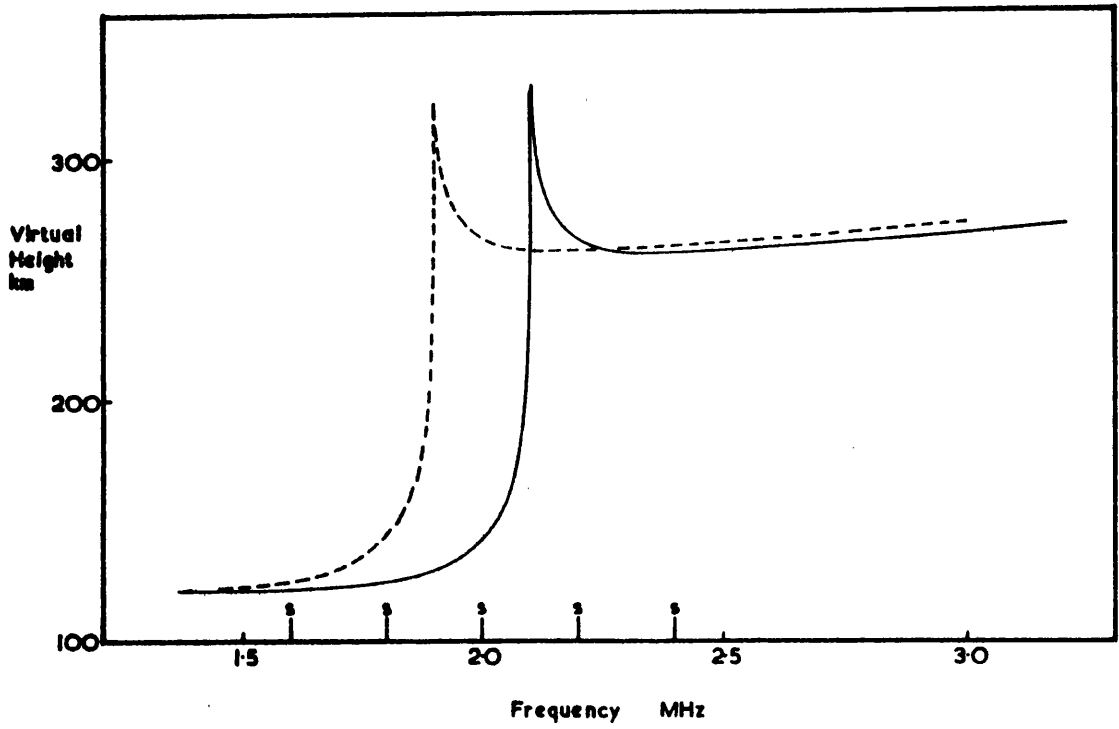


FIG.3.5.2 Test virtual height-frequency curve D (scaling points s).

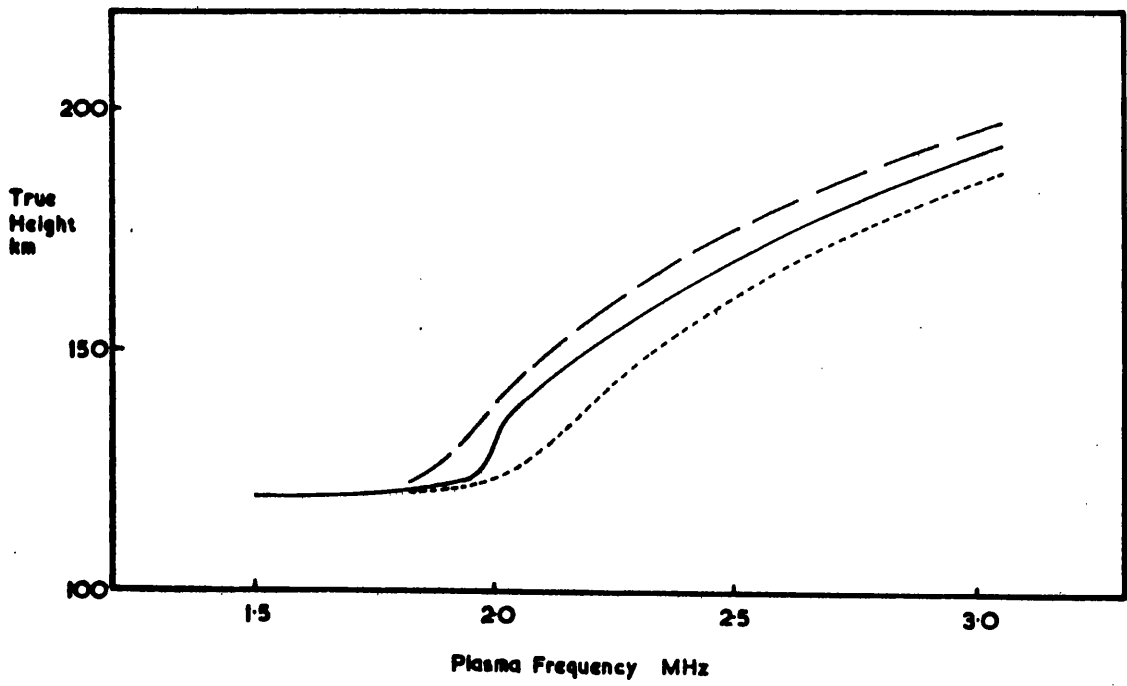


FIG.3.5.3 Monotonic profiles resulting from the movement of a cusp feature (fig.3.5.2) between the scaling points.

altered. Thus to obtain a profile which might represent the virtual height data as closely as possible it was considered that the cusp structures of the ionogram should be located as accurately as possible by employing the smallest practicable scaling interval. This was found to be 0.05 MHz. Further interpolation between the frequency markings of the ionograms may entail large errors since, by virtue of the servo-tuning control system employed, the receiver frequency is generally not a simple function of time. Thus the frequency mark spacing on the ionograms may be irregular.

In recomputing the matrices for the analysis it was considered necessary to use a three point Simpson's Rule to evaluate the quantities $\bar{\mu}'_{ij}$ in the last six frequency steps where the proximity of the reflection height renders the simple linear assumption inadequate. The difference between the coefficients $\bar{\mu}'_{ij}$ calculated by the two methods was approximately one percent for the sixth coefficient, $j = i - 7$, and eight percent for the last step. The electron density profile obtained by this modified analysis has been included in figure 3.5.3. and demonstrates clearly the increase in profile definition obtained by the use of the narrower scaling interval. This improvement has been further illustrated in figure 3.5.4 in which the results obtained from the two analyses and the test curve A have been presented. The two peaks which give rise to the cusps of curve A are clearly defined by the modified analysis while the original coarse reduction gives little or no indication of these structures.

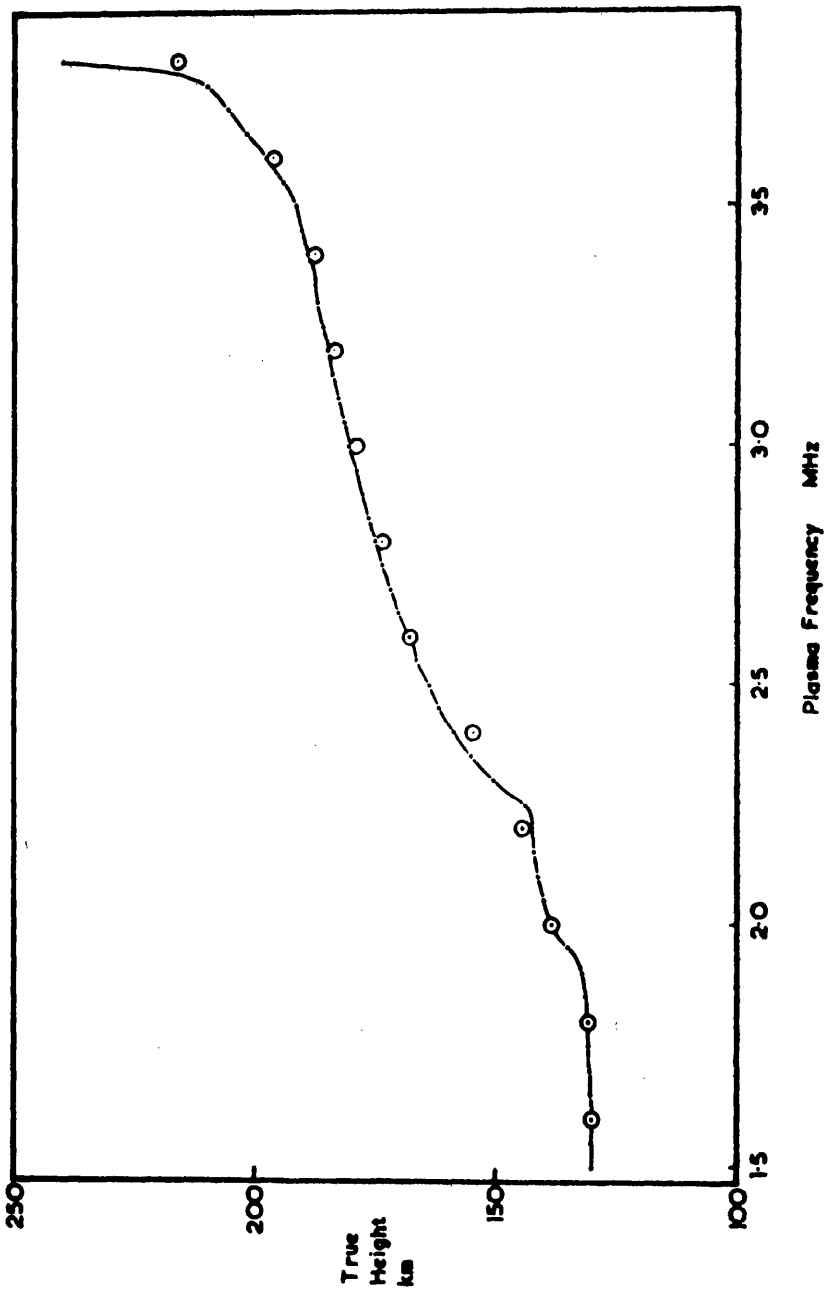


FIG.3.5.4 Monotonic profiles obtained by analyses employing scaling intervals
 (a) \circ 0.2 MHz, and
 (b) \cdots 0.05 MHz.

3.5.3. Comparison with Analytic Profiles

The three analytic profiles given by the equations of 3.5.1 and illustrated in figures 3.5.5, 3.5.6 and 3.5.7 were used to test the validity of the reduction technique.

$$\begin{array}{ll}
 \text{Linear layer} & f_N^2 = \alpha(z - h_0) \quad z > h_0 \\
 \text{Parabolic layer} & f_N^2 = f_p^2 \left[1 - \frac{(z - z_m)^2}{a^2} \right] \quad (z - z_m) \leq a \\
 & f_N^2 = 0 \quad (z - z_m) > a \\
 \text{Exponential layer} & f_N^2 = F^2 e^{\alpha(z - h_0)} \quad z > h_0
 \end{array} \quad 3.5.1.$$

In each case the corresponding virtual height profile was calculated using the expressions for the no field case derived by Budden (1961) and these profiles were then processed by the reduction analysis.

The technique described by Titheridge (1961a) was used to obtain the curves marked A in the figures listed above. In this analysis the real and virtual heights at a starting frequency of 1.5 MHz, f_1 , were set equal and the computation begun at the frequency $f_2 = f_1 + \Delta f$, where Δf was the step length. It was noted that the resulting profiles were too high by 3.5, 2.0 and 9.0 km for the linear, parabolic and exponential layers respectively at 1.5 MHz. This discrepancy has been attributed chiefly to the neglect of ionisation below the reflection level of the 1.5 MHz wave. However the approximations used by Budden in computing virtual heights in the absence of a magnetic field would also contribute to the poor agreement. In order to take account of the low lying ionisation the starting assumption to the analysis has been modified.

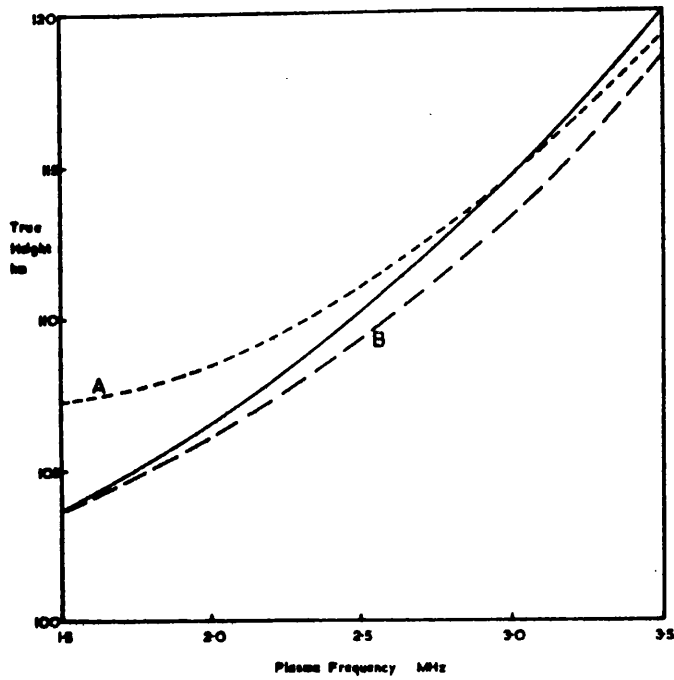


Fig.3.5.5 Comparison of computed electron density distributions with a linear model.
 — linear model
 - - - profile A, no starting correction
 - · - profile B, starting correction

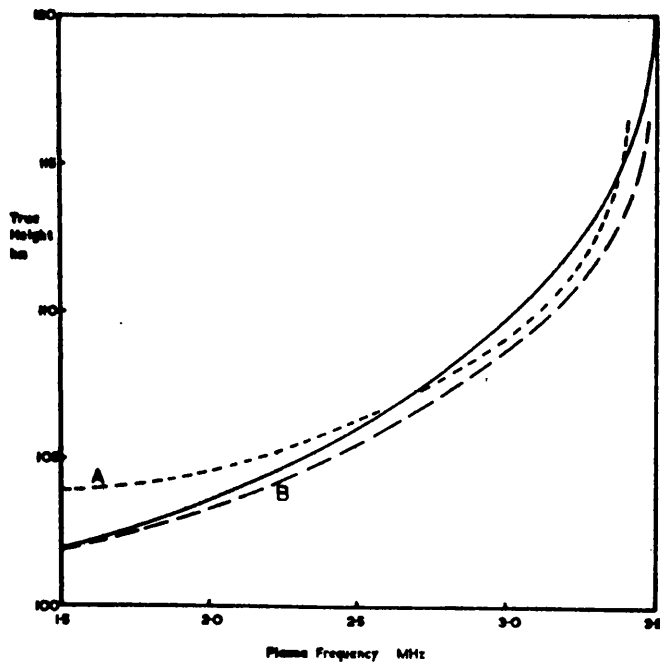


Fig.3.5.6 As above with a parabolic model.

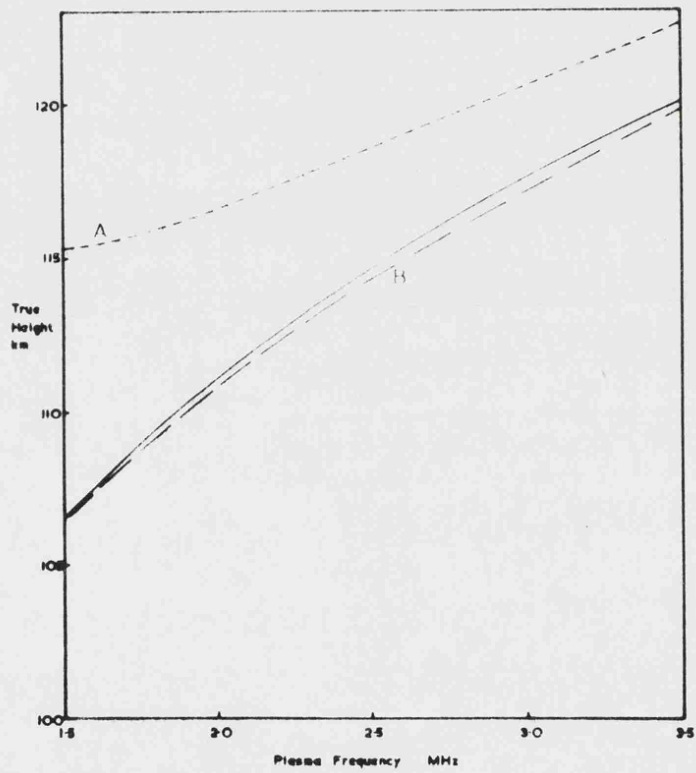


FIG.3.5.7. Comparison of computed electron density distributions with an exponential model.
 — exponential model
 - - - profile A
 - · - profile B

The virtual height h'_{i-1} was assumed to be equal to h'_i and the extent of the group retardation of the wave frequency f_{i-1} was estimated. The base height, h_0 , was then set at a value equal to the real height h_{i-1} i.e. h'_{i-1} minus the estimated group retardation. The analysis was then applied as before starting at the first scaling point. Thus for the frequency f_i the partial virtual heights

$$H'_{i-1, i-2} = h'_{i-1} - h_0$$

and
$$H'_{i, i-1} = h'_i - h_0$$

take a non-zero value and lead to a new computation of h_i .

Further, at a frequency f_{i+2} the value of

$$H'_{i+1, i} = h'_{i+1} - \left[h_0 + \bar{\mu}'_{i+1, i} (h_i - h_{i-1}) \right]$$

is modified by addition of the term $\bar{\mu}'_{i+1, i} (h_i - h_{i-1})$ which is no longer zero.

This modified analysis was applied to the analytic test profiles and the resulting curves, marked B in figures 3.5.5, 3.5.6 and 3.5.7., were obtained and show agreement over the frequency range to better than 1 km.

3.5.4. Comparison with the Lamination Method

The virtual height test curves A and B of figure 3.5.1 representing typical winter and summer profiles were analysed by the reduction analysis described above and by the Lamination Method as formulated by Thomas and Vickers (1959). The resulting profiles are shown in figure 3.5.8. and the mean difference has been calculated to be 1.9% for the winter, 1.2% for the summer profile. Further comparison with

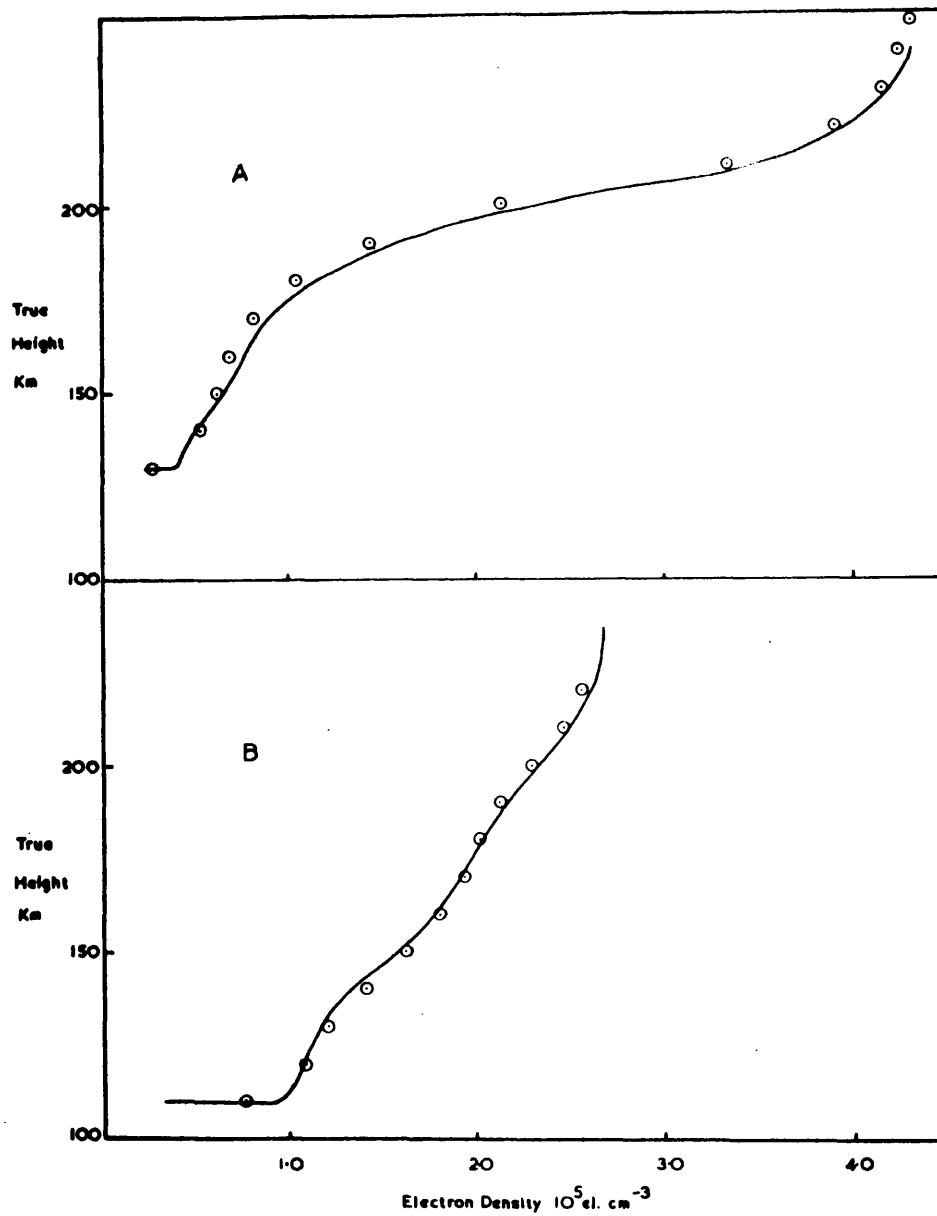


FIG.3.5.8 Monotonic electron density profiles computed from the models A and B of fig.3.5.1 by
 (a) \circ Lamination method,
 and (b) — Polynomial method.

the lamination method was obtained by analysing the test data published by Thomas and Vickers (1959). The results of these computations agree with those obtained by Thomas and Vickers as can be seen from figure 3.5.9. From the observations and comparisons made above it is concluded that the Modified Titheridge reduction analysis with a frequency scaling interval of 0.05 MHz produces a monotonic electron density distribution representative of the virtual height data with an accuracy comparable with that of other methods available for use on a small computer.

The modified polynomial reduction discussed in detail in this chapter has been employed at Leicester and the electron density distributions obtained feature in the comparative studies discussed in Chapter 7. In conjunction with these and other experimental and theoretical models, the phase integral analysis has been extensively used to compute both absorption and virtual height. The results of these calculations are discussed in detail in Chapters 7 and 8.

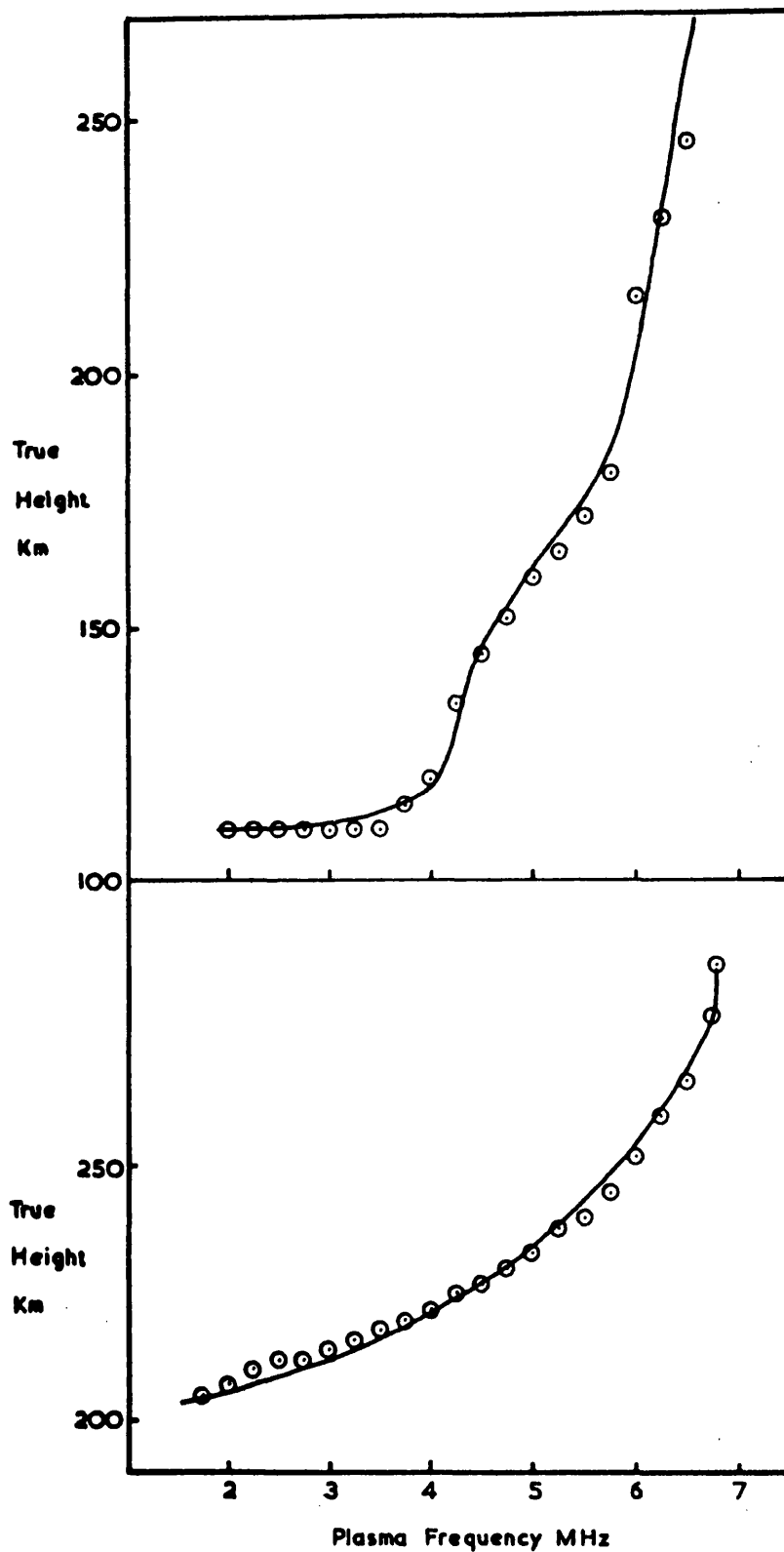


FIG.3.5.9 Monotonic electron density profiles computed from Thomas and Vickers (1959) models by (a) Lamination method, \circ and (b) Polynomial method, —.

Chapter 4

Previous Experimental Studies of absorption and Virtual Height

4.1. Pulse Techniques

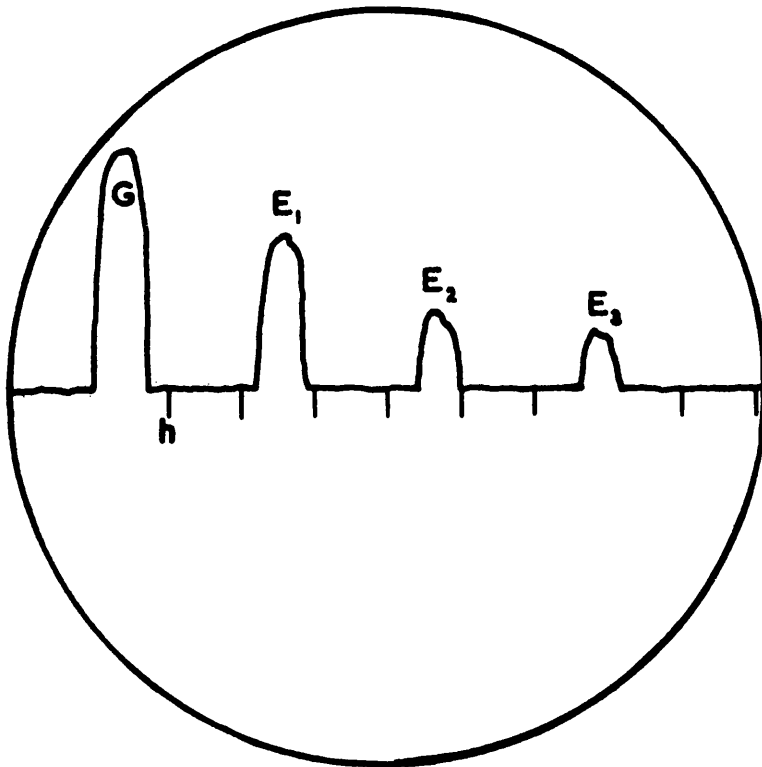
Appleton (1928) has reviewed the experimental techniques available at that time for the measurement of the virtual height of reflection of radio waves by the ionosphere. These methods were (i) the 'angle of incidence' method described by Appleton and Barnett (1925a), (ii) the 'frequency change' method, Appleton and Barnett (1925b) and (iii) the 'group retardation' method, Breit and Tuve (1925). The first two techniques employed continuous radio waves travelling over horizontal distances of the order of 150 km whereas the third required the transmission of a short duration pulse of radio waves along a nearly vertical path to the ionosphere and has since been called the 'pulse' method. Appleton and Builder (1932) have described some experiments carried out in England to compare the results obtained from the 'frequency change' and 'pulse' methods. The pulse technique described by these authors and its application to the measurement of virtual height has been widely adopted and is employed in this study. Appleton and Builder also commented upon the variability of the size of the reflected pulse and further development of their technique enabled many workers to measure the total absorption of a radio pulse in its passage through the ionosphere (Piggott 1953). In discussing the later development of pulse techniques it is convenient to treat the observa-

tions of virtual height and absorption separately.

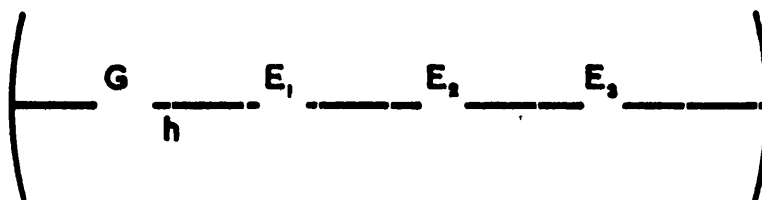
(a) Pulse Sounding

Figure 4.1.1.(a) illustrates a typical form of display obtained by the Appleton and Builder (1932) technique and indicates both the virtual height and amplitude of each echo. However the measurement of virtual height alone is more conveniently obtained from the B scan display, figure 4.1.1.(b), upon which Gilliland (1934) based the first automatic sounder. As the operating frequency of the instrument was steadily increased, photographic film was drawn perpendicularly past the trace thus producing a record similar to that illustrated in figure 4.1.1(c). Naismith (1933, 1936) developed a similar instrument with which Appleton and Naismith (1935) made one of the first synoptic studies of the features of the virtual height variation with frequency.

Wright, Knecht and Davies (1957) have reviewed the development of these techniques prior to the I.G.Y. and list the specifications for fourteen ionosondes incorporating the basic principles of the pulse sounding technique. The Union Radio mark II ionosonde described by Clarke and Shearman (1953) has been used at Leicester and will be described in more detail in Chapter 6. Following the I.G.Y. several further modifications to the technique have been described in order to improve noise discrimination and to facilitate record scaling as well as to increase the transmitted power and frequency response. These developments and the adaptation of sounding techniques to operation in artificial satellites to enable topside sounding to be carried out have recently been



A - SCAN



B - SCAN

FIG.4.1.1 Types of ionosonde display,
 (a) A-scan
 (b) B-scan

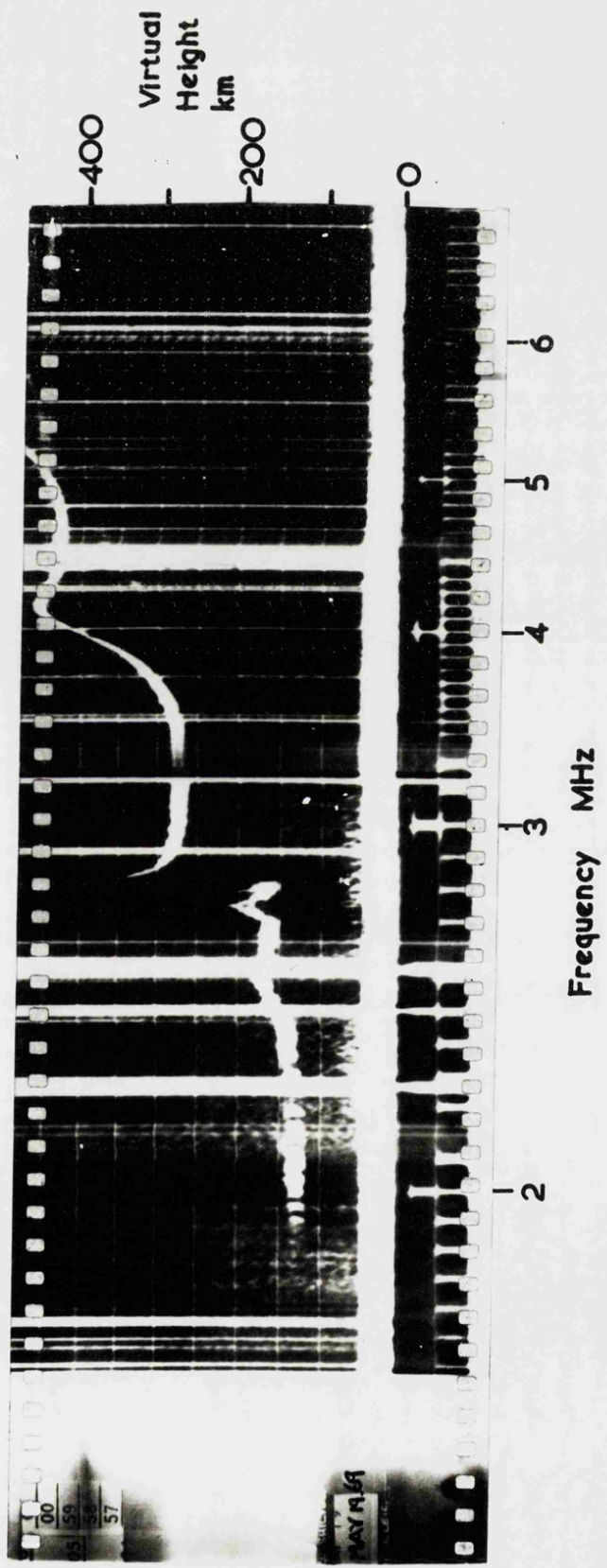


FIG.4.1.1(c) Typical Morning Ionogram

reviewed by Eccles and King (1970). These authors also describe some new sounding techniques which depart from the basic system discussed above, for example the 'Chirp' sounder described by Fenwick and Barry (1967) and the pulse compression techniques investigated by Coll and Storey (1965).

(b) Measurement of absorption

The first attempt to measure the amplitude of radio waves reflected from the ionosphere was made by Appleton and Ratcliffe (1930) using the frequency change method. The introduction of the pulse technique by Appleton and Builder (1932) greatly simplified the observations and made accurate measurements possible. Many workers (White 1933, White and Brown 1936, Best and Ratcliffe (1938) employed this simple manual technique to observe the variations of ionospheric absorption with frequency, time and season. Much of this work has been summarised by Piggott (1953) and Appleton and Piggott (1954) in reporting the findings of their observations over two sunspot cycles.

The manual pulse absorption technique requires the continuous services of a skilled operator and it is therefore impracticable to make observations over a long period of time. To overcome this problem Jenkins and Ratcliff (1953) have described a fully automatic recording system employing a gated amplifier in conjunction with a constant gain receiver. Many modifications of this technique (Madden 1967, Henry 1966), designed to meet local requirements, have been discussed. The system developed by Madden (1967) has been used as a basis for the recording equipment developed at Leicester which is described in Chapter 6.

4.2. The experimental studies of the regular features of the ionosphere

In the Annals of the I.G.Y., Piggott, Beynon and Brown and Little (1957) have described in detail the measurement of absorption and discussed the main experimental and theoretical conclusions drawn by the early workers. Further observations of these regular phenomena have been discussed by Bibl, Paul and Rawer (1965).

Appleton and Piggot (1954) have shown that the frequency dependence of the non-deviative absorption is given by the formula

$$L = \frac{A}{(f \pm f_m)^2}$$

and the solar cycle variation by

$$L = a(1 + bR_z)$$

These authors have also found that the diurnal variation of absorption can be represented by the expression $L = C \cos^n X$, in which the constant C may vary with season and magnetic activity. Much discussion of these empirical relationships has been undertaken especially that describing the diurnal variation of absorption. Bibl, Paul and Rawer (1965) have found a seasonal variation in the exponent n and Davies (1965) demonstrates the latitude dependence of n and also suggest that the form

$$L = A + B \cos X$$

better describes

conditions at sunrise and sunset. Recently Rai (1969 a, b) has reviewed the available estimates of n and has investigated, both experimentally and theoretically, the dependence of non-deviative absorption upon X and frequency at large values of the zenith angle.

The routine observation of virtual height by sounding techniques has provided extensive world wide data from which the diurnal, seasonal, solar cycle and latitude variations of the layer parameters such as the E region critical frequency, $f_o E$, have been derived. The observations of Appleton and Naismith (1935) established the structure of the ionosphere above 100 km by indicating two distinct reflecting regions referred to as the E and F layers. These authors also observed an irregular reflecting region near 100 km which they called the abnormal E. Further studies of the virtual height variation with frequency, $h'(f)$, were made by Halliday (1936) who observed irregularities around $f_o E$ on ionograms recorded manually at noon. Robinson (1960a) has discussed in detail observations of the E region and has compared the regular variations of this layer with those predicted for a theoretical layer by Chapman (1931). To facilitate such studies Wright, Knecht and Davies (1957) and later Piggot and Rawer (1961) have formulated systems by which the interpretation of ionograms may be formalised. The results of synoptic studies of ionogram data have shown the E layer to be a well behaved layer following closely the predictions of the Chapman theory and the F region to consist of two closely associated layers, F_1 and F_2 of which the F_1 approximates to the Chapman theory while the upper layer is far less predictable.

4.3. Irregular ionospheric features in the E-F transition region

The study of the regular features of the ionosphere between 110 and 170 km is complicated by the occurrence of several irregular phenomena. The most important of these is the occurrence of Sporadic E which was first observed by

Appleton and Naismith (1935) and has received much attention since (Smith and Matsushita 1962). In addition further minor features of the E-F transition region producing multiple cusp structures upon ionograms have been observed over many years. Naismith (1933) observed a single intermediate trace between the E and F layer traces of the ionogram which he designated the E_2 layer. These observations gave support to the work of Appleton (1933) who concluded that the intermediate layer was as thick as the normal E layer and was produced by the same ionising radiation. Gilliland (1935) and Halliday (1936) observed multiple cusp structure on ionograms and the work of these and several other authors has been reviewed by Becker and Dieminger (1950) who suggested that the occurrence of the E_2 should be adopted as a regular phenomenon and its minimum virtual height and critical frequency be tabulated by the routine sounding stations. Becker and Dieminger have also carried out a synoptic study of the occurrence of the E_2 trace and have found it to be a common feature near sunrise and sunset but less frequent at midday. Furthermore, these authors conclude that the E_2 layer has the characteristics of a thin homogeneous layer which has a critical frequency 200 to 300 kHz above that of the normal E layer and which develops in a regular fashion throughout the day.

Whale (1951) has commented upon this fine structure and has attempted by an ionogram reduction analysis to obtain representative electron density profiles of the upper E region and E-F transition. These profiles showed minor ledges in the monotonic profile to which Whale attributes the fine cusp structure. A similar study was undertaken by Munro and Heisler (1956) in the temperate latitude F region following

the observation of fast moving cusp structures in the tropical F layer by Skinner, Brown and Wright (1954). Munro and Heisler have traced model travelling disturbances through the F region and illustrated by calculation how such structures could produce the fast moving cusps observed. However it was further suggested that the effect of such disturbances would be very small in the E layer.

The observation of fine structure and the regular occurrence of a prenoon dip in the development of f_oE with λ has led Appleton and Lyon (1957) to discuss the departures of the E layer from the predictions made for a Chapman layer. These authors have proposed that a transport term should be included in the continuity equation for the E layer, thus

$$\frac{dN}{dt} = q(t) - d(N) - \text{div}(N\mathbf{v})$$

This transport or vertical drift term has been described by Martyn (1947) and attributed to the movement of ionization under the influence of the Sq current system, described by Chapman and Bartells (1940), and of the horizontal component of the earth's magnetic field. During experimental studies of the effect of Sq currents upon f_oE , Beynon and Brown (1959) and Appleton and Lyon (1961) have noted some ambiguity in recording the value of f_oE and have attributed this to small fluctuations in the electron density distribution near the E layer peak. Robinson (1960 b) has continued the work of Whale (1951) and Bibl (1951, 1953) in investigating the perturbations of the electron density distribution associated with these small cusps occurring near f_oE . Dieminger (1962) has considered the multiple cusp irregularity in terms of the highly complex electron density profiles observed from

rockets. These profiles, which may differ in detail between the ascent and descent of the same rocket, show many small undulations in the profile which Dieminger regards as the result of highly localised regions of increased ionization within the regular layer. This is, however, in contradiction to the observations of Robinson (1960 b). Furthermore, Dieminger has studied the lifetime of the ionogram fine structure during the afternoon and evening and has found that the subsidiary cusp structures have a faster decay rate than does f_oE and that half the cusps observed have a lifetime of less than two minutes.

The observations of Becker and Dieminger (1950), discussed earlier, indicate that the occurrence of fine structure is particularly noticeable near sunrise, thus suggesting that the electron density distribution between 110 and 170 km at this time may depart markedly from that predicted by Chapman theory.

The measurements of absorption discussed in a previous section have been made chiefly around noon, remote from the disturbed sunrise and sunset periods, although Rai (1969 a) has described an experiment to measure the absorption of frequencies reflected by the F layer in order to investigate the dependence of the exponent n on the zenith angle during sunrise and sunset. However a number of studies of the sunrise and sunset periods have been made using virtual height data.

The so called 'sunrise effect', observed by Appleton and Naismith (1935) as a marked increase in the F layer virtual height some minutes before sunrise, has been investigated and

Baral (1955) has suggested an explanation in terms of the dawn line tilt in the isoionic contours. Bourne Setty and Smith (1964) have observed multiple fine structure on ionograms at Armadale and have attempted to predict the development of the E and E-F transition regions following the sunrise by combining a nighttime E region model with a modified Chapman development of ionization. These authors have adopted several nighttime models of the E region electron distribution. Direct studies of electron densities at night have been undertaken by several workers (Watts and Brown 1954, Belrose 1963) and these have been discussed by Wakai (1966).

Although attention has been drawn to the existence of minor structure in the electron density distribution near the E layer peak and the form of the E-F transition region has been discussed theoretically, few experimental studies have been made of these regions. Thus, this investigation has been undertaken in an attempt to produce electron density profiles consistent with both experimental and theoretical observations.

Chapter 5

Pulse Measurements in the Ionosphere

5.1. Absorption

5.1.1. Principle of measurements

The absorption of a radio wave is attributed, according to the magneto-ionic theory, to the loss of energy suffered by electrons undergoing collisions with the other constituent particles of the medium and can be expressed in terms of an apparent reflection coefficient. Appleton and Ratcliffe (1930) have defined this coefficient, ρ , as the ratio of the amplitude, I , of a wave reflected once in the ionosphere and that which would have been received, over the same path, in the absence of dissipative attenuation. If an absorption coefficient, k , is assumed these amplitudes can be related by the expression

$$I = I_0 e^{-ks} \quad 5.1.$$

in which s is the path length. In the ionosphere k is a function of the refractive index, the wave frequency, the electron density distribution and the effective electron collision frequency which vary along the path and the relationship above must therefore be expressed as

$$I = I_0 e^{-\int k ds} \quad 5.2.$$

Thus the apparent reflection coefficient may be expressed in the form

$$L = -\log_e \rho = \int k ds \quad 5.3.$$

in which nepers are the units of the absorption, L . If equation 5.3 is expressed in logarithms to the base ten the units of absorption are decibels and this system has been employed throughout this study. The absorption L may thus be determined experimentally by measurement of the quantity $\log \rho$

. In the absence of dissipative loss, the amplitude, I , of a wave suffering a single ionospheric reflection is related to its virtual height of reflection, h' , by the expression

$$(Ih') = G \quad 5.4.$$

where G may be considered as a calibration constant. Similarly when the wave suffers attenuation

$$(Ih')_A = \rho G \quad 5.5.$$

and the absorption may be expressed as

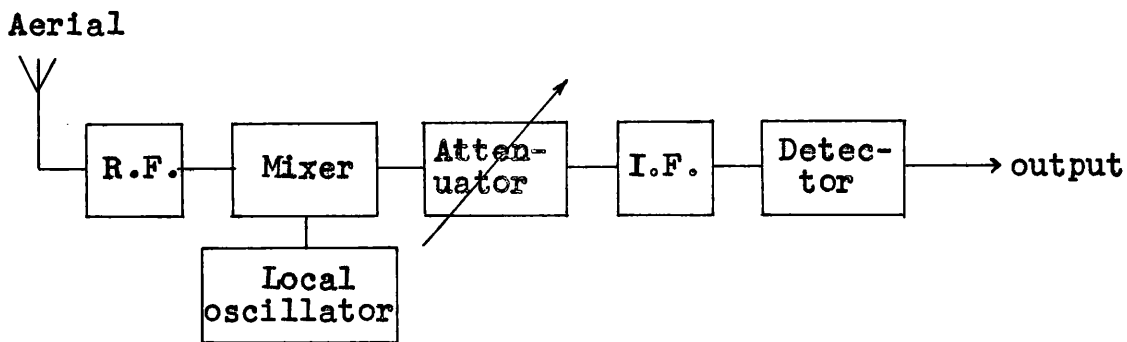
$$-\log \rho = \log G - \log (Ih')_A \quad 5.6.$$

and computed from measurements of I , h' and the calibration constant G .

5.1.2. Experimental techniques

In the previous section it has been shown that in order to estimate the ionospheric absorption loss the amplitude and the virtual height of reflection of a radio signal reflected by the ionosphere must be measured. The determination of virtual height is discussed in section 5.2 and the various techniques for the measurement of the amplitude of pulse transmissions are outlined here.

The schematic diagram shown overleaf illustrates the fundamental requirements of an amplitude measuring system.



In this study pulses of radio waves are considered throughout and the modifications necessary to a communications receiver for the reception of this form of modulation are discussed in Chapter 6. The inclusion of an attenuator before the I.F. amplifiers enables the gain of the system to be varied either by set amounts or continuously. The modulation envelope is produced by a detector stage incorporating a suitable time constant and the video output may be displayed on an oscilloscope in the form of an A-scan or passed to further circuitry for automatic monitoring.

The amplitude, I , of the returned echo is measured either by recording the attenuator settings as they are varied to maintain a constant echo output or by operating at constant gain and recording the extent of the echo output. The accuracy of these measurements depends upon the stability of the transmitter power, aerial gain and receiver characteristics, and upon the independence of these systems to the form of the wave modulation. Precautions must also be taken to ensure that sufficient observations are made to overcome the sampling errors discussed in the previous chapter.

The constant output technique was widely used in early manual experiments. However, the more recent development of automatic monitoring systems has resulted in the general

adoption of the constant gain method. Automatic measurement of echo amplitudes requires that the receiver should give an output proportional to the input over a wide range of input voltages and it may be necessary to change the gain by fixed steps in order to extend this range. The monitoring of the echo amplitude in such an automatic system is discussed later with special reference to the equipment designed by Madden (1967).

The calibration of an automatic constant gain system is undertaken in two stages. Firstly, the stability of the receiver gain is regularly checked against a standard signal generator which is also used to obtain conversion coefficients for the different gain settings employed. Secondly, the calibration constant, G , is estimated by observing the amplitude and virtual height of the echo received after a single reflection by the ionosphere when reflection conditions are such that the absorption is negligible and ρ may be assumed equal to unity. At temperate latitudes such conditions occur in the early morning hours when reflections from the F region are particularly stable and when extensive blanketing Es occurs at night. However, occasions on which spread F or partial Es reflections are in evidence must be avoided.

5.1.3. Non-Dissipative Attenuation

In addition to the dissipative attenuation discussed above the amplitude of the reflected radio wave will depend on a number of non dissipative phenomena such as

- (a) Polarization
- (b) Dispersion
- (c) Spatial attenuation

(d) Partial reflection

(e) Fading

(a) Polarization

The magneto-ionic theory indicates that a wave of arbitrary polarization incident on the ionosphere will produce two characteristic waves, the ordinary and extraordinary, which are generally propagated independently through the medium and return to the receiver with a small time difference. If however this difference is small the two components interfere to an extent governed by their relative amplitudes and phases giving rise to the polarization fading effect. Piggott (1953) has pointed out that in most cases the echo pulses are separated sufficiently either in time or amplitude to give satisfactory separation of the modes. Complete separation of the characteristic waves can be achieved by the use of a polarized aerial system as described by Phillips (1951).

(b) Dispersion

Since a pulse of radio waves consists of a complete spectrum of frequencies centred on the wave frequency, the dispersive properties of the transmitter, the ionosphere and the receiver will result in the distortion of the pulse. This distortion has been discussed in detail by Budden (1961) and is overcome in the present experiment by employing a pulse width sufficient to render the amplitude of the echo independent of the pulse shape.

(c) Spatial Attenuation

Breit and Tuve (1925) have shown that, when the inverse square law is applied to the passage of a radio pulse through the ionosphere, the amplitude of the wave varies inversely as the apparent path length, h' in the case of vertical incidence. This is not strictly applicable in the presence of a magnetic field but the departure is considered to be small in practice.

(d) Partial reflection

The path of a radio pulse to its reflection height may be interrupted by dense clouds of ionisation which give simultaneous reflections from a lower level. Thus the division of the wave energy by partial reflections from sporadic E clouds render accurate measurements of absorption impossible.

(e) Fading

The fading of the echo amplitude due to the superposition of two pulses has been discussed above. However fading may also result from random perturbations and drifts in the reflecting strata when only a single echo is present. This phenomenon exhibits the same fading patterns as the random noise which possess two independent fading rates, fast fading with a quasi period of 1 to 10 secs and slow fading with a period 5-15 minutes. These effects may be eliminated by suitable sampling techniques.

5.1.4. Sampling

Fading phenomena have been studied statistically by McNicol (1949) and the sampling techniques employed to

eliminate them have been discussed in detail by Beynon and Davies (1954) and Piggott, Beynon, Brown and Little (1957). These authors have shown that in practice the minimum sample, giving reasonable minimization of fading and sampling errors, is one incorporating twenty independent observations. Since the recorded signal amplitudes show a correlation over time intervals comparable with the fading period only a limited number of independent observations can be obtained from a continuous record. In the case of fast fading the quasi-period is generally 2-6 secs thus giving between ten and thirty independent observations per minute and in consequence a sampling error of the order of 10% in the output of an automatic integrator operating for one minute. The aim of the present study was to observe changes in absorption having a period similar to that for slow fading. Therefore the effect of fast fading was minimized by the automatic integration technique and five minute running means of the integrated output were employed, following the recommendations made by Piggott (1953) for the study of slow fading.

5.2. Virtual height

5.2.1. Principle of measurements

The virtual height of reflection has been defined by the expression

$$h' = \frac{1}{2} c \tau$$

in which τ is the time taken to travel from the ground to the ionospheric reflection level and back to the ground. The measurement of this short time interval in terms of the displacement of the echo pulse from the ground pulse on an A or

B scan display (figure 4.1.1.) thus constitutes a measurement of the virtual or group height.

5.2.2. Distortion

The distortion of the pulse shape, by virtue of the dispersive effects of the equipment and the ionosphere, plays an important part in determining the accuracy to which the virtual height can be estimated. Lyon and Moorat (1956) have discussed the effects of this distortion and have found by observation that the output pulse may be represented by a pulse whose leading and trailing edges have constant rise times. Figure 5.2.1. illustrates such a pulse and an arbitrary threshold level for the equipment. It can be seen that a noticeable overestimation of the virtual height will be made if the effects of distortion are not accounted for. This can be achieved by applying the correction technique described by Lyon and Moorat and discussed in the following section.

5.2.3. Lyon and Moorat Correction

In addition to the distortion error mentioned above a small delay is experienced in pulse transmitters between the triggering of the modulation pulse and the appearance of the radio pulse on the aerials thus introducing a further error of the order of 2 km into the estimation of h' . Lyon and Moorat (1956) have shown that the total error in h' may be expressed in the form

$$\Delta = a - bw$$

where w is the width of the recorded echo and the coefficients a and b may vary with frequency and from one

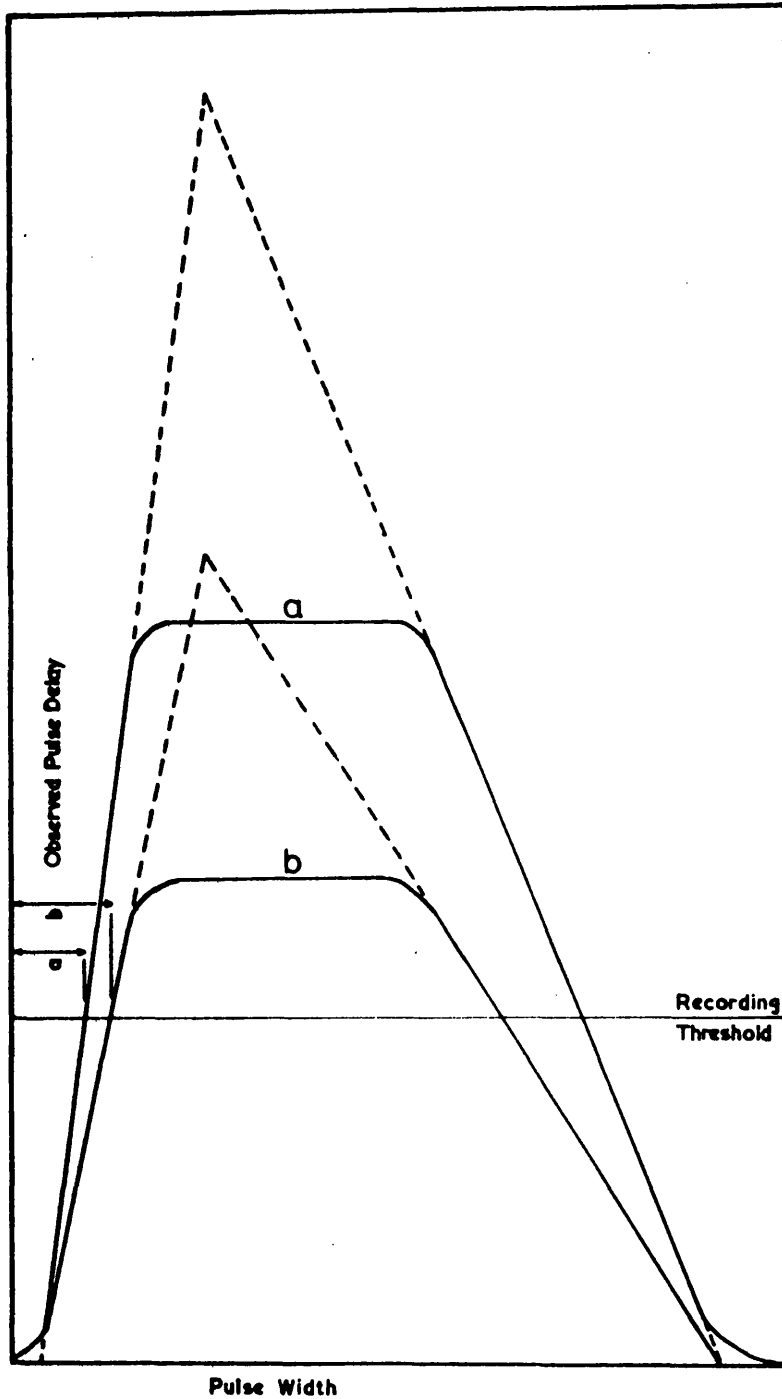


FIG.5.2.1 Equivalent pulse shape indicating the dependence of pulse delay on the pulse width at the recording threshold level.

instrument to another. These authors have described an experiment to measure the coefficients a and b when the ionospheric distortion is neglected, and claim an accuracy of ± 2 km in the adjusted E region virtual heights. The representation of the above expression on a transparent overlay allows the correction to be made directly during the scaling of ionograms and this has been done throughout this study.

Chapter 6

Experimental Studies

6.1. Equipment

6.1.1. Radio Ionosonde

Clarke and Shearman (1953) have described in detail ionospheric sounding equipment which produces a photographic record of virtual height against frequency in the range 0.65 to 25 MHz. A commonly produced version of this instrument, the Union Radio Ionosonde Mark II, has been used in Leicester throughout the present study.

A schematic diagram of this equipment is presented in figure 6.1 and a typical record has been included in figure 4.1.1. The transmitter, which covers the frequency band in five stepped ranges, consists of a pulse modulated master oscillator coupled to an aperiodic power amplifier. The receiver is of the superheterodyne type and is tuned separately from the transmitter, synchronisation being maintained by a frequency sensitive servo-system. The 1 MHz and 100 kHz frequency markings presented on the record are derived from a 1 MHz crystal oscillator by frequency division and harmonic selection within the receiver. The crystal output is further divided to give narrow 3 kHz pulses which, when superimposed upon the B scan display, correspond to height markings at 50 km intervals. Finally a 60 Hz supply is derived upon which the master clock is operated.

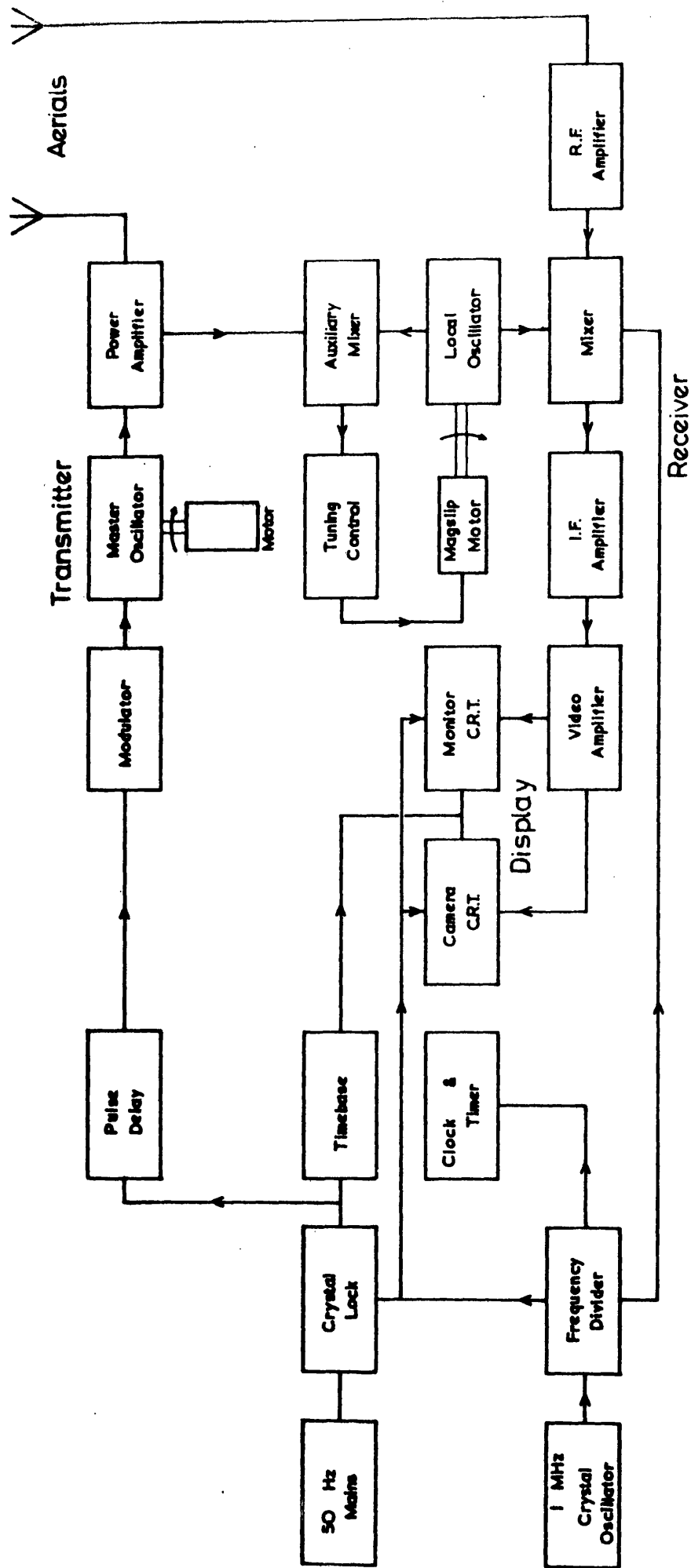


FIG. 6.1 Schematic diagram of the Union Radio Ionosonde Mk. II

The pulse repetition frequency of this instrument is approximately 50 Hz, the transmitter modulating pulse being locked to the 3 kHz height markers. A transmitted pulse width of $200\ \mu\text{sec}$ was used throughout the study and the power supplied to the aerial was approximately 1 kw in the frequency range employed, 1.5 to 7 MHz. The aerial system (figure 6.2.) was switched at 3.2 MHz, the lower frequencies being transmitted from a delta aerial loaded at its apex with $600\ \Omega$, and the higher frequencies from a vertical rhombic again top loaded with $600\ \Omega$. A similar aerial array, close to the first and in a parallel plane, was used for receiving, and balanced transformers were used to match the $75\ \Omega$ input impedance of the receiver to the aerial impedance of $600\ \Omega$. The radio frequency stages of the receiver were adjusted to give a constant response with frequency in two ranges 1.5-3.2 MHz and 3.2-7 MHz, and the receiver was tuned so that an input signal of $1\ \mu\text{v}$ gave 2 cm deflection of the trace on the A scan (figure 4.1.1) monitor at maximum gain. The display time base was arranged such that a virtual height of 500 km was recorded across the camera film and provision was made to enable the instrument to be switched automatically between routine and continuous running during predetermined periods of the day.

6.1.2. A1 absorption equipment

The A1 absorption experiment was arranged so that a very steep path was monitored following the practice of early workers (Appleton and Builder 1932). The transmitting station was located 12 km from the receiver and the azimuth of the path was $73^{\circ} 30'$ east of magnetic north thus giving an angle of incidence in the E region of approximately $3^{\circ} 30'$.

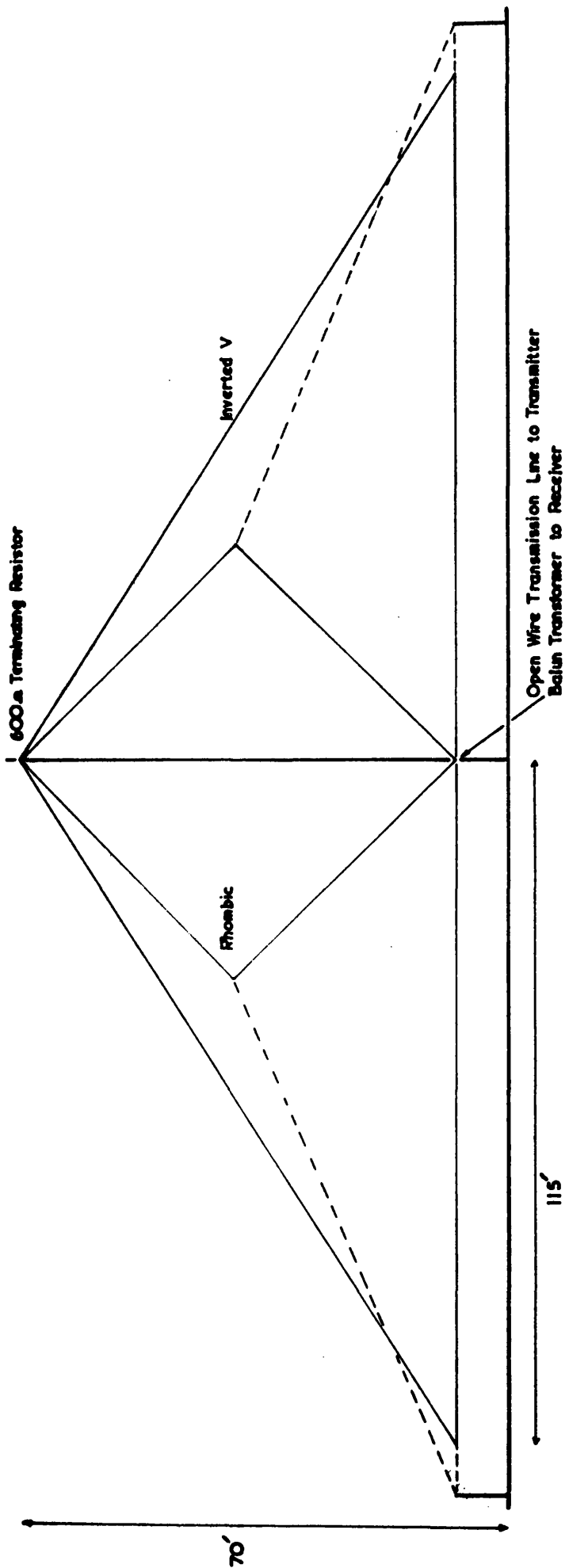


FIG. 6.2 Schematic representation of Rhombic and Inverted V aerial systems.

The propagation conditions along this path were compared with those at vertical incidence for a single ionospheric model by computing the absorption and virtual height at 2 MHz by the Jones (1966) ray tracing programme. The discrepancy was found to be 300 meters in the virtual height and 0.016 dB in absorption representing an error of less than 0.2% in each case. This error may be neglected in view of the larger errors discussed in the previous chapter and this 12 km path can be approximated to vertical incidence propagation.

(a) Transmitter

Diagrams 1, 2 and 3 present the circuits employed in the construction of the pulse transmitter used throughout this study. A crystal controlled Pierce Miller oscillator was arranged to give maximum output of the fundamental frequency. This continuous signal was then amplified by a tuned pentode amplifier stage (diagram 1) and the resulting 700 v peak to peak signal was applied to the push-pull amplifier stage, V_5 and V_6 (diagram 2), through the transformer T_1 . This second amplification stage was operated in class C by superimposing the oscillator r.f. signal on to a modulation pulse, 180 μ secs wide, drawn from the mains locked modulator (diagram 3) and amplified and inverted by the valves V_3 and V_4 . The output from the tuned anodes of this stage was applied to a wide band power amplification stage by means of a matching transformer, T_2 . This final stage consisted of a push-pull amplifier operated in class C and was matched to the 600 Ω aerial by means of a further matching transformer T_3 . The power supplied by this equipment in a 180 μ sec pulse was estimated to be

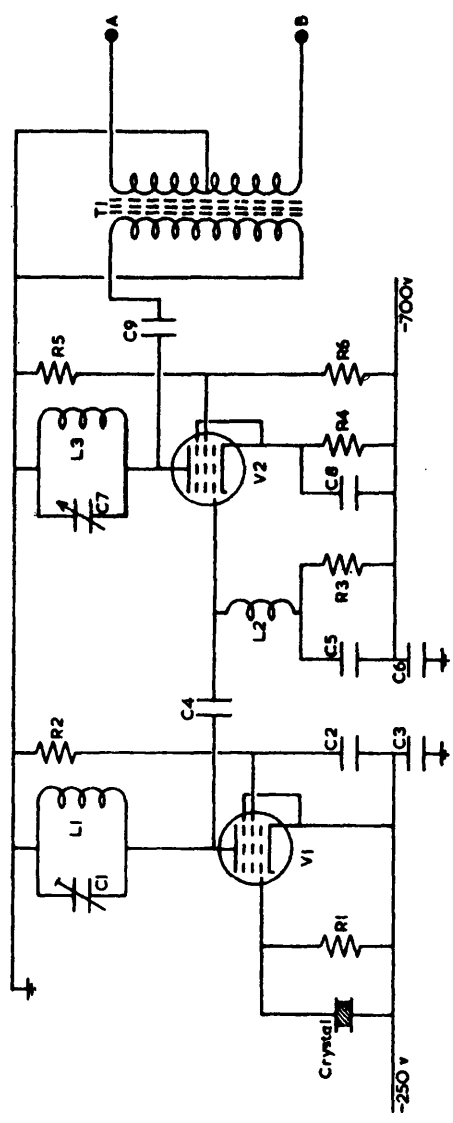


Diagram 1 Transmitter Oscillator

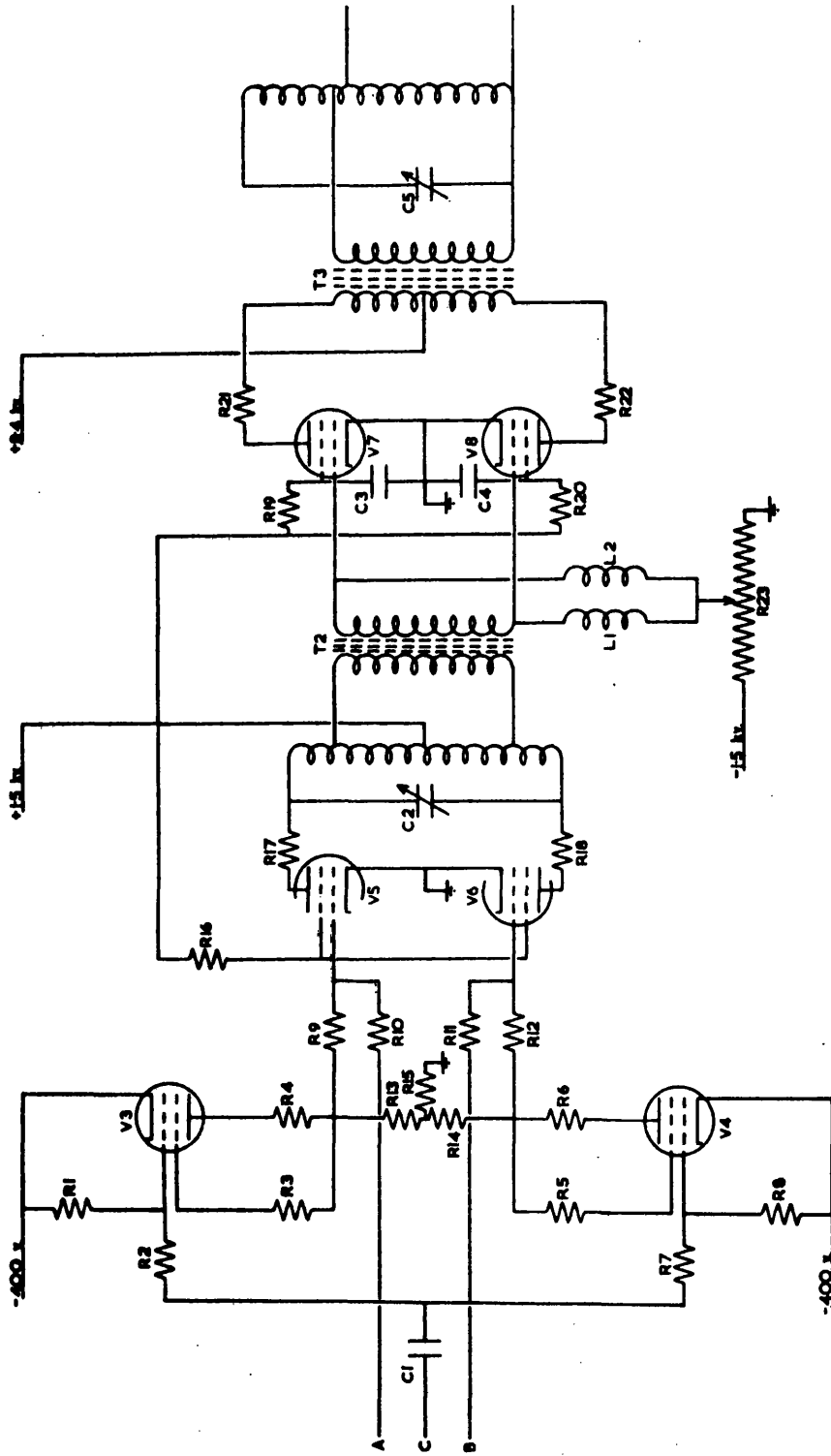


Diagram 2 Transmitter Power Amplifier

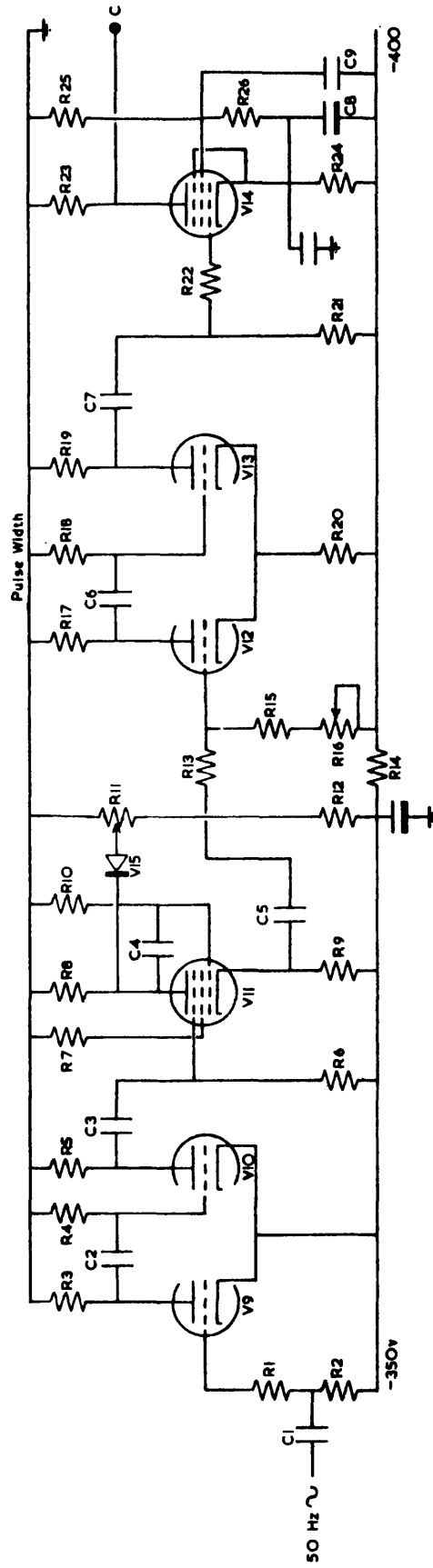


Diagram 3 Transmitter Modulator

approximately 5 kw and the peak to peak voltage to be 14 kv.

(b) Receiver

The receiver used in this work was a Marconi C52 remote receiver with the intermediate frequency and detector stages modified for pulse reception. The standard 470 kHz i.f. transformers were replaced by similar transformers in which the coil spacing had been reduced to 6 mm thus giving a receiver bandwidth of 20 kHz at the 3 dB point. The two i.f. amplification valves (ARP 3) were replaced by constant μ valves (EF 80) and the cathode by-pass capacitors and all decoupling capacitors were changed to facilitate pulse reception. In addition the detector stage was modified using a solid state diode (OA 81) and the time constant of this circuit was arranged to be 12μ sec. In order to ensure gain stability the receiver was operated from a stabilized power supply and provision for further stabilization of the screen grid supply was made.

(c) Monitoring System

The monitoring systems employed in the measurement of the absorption and virtual height were developed from those described by Madden (1967) and are illustrated in the schematic diagram of figure 6.3. The measurement of the echo amplitude is achieved by means of a gated amplifier in which the strobe is automatically locked to the echo pulse. By this arrangement the echo pulse present in the receiver video output is used to produce the strobe for the amplifier, thus any change in the virtual height of the pulse is overcome by an

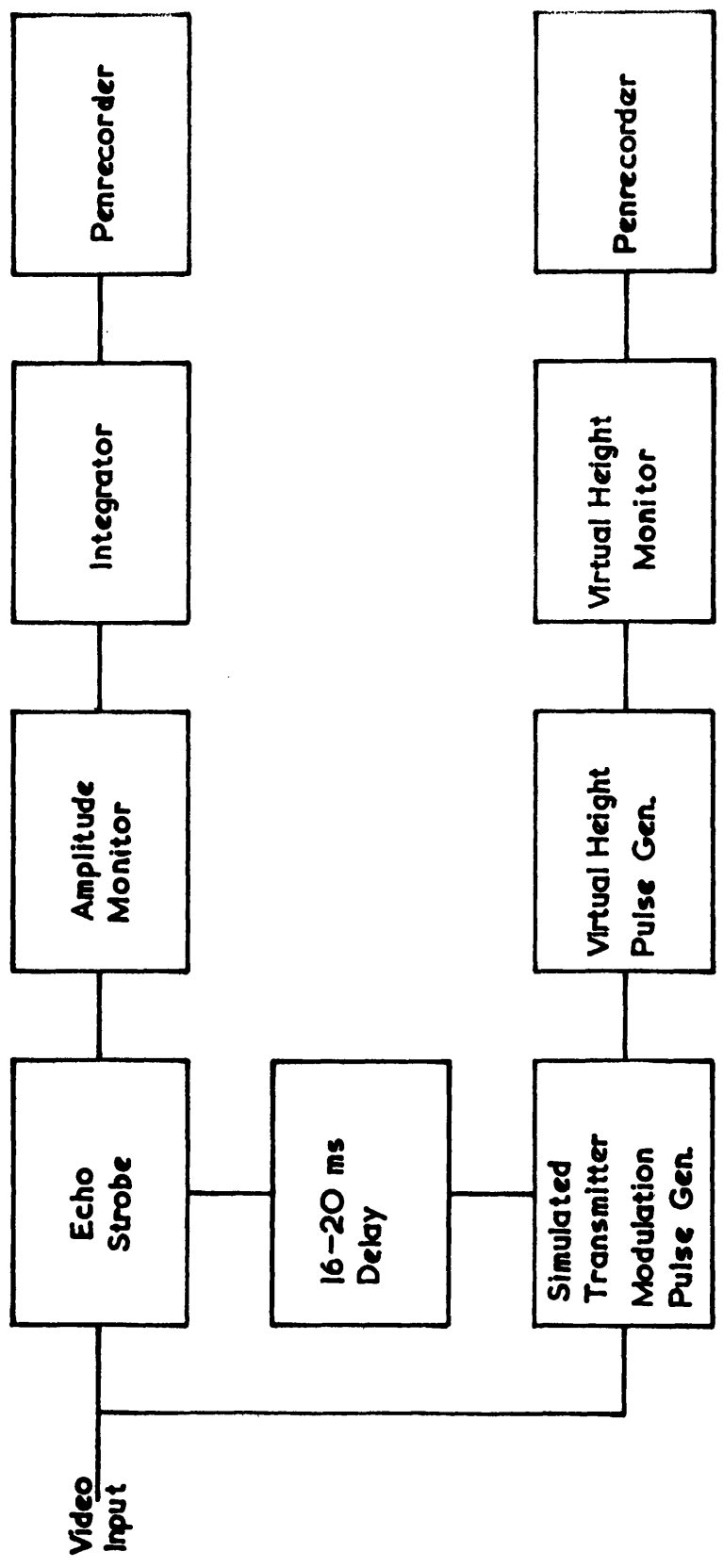


FIG. 6.3. Schematic diagram of the amplitude and virtual height monitoring system.

equivalent movement of the strobe. The arrangement of the transmitting and receiving sites 12 km apart has necessitated the modification of the initial triggering circuits since the direct input of the transmitter modulation pulse was not possible. The nominal 50 Hz mains frequency varied between the sites, and the circuits illustrated in diagram 4 were designed to provide a simulated transmitter modulation pulse from the receiver video output.

A mains locked trigger pulse of variable phase was obtained from the phantastron circuit of V_3 (diagram 4) and was used to produce a wide positive going pulse (~ 1 msec) in the monostable constituted by valves V_4 and V_5 . The arrangement of valves V_6 and V_7 has been taken from Madden (1967) and leads to the selection of the ground pulse which is reformed in valves V_8 and V_9 and output as a trigger pulse at point A. The circuits illustrated in the lower portion of the diagram have again been taken from Madden and are used for the selection of the echo pulse, this being output at B. The output pulses at A and B are compared directly by the Madden Virtual height recorder and the resulting output is fed to a pen recorder. The trigger pulse at A is further delayed in the circuit of V_{20} and V_{21} by almost 20 msec and forms the simulated transmitter modulation pulse for the absorption monitor in the next cycle of the mains voltage. Thus the echo is maintained on the narrow strobe of this monitor throughout the observing period. The output from the monitor was integrated by means of a Philbrick operational amplifier, P65AU charging a $16 \mu\text{F}$ capacitor. The integration was carried out over 50 secs and the accumulated voltage was then allowed to operate a pen recorder. The capacitor was finally

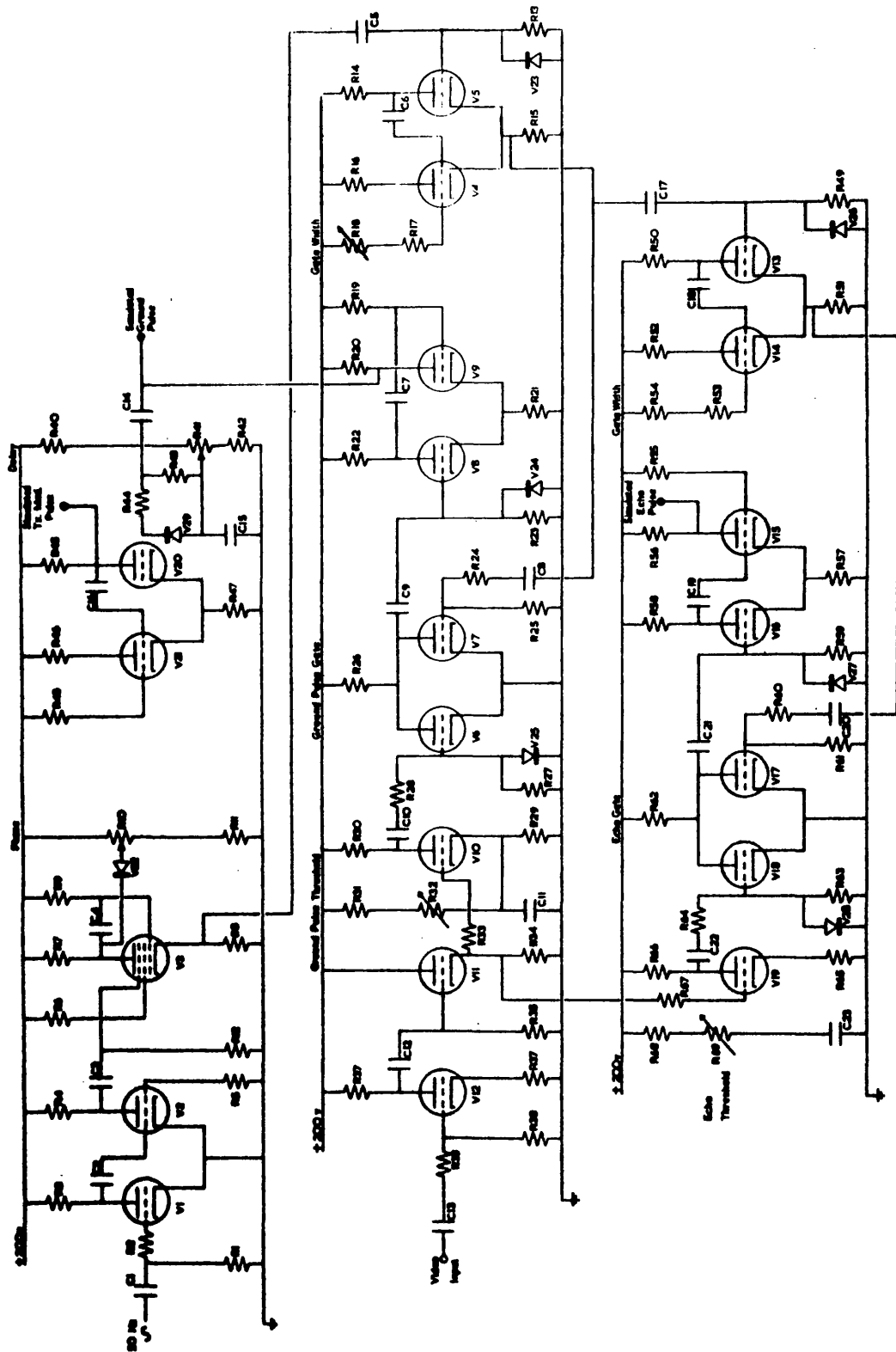


Diagram 4 Modified strobe unit for absorption and virtual height monitors.

shorted out before a further 1 minute cycle was begun.

In addition to the electrical measurement of virtual height the video output of the receiver was used to produce a B scan display which was photographically recorded during the observing periods. A typical record, taken when the observing frequency was close to f_oE , is shown in figure 6.4.

(d) Aerials

At both the transmitting and receiving sites halfwave folded dipoles loaded with 600Ω at the centre were employed. These aerials were approximately 75 m in length and suspended 10 m above the ground. The transmitting aerial was fed by a transmission line and the receiving aerial was matched to the 75Ω input of the receiver by a ^{-unbalance} balance transformer. In order to increase the suppression of the ground pulse the aerials were arranged to be perpendicular to one another.

6.2. Observations

6.2.1. Ionospheric Soundings

Routine hourly soundings of the ionosphere have been made since June 1966 of the frequency range 1.5 to 7.0 MHz to a maximum virtual height of 500 km. In addition on 20 days between January and June 1969 this frequency range has been sounded continuously between ground sunrise and noon thus giving an ionogram record every 3 minutes during this time. The correction technique described by Lyon and Moorat (1956) discussed in Chapter 5 has been applied in the scaling of these records giving virtual height data to an accuracy of ± 2 kms.

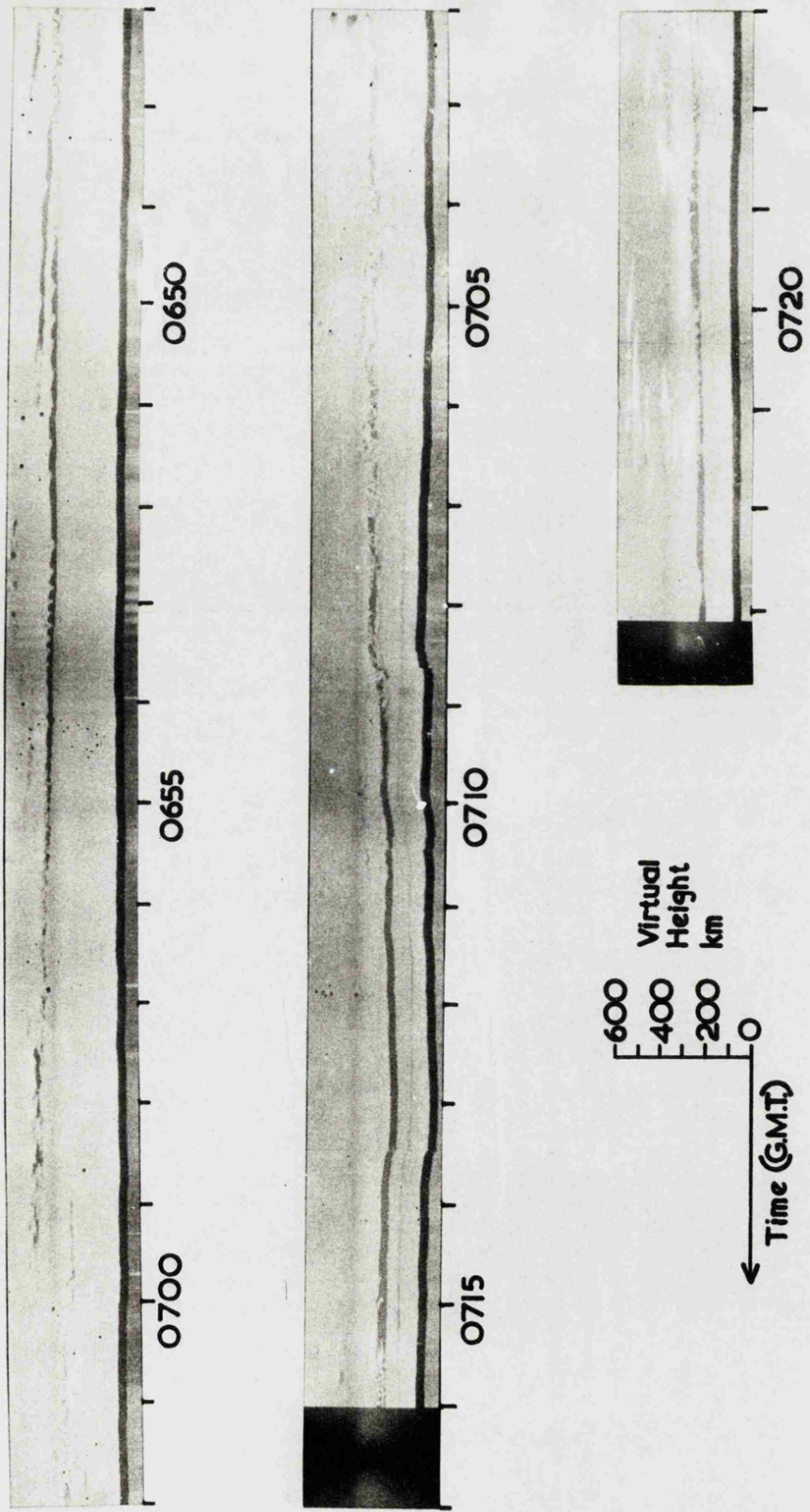


FIG. 6.4 Typical Photographic $h'(t)$ record (14th March 1969)

6.2.2. Absorption Measurements

The steep propagation path, described in an earlier section, and the perpendicular arrangement of the folded dipole aeriials diminish the ground wave signal so that the recorded ground pulse is comparable in amplitude to the night-time reflections. Hence it is unnecessary to desensitise the receiver during reception of the ground wave and the ground pulse can be monitored directly at any time as a check upon the gain stability of the system.

Observations of absorption and virtual height were made on a number of days each week between February and June 1969 from a time shortly before ground sunrise until noon. The operating frequency was 2.05 MHz for measurements made before the 15th April and was then changed to 2.266 MHz for the remaining observations. The receiver gain was measured periodically and ionospheric calibrations were carried out at regular intervals throughout the period. Such calibrations were made during the early morning hours using both F region and Es reflections and the calibration constants derived were found to be compatible. Absorption values in dBs were obtained by computer analysis of the integrated amplitude output produced each minute by the monitoring system. A further facility of this data analysis was the provision for the calculation of 5 and 15 minute running means of absorption.

6.2.3. Virtual Height

Measurements of virtual height were made continuously as an integral part of the absorption observation of 2.05 MHz and later on 2.266 MHz employing both the electronic monitor

and the photographic records discussed earlier. The sensitivity of the electronic monitor was found to be poor and subject to interference from broadcast and local noise which did not disrupt the photographic records to the same extent. Consequently the electronic monitor was used in a qualitative manner to assist in the interpretation of the photographic records.

The photographic records were calibrated at regular intervals against the 3 KHz output of a square wave generator and were scaled each minute throughout the observing period. In the scaling procedure a modified Lyon and Moorat (1956) correction technique was employed to account for the time of flight of the ground pulse in addition to the normal sounding errors already discussed.

Initial observations of both amplitude and virtual height were made on a night of strong sporadic E reflections and the resulting records were analysed by the following procedure. When the amplitude of the first and second Es reflections were equal, the delay between them was taken to be a measure of the true virtual height. A time at which the first echo and the ground pulse have equal amplitude was then considered and the assumption was made that the virtual height of the Es reflection remained constant throughout the observation period, approximately one hour. The virtual height indicated by these two pulses is less than the true virtual height by an amount h_p (figure 6.5) which is a measure of the time of flight of the ground pulse over 12 km and the ground pulse distortion at a particular receiver gain setting. During the observation the width, w_0 , and amplitude of the

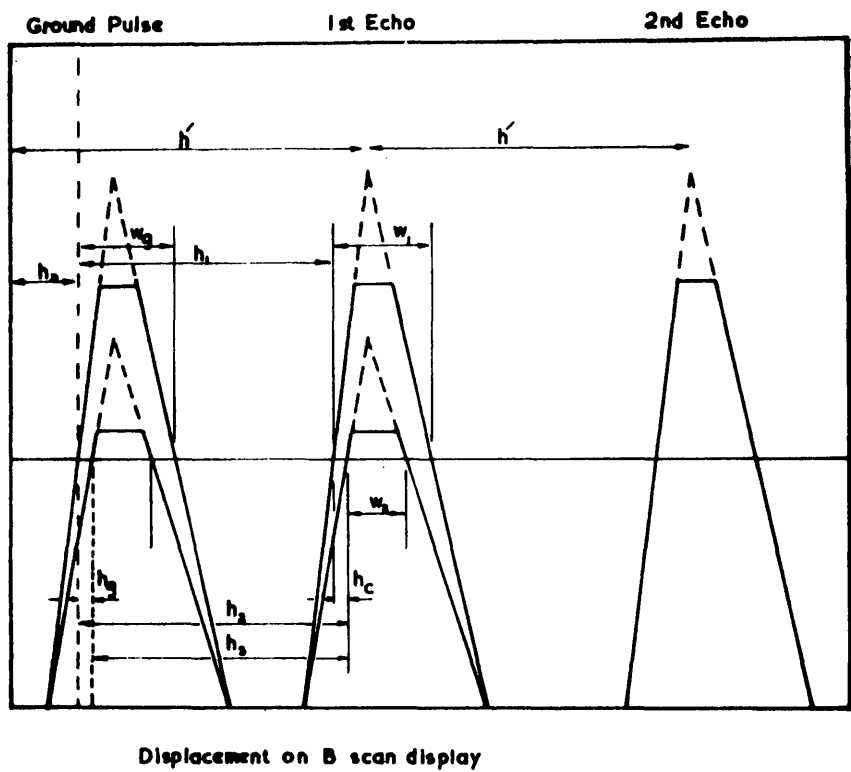


FIG. 6.5 The effect of pulse distortion and ground pulse delay on virtual height measurements on a steep incidence path.

ground pulse remained constant and the difference between the 'true' virtual height, h' , and the recorded height plus h_p was plotted against the echo width, w . This difference constitutes the echo distortion correction, h_c , and may be represented as a function of echo width on a transparent overlay for routine scaling. h_c will have positive values when the apparent echo pulse width is greater than that of the ground pulse. The additional error, introduced when the receiver gain was changed, was accounted for by assuming that the distortion of the ground pulse took the same form as that of the echo and correction values, h_g , were obtained for each attenuator setting. The correction h_g will have a negative value for gain settings above that at which the correction curve for h_c was constructed. Thus the fully corrected value for the virtual height will be given by the expression

$$h' = h_s - h_c + h_g + h_p$$

in which h_g and h_p are constants and h_c can be obtained from the echo width by the overlay scaling grid technique.

Chapter 7

The post-sunrise changes in the virtual height- frequency variation

7.1. Introduction

The virtual height of reflection and the absorption of radio wave pulses, observed by means of the techniques described in Chapter 6, will now be discussed in some detail. This chapter is devoted exclusively to the variation of virtual height with frequency and the discussion of the simultaneous virtual height and absorption data observed on a single fixed frequency will constitute Chapter 8.

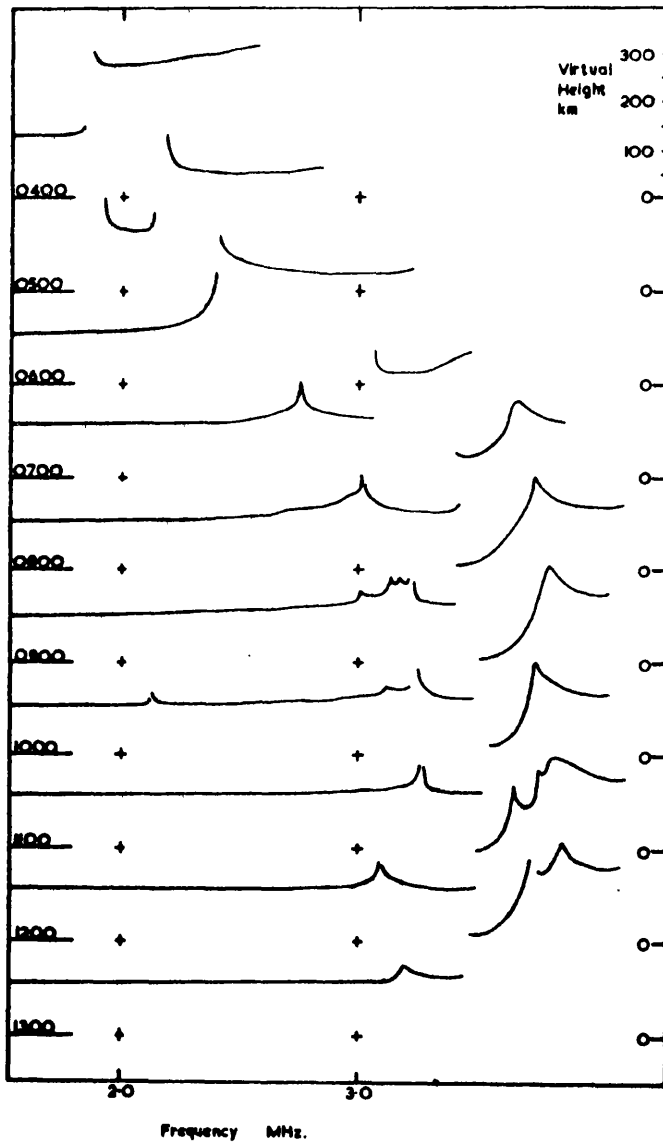
Following the work of Halliday (1936), many workers have commented upon the complexities observed near the E layer critical frequency on ionograms recorded at temperate latitudes and several attempts have been made to set down rules by which this critical frequency might be recognised and hence reliably tabulated (Becker and Dieminger 1950, Beynon and Brown 1959, Piggott and Rawer 1961). A synoptic study of this fine structure has been undertaken with special reference to the growth of the E layer peak and the E-F transition region following the sunrise. A theoretical study of these conditions made by Bourne, Setty and Smith (1964) will be related to two independent experimental observations of the electron density distribution with height. These are (a) the profiles computed from virtual height data recorded at Leicester and (b) the profiles measured by Taylor (1969) at the

Royal Radar Establishment, Malvern, by a Thomson scatter experiment. The latter group of profiles will be referred to as the Thomson scatter profiles in the following chapters.

7.2. Occurrence of Fine Structure on Ionograms

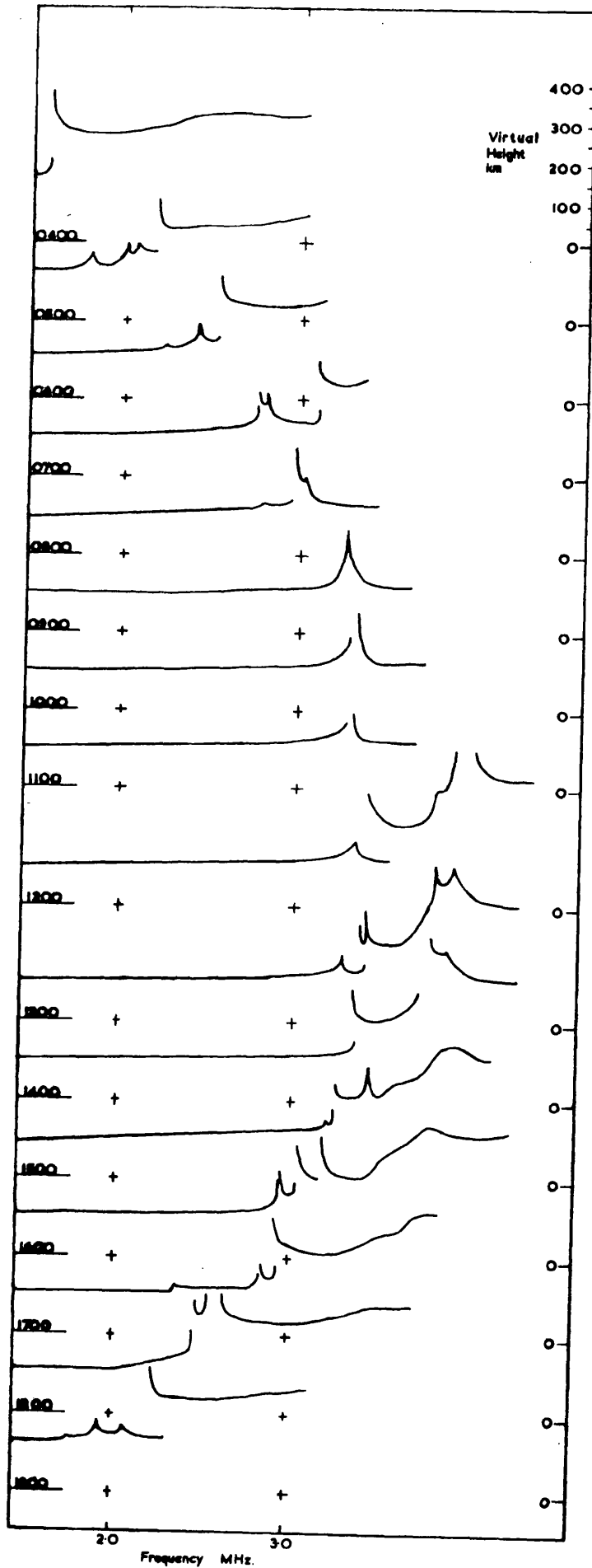
Figure 7.2.1. represents a number of typical ionograms recorded at Leicester between June 1966 and May 1967. All these records show one or more regions of high group retardation which are commonly referred to as cusps (Piggott and Rawer 1961) and which may be associated with irregularities in the electron density profile. The section of the record separating two of these cusps will be referred to as an intermediate trace and this may possibly represent an intermediate layer. Thus on a typical daytime ionogram in the absence of sporadic E, the trace at the lowest frequencies recorded will represent E region reflections and the trace will be terminated by a cusp. This cusp may be followed, as the frequency is increased, by the F region trace if only one cusp is present or by a series of intermediate traces separated by cusps. The presence of several cusps and intermediate traces, collectively called fine structure, has been observed as a regular feature on the Leicester ionograms, being most common in the early morning and late afternoon.

In order to assess the extent of the fine structure a qualitative scale 0-3 was devised to grade each half day throughout the period. This activity scale is illustrated in figure 7.2.1. In estimating the activity, records displaying strong Es were discarded as were days on which Es was predominant for an appreciable part of the day. This procedure



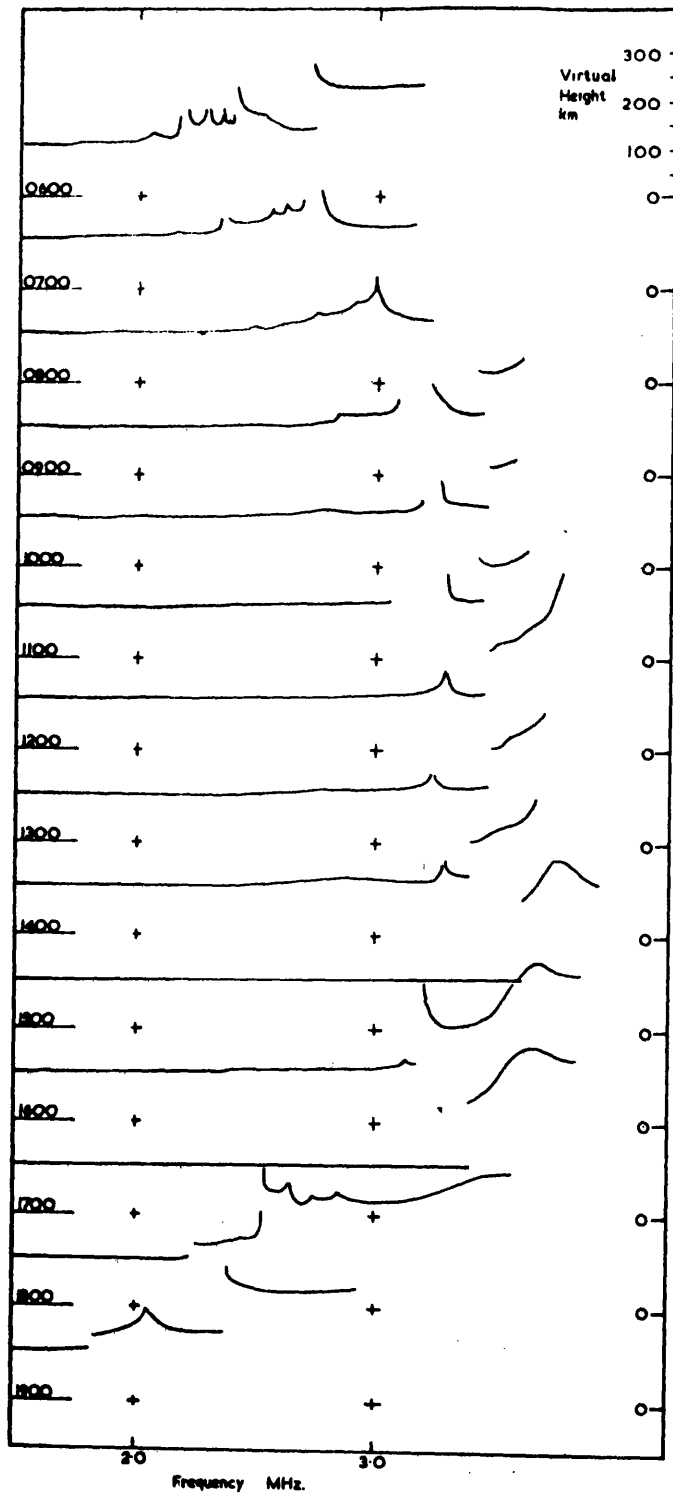
(a) 4.666 Activity No. $\frac{1}{2}$ pre-noon
 $\frac{1}{2}$ afternoon

FIG.7.2.1 Typical sequences of hourly ionograms representing summer, equinox and winter conditions as observed at Leicester.



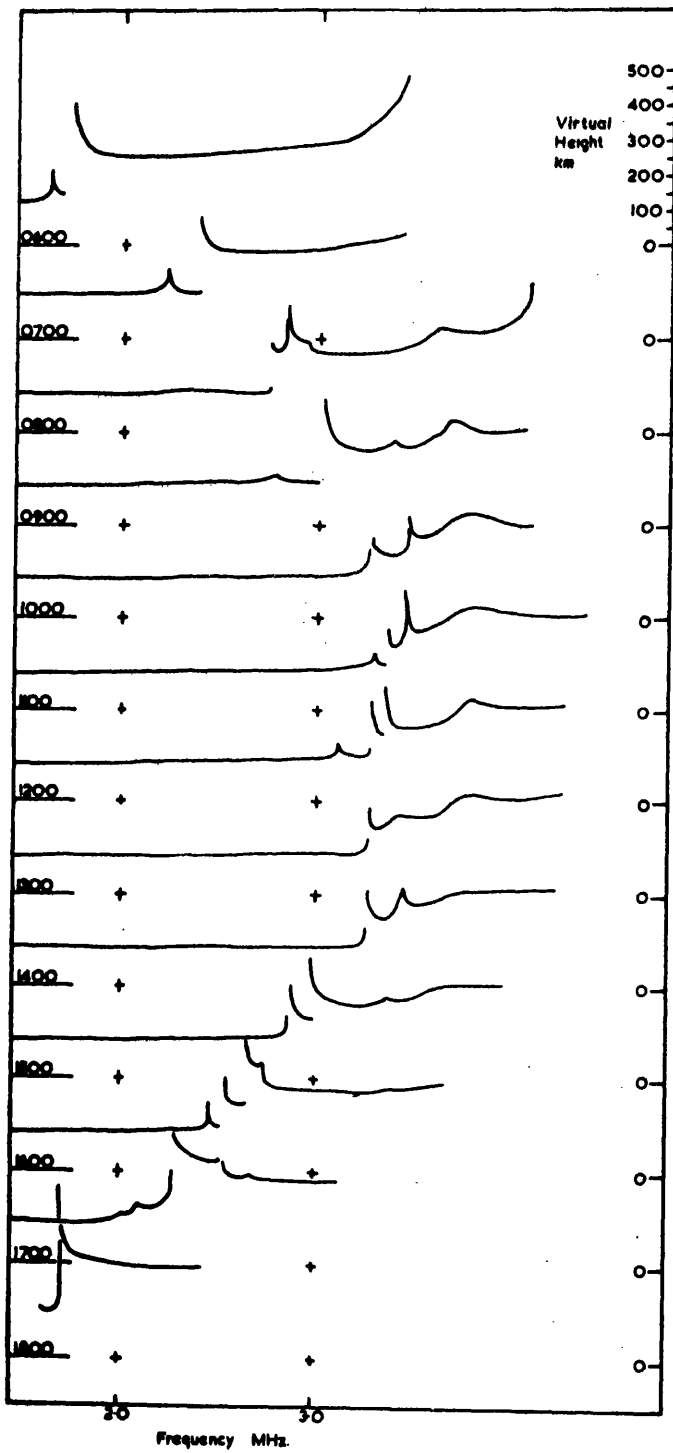
(b) 8.6.66

Activity No. | pre-noon
| afternoon



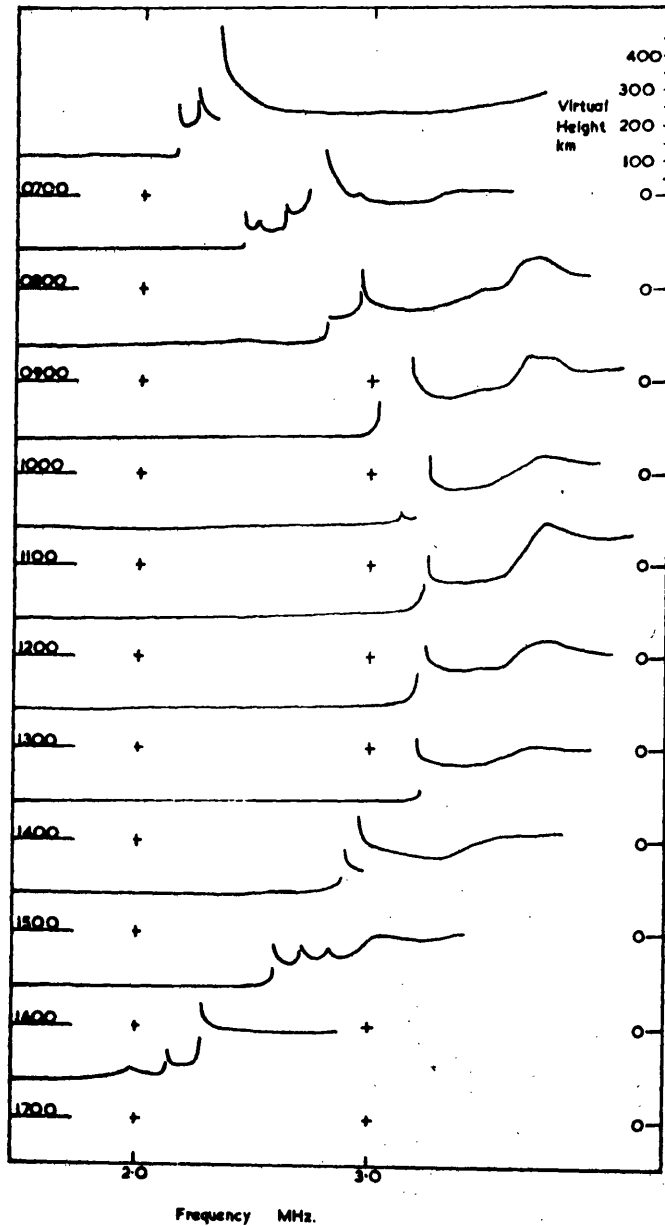
(c) 22.6.66

Activity No. 1 pre-noon
 1/2 afternoon



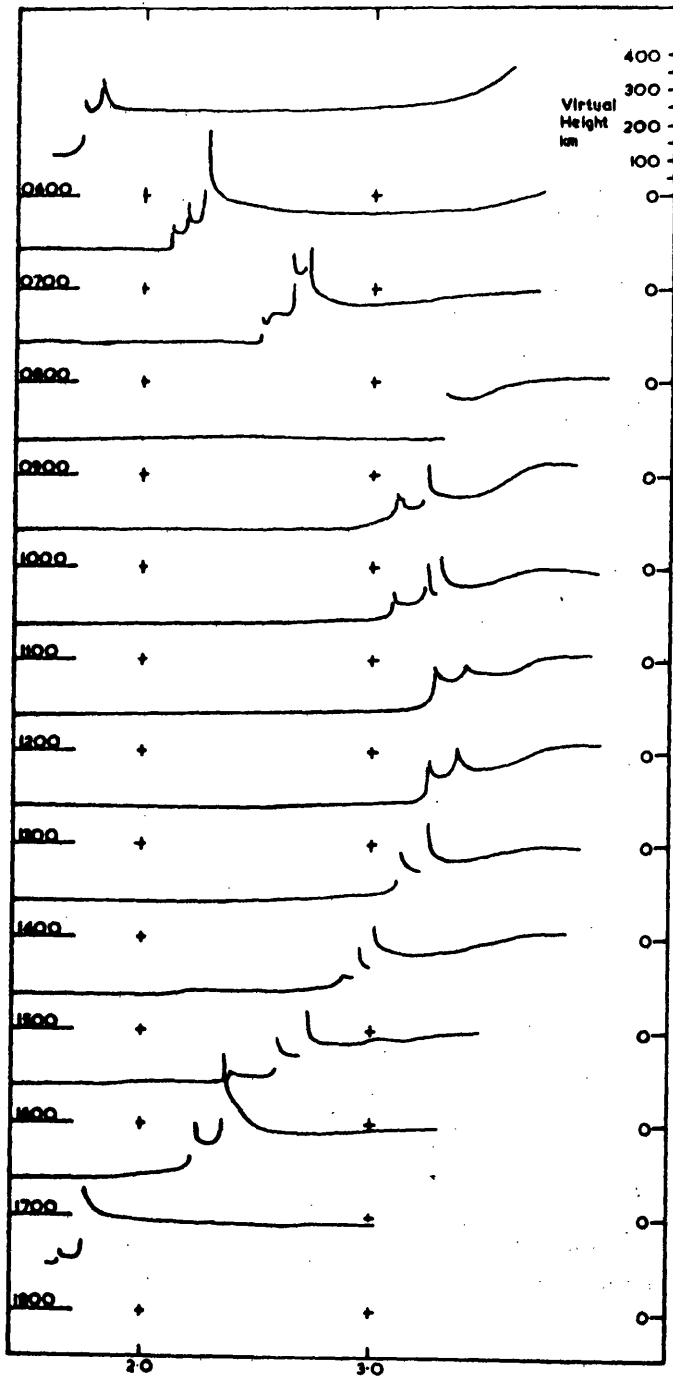
(c) 14.9.66

Activity No. 1/2 pre-noon
1 afternoon



(e) 15.966

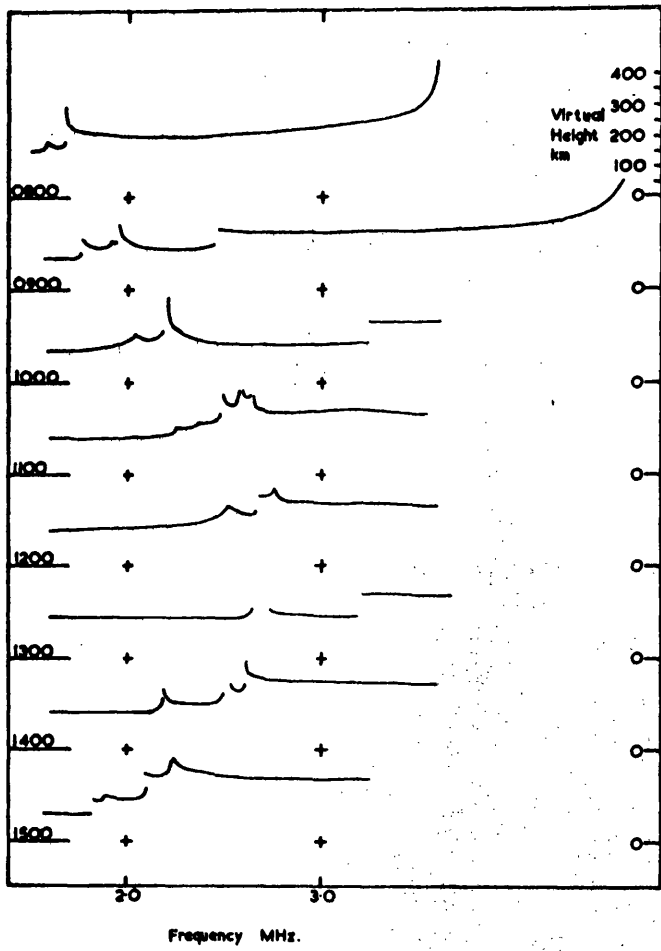
Activity No. 1 pre-noon
1/2 afternoon



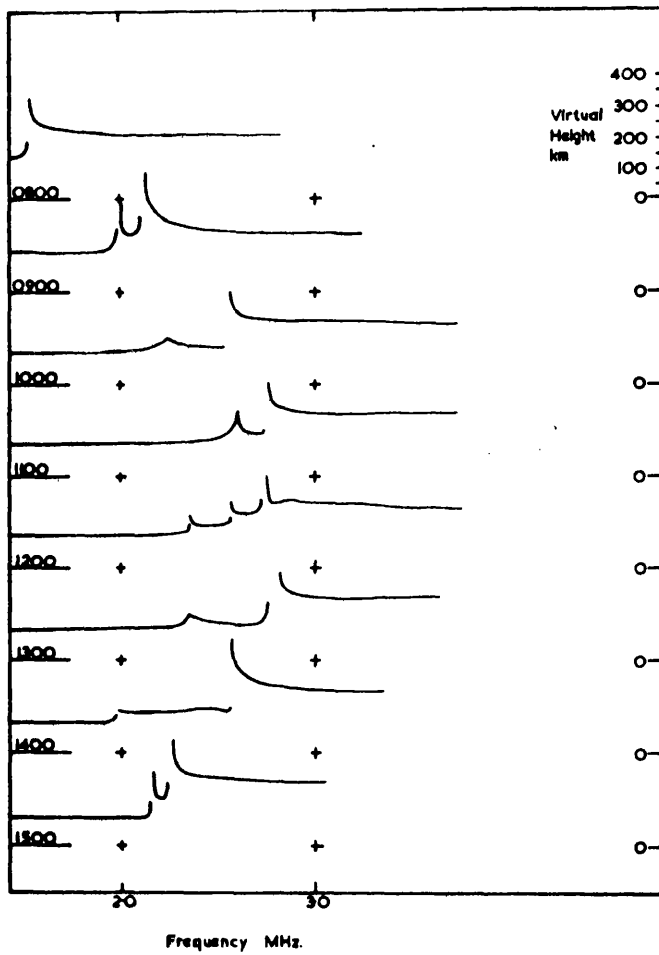
Frequency MHz.

(f) 16.966

Activity No $\frac{1}{2}$ prenoon
 $\frac{1}{2}$ afternoon

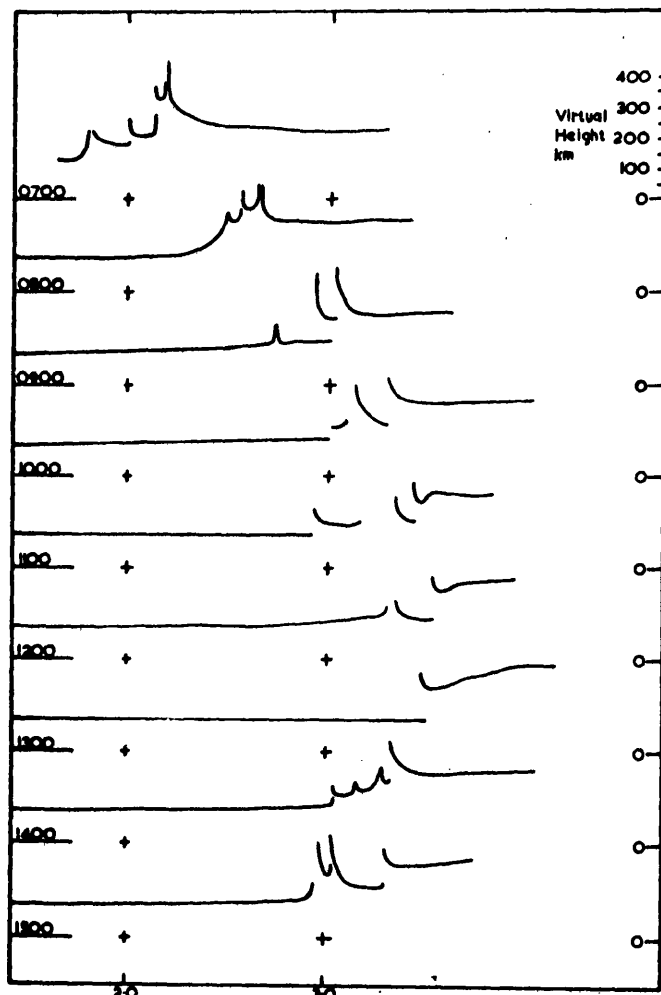


(g) 30.12.66 Activity No. 1/2 pre-noon
 1 afternoon



(7) 4.1.67

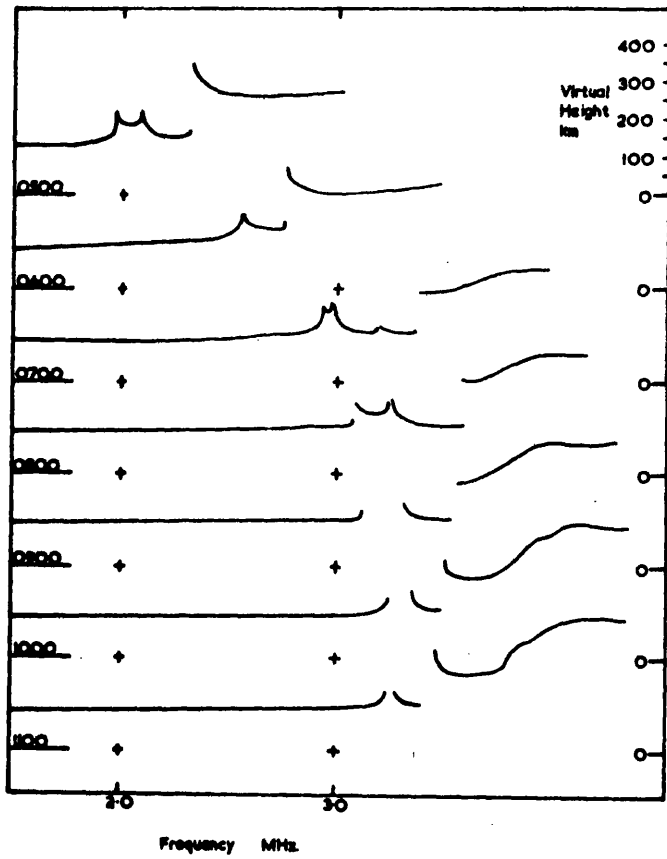
Activity No. - 1/2 pre-noon
- 1/2 afternoon



Frequency MHz.

(1) 16.3.67

Activity No. 1 pre-noon
 1 afternoon



(j) **215.67** Activity No. - 1/2 pre-noon

gave a sample of 151 prenoon and 181 afternoon periods, 131 days having an activity number for both periods. Of these days 55 showed equal activity before and after noon, while the number of days having greater activity in the morning or in the afternoon were 39 and 37 respectively. Although a large number of days showed equal activity in both periods it can be seen from figure 7.2.1. that the type of structure which occurs may differ greatly between the morning and the afternoon. As a further comparison, monthly mean activities were computed for both half days and have been plotted in figure 7.3.1. The activity was seen to be substantially the same for the prenoon and afternoon periods, the yearly means being 0.76 and 0.77 respectively. The number of hours for which fine structure was observed before and after noon has also been recorded and the means for the two periods taken for the year were found to be 2.9 and 2.6 hours respectively. Furthermore, on 24% of all days considered fine structure was present at noon.

The seasonal dependence of this phenomenon has been investigated by considering in more detail the results for the months of June and December 1966, March 1967 and January 1969. The various cusp frequencies and the minimum virtual heights of the intermediate traces were recorded. In addition the six most common cusp shapes were identified and are reproduced in figure 7.2.2. The distinguishing features of these cusps and the descriptive letters are listed in table 7.2.1.

The data for various times of the year presented in figure 7.2.1. indicates no marked difference in the fine structure pattern from season to season. This point has been

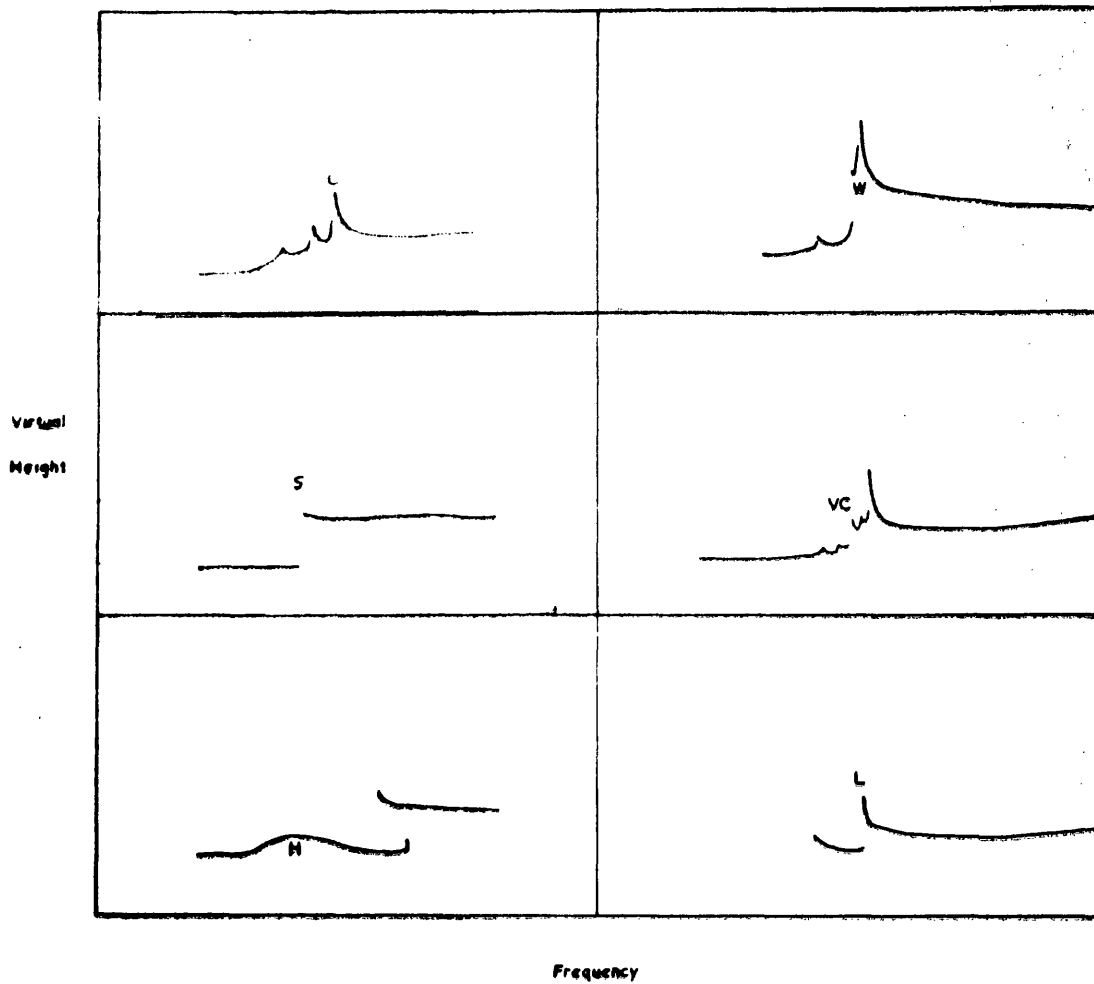


FIG. 7.2.2 Typical ionogram cusp shapes.

Descriptive Letter	Distinguishing Features
C	Symmetrical feature. Clearly defined discontinuity between regions of comparable group retardation.
S	No group retardation at the high frequency limit of the lower trace. Group retardation may be evident on the higher trace. Characteristic of Es.
H	Increased group retardation over a wide range of frequency without any discontinuity.
W	Rapid increase in group retardation of the upper and lower traces are displaced in frequency. A central trace may occur at a great height or may suffer large attenuation and hence remain undetected.
VC	A range of small cusps too closely spaced to be satisfactorily distinguished on the frequency scale.
L	Asymmetrical cusp. Little group retardation on the lower trace but normal retardation is evident on the upper trace. Characteristic of E2 echo described by Becker and Dieminger(1950)

Table 7.2.1 Descriptive Letters and Distinguishing Features of six typical Cusp Structures.

confirmed by the more extensive study of the selected months mentioned above. Table 7.2.2. presents the distribution figures for the various cusp types observed in each month. On average 2.04 cusps occurred on each ionogram recorded in summer compared with 1.95 at the equinox and 1.98 in winter. The cusp type S, which may be associated with the existence of sporadic E, was more common in summer, accounting for 22.4% of all cusps recorded, than in winter, when its contribution falls to 11.4%. No seasonal trend was evident in the other cusp types; the common C type giving 63% and the L type 13% of the structure throughout the year. The VC and W types may have larger occurrence percentages than those shown, but their recognition is strongly dependent upon the record quality.

Although the independence of morning and afternoon traces has been emphasised it has been noted that ionogram irregularities are sometimes long lived and can be traced throughout the day. For example, the ionograms for the 16th September 1966, illustrated in figure 7.2.1., show an intermediate trace which persisted from 0600 until 1800 hours. The changes in the shape of the cusp at the high frequency end of this trace are noticeable and variations of this type will be discussed later in this chapter. Further consideration of the data of figure 7.2.1. indicates that the upper and lower frequency limits of the cusp features appear to follow the zenith angle variation predicted by the Chapman theory. This observation has been confirmed by the detailed study of 20 days between January and June 1969 during which the ionosonde was run continuously throughout the morning giving an ionogram every three minutes. On these days the frequencies of all inflections and cusps appearing below the F_1 layer trace were

Cusp Type	Cusp Occurrence							
	June 1966		December 1966		March 1967		January 1969	
	number rec.	percent. total	number rec.	percent. total	number rec.	percent. total	number rec.	percent. total
C	232	55.6	129	66%	119	75%	63	57%
S	95	22.4	25	12.8	16	10	11	10
H	44	10.4	12	6	7	4.4	16	14
W	0		1		0		1	
VC	1		0		0		0	
L	51	12	26	13.3	16	10	19	17
Total cusp record	423		196		158		111	
Total Ionogram Sample	207		105		81		53	
Mean cusps per Ionogram	2.04		1.87		1.95		2.09	

Table 7.2.2 Cusp Occurrence for months representing different seasons.

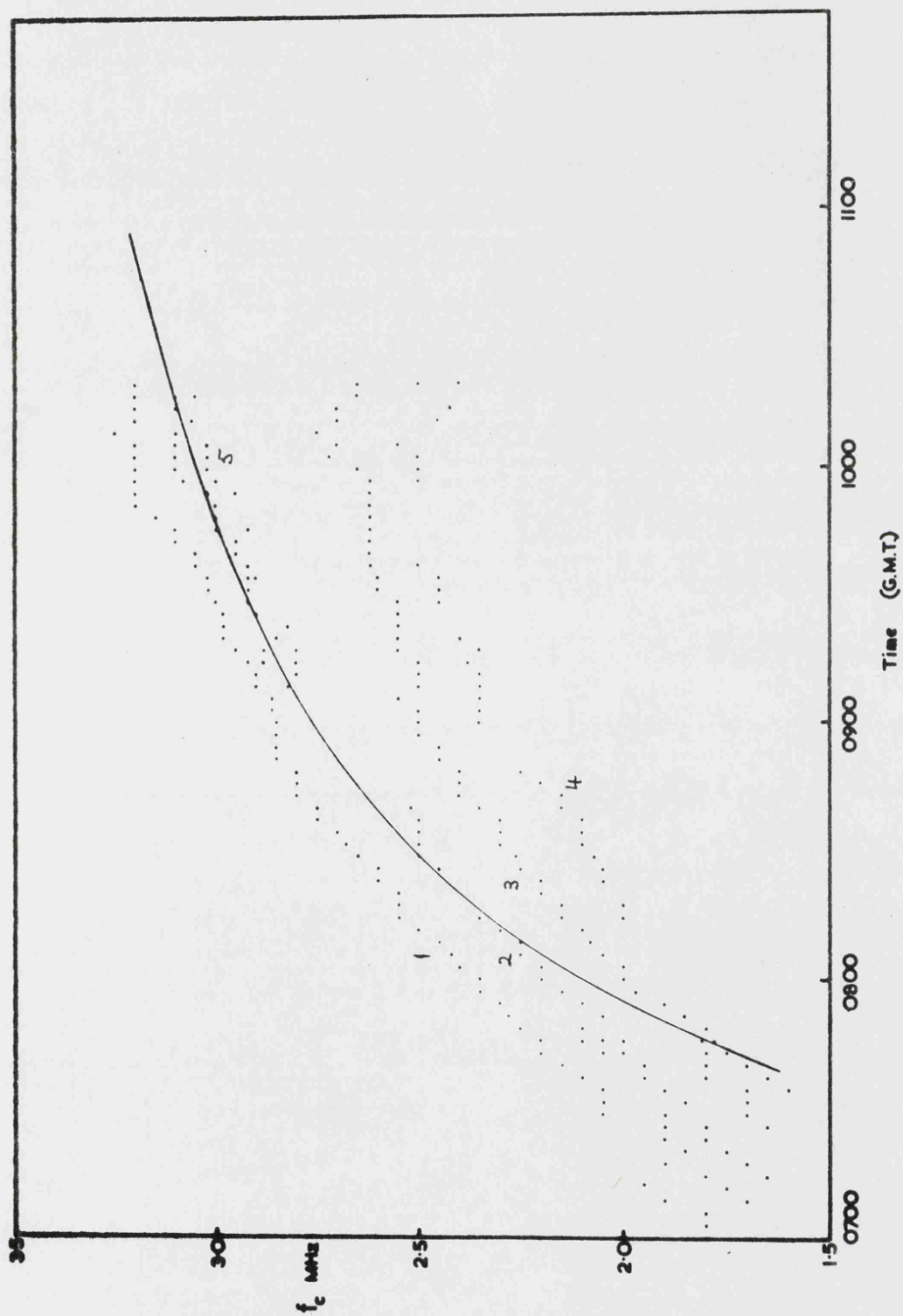


FIG. 7.2.3(a) Variation of cusp frequencies, f_c , with time for 26.2.69 ($f_o F_{2min}$ 3.4MHz)

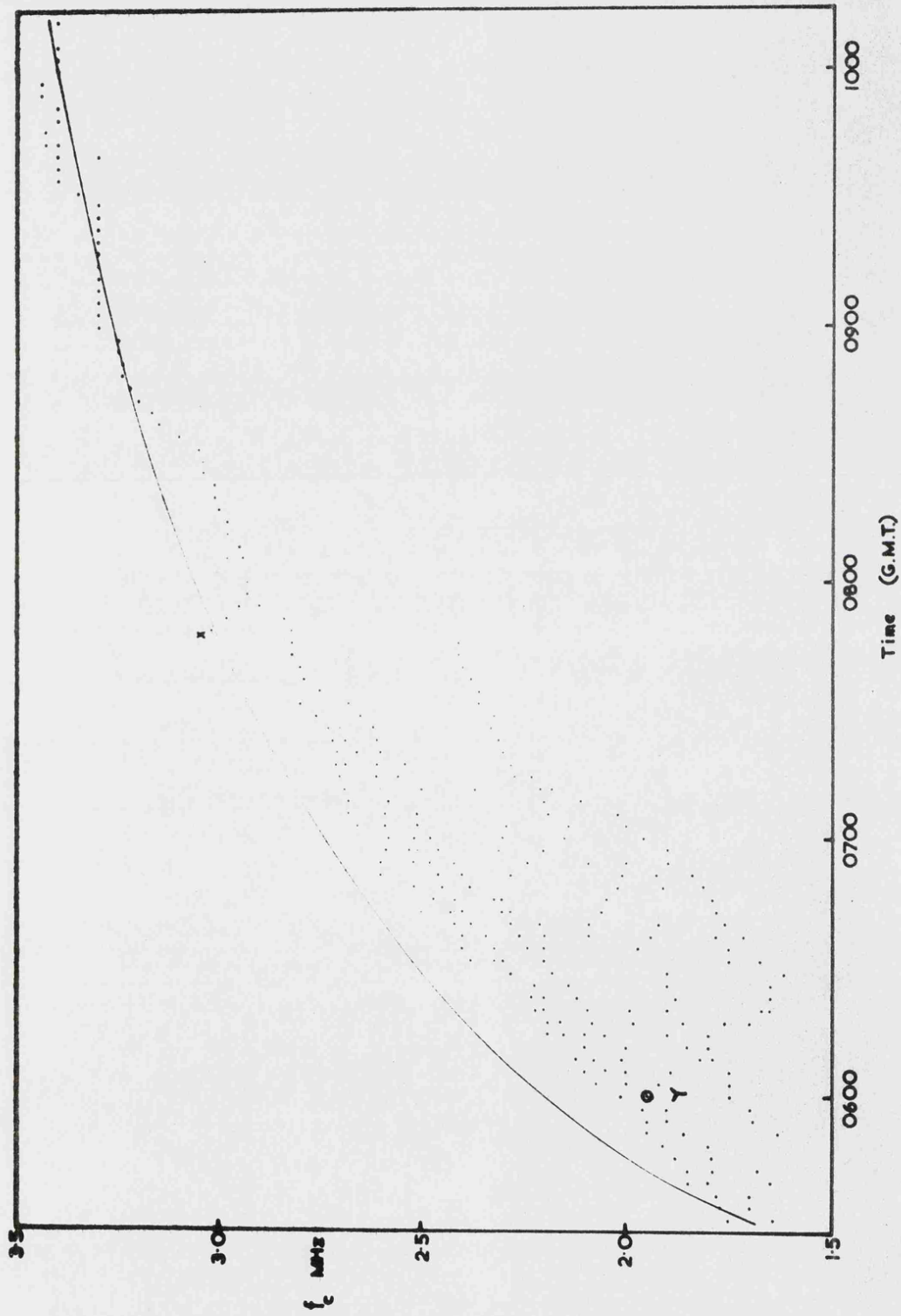


FIG. 7.2.3(b) Variation of cusp frequencies, f_c , with time for 10.4.69 ($f_o E_{min} = 3.5\text{MHz}$)

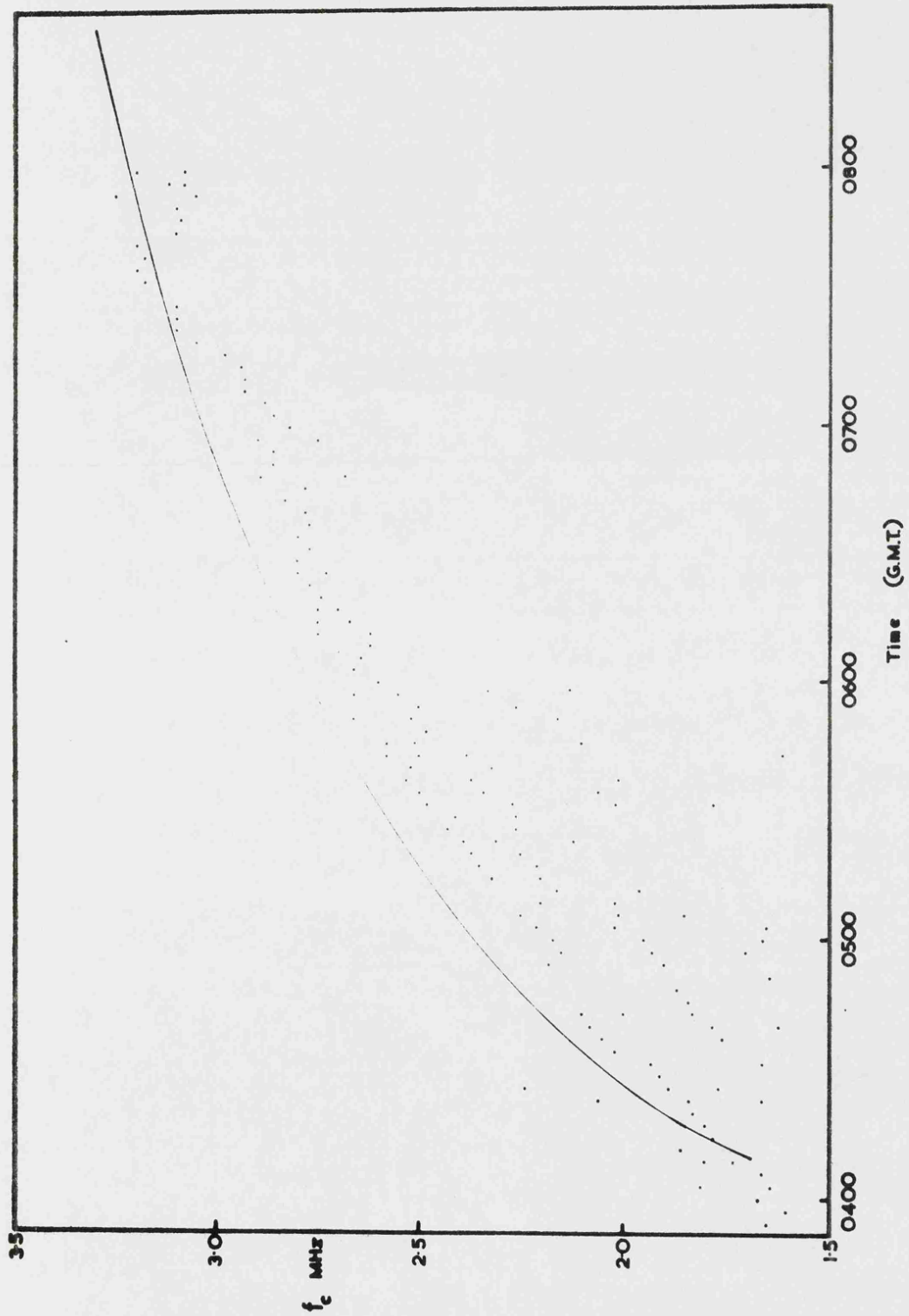


FIG. 7.2.3(c) Variation of cusp frequencies, f_c , with time for 17.6.69 ($f_0 E_{\text{noon}} 3.6\text{MHz}$)

noted. The cusp frequencies have been plotted against time in figure 7.2.3. for three days representing typical conditions during the three seasons. Also included in this figure is the variation of the E layer critical frequency, f_oE , calculated from its observed value at noon and the relationship

$$(f_oE)^n = A \cos \chi \quad 7.2.1$$

in which n has been set equal to 4 thus representing a Chapman layer. In all seasons the frequency variation of the fine structure follows fairly closely the theoretical predictions. The agreement is, however, less marked in the summer months but this may be attributed to the greater occurrence of sporadic E. Consideration of the lifetime of a particular cusp in figure 7.2.3. leads to the conclusion that the disturbance in the electron density distribution which produces it has a shorter life in summer than in winter. A single structure can be followed for between 30 and 40 minutes in summer, 40 and 60 minutes at the equinox and for times in excess of one hour in winter. Considering more closely the results for the 26th February in figure 7.2.3(a) the long persistence winter features have been used to examine the validity of the Chapman relationship of equation 7.2.1. in describing the conditions existing in the early morning. In figure 7.2.4. the logarithms of the various cusp frequencies, $\log_{10} f_c$, have been plotted against $\log_{10} \cos \chi$ in order to determine the exponent n , in equation 7.2.1., for each numbered trace of figure 7.2.3(a). The Chapman prediction with n equal to 4 has again been superimposed. The values of n obtained for each line have also been included in the figure and those obtained from the traces 1 to 4 show a mean value of $n = 5$. This deviation from the Chapman-like behaviour of the region is to be expected as

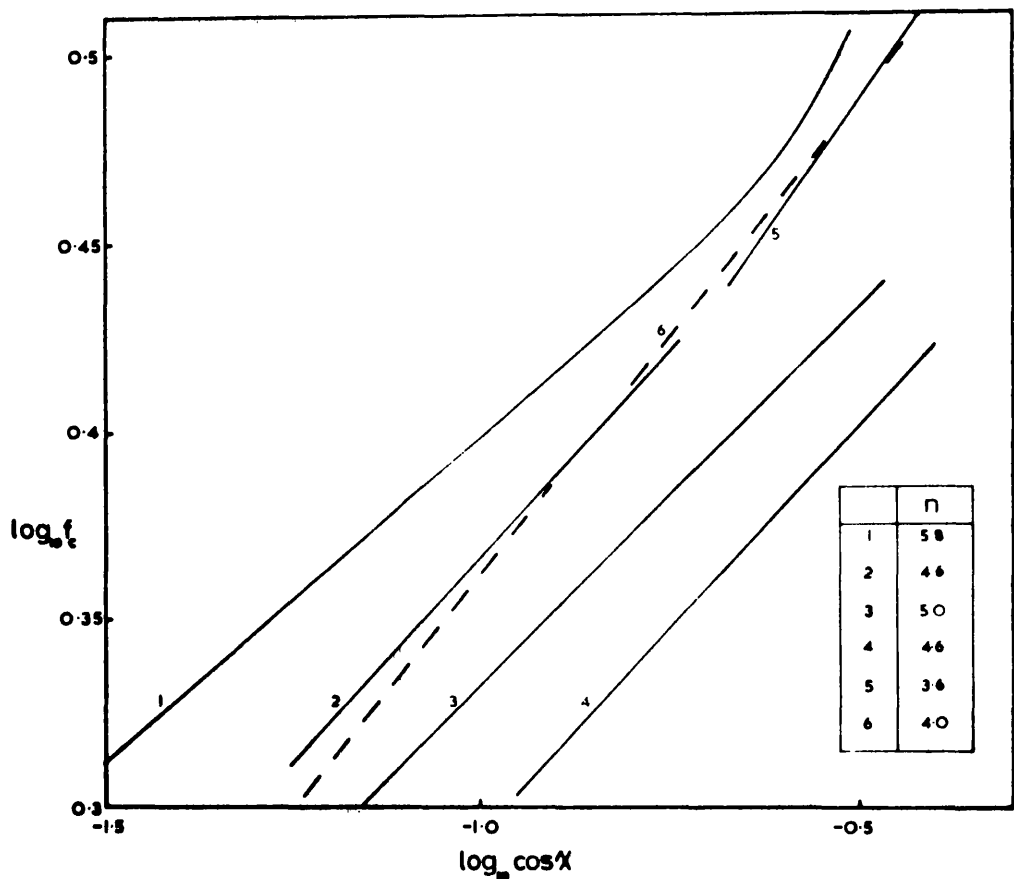


FIG. 7.2.4 $\log_{10} f_c$ against $\log_{10} \cos \lambda$ for various persistent cusp features

the solar zenith angle tends to 90° . The value of n for trace 5 and the gradient change of trace 1 at lower values of χ indicates the adjustment of the layer to Chapman-like development towards noon. A further notable feature of figure 7.2.4. is the displacement of the lines indicating different values of the constant A . It can be concluded from these observations that the disturbances in the electron density profile responsible for the fine structure develop in a regular Chapman-like manner but with an increased value of n typical of early morning conditions. Furthermore the values of n are approximately the same for the growth of each disturbance and only the value of the coefficient A distinguishes their growth pattern.

Close inspection of figure 7.2.3. also reveals traces which do not follow the Chapman growth pattern. These traces may form complex patterns of cusp development, for example the appearance of three cusps at the point marked Y in figure 7.2.3(b). These complexities can be explained in terms of redistribution of ionization in the region producing the parent cusp. In considering the example at Y, where a single cusp was split to produce three independent cusps, one rising in frequency, one falling and the third following the original growth pattern, the profile represented by the full line in figure 7.2.5. has been adopted. This profile would originally produce a single cusp at the plasma frequency 1, however redistribution of ionization due to two highly localised vertical drifts will produce the profile indicated by the broken line. The profile thus produced will give cusps at plasma frequencies 1, 2 and 3. Furthermore if the lower re-

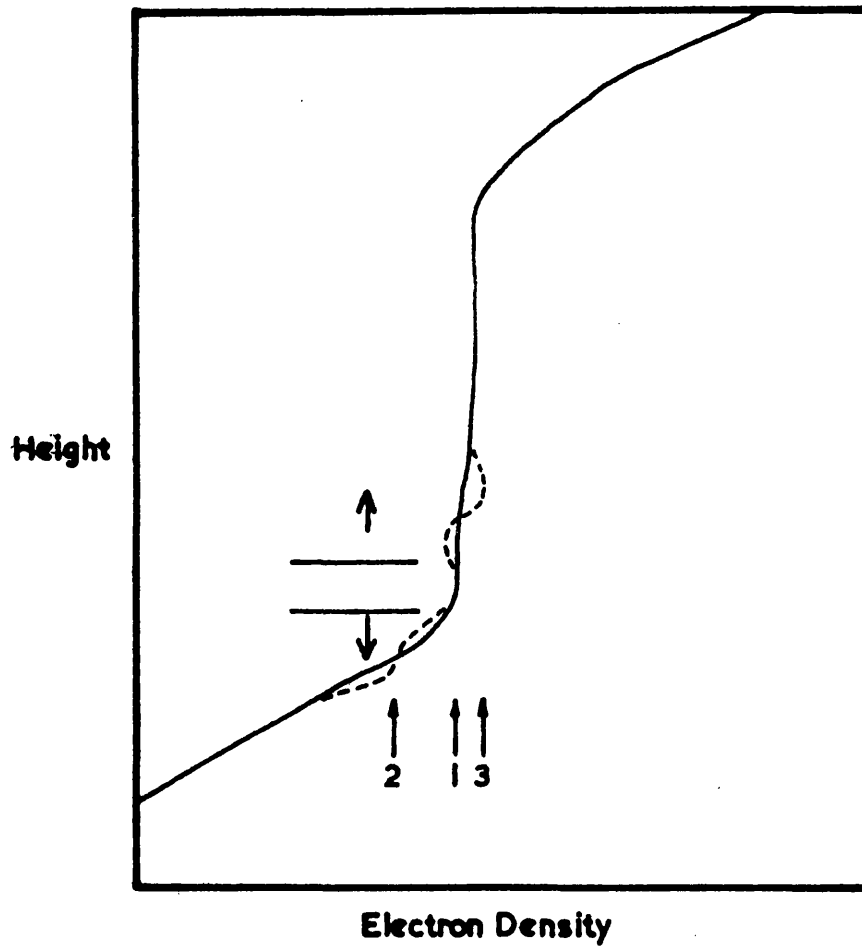


FIG. 7.2.5 Modification of the E layer peak by localised vertical drifts.

distribution moves the ionization down at a faster rate than it is produced at this height, the cusp 2 will appear to fall back in frequency as shown by the lower trace from the point Y. The extent of the redistributions required to achieve this effect will be discussed in section 7.4. and the implications of this explanation will be considered in Chapter 9.

Munro and Heisler (1956) have discussed the cusp structure observed in the F region and have suggested the use of travelling waves in the ionosphere to account for the phenomenon. The passage of such a travelling disturbance from the F₁ layer into the E-F transition region is thought to be responsible for the trace labelled X in figure 7.2.3(b). Only one trace of this kind was observed in this study thus giving weight to Munro and Heisler's statement that the disturbances which they describe would have little effect in the E region.

7.3. Correlation of Cusp Activity with Magnetic and Solar Indices.

The monthly mean activity figures together with the monthly mean values of, (a) the hourly measurements of the horizontal and vertical components of the earth's magnetic field at Hartland, (b) the Zurich sunspot numbers and (c) the flux of 2800 MHz solar radio noise are presented in figure 7.3.1. The particularly high activity figure for February results from four exceptionally active days, the 18th, 19th, 20th and 21st, and may be considered an anomalous feature. Thus, by omitting the morning value for February there appears to be evidence of a negative correlation between the cusp and solar activities. A less detailed and purely qualitative

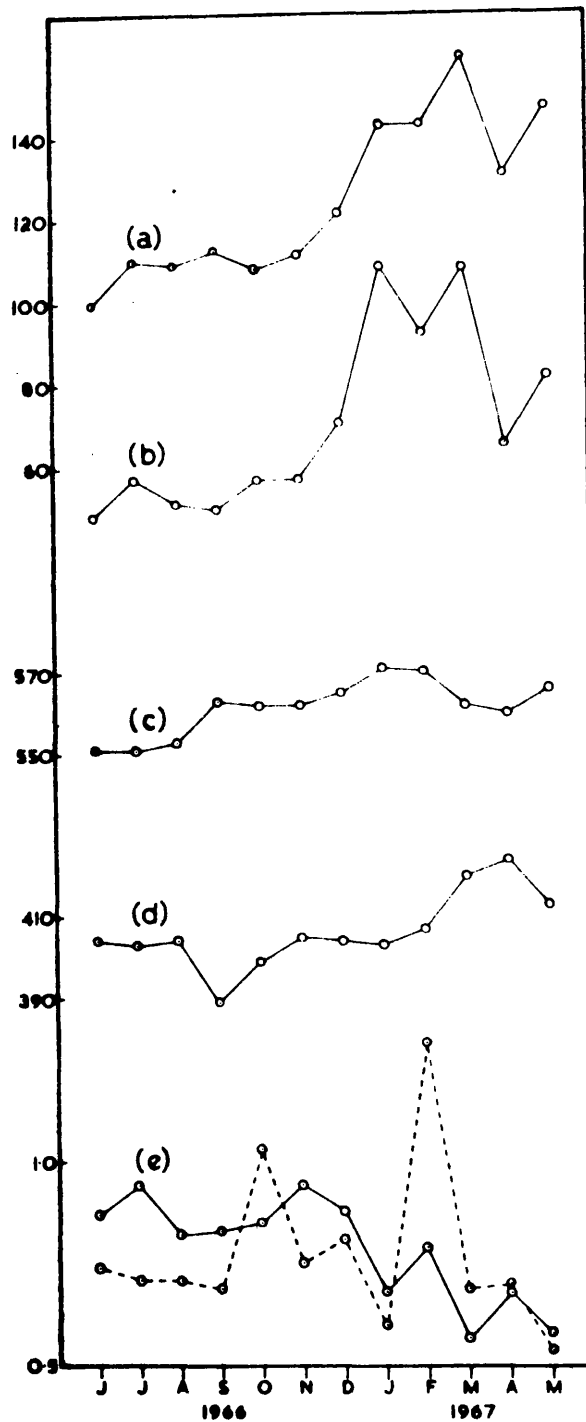


FIG. 7.3.1 Monthly mean cusp activity index against magnetic and solar parameters
 (a) Solar flux of 2800 MHz in $\text{W.m}^{-2}.\text{Hz}^{-1}$
 (b) Zurich sunspot number
 (c) Vertical component of the earths magnetic field - 43000γ
 (d) Horizontal component of the earths magnetic field - 18500γ
 (e) Monthly mean cusp activity index --- a.m.

 --- p.m.

inspection of records taken at sunspot maximum are in agreement with this observation. It has been suggested by Morgan (1966) that there may be a negative correlation between the occurrence of sporadic E and the horizontal component of the earth's magnetic field. In order to ascertain whether the cusp structure on ionograms is a transient or a regular feature, the parameters listed above were plotted for each day from June 1966 to May 1967. A portion of the resulting diagram is presented in figure 7.3.2. in which there is some evidence that the periods of high cusp activity follow within a few days of high magnetic activity and low horizontal magnetic field; conditions which favour the formation of sporadic E as described by Whitehead (1962). For example, the records for the 16th of September discussed in the previous section were dominated by an intermediate trace and inspection of the magnetic data showed the 15th to be an active day and to have a low horizontal field component compared with the days around it. Furthermore, it has been noted on several sequences of ionograms that the collapse of intense sporadic E was sometimes followed by cusp activity. These observations are supported by the figures of table 7.3.1. It can be seen that days of low cusp activity are generally days of (a) low magnetic activity, (b) high horizontal magnetic field and (c) high sunspot number in contrast to the conditions for the 'cusp' active days. There are, however, two days listed which do not fit into this pattern, suggesting that although the combination of conditions mentioned above may effect the formation of fine structure they are not the only criteria. The daily meteor counts have also been included as a source of additional ionization in the 90-120 km region but no direct

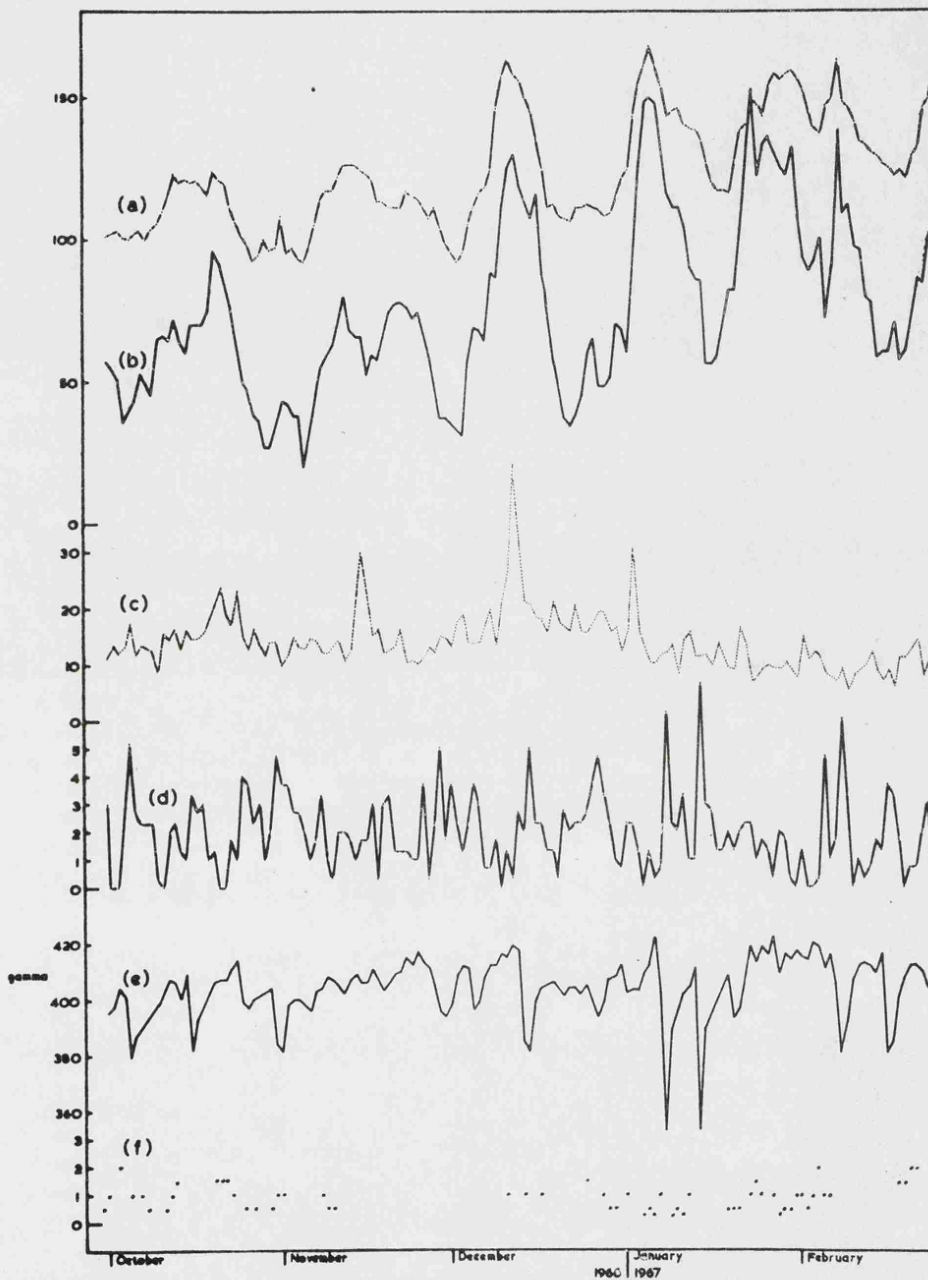


FIG. 7.3.2 Day to day variations of cusp activity compared with (a) 2800MHz solar radiation flux (b) Zurich sunspot number (c) Mean hourly meteor count (d) Kp index for the first 3 hours of each day (e) Horizontal components of the earth's magnetic field less 18500 γ

Days of High Cusp Activity

Days of Low Cusp Activity

Date	Cusp Activity		Magnetic Field H gamma +0.500	R ₂	Meteor Count	Date	Cusp Activity		Magnetic Field H gamma +0.500	R ₂	Meteor Count
	a.m.	p.m.					a.m.	p.m.			
8.11.66	1	1-5	404	51	12-1	11.10.66	5	5	403	66	16-3
25.12.66	1-5	1-5	405	60	15-3	6.1.67	5	0	422	148	9-4
21.2.67	2	6	412	71	13-8	22.3.67	5	5	412	108	8-4
24.6.66	2	1-5	415	63	11	30.3.67	5	0	423	130	10-4
21.7.66	1-5	1-5	406	55	12-1	8.5.67	5	0	417	18	14-5
21.10.66	1-5	1	407	96	24-3	23-4-67	5	5	427	94	10-8
MEAN			408	66	14-8	MEAN			417	94	11-6
Mean emitting 21.10.66			408	60	12-9	Mean emitting 23.4.67			415	94	11-8

Table 7.3.1 Comparison of high and low cusp activity days

effect, even of intense meteor showers, has been noted.

7.4. Interpretation of model cusp structures in terms of disturbances in the electron density profile

In section 7.2. the complex movement of small cusps along the frequency scale has been attributed to small redistributions of electrons in the transition region between the E and the F layers and around the E layer peak. The extent of this redistribution has been studied by computing, by means of the Titheridge (1961a) analysis, monotonic electron density distributions from models in which particular features of the virtual height data have been represented. The virtual height models A, B and C of figure 7.4.1. have been constructed, such that only the position of the central cusp changes between models. The electron density profiles computed for the three cases are presented in figure 7.4.2. Curves A, B and C of this figure show the movement of a central bulge through approximately 3 km. Figure 7.4.2(d) illustrates that the extent of the fluctuation in electron density at a fixed height of 127 km was of the order of 2×10^3 electrons/cm³ and that the change in height at constant electron density of 10^5 electrons/cm³ was less than 1.5 km. Thus it may be concluded that the redistribution of approximately 2% of the ionization over a height range of less than 1.5 km can move a minor feature of the profile by 3 km and cause its corresponding cusp on the $h'(f)$ curve to move by 0.1 MHz.

The models presented in figures 7.4.3. and 7.4.5. have been devised to investigate the effect of (a) the width of the intermediate trace and (b) its depth. In figure 7.4.3.

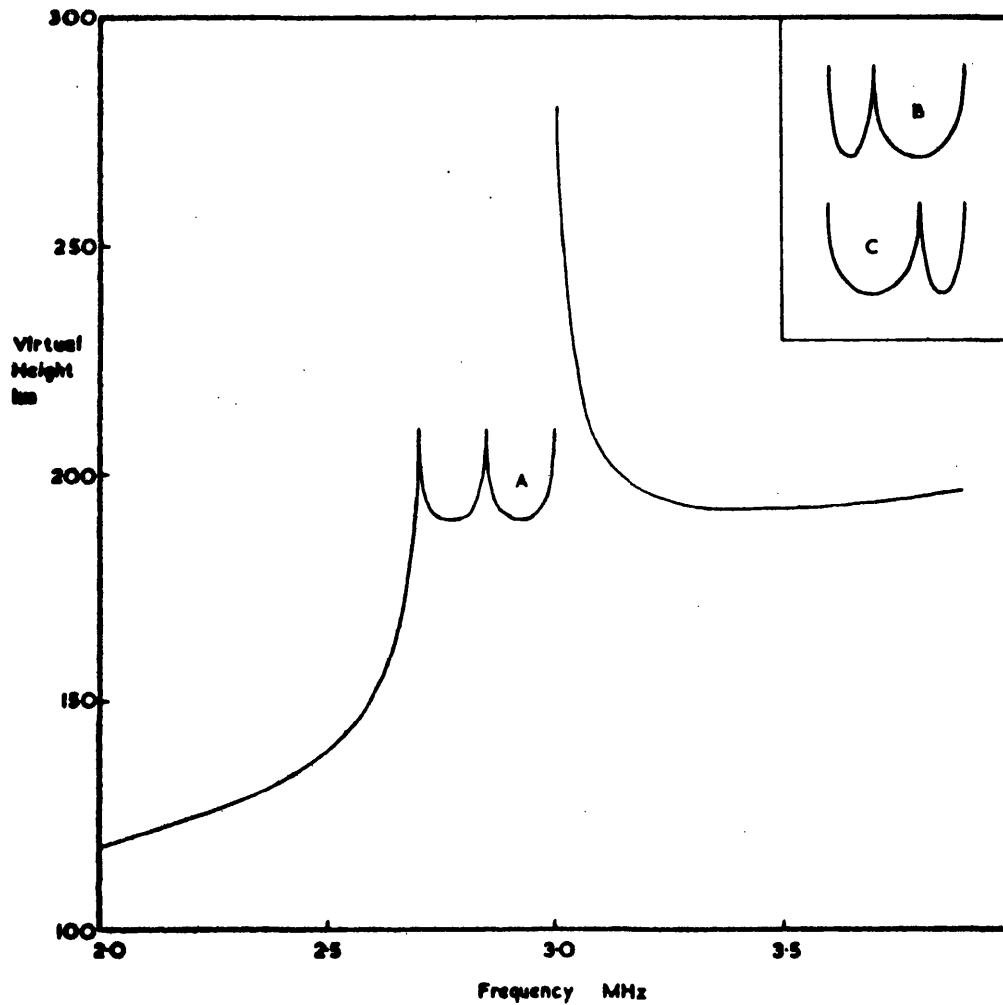


FIG. 7.4.1 Model $h'(f)$ curves with central cusp displaced. Inset are alternative intermediate traces B and C.

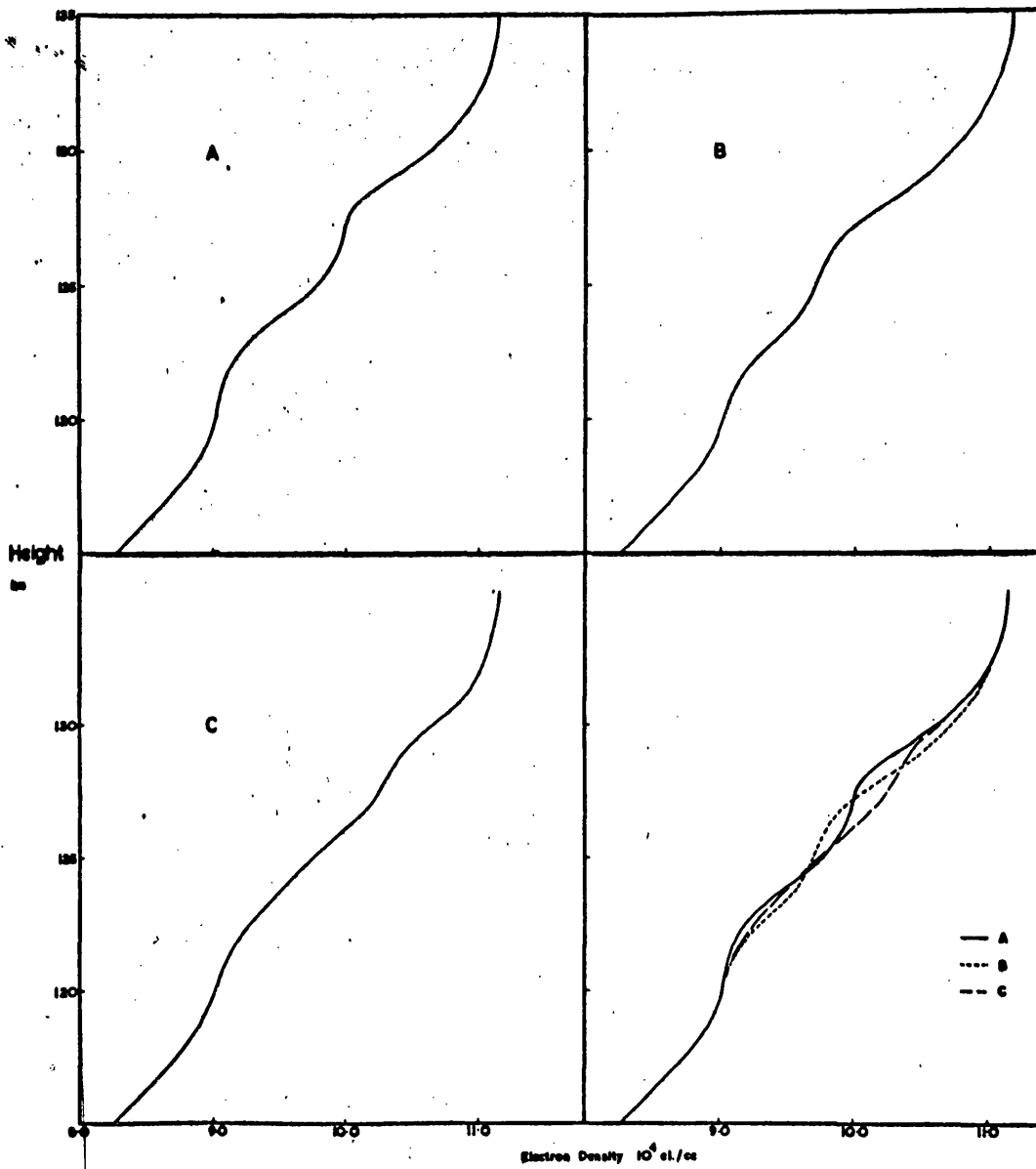


FIG. 7.4.2 Monotonic electron density profiles computed from the model h (f) curves of figure 7.4.1.

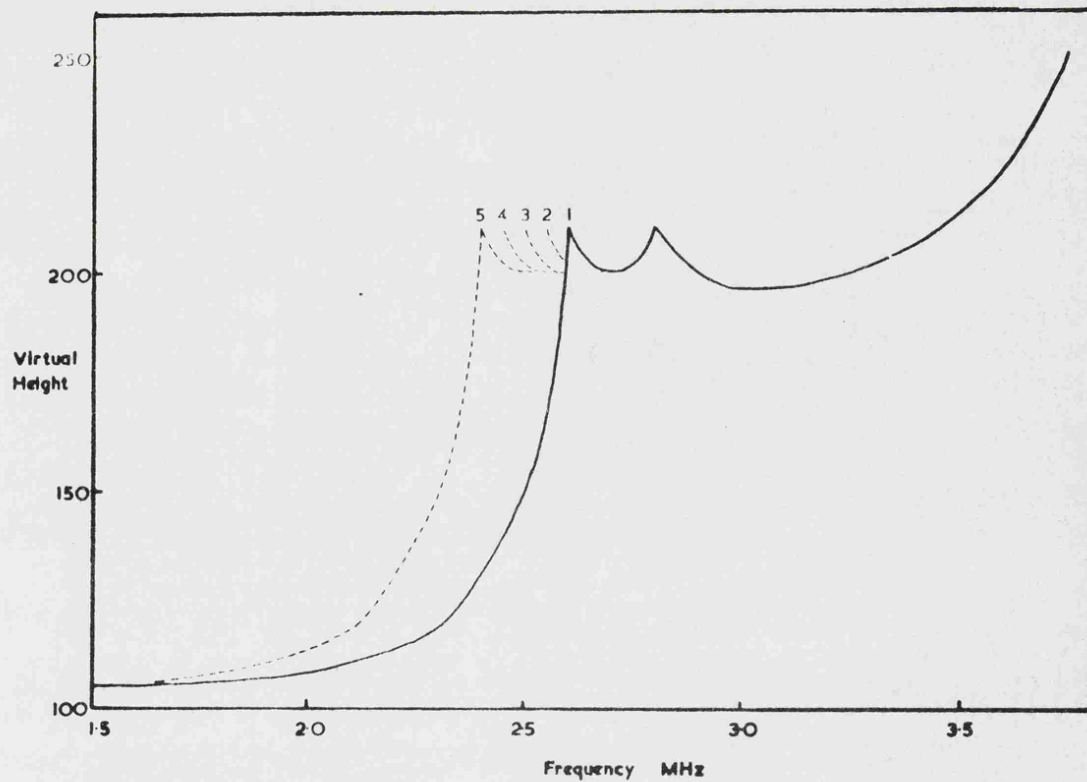


FIG.7.4.3 Model $h'(f)$ curves with various intermediate trace widths

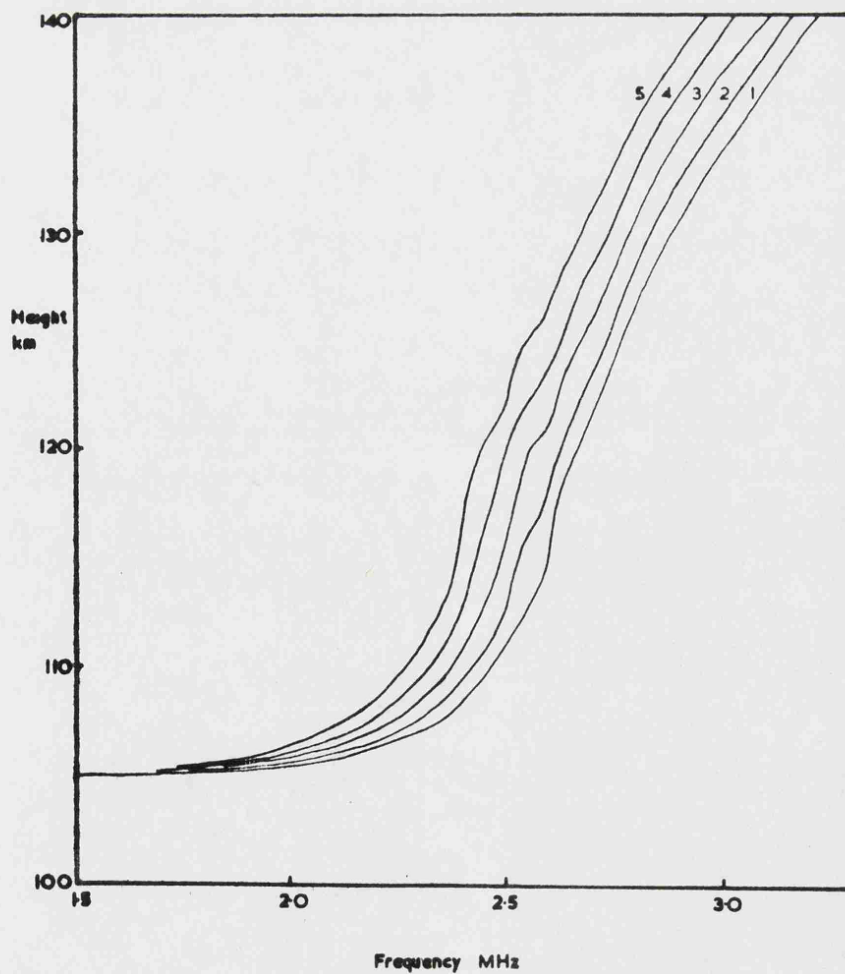


FIG.7.4.4 $N(h)$ profiles computed from $h'(f)$ curves shown in fig.7.4.3

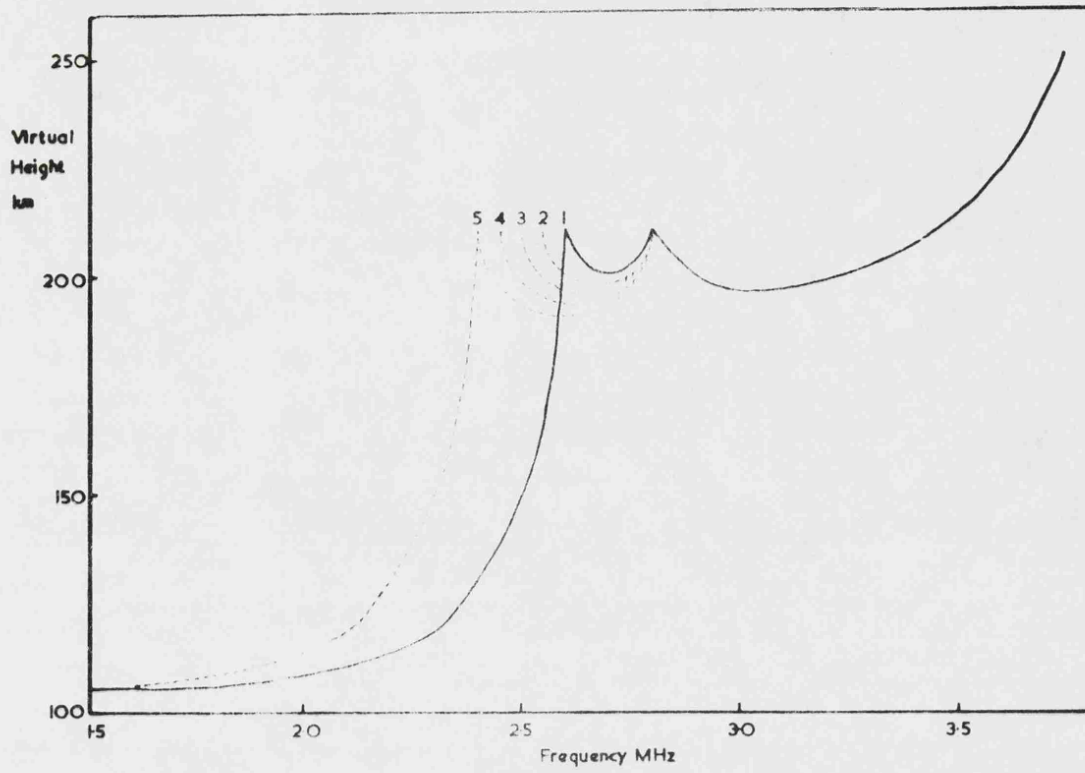


FIG.7.4.5. Model $h'(f)$ curves with various intermediate trace sizes.

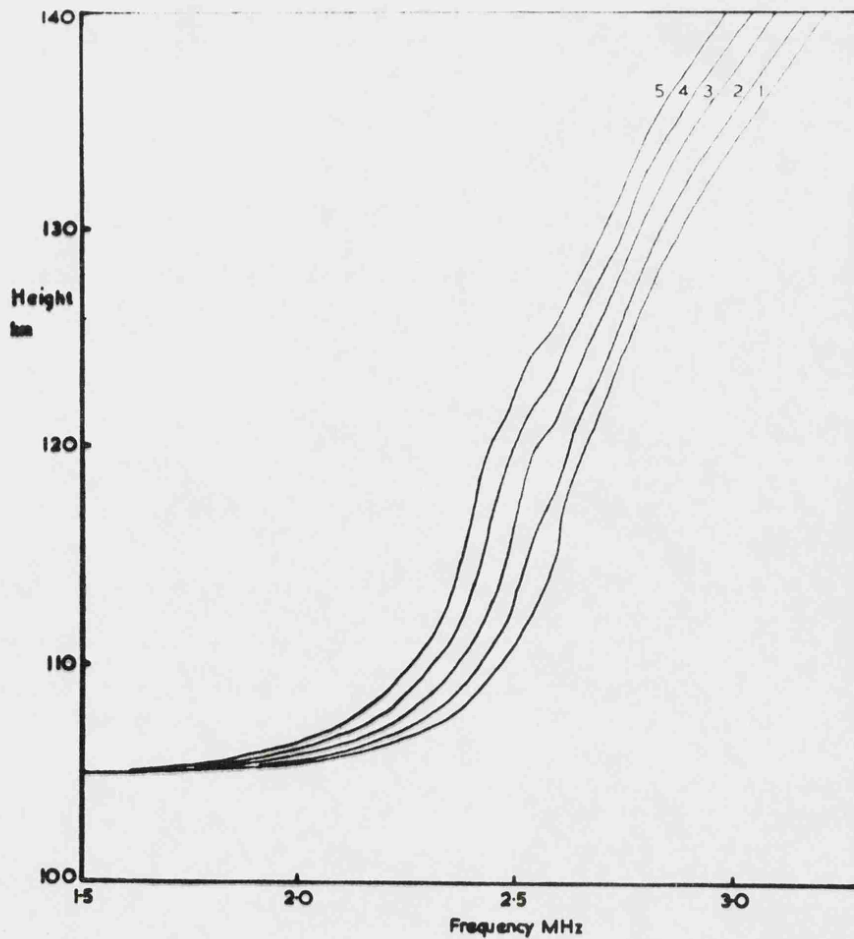


FIG.7.4.6. $N(h)$ profiles computed from $h'(f)$ curves shown in fig.7.4.5.

the spacing between the cusps has been steadily increased in 50 kHz steps to produce a series of virtual height curves in which the E layer trace has been moved to accommodate the widened constant depth cusp. The computed electron density profiles are illustrated in figure 7.4.4. The frequency shift in the E region trace has produced a predictable change in the computed electron density in this region and has also produced a shift in the F region distribution although the F layer virtual heights have not been altered. Since a decrease in the electron densities in the E layer would normally produce a decrease in the F layer virtual heights, it is to be expected that keeping these heights constant would result in the height of the electron density distribution representing the F layer being increased. In addition to these gross features the profiles of figure 7.4.4. show the movement of the small undulations responsible for the cusp structure of the virtual height curves. The electron density profiles of figure 7.4.6. which have been computed from the virtual height profiles containing intermediate traces of varying depth, figure 7.4.5., incorporate the same gross features as those discussed earlier. The small undulations are again present but the limited scaling interval of the analysis prevents any comparison of their form with those discussed above and hence the fluctuations in electron density responsible for the changes in the width and depth of the intermediate traces cannot be recognised.

The virtual height curves discussed above have been concerned with the variations in shape of the intermediate trace and it has been shown that using the present analysis

these variations have little noticeable effect upon the fine structure of the electron density profile. In order to investigate the variations in the $N(h)$ distribution due to a general increase in the group retardation of the intermediate trace, the models presented in figure 7.4.7. have been reduced to electron density profiles. In figure 7.4.7. the virtual height of a given intermediate trace has been lowered in steps of 10 km and the E region trace suitably adjusted in each case. The resulting electron density profiles given in figure 7.4.8. indicate the progressive growth of the E layer and an additional intermediate layer. Again the apparent change in the height of the F region results from holding the F layer virtual heights constant while the electron densities in the E region were increased.

A series of analytic profiles incorporating the various cusp movements discussed separately above have been developed to represent observed movements in the intermediate layer and are presented in figure 7.4.9. The computed electron densities for these models are given in figure 7.4.10. This figure illustrates the formation of an intermediate layer which decreases in height and finally assumes the form of a sporadic E layer. Such a development has been described by McNichol and Gipps (1951) and the layer, which was attributed to ionization moving down from the F region into the E-F transition region, has been referred to as the 'Sequential Es'. Following the conclusions of Munro and Heisler (1956) that interaction between the F and the E regions is slight it is considered that this type of intermediate layer development is due to local redistribution of ionization. The

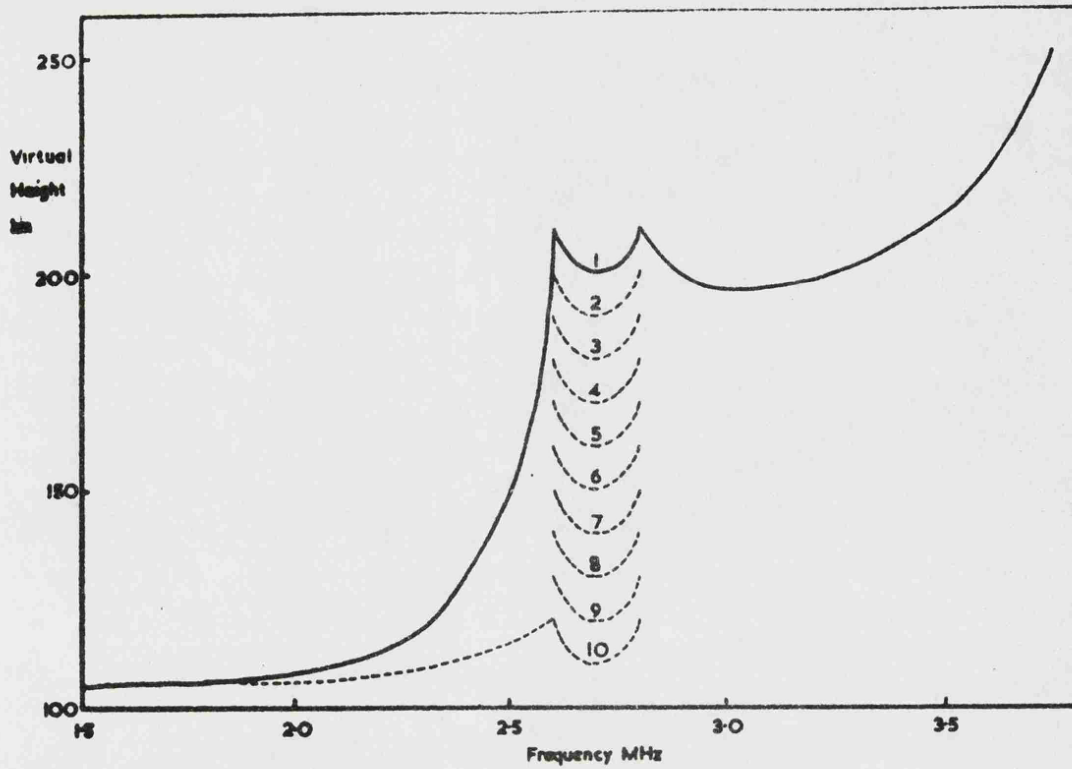


FIG.7.4.7 Model $h'(f)$ curves with various intermediate trace heights

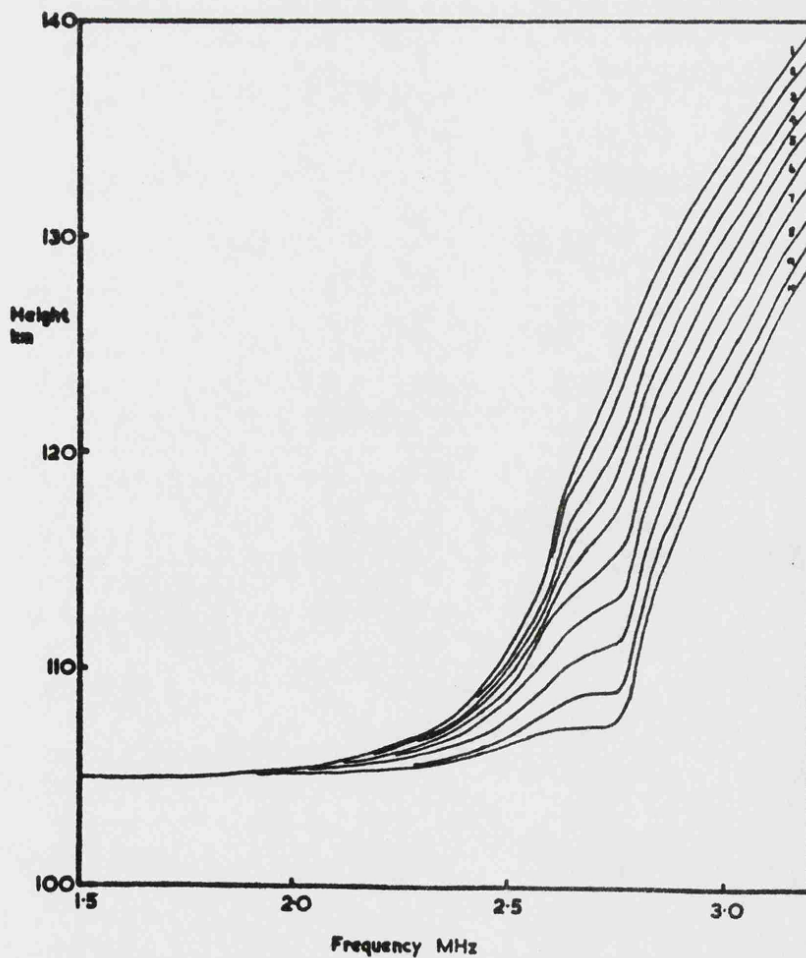


FIG.7.4.8 $N(h)$ profiles computed from $h'(f)$ curves shown in fig.7.4.7

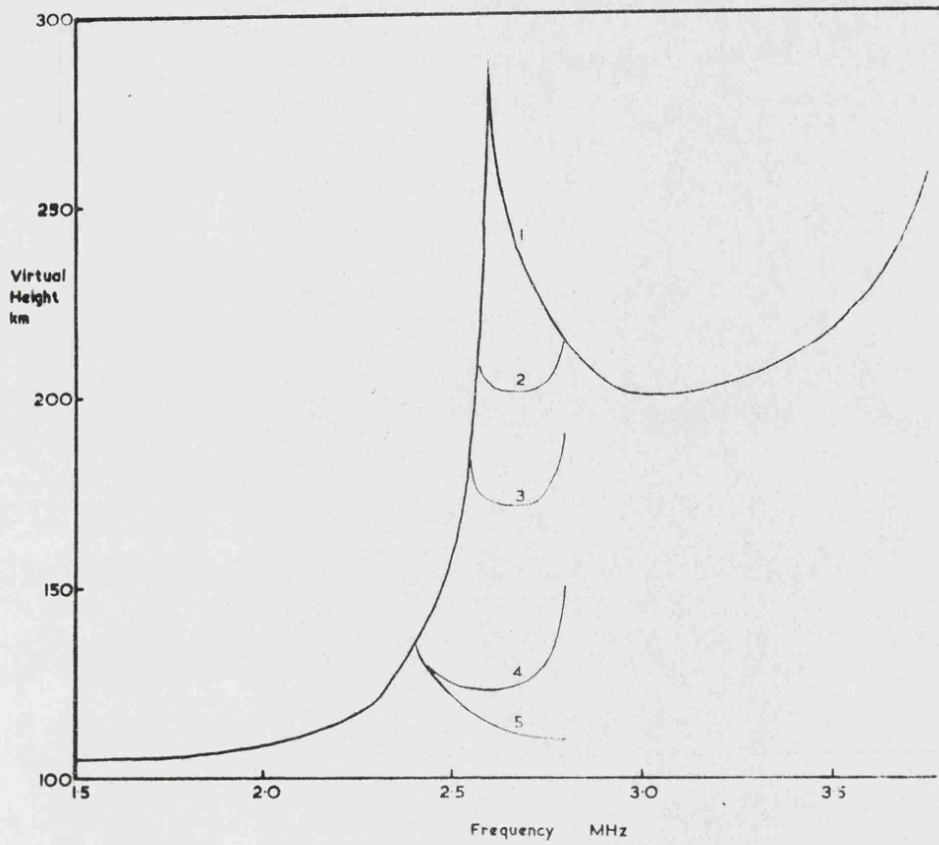


FIG.7.4.9 Model $h(f)$ curves with various intermediate traces

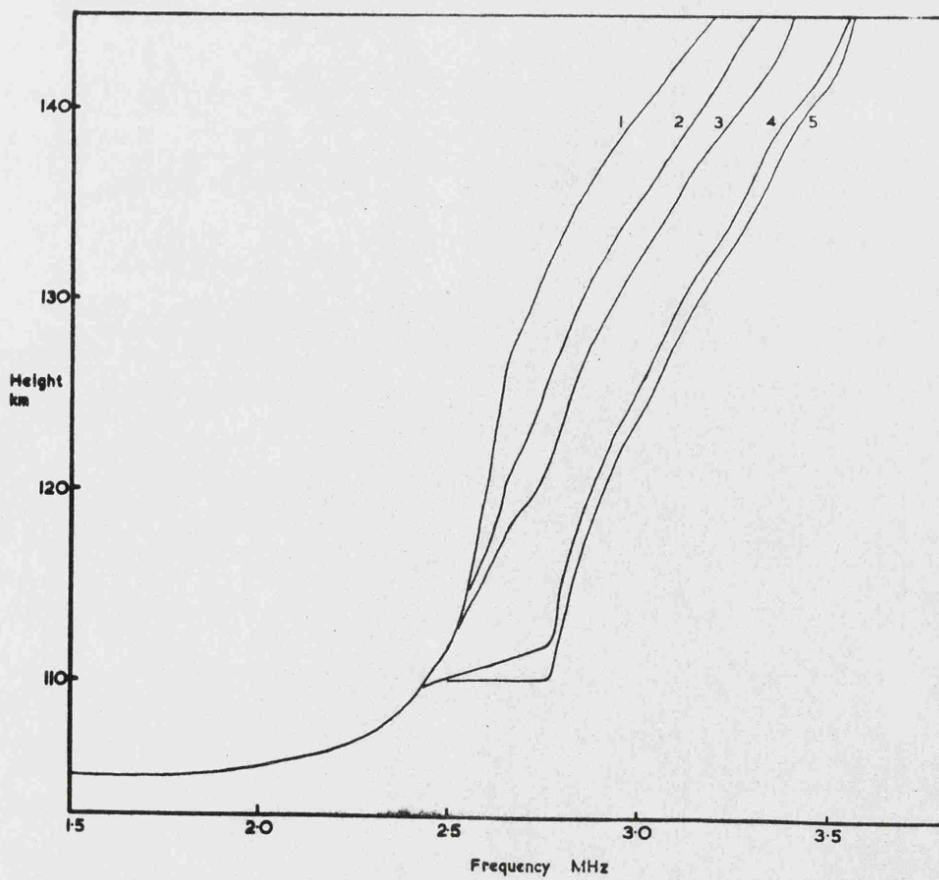


FIG.7.4.10 $N(h)$ profiles computed from $h'(f)$ curves shown in fig.7.4.9

extent of the apparent change in the electron distribution having been exaggerated by the monotonic form of the electron density distribution. The apparent decrease in height of the forming layer can be attributed, at least in part, to the omission of any re-entrant regions in the distribution.

In figure 7.4.11. a series of model electron density distributions are presented illustrating various simple forms for the E-F transition region. The phase integral analysis, discussed in Chapter 3, has been used to compute the variation of the virtual height with frequency for each of these models and the resulting cusp shapes are illustrated in figure 7.4.12. The electron density models numbered 122 to 127 are re-entrant between the peak of the E layer and the lower F layer and the corresponding $h'(f)$ curves of figure 7.4.12. contain a clearly defined cusp. It is noticeable from these $h'(f)$ curves that as the re-entrant portion of the electron density model becomes less marked so the group retardation of frequencies close to the E layer penetration frequency (3.47 MHz) increase. Considering the models 127 and 120 the group retardation of a frequency 3.5 MHz just above the E layer penetration frequency increases from 384 to 740 km as the electron density in the transition region increases by 5×10^3 electrons/cm³ and the re-entrant portion of the profile finally disappears. Thus very shallow re-entries in the electron density profile produce a very marked effect upon the group retardation of frequencies close to the penetration frequency. The remaining models 128 to 134 represent monotonic distributions and again produce a reduction in the group retardation of frequencies slightly in excess of the E layer critical. However, this is accompanied by increasing distortion and widening of the cusp region as the two layers become less well defined. Thus

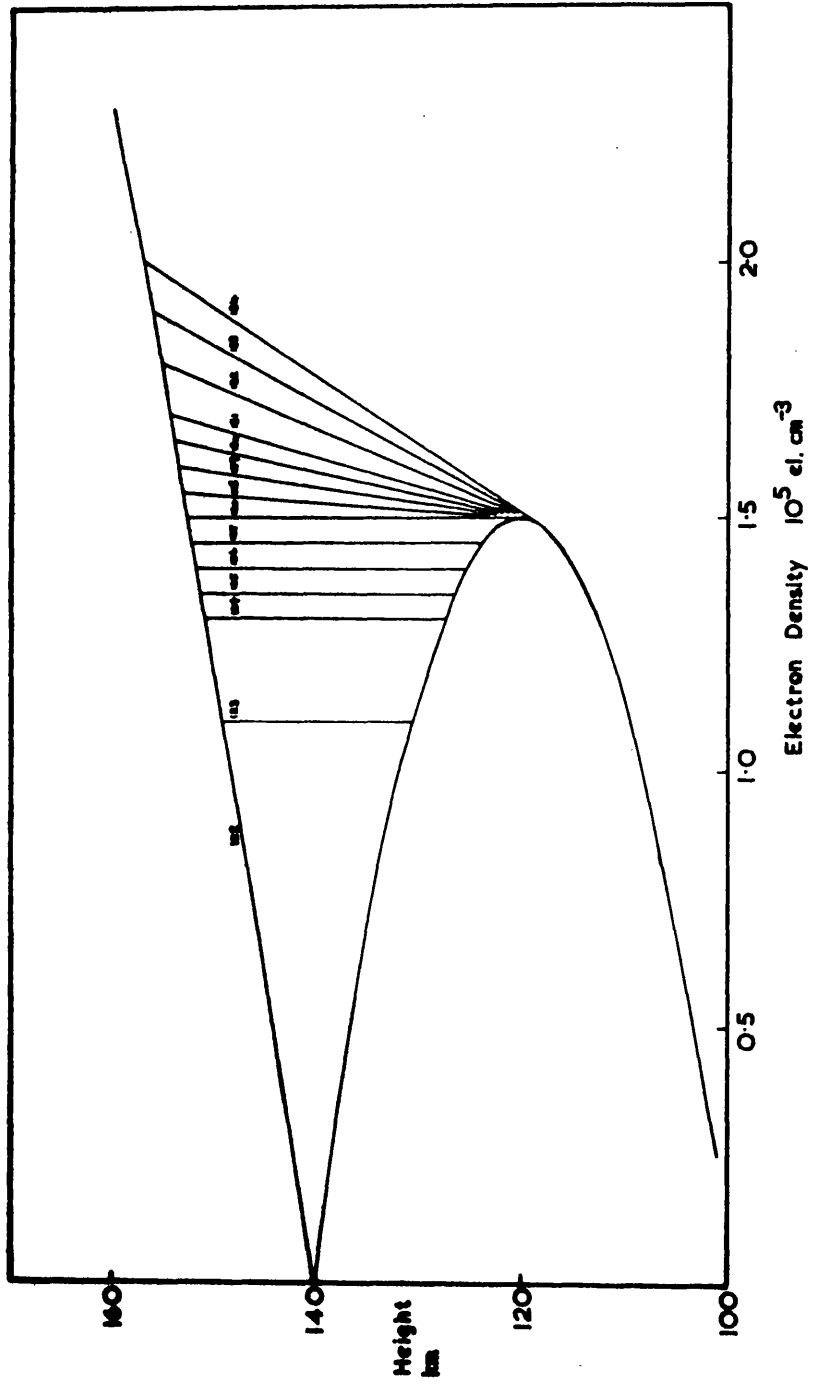


FIG. 7.4.11 Model electron density profiles with various transitions between parabolic E and F layers.

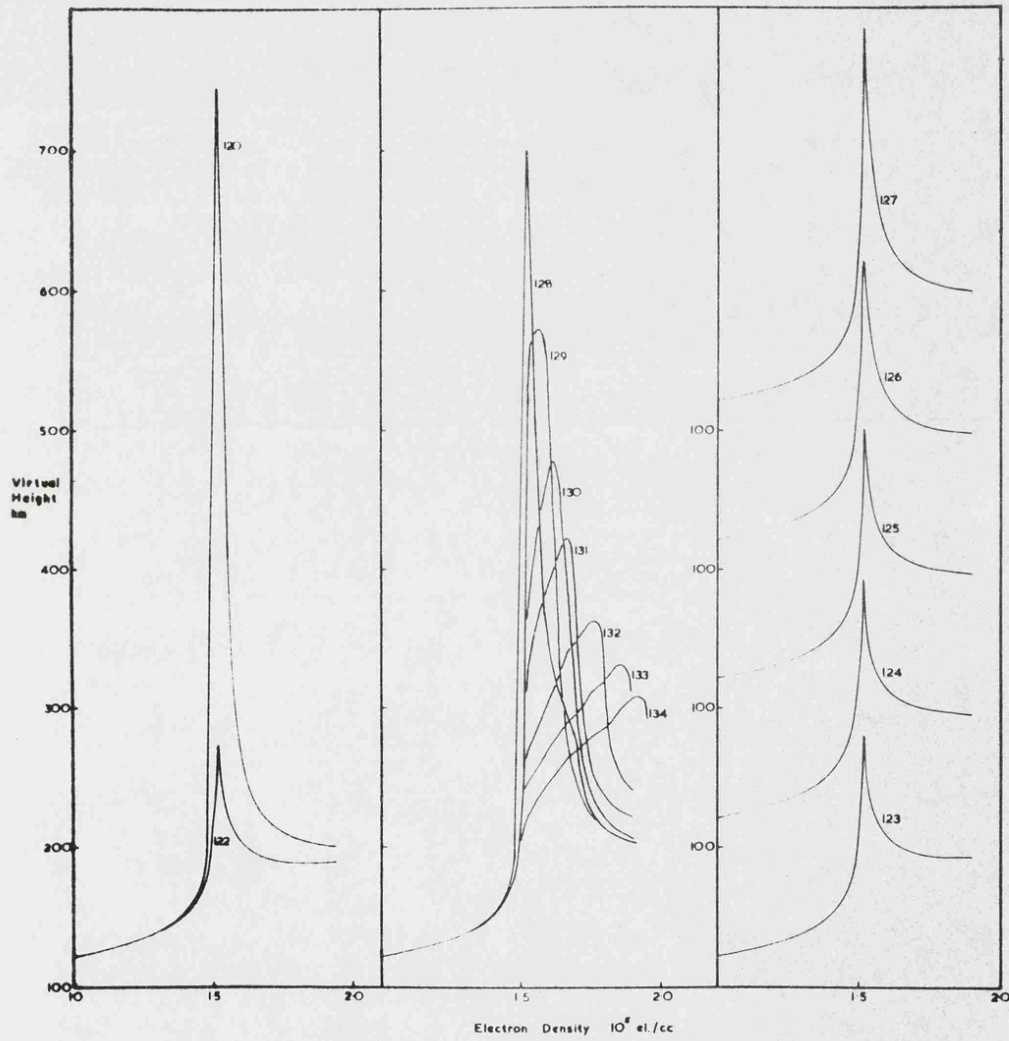


FIG. 7.4.12 Variations of virtual height with frequency for the model profiles illustrated in fig. 7.4.11

very sharp cusps accompanied by large group retardations will result from electron density profiles in which the E-F transition has an approximately constant electron density or forms a shallow re-entry into the electron density profile. Profiles containing a more extensive minimum or a steady increase in electron density in the E-F transition will produce sharp cusps accompanied by lower group retardations at adjacent frequencies or highly distorted cusps which may not contain a clear discontinuity.

7.5. Cusp Development following sunrise

In the previous section an ionogram reduction method was used to relate model cusp structures to changes in the electron density distribution. It is of interest to consider the inverse problem i.e. to calculate the $h'(f)$ changes in the vicinity of f_oE produced by typical $N(h)$ distributions. Three sources of $N(h)$ profiles are considered (a) the model profiles described by Bourne, Setty and Smith (1964), (b) the distributions deduced from ionograms taken at Leicester and (c) the electron density profiles measured by Taylor (1969) from Thomson Scatter observations.

7.5.1. Theoretical Profiles

Bourne, Setty and Smith have modified the techniques of Chapman (1931) by postulating a variation in the scale height of the ionosphere above 100 km to account for the increase in the group height of the lower F region before ground sunrise, commonly referred to as the 'sunrise effect'. The scale

height was allowed to increase linearly according to the formula

$$H = H_0 + \beta (h - h_0)$$

published by Nicolet (1951), in which H_0 was 5 km at an altitude h_0 of 100 km and $\beta = 0.4$. The profiles calculated from this analysis for various periods after the ground sunrise are shown in figure 7.5.1. By adding this additional ionization to an assumed model of the nocturnal E region the distributions at various times were obtained for up to 80 minutes after sunrise and these are presented in figure 7.5.2. The models have been extended to D region heights by the addition of appropriate Smith (1966) models of this lower region. The virtual height variations with frequency for these profiles were computed and the results are presented in figure 7.5.5. It is evident that reflections from the E region will not be observed above 1.5 MHz until approximately 40 minutes after sunrise by which time the original extreme stratification of the nocturnal profile has disappeared and the developing profile represents a simple E layer with a shallow valley above. This shallow valley gives rise to very sharp discontinuities in virtual height as predicted by the theoretical considerations of section 7.4. Furthermore, the undulations in the derived virtual height curve in regions away from the main cusp illustrate that small irregularities in the electron density profile around the reflection level, which are not reproduceable in the diagram, greatly influence the group retardation.

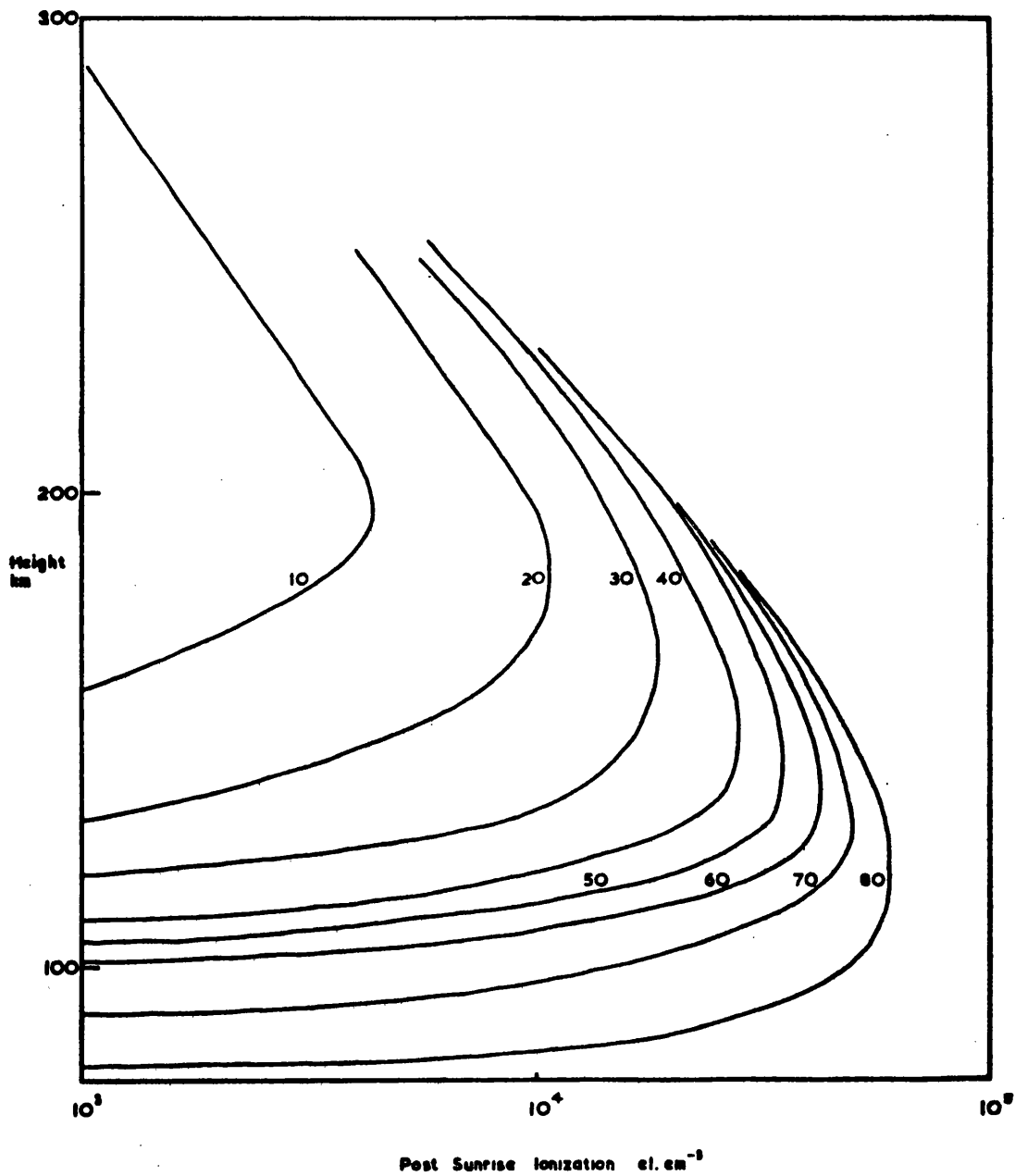


FIG. 7.5.1 Bourne, Setty and Smith (1964) ionization production curves for various times after ground sunrise (shown in minutes).

7.5.2. Direct observations of Virtual Height at Leicester

Ionograms have been observed continuously during the early morning hours of 20 days between February and June 1969 by the experimental technique described in Chapter 6. From these records four typical days have been selected for close examination. In figure 7.2.4(a) and (b) the observed cusp frequencies for two of these days, 26th February and 10th April have been presented. It was concluded above that the lifetime of the fine structure was greater in winter than in summer and this point is further illustrated in figure 7.5.6., in which the ionogram data for a short period following the appearance of fine structure is reproduced. In addition these ionogram sequences demonstrate that the form of the fine structure undergoes rapid changes especially in the summer and equinox months. The pattern of the fine structure observed on the 26th February is fairly stable throughout the period of observation whereas that for the 10th April indicates that while the cusp frequency increases in a regular fashion the shape of the trace between cusps may change appreciably within the 3 minute period between records. Furthermore these differences in the cusp pattern appear, at times, to occur as discrete changes. For example, on the 10th April a single intermediate trace developed between 0618 h and 0630 h and then suddenly subdivides to form a further cusp which persist until 0800 h.

The ionograms recorded on the four days have been reduced to electron density profiles by the analysis outlined in Chapter 3 and the quarter hourly profiles are reproduced in figure 7.5.3. As a check upon this analysis the virtual

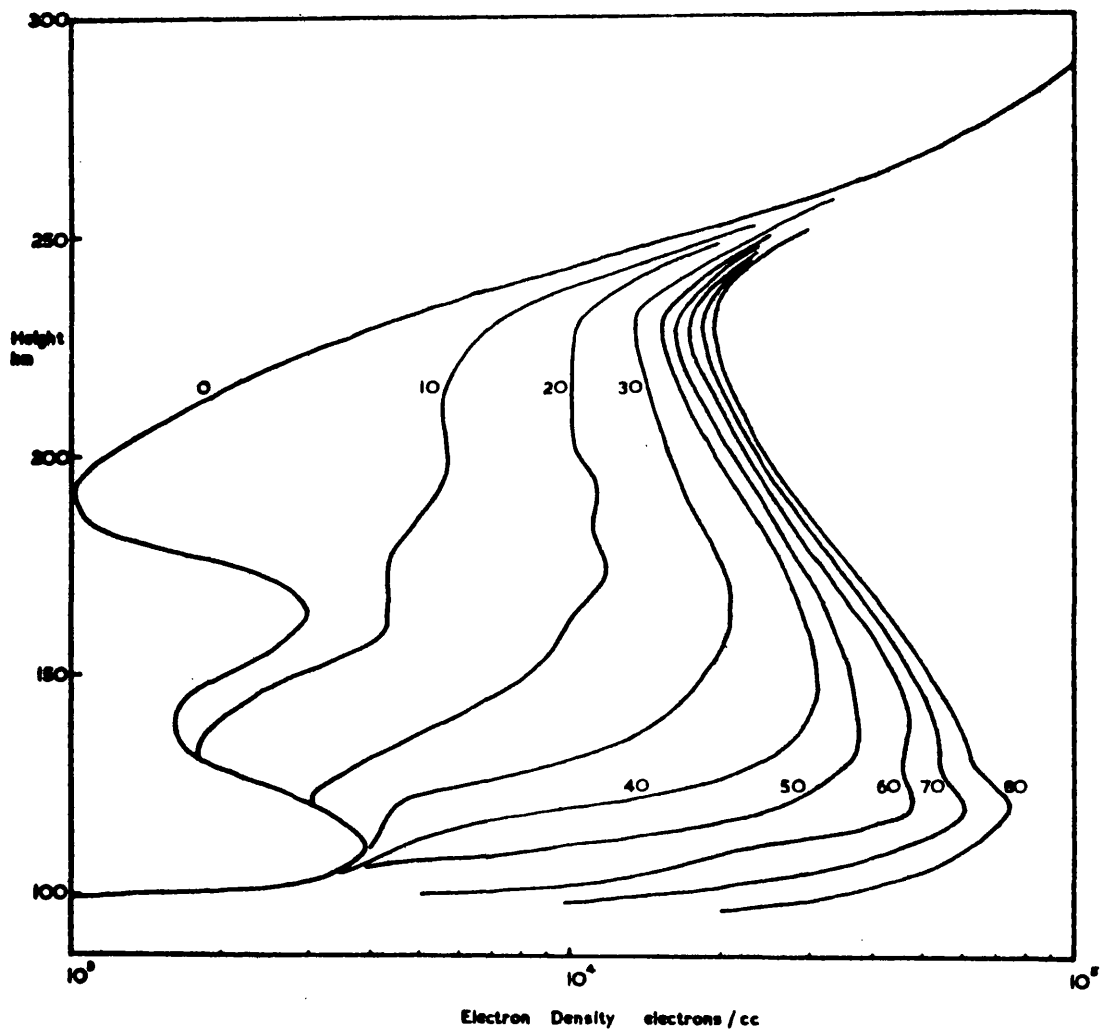


FIG. 7.5.2 Theoretical electron density models after Bourne, Setty and Smith (1964)

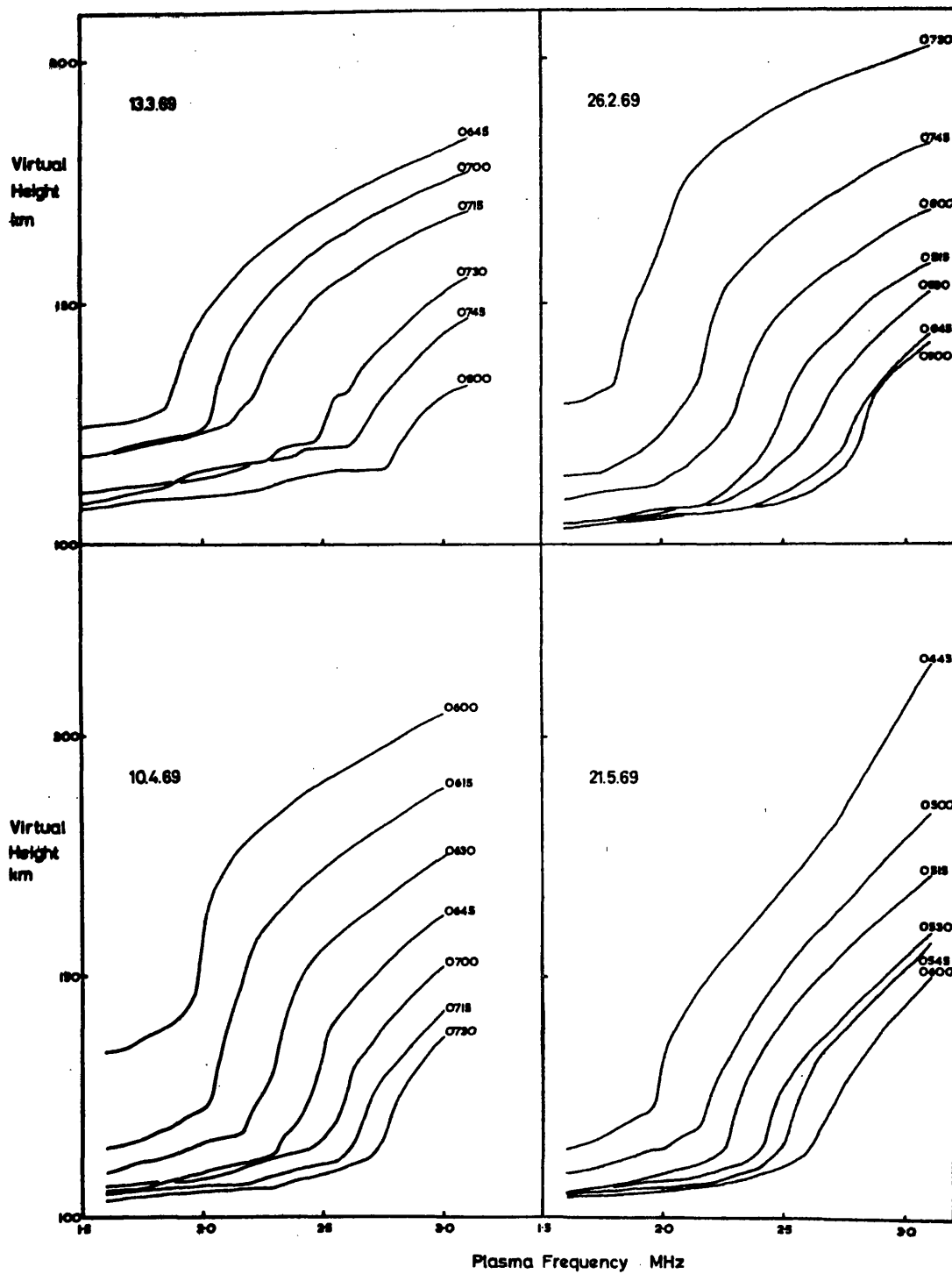


FIG.7.5.3 Quarter hourly profiles computed from Leicester ionograms recorded during the mornings of the days shown.

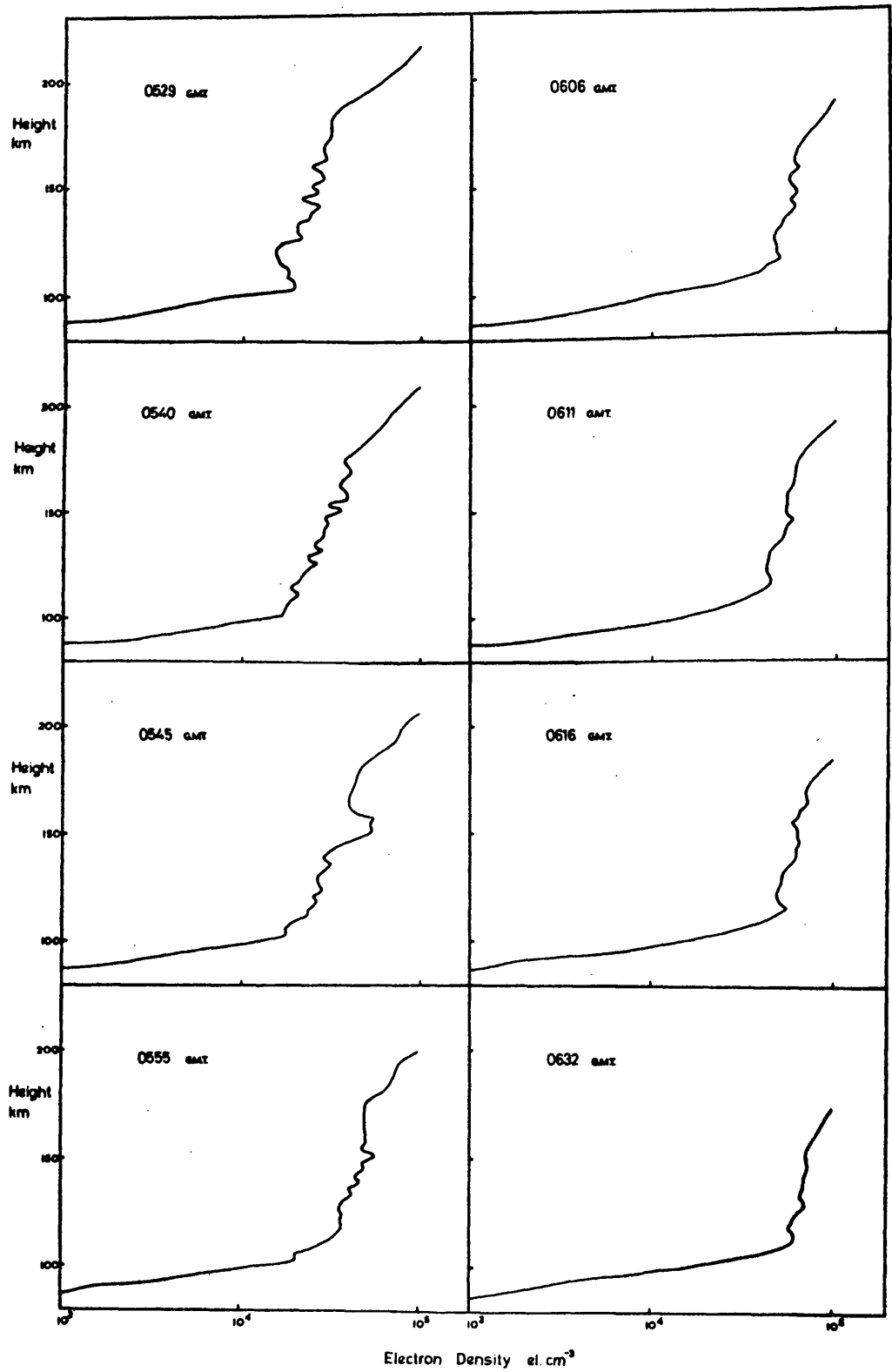


FIG.7.5.4 Thomson Scatter profiles for 11th April 1969.

heights for a range of frequencies have been recalculated from these profiles and the results for the 10th April are presented in figure 7.5.7. together with the observed $h'(f)$ curves. A good correlation was obtained between the observed and calculated values and although the fine structure was not reproduced in detail irregularities are present in the virtual height data in the vicinity of the cusps. The figure indicates that much of the observed fine structure occupies a frequency range less than the scaling step of 0.05 MHz and this would not be effective in modifying the derived electron density profile. Further reduction of this scaling step is impracticable as it would greatly increase the size of the matrices involved in the Titheridge reduction. This analysis does however give distributions which represent the virtual height data to an acceptable degree of accuracy.

7.5.3. Electron Densities observed by Thomson Scatter

The electron density profiles measured by the Thomson scatter technique at Malvern (Taylor 1969) during the early morning of the 11th April 1969 and reproduced in figure 7.5.4. have a lower limit of 95 km below which the experimental results are unreliable. It was therefore necessary to extrapolate these profiles to lower heights in order to obtain a complete representation of ionospheric conditions. Two of the Thomson Scatter profiles were fitted to Smith (1966) D region models by the four different extrapolations illustrated in figure 7.5.9. and also to the Deeks (1966) sunrise model included in the figure. The two sets of five profiles produced were used in the derivation of virtual heights for a number of frequencies and these results are presented in table

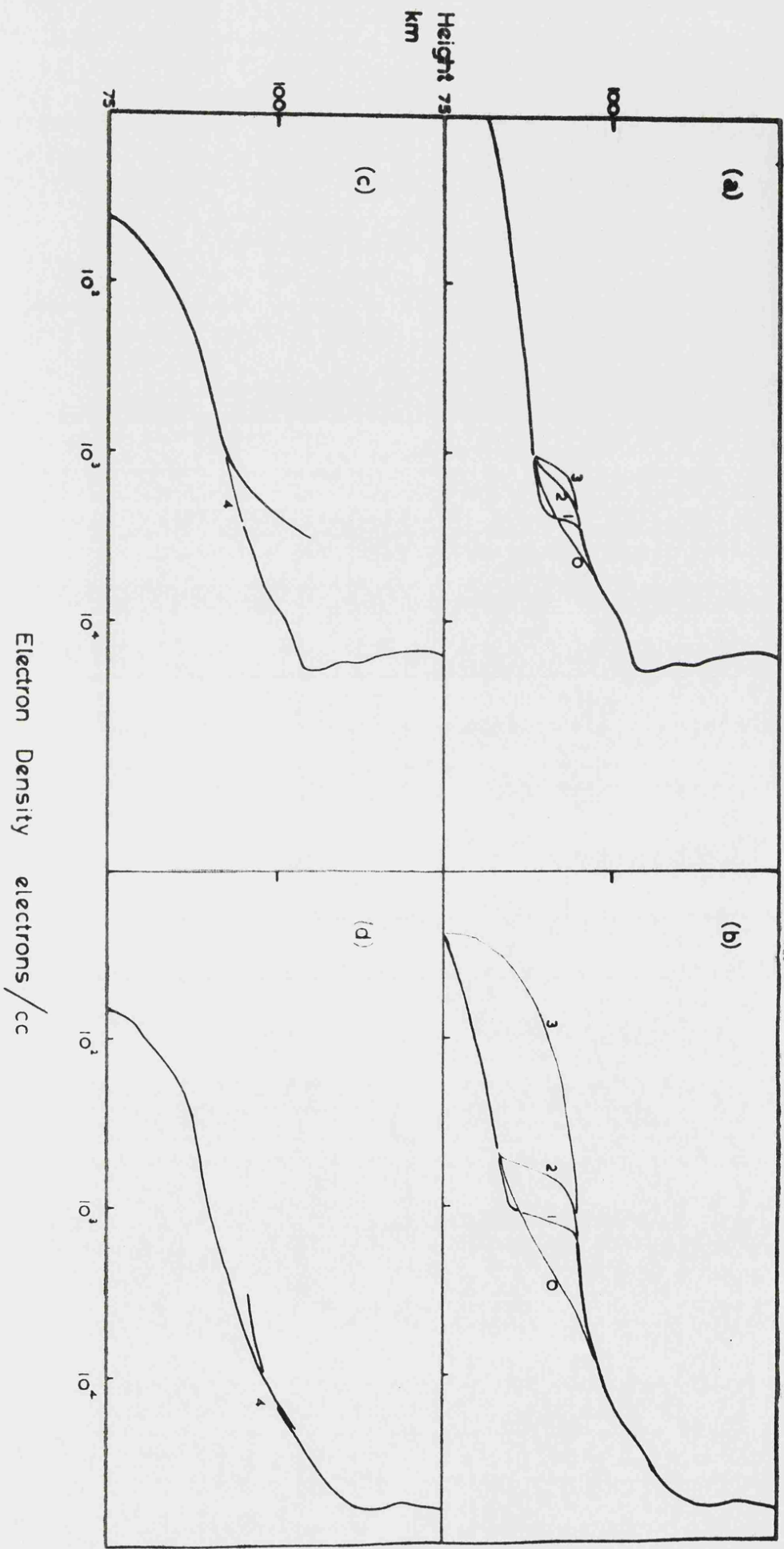


FIG. 7.5.9 Model extrapolations from Thomson Scatter profiles to (a) and (b) Smith (1966) D region model, (c) and (d) Deeks (1966) D region

(a)

Frequency MHz	Virtual Height km				
	0	1	2	3	4
1.5	224.88569	224.86167	224.82624	224.81805	224.80153
1.6	381.53394	381.52253	381.48660	381.47510	381.45576
1.7	272.98932	272.97061	272.94241	272.93247	272.91484
1.8	240.16102	240.14659	240.11987	240.11044	240.09359
1.9	236.25232	236.23428	236.21322	236.20716	236.19059
2.0	239.66212	239.64703	239.62820	239.62267	239.60870
2.1	243.00066	242.98841	242.96704	242.96096	242.94945
2.2	244.71803	244.70806	244.68784	244.68188	244.66891
2.3	245.71449	245.70461	245.68540	245.67930	245.66816
2.4	247.16172	247.15168	247.13507	247.13029	247.12003
2.5	251.75190	251.74237	251.72685	251.72229	251.71090

(b)

1.5	115.11745	115.02150	114.98657	114.94394	115.10098
1.6	115.78908	115.69699	115.66247	115.61931	115.76649
1.7	116.54074	116.46311	116.43208	116.39613	116.51702
1.8	119.91632	119.84615	119.81846	119.78630	119.89620
1.9	121.91770	121.85445	121.82537	121.78687	121.89283
2.0	123.10932	123.04113	123.01650	122.98878	123.08997
2.1	132.26923	132.19940	132.17827	132.15025	132.24967
2.2	136.90139	136.85638	136.83586	136.80886	136.88520
2.3	199.32363	199.29221	199.26233	199.24380	199.30958
2.4	342.62965	342.58337	342.56535	342.54850	342.61758
2.5	293.91932	293.85133	293.83479	293.81888	293.90112

Table 7.5.1 Virtual Height calculated from the profiles of fig.7.5.9. representing variations upon the Thomson Scatter profiles for
(a) 0529h ,and (b) 0632h 11th April 1969.

7.5.1. The first profile, observed at 0529 h, gives virtual height data representing only F region reflections and the agreement obtained between the various D region models and extrapolations was better than 100 meters at all frequencies observed. The second profile recorded at 0632 h displays E region reflections up to 2.3 MHz and the virtual heights obtained from the different models agree to within 200 meters. Thus it can be concluded that the effect of the shape of the D region model and its extrapolation to the E region has very little effect upon the calculated virtual heights, the variation being very much less than the errors involved in the direct observation of virtual height. In the present study the Thomson Scatter profiles were linked to Smith (1966) D region models for corresponding zenith angles by smoothly matching the gradients at the extremities of the two curves as illustrated by the models marked '0' in figure 7.5.9.

The virtual height was computed as a function of frequency by means of the Phase Integral analysis (Chapter 3) and the results are presented in figure 7.5.8. The calculations were first made at intervals of 0.05 MHz but as the complexity of the distributions became evident additional points were computed to clarify the detailed cusp structure. The resulting $h'(f)$ curves of figure 7.5.8. display extensive fine structure consisting of several major cusp structures often accompanied by other smaller irregularities either in the form of cusps or regions of increased group retardation without the formation of a discontinuity. The sharp cusp predicted at 1.6 MHz by the 0529 h profile shows a large increase in the group retardation over a comparatively small frequency range and corresponds on the electron density profile of figure

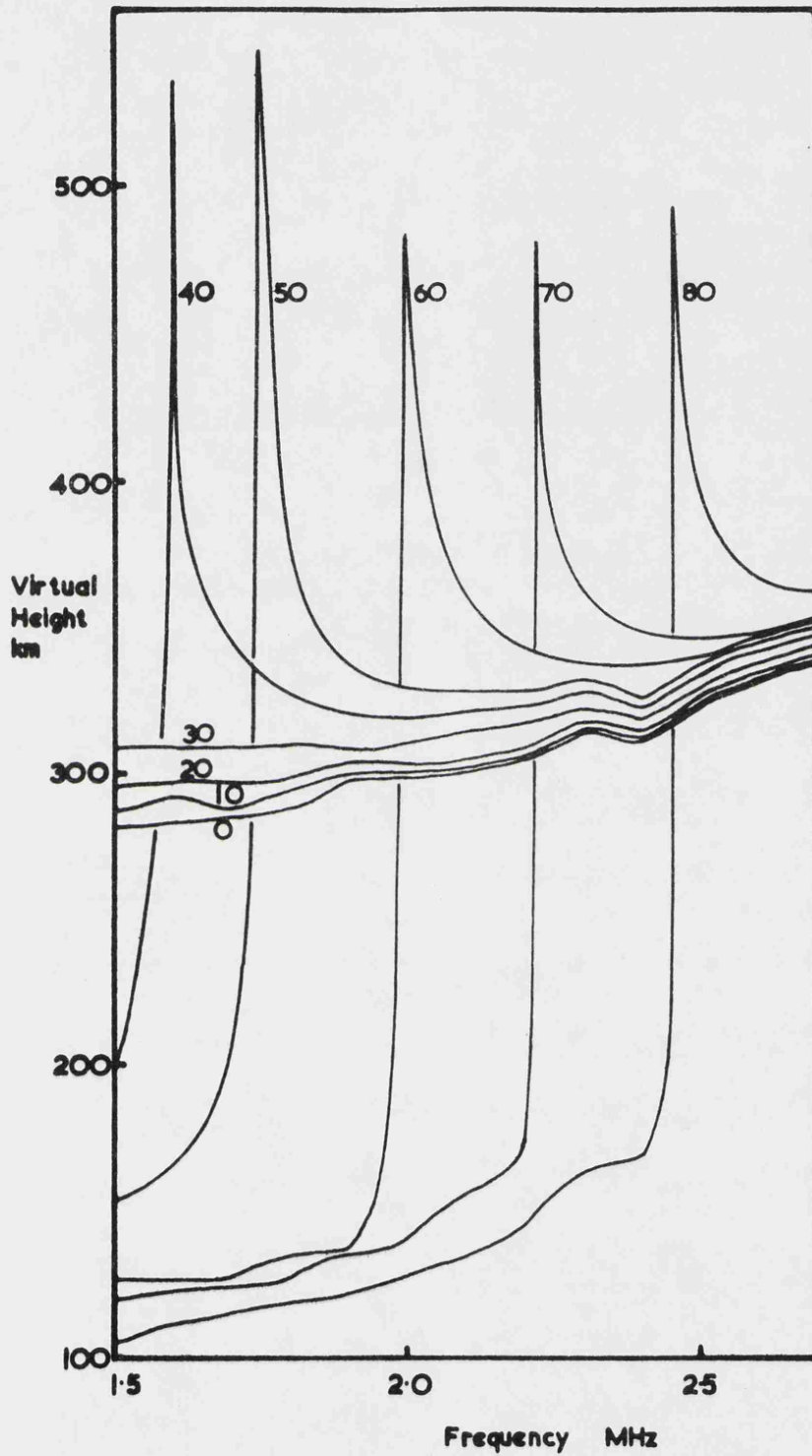


FIG. 7.5.5 $h'(f)$ curves computed from the theoretical models illustrated in fig. 7.5.1

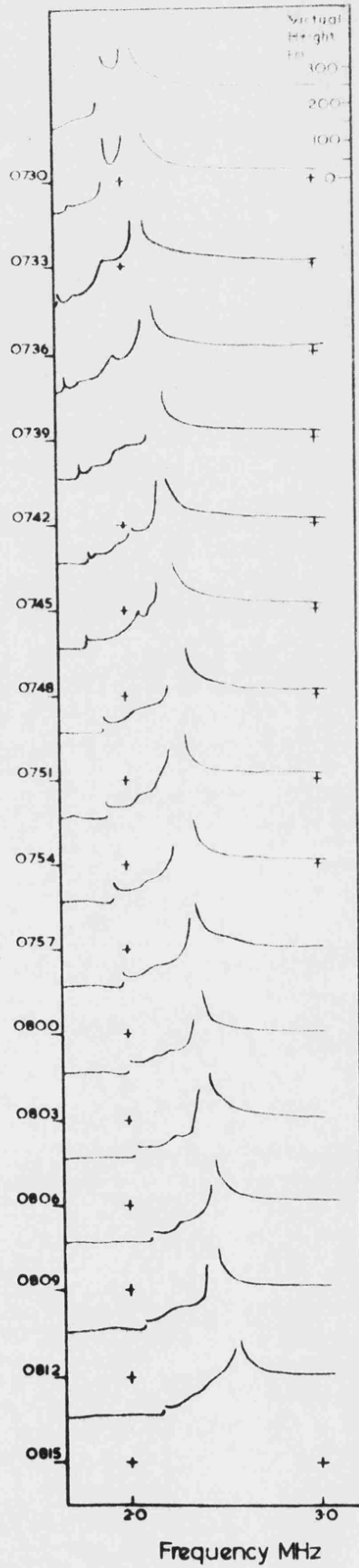


FIG.7.5.6 (a) Continuous Ionogram records for 26.2.69

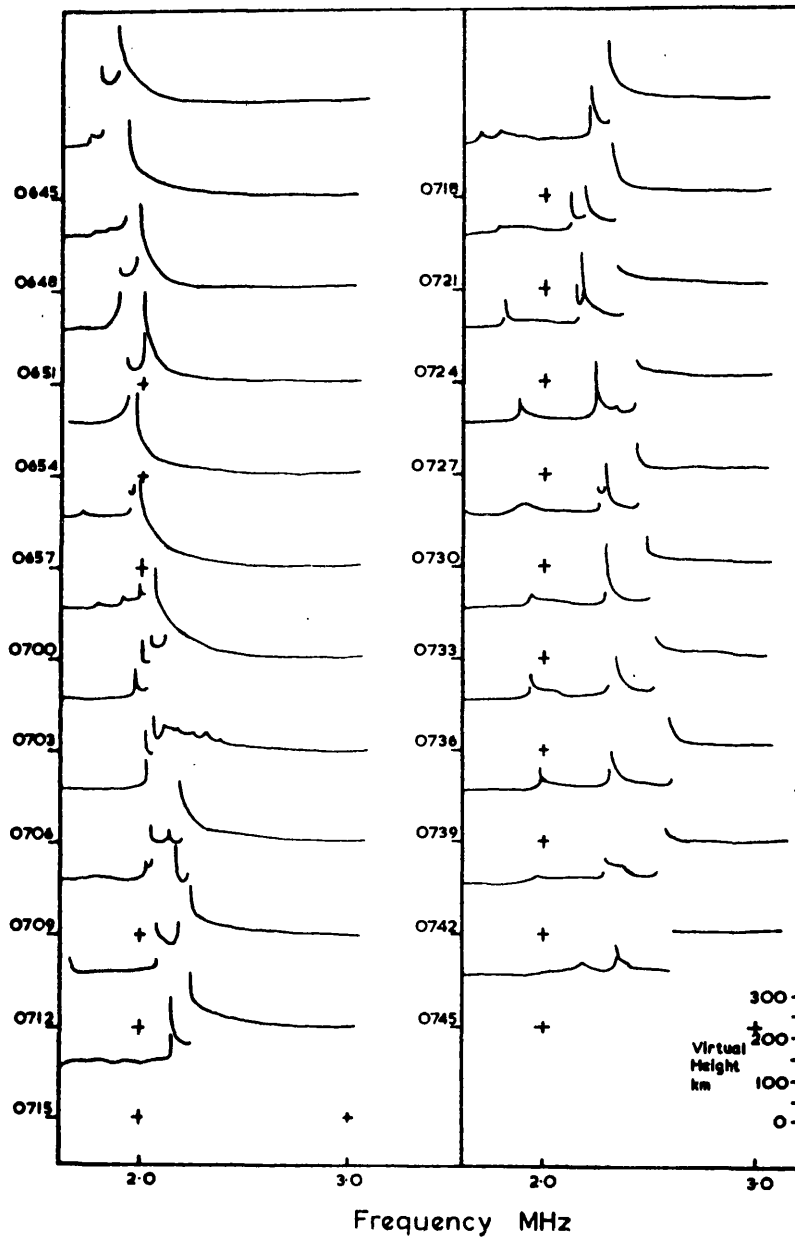


FIG.7.5.6 (b) Continuous Ionogram records for 13.3.69

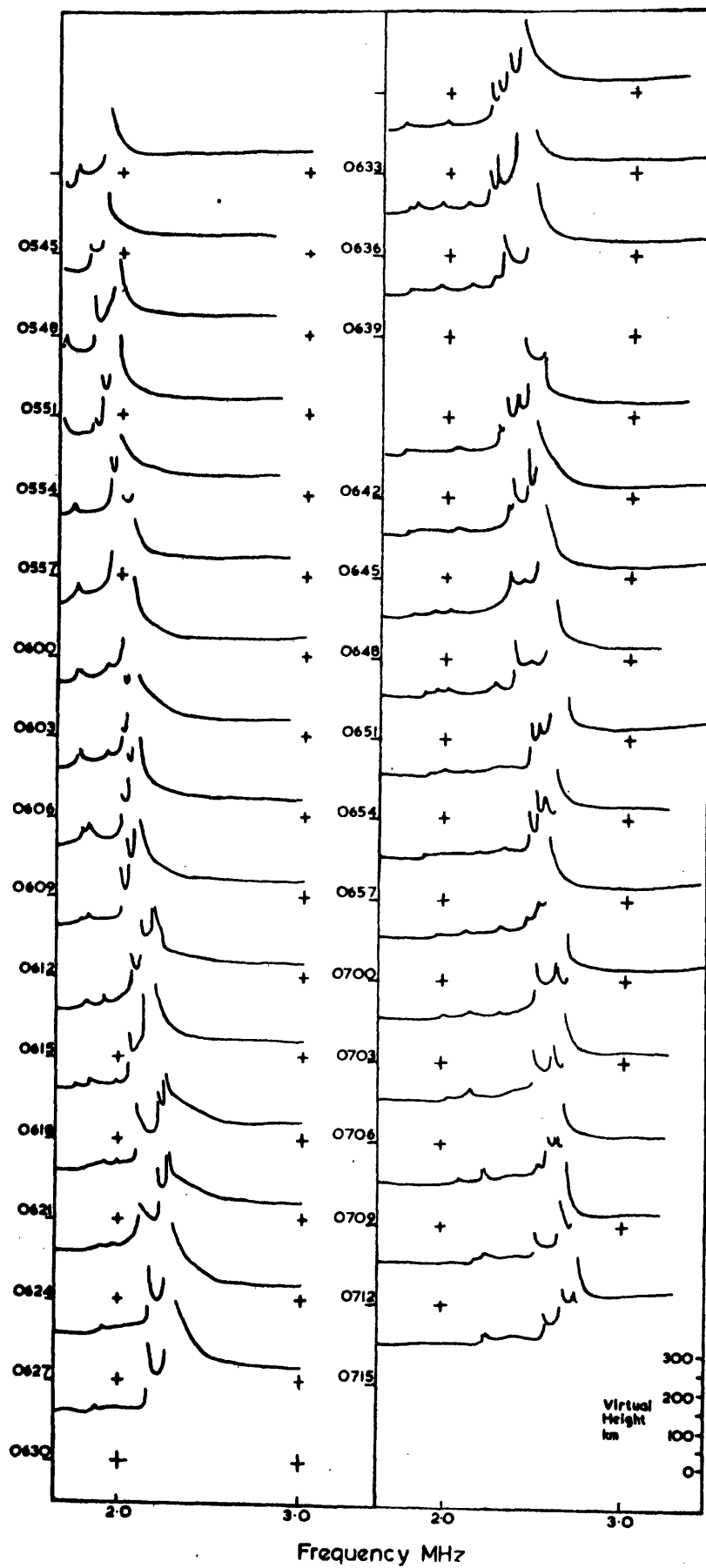


FIG.7.5.6 (c) Continuous Ionogram records for 10.4.69.

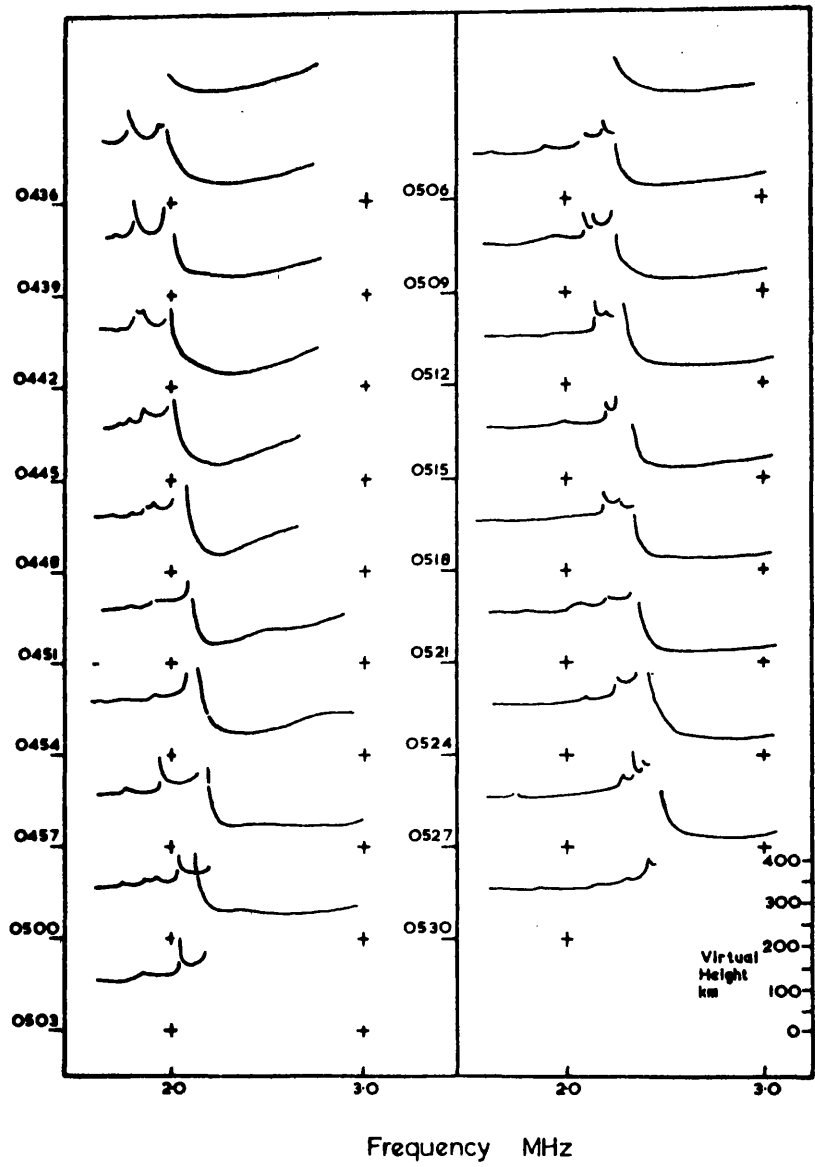


FIG.7.5.6 (d) Continuous Ionogram records for 21.5.69.

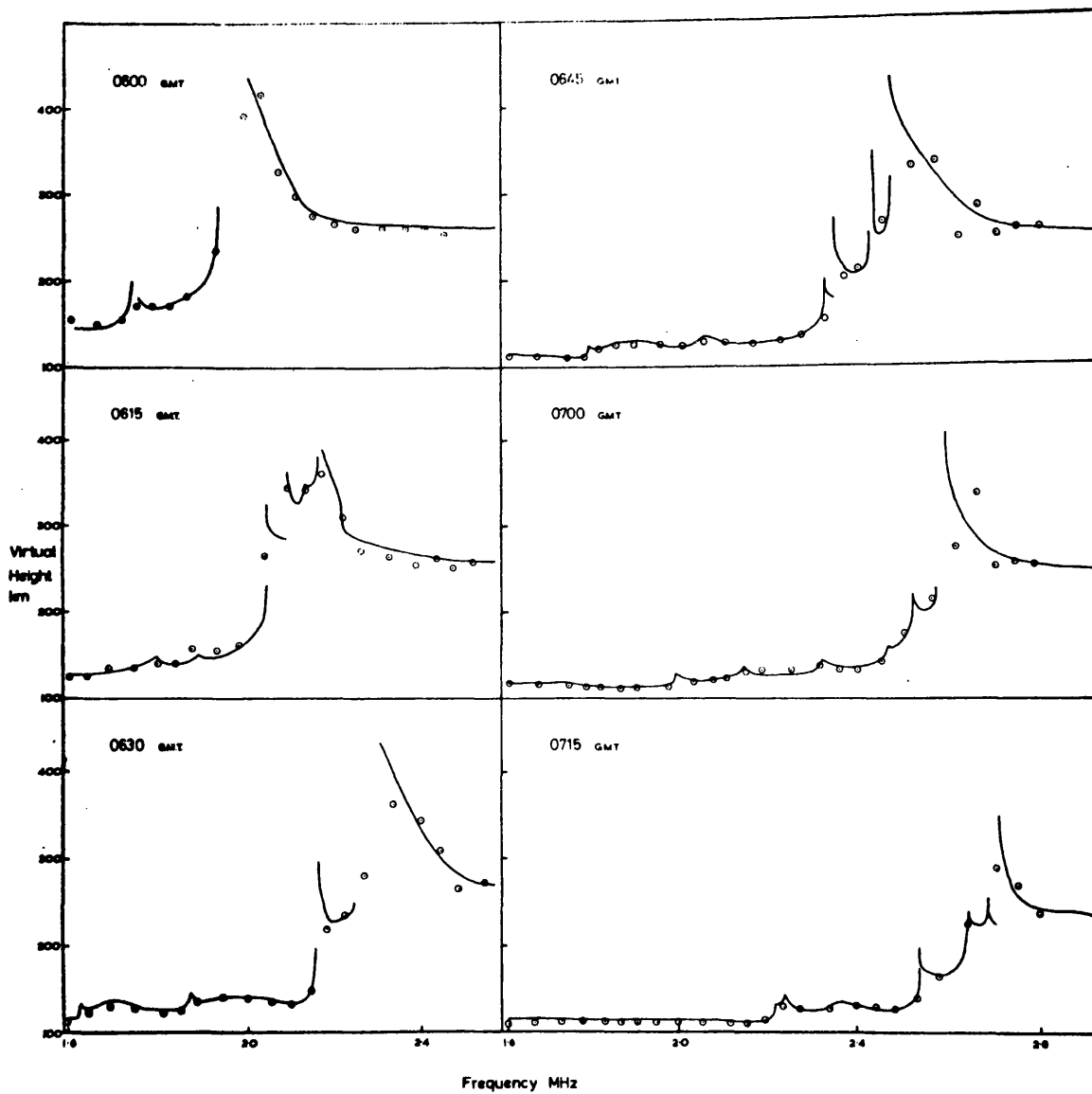


FIG.7.5.7 $h'(f)$ computed from the Leicester monotonic profiles compared with the original ionogram.

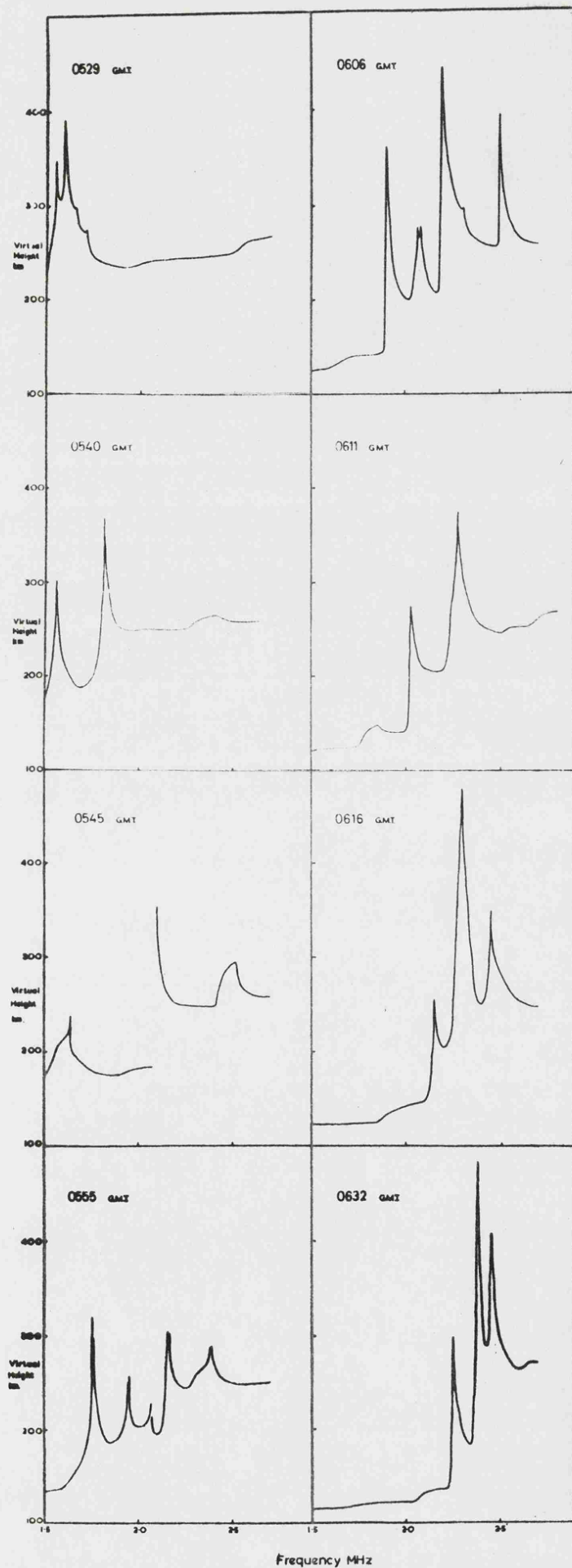


FIG.7.5.8 $h'(f)$ curves computed from the Thomson Scatter profiles for 11th April 1969.

7.5.4. to a region in which the electron density is almost constant with height. This observation is in agreement with the theoretical observations made in section 7.4. Similarly the increase in group retardation observed around 2.5 MHz on the $h'(f)$ curve for 0545 h is associated with a gradient change in the corresponding profile of figure 7.5.4. and may be compared with the distorted 'cusp' regions shown in figure 7.4.12. The sharp layer illustrated on the 0545 h profile at 150 km produces the rapid increase in group retardation with very little curvature on the low frequency side, a characteristic of a sporadic E layer. Furthermore, since this layer does not appear on the 0540 h curve and has all but disappeared on the 0555 h profile, it must be recognised as a minor high sporadic E layer. Several other 'sporadic E' type cusps have been observed and these are considered to be due to the presence of highly localised sharp peaks in the electron density distribution. Such structures are a very marked feature of the transition region as measured by the Thomson Scatter technique.

7.6. Comparison of the virtual height profiles for the post sunrise period

The variation of virtual height with frequency calculated from the electron density profiles computed at Leicester were found, in section 7.5.2., to agree very well with the observations. This agreement has been illustrated in figure 7.5.7. which presents the data for the 10th April 1969. Further calculations have been described in the previous sections in which the theoretical profiles derived by Bourne, Setty and

Smith and the Thomson Scatter profiles have been used to obtain the virtual height variation. These results have been presented in figures 7.5.5. and 7.5.8. respectively. The Bourne, Setty and Smith profiles have been constructed at Armidale (30.5° S) to represent midsummer conditions in temperate latitudes. However the Thomson Scatter and Leicester profiles used in this comparison describe approximately equinox conditions in temperate latitudes.

The reproduction of extensive fine structure on virtual height data computed from the Thomson Scatter and Leicester profiles is in general agreement with the observed conditions illustrated in figure 7.5.6. However the virtual height curves, derived from the Bourne, Setty and Smith models and presented in figure 7.5.5, display a single well defined cusp accompanied by small undulations. This disagreement with the observed virtual height variation will be discussed further in the next section.

It is noticeable that although the virtual heights calculated from the Thomson Scatter profiles give similar fine structure patterns to those observed on ionograms, the fine detail is often more marked than on the ionograms. This may be due to small errors in the interpretation of the ionogram traces. During the scaling of ionograms the appearance of 'off vertical' reflections, broadcast interference bands and signal fading often render the records difficult or even impossible to read accurately. Thus some fine detail may have been omitted from the ionogram tracings as a result of misinterpreting these features as being due to one of the three interfering factors listed above. This observation is further

illustrated by the comparison of the structure of the lower F layer trace in figures 7.5.7. and 7.5.8. The extreme complexity often observed in this part of the ionograms has been approximated, in figure 7.5.7, by a single trace of fairly low negative gradient. However, the results represented in figure 7.5.8. sometimes display small cusps or undulations in this region. It is noticeable, especially in the first curve in each figure, that if this F layer fine structure were neglected the resulting trace would have a gradient very similar to that observed on the ionogram.

In addition to the fine structure discussed above, the F region virtual heights represented in figure 7.5.8. display a far more disturbed variation with frequency than is observed on ionograms. These undulations in the curve are considered to be the result of decreased definition above 160 km on the Thomson Scatter profiles since the data points were spaced at 3 km below this height and at 6 km above. The increased spacing in conjunction with the logarithmic interpolation procedure could lead to small bulges in the profile between data points and hence undulations in the computed virtual height variation.

The electron density profile observed at Malvern at 0606 G.M.T. 11th April 1969 has been used to compute the virtual height variation with frequency which is presented together with the ionogram observed in Leicester at 0600 h on the same day in figure 7.6.1. This time difference is considered to be responsible for the displacement between the curves on the frequency scale. Reference to figure 7.2.3.(b) indicates that at this time of year the time difference would result in a frequency movement of the cusps of approximately

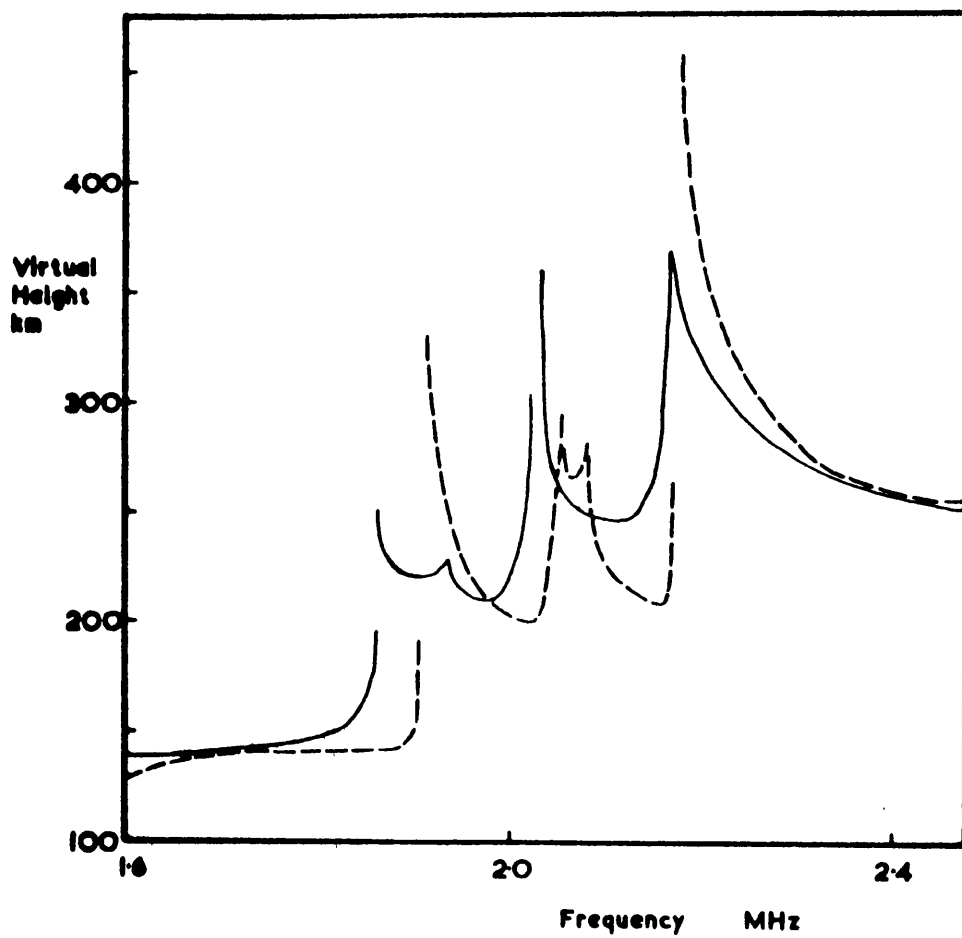


FIG. 7.6.1 Comparison of observed virtual heights and those computed from a Thomson Scatter profile
 — Leicester Ionogram 0600 11.4.69
 --- Thomson Scatter 0606 11.4.69

100 kHz. The movement observed in the highest cusp in figure 7.6.1. was 100 kHz while that of the other two cusps has been exaggerated by modification of the cusp shape. This modification results from changes in the electron distribution due either to the time difference or to the different observing location. Following the discussion of section 7.5.2. changes of this kind could take place in this period of time. The difference in location, 87 km, may also lead to such changes since small modifications in the electron density profile can give rise to appreciable distortion of the virtual height curve. Although the minor structure has changed between the two curves in figure 7.6.1. the main features, two intermediate traces, are reproduced on both. Thus it can be concluded that not only are the gross features producing ionogram structure maintained over the period of six minutes but are also features of the ionosphere over a distance of at least 87 km.

It has been found that the Thomson Scatter profiles give virtual height variations which agree well with those observed directly at Leicester. Furthermore, it is concluded that the difference in fine detail results from the limited accuracy of the ionogram interpretation. It is reasonable to assume that since the computed virtual heights are obtained from a single well defined electron density profile they should show more fine detail than the direct observations which are necessarily the result of illuminating a considerable region of the ionosphere and recording the accumulative signals from many reflection paths. The theoretical profiles constructed by Bourne, Setty and Smith do not predict virtual height variations in agreement with those observed. This may

be a direct result of the choice of the residual presunrise electron distribution. This point will be discussed in the next section.

7.7. Comparison of the true height profiles for the post sunrise period

The true height profiles which have been employed in the calculations of virtual height discussed in the previous section will now be compared. The three sets of profiles obtained theoretically by Bourne, Setty and Smith and experimentally at Leicester and at Malvern have been presented in figures 7.5.2, 7.5.3 and 7.5.4. respectively.

Considering first the Thomson scatter profiles for 11th April 1969, figure 7.5.4, and those derived from ionograms observed at Leicester for the 10th April 1969, figure 7.5.3, two marked differences have been noted. Firstly the Leicester profiles, being monotonic, display little of the fine layer structure which is such a noticeable feature of the Thomson Scatter profiles. Secondly a considerable discrepancy exists between corresponding profiles in the height range 100-130 kms. Figure 7.7.1 represents the change in the reflection heights of various frequencies with time as indicated by the two sets of profiles. The reflection height of 2.5 MHz remains comparatively high during the period represented by the figure and the predictions of the two profile sets agree fairly well. However, the curves for 1.6 and 2.0 MHz show a difference in their heights of reflection of about 20 km. This point has been further illustrated in figure 7.7.2. in which the Thomson Scatter profile for 0606 11th April 1969

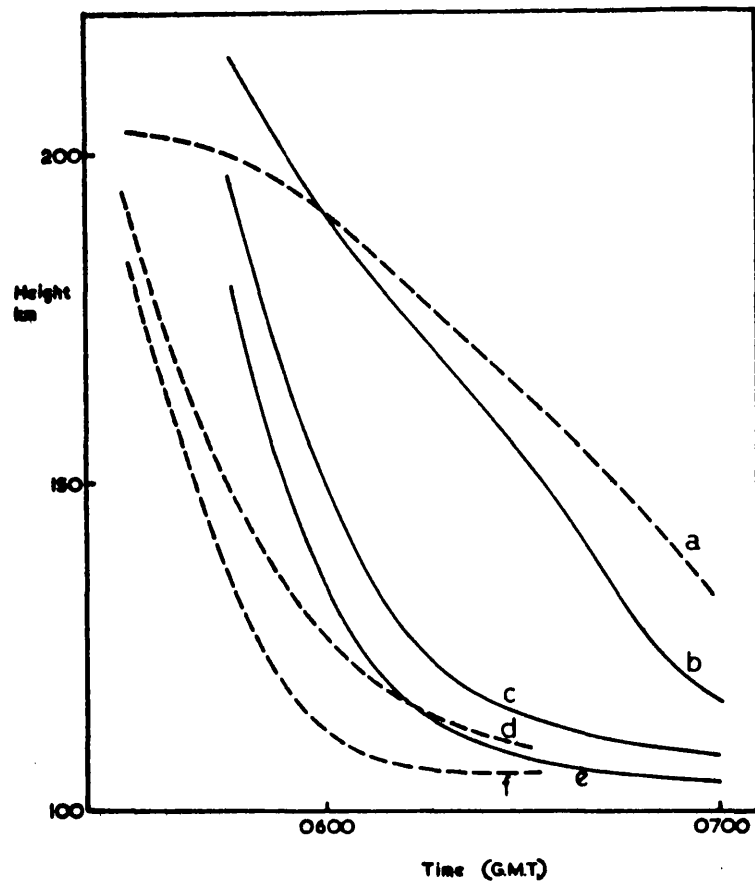


FIG. 7.7.1 Variations of height of reflection with time
 (a) Thomson Scatter profile, frequency 2.5MHz
 (b) Leicester profile 2.5MHz
 (c) Leicester profile 2.0MHz
 (d) Thomson Scatter profile 2.0MHz
 (e) Leicester profile 1.6MHz
 (f) Thomson Scatter profile 1.6MHz

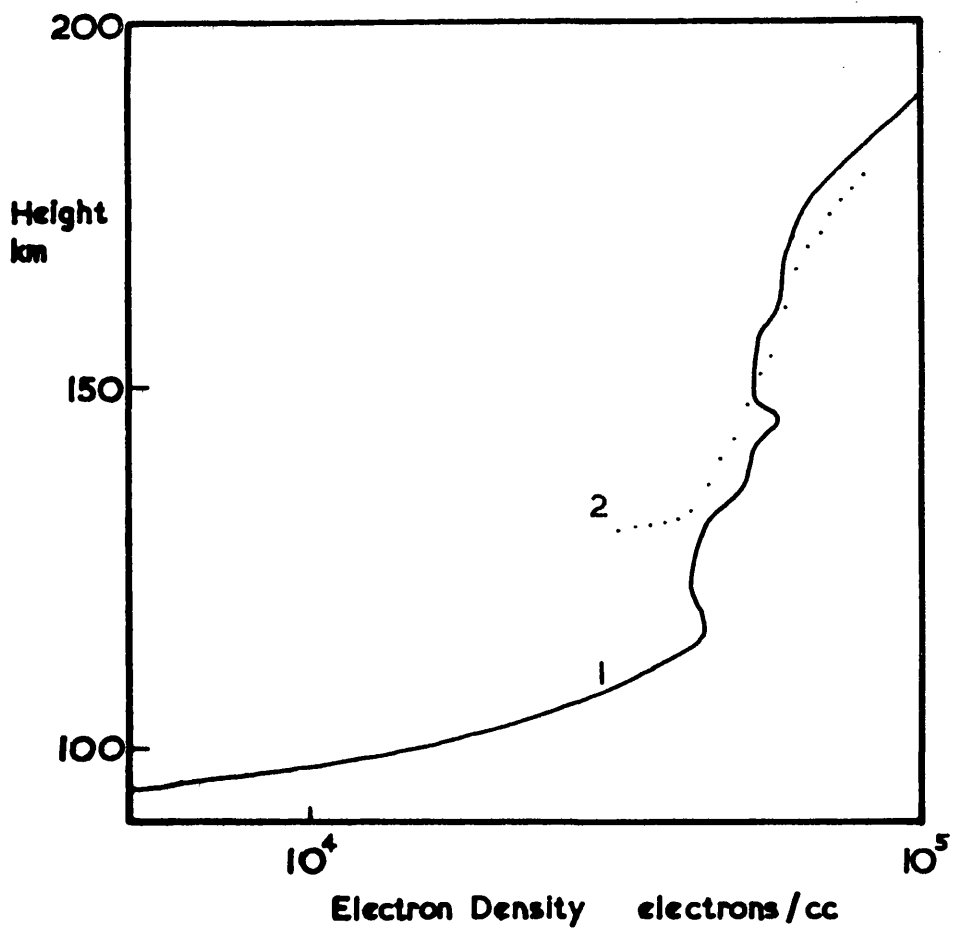


FIG. 7.7.2 Comparison of the monotonic electron density profile computed for 0600 11th April 1969 with the Thomson Scatter profile for 0606h on the same day
 (1) — Malvern (2) Leicester

and the profile computed at Leicester for 0600 on this day have been presented. The discrepancy is clearly marked and is 21 km for an electron density of 3.2×10^4 electrons/cm³. Consideration of the Thomson Scatter profiles of figure 7.5.4. shows that the almost constant ionization growth rate between 100 and 170 km could result in considerable ionization existing below the reflection height of 1.6 MHz, the lowest frequency recorded on the Leicester ionograms. This frequency corresponds to a plasma frequency of 3×10^4 electrons/cm³. The neglect of such ionization in the computation of the electron density profile by the Titheridge analysis (Chapter 3) would lead to appreciable errors in the low density section of the profile. However figure 7.7.2. also illustrates the agreement between the profiles above 130 km. This suggests that although the neglect of ionization less than 3×10^4 electrons/c.c gives rise to appreciable errors below the E layer peak, the monotonic profile may not be excessively in error above 130 km.

The uniform development of the transition region, 110-170 km, predicted by the Thomson Scatter profiles and supported to some extent by the computed Leicester profiles is in contrast to that predicted by the Chapman theory as presented by Bourne, Setty and Smith, figure 7.5.2. Two major differences in the growth pattern are noticeable from a comparison of the profiles of figure 7.5.2 and 7.5.4. The theoretical models show an initial growth in ionization density between 150 and 220 km which is later overtaken by the growth at E region heights, 100-120 km. The night time model used by Bourne, Setty and Smith (figure 7.5.2.) has been replaced by the Thomson Scatter profile recorded at 0519 11th April 1969 (7 minutes before

ground sunrise) in the construction of the profiles in figure 7.7.3. from the production curves presented in figure 7.5.1. A comparison between the profiles of figures 7.7.3 and 7.5.4 illustrates the inadequacy of the theoretical analysis. The initial increase in electron density above 150 km results in the persistence of the marked valley between 103 and 140 km for approximately 40 minutes in contrast to the growth predicted by the Thomson Scatter observations in which this valley has almost disappeared within 10 minutes. Furthermore the profiles of figure 7.7.3 indicate the formation of a re-entrant region above 150 km at approximately 40 minutes after sunrise. However none of the Thomson Scatter profiles considered show an extensive re-entrant region.

In the previous section the choice of a night time electron density model on which to base the Bourne, Setty and Smith profiles was mentioned as a possible source of error in producing representative profiles. The results discussed above have shown that, if an observed electron density distribution is employed as the basis for this theoretical approach, the derived profiles deviate greatly from those observed by experiment.

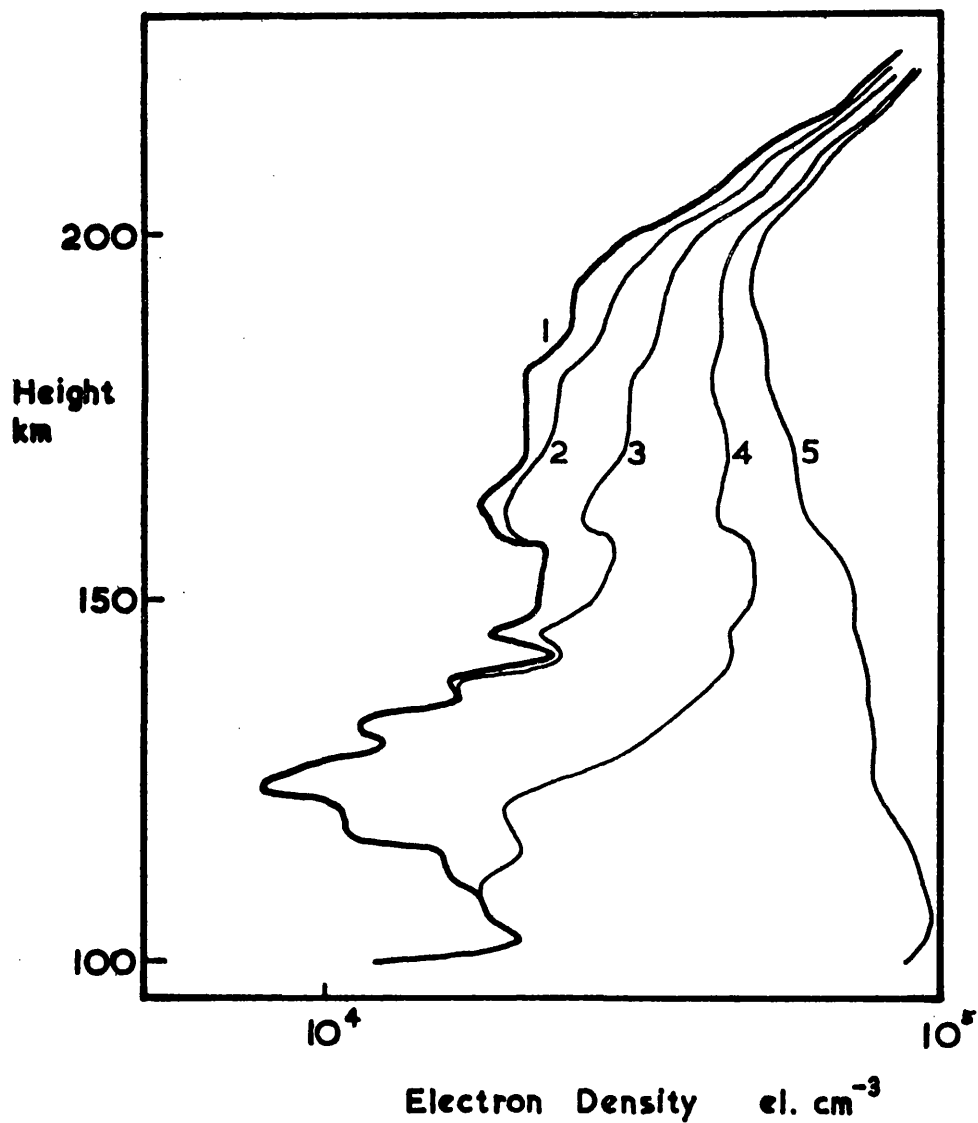


FIG. 7.7.3 Theoretical sunrise profiles based upon a pre-dawn Thomson Scatter profile

(1)	Thomson Scatter profile for 0519 h
(2)	10 minutes after sunrise
(3)	20 " " "
(4)	40 " " "
(5)	60 " " "

Chapter 8

The variation of Absorption and Virtual Height of a fixed frequency following sunrise

8.1. Introduction

In the previous chapter the variation of the virtual height with sounding frequency has been discussed. Attention is now given to the variation of the virtual height of reflection and absorption of a fixed frequency with time during the early morning growth of the ionosphere. The observation of these parameters, made on 2.05 MHz and later on 2.266 MHz as described in Chapter 6, will be considered in detail and compared with the computed variations obtained from the Bourne, Setty and Smith (1964) theoretical models, the monotonic electron density distributions derived from the Leicester ionograms and the Thomson Scatter profiles measured at Malvern. Various models of the lower ionosphere, which include the D-E transition region, have again been used to extend the various distributions, and the composite models are employed in conjunction with the Phase Integral programme to compute the absorption and virtual height for the frequencies employed in the experimental work. Thus an estimate is made of the part played by the low lying ionization in determining the absorption and virtual height of frequencies reflected by the E layer and the E-F transition region. In addition, the variation of the absorption with frequency has also been computed from the three sets of profiles and these results

are also included in this chapter. Special reference will be made to the observations for the 11th April 1969 since this is one of the few days on which data from both Leicester and Malvern was available.

8.2. Simultaneous observations of absorption and virtual height at a fixed frequency

The variations of both absorption and virtual height during the hours following the ground sunrise were recorded on 42 days between February and June 1969. Four typical records are presented in figure 8.2.1. and the record for the 11th April 1969 in figure 8.2.2. In studying these observations it is convenient to consider the amplitude and virtual height results separately.

8.2.1. Variation of virtual height with time

Figure 8.2.1. illustrates four typical variations of virtual height with time. In each case the movement of the reflection height of the fixed frequency from the F to the E region is typified by fine structure on the record, similar in form to that already described for the ionogram observations. This fine structure is particularly noticeable in figure 8.2.1(d) in which the virtual height increases to a discontinuity at 0440 G.M.T., thus producing a cusp like structure. This is followed closely, as time progresses, by several smaller features preceding the appearance of the regular E region reflection. Figure 8.2.1(b) clearly shows the characteristic cut off of the higher reflection by a developing sporadic E layer. The two remaining sections of the

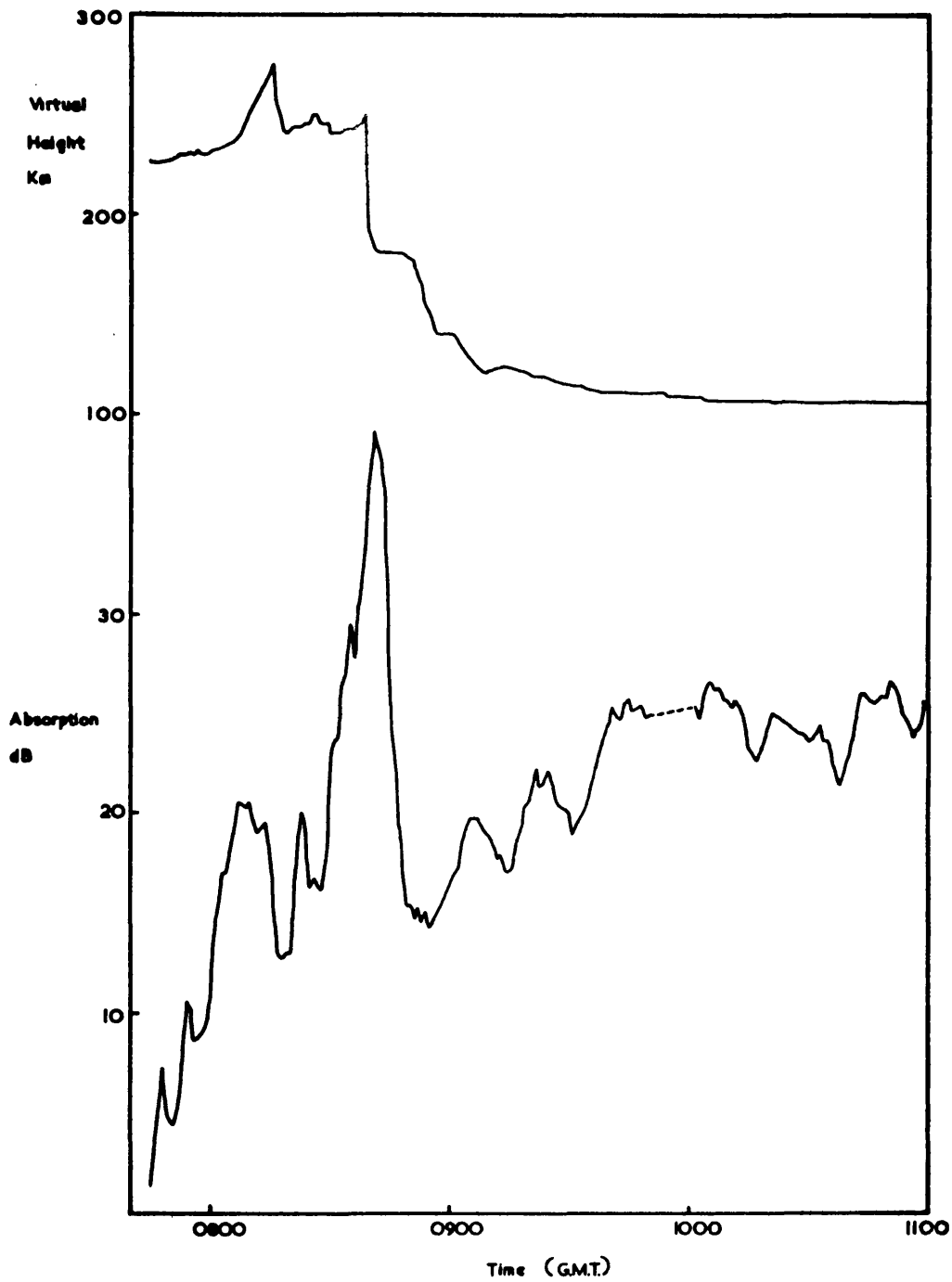


FIG. 8.2.1(a) Experimental observations of virtual height and absorption of 2.05MHz on 5th February 1969

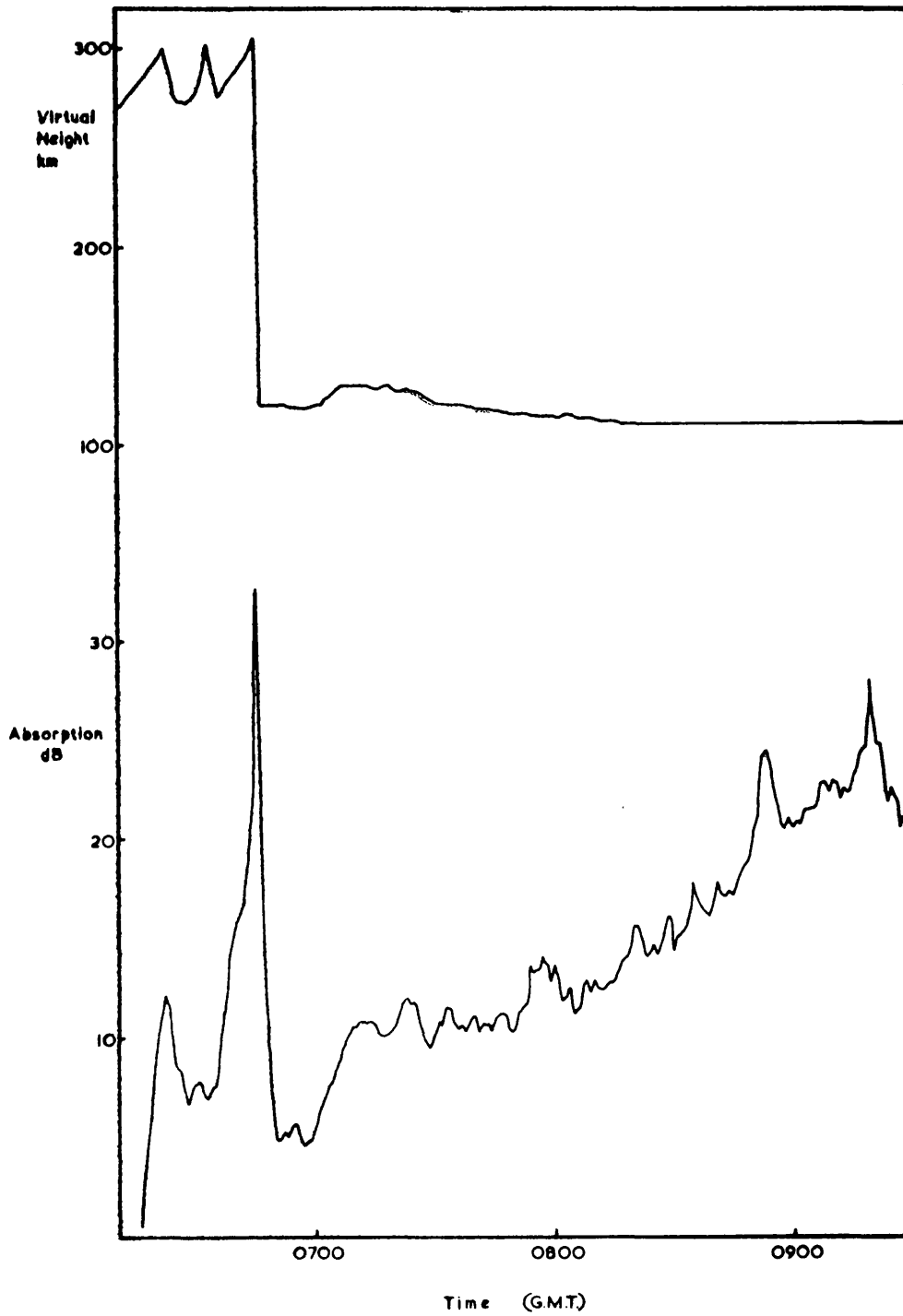


FIG. 8.2.1(b) Experimental observations of virtual height and absorption of 2.05MHz on 19th March 1969

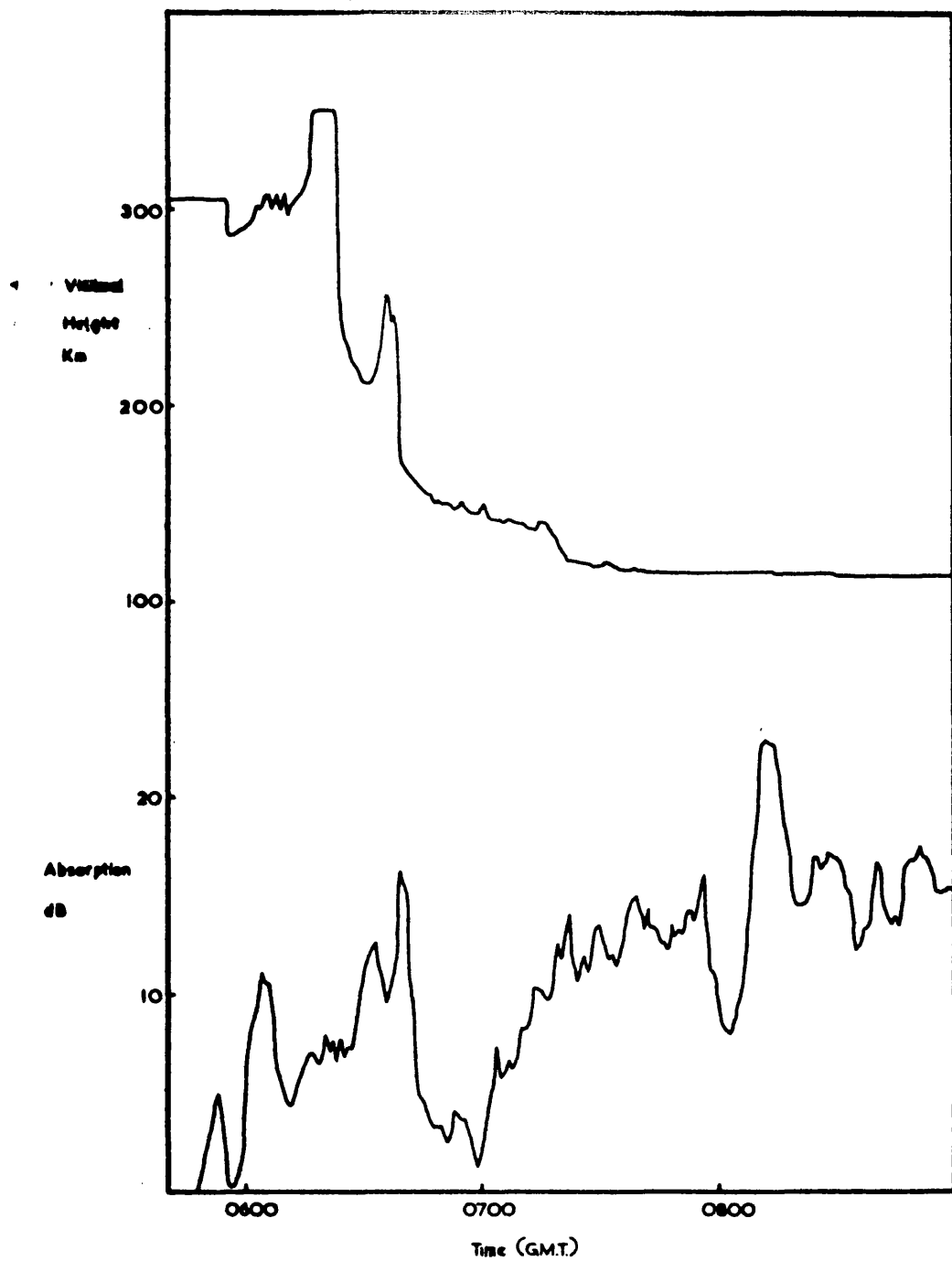


FIG. 8.2.1(c) Experimental observations of virtual height and absorption of 2.05MHz on 1st April 1969

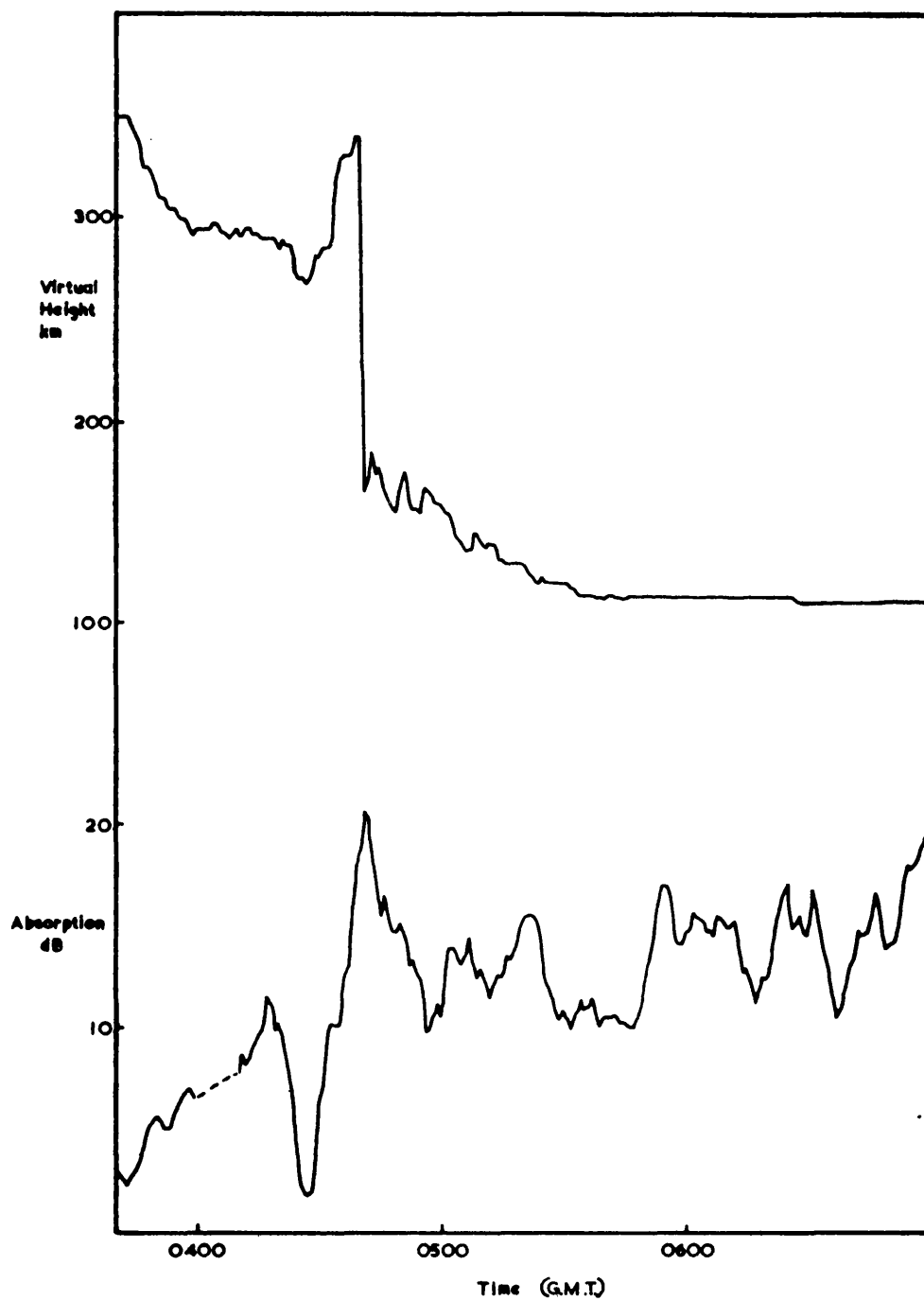


FIG. 8.2.1(d) Experimental observations of virtual height and absorption of 2.266MHz on 16th June 1969

figure illustrate a distinct intermediate trace similar to those seen on the ionograms of figure 7.2.1. The intermediate trace represented in figure 8.2.1(a) exhibits no appreciable increase in the group retardation prior to the movement of the reflecting height to the E layer. This suggests a filling in of the electron density profile rather than a fall in the reflection level to another maximum in the N(h) profile.

The solar zenith angle (χ) was determined for those times at which the change in reflection level from the F layer to a lower region was clearly marked. An appreciable day to day variation of these χ values is evident from figure 8.2.3. For comparison, the Zurich sunspot number and the horizontal component of the earth's magnetic field are also included in the figure although no marked correlation is evident between these parameters and the 'change over' zenith angle values.

The variation in this 'change over' time could be attributed to three factors; fluctuations of the growth rate of the transition region, redistribution of the ionization by drifts or the variable extent of the nocturnal ionization in this region. The major sources of ionization at these heights during daylight hours are known to be solar X radiation in the wavelength band 10-200 Å and E.U.V. 800-1100 Å. If changes in these radiations were to produce this phenomenon some correlation with sunspot number would be expected. No correlation can be detected. In confirmation of this observation it is well known that E.U.V. radiations are very stable even during flares and that the changes in the 10-100 Å x ray spectrum are very much less than those observed in the 1-10 Å range resulting in the great stability of the E layer

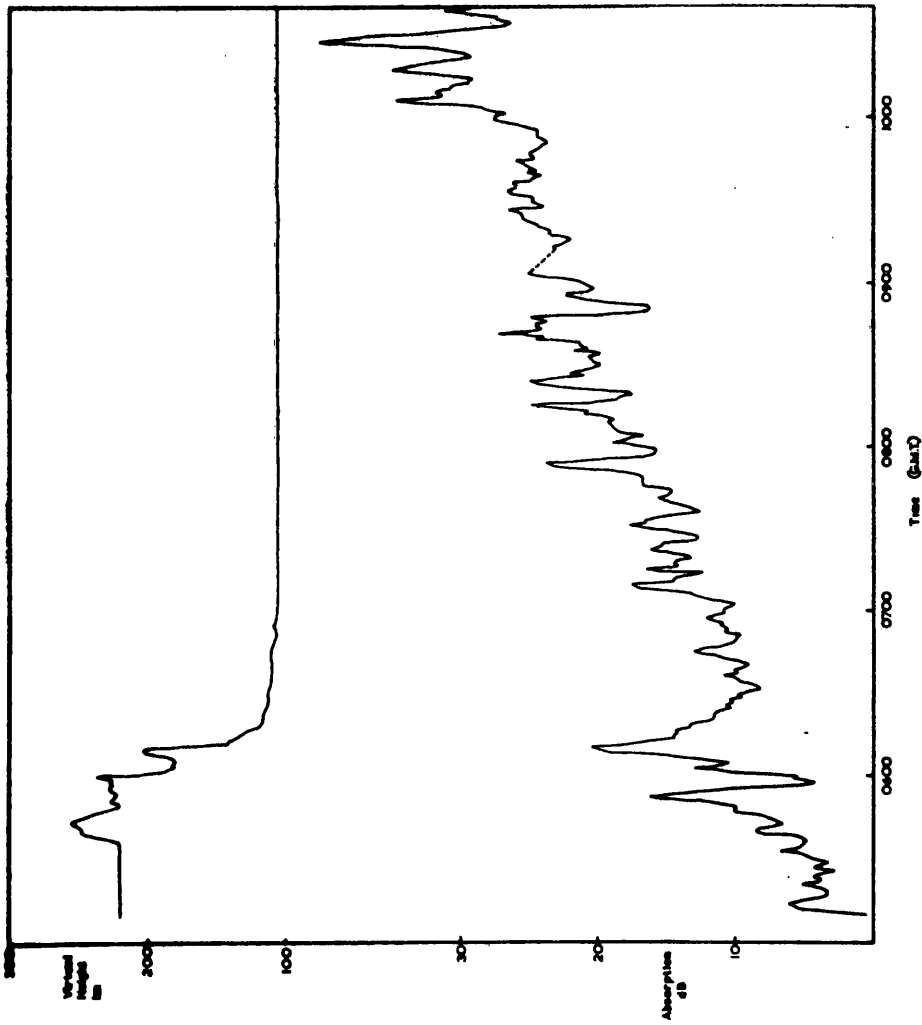


FIG. 8.2.2 Experimental observations of virtual height and absorption of 2.05MHz on 11th April 1969

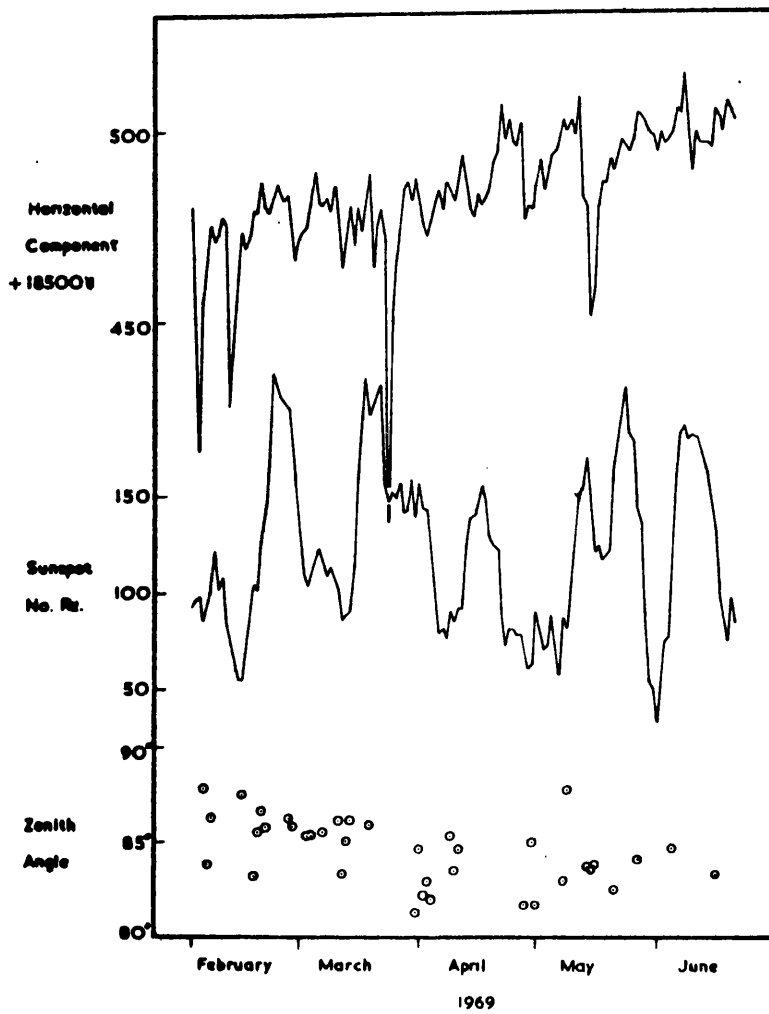


FIG.8.2.3 'Change over' zenith angle against sunspot number and the horizontal component of the earth's magnetic field.

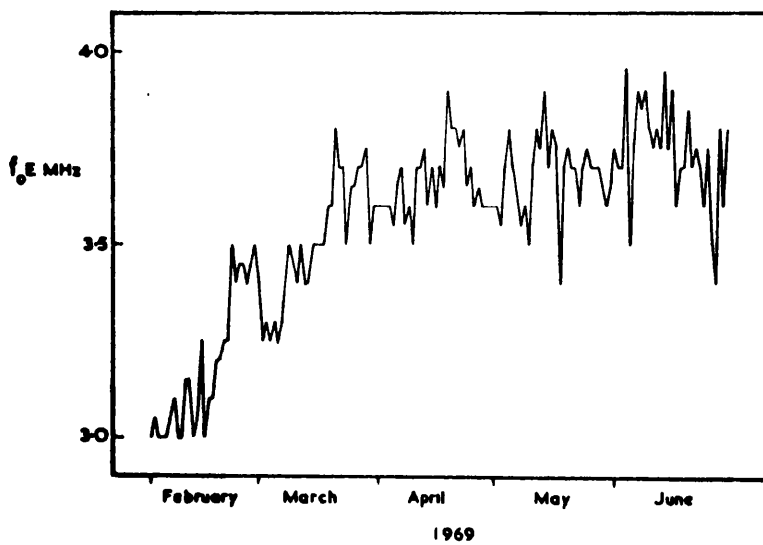


FIG.8.2.4 The variation of f_0E from day to day.

with respect to solar activity, even during flare conditions.

8.2.2. Variation of Absorption with time

The variation of the absorption with time, as typified by the curves of figure 8.2.1., displays periods of enhanced absorption which correspond closely to the cusp like features in the virtual height curves. As discussed in Chapter 6 the measurement of absorption is complicated by the presence of fading; this has been minimized for the data of figure 8.2.1. by taking 5 minute running means of the measured values. Following Piggott (1953), this analysis reduces the effects of fast fading to a minimum while giving a clear indication of the short term changes in absorption which occur in intervals similar to the quasi-period of the slow fading. The change from F region reflections to those from lower layers will, however, not produce such an abrupt change in the running mean absorption as was the case in h'_{p} . Nevertheless, the absorption curves do show the effect of various forms of reflecting layer. For example, figure 8.2.1(b) illustrates very clearly the effect of the imposition of a sporadic E layer on the absorption of the radio pulse initially reflected from the F layer. Several records, similar to that illustrated in figure 8.2.1(d), show that the absorption on frequencies reflected below the F region is maintained at an abnormally high level for periods in excess of 20 minutes following the layer change. This effect has been attributed to the occurrence of reflections from fine undulations in the electron density distribution near the E layer peak which may not be sufficiently large to appear as separate features on either the absorption or virtual height curves.

The comparability of the absorption data measured at Leicester and at Freiburg has been investigated and the results presented in figures 8.2.5. and 8.2.6. It was first noted that at the latitude of Freiburg, 48° N, the zenith angle at noon varied between 25° in summer and 72° in winter. Since the Leicester absorption data was taken in the hours immediately following the ground sunrise and therefore in a fixed range of χ , it was necessary to remove, at least in part, the zenith angle variation inherent in the Freiburg noon data. An investigation of the variation of the absorption with in terms of the formula

$$A = A_0 \cos^{\frac{1}{n}} \chi \quad 8.2.1.$$

was undertaken and the results for 3 typical days are presented in figure 8.2.7. Fifteen minute running means of the Leicester absorption data were computed for this following the 'change over' time and the logarithms were plotted against $\log_{10} \cos \chi$. The gradient of the best straight line through these points was taken as a measure of the exponent $\frac{1}{n}$. Large variations in this parameter are observed for the days included in figure 8.2.7. This point has been discussed by Rai (1970), who has reviewed the estimates of the exponent made by many workers which range between 0.3 and 1.3 varying both with latitude and zenith angle. In order to determine the equivalent Freiburg absorption for $\chi = 75^{\circ}$ it was considered sufficient in this study to use equation 8.2.1. with $n = 1$. The correlation between the values obtained by this method and those observed at Leicester for $\chi = 75^{\circ}$ is illustrated in figure 8.2.5. Some discrepancies are evident and these are attributed to the

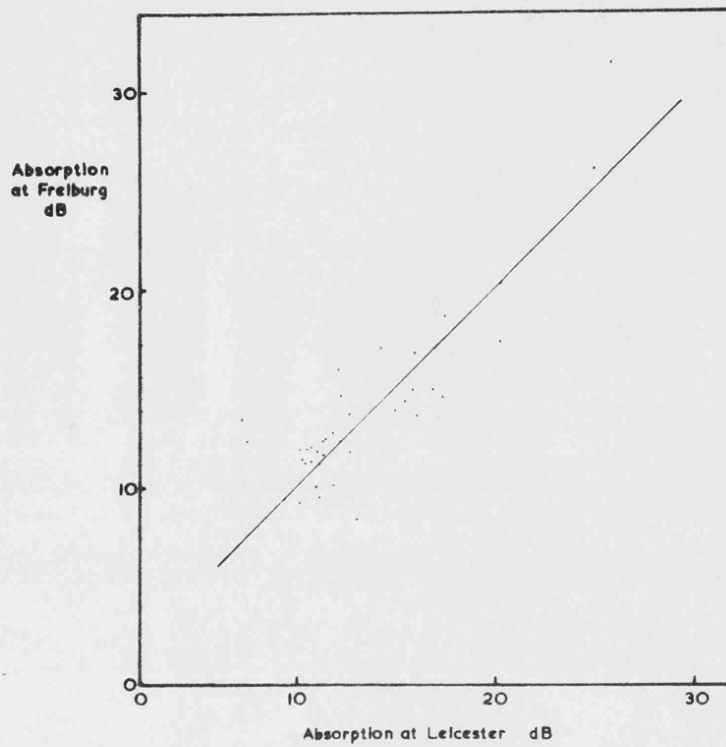


FIG.8.2.5 Comparison of measurements of absorption of 2.05 MHz made at Leicester and Freiburg for $\chi = 75^\circ$

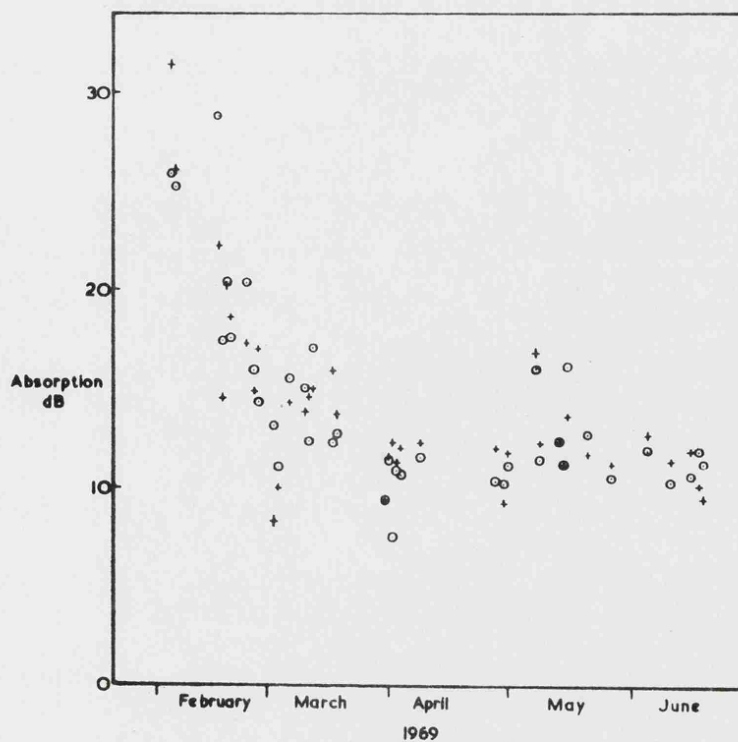


FIG.8.2.6 Variation of absorption from day to day
 (a) + 2.05MHz at Freiburg
 (b) ⊙ 2.05MHZ before 15.4.69 and 2.266MHZ after this date at Leicester

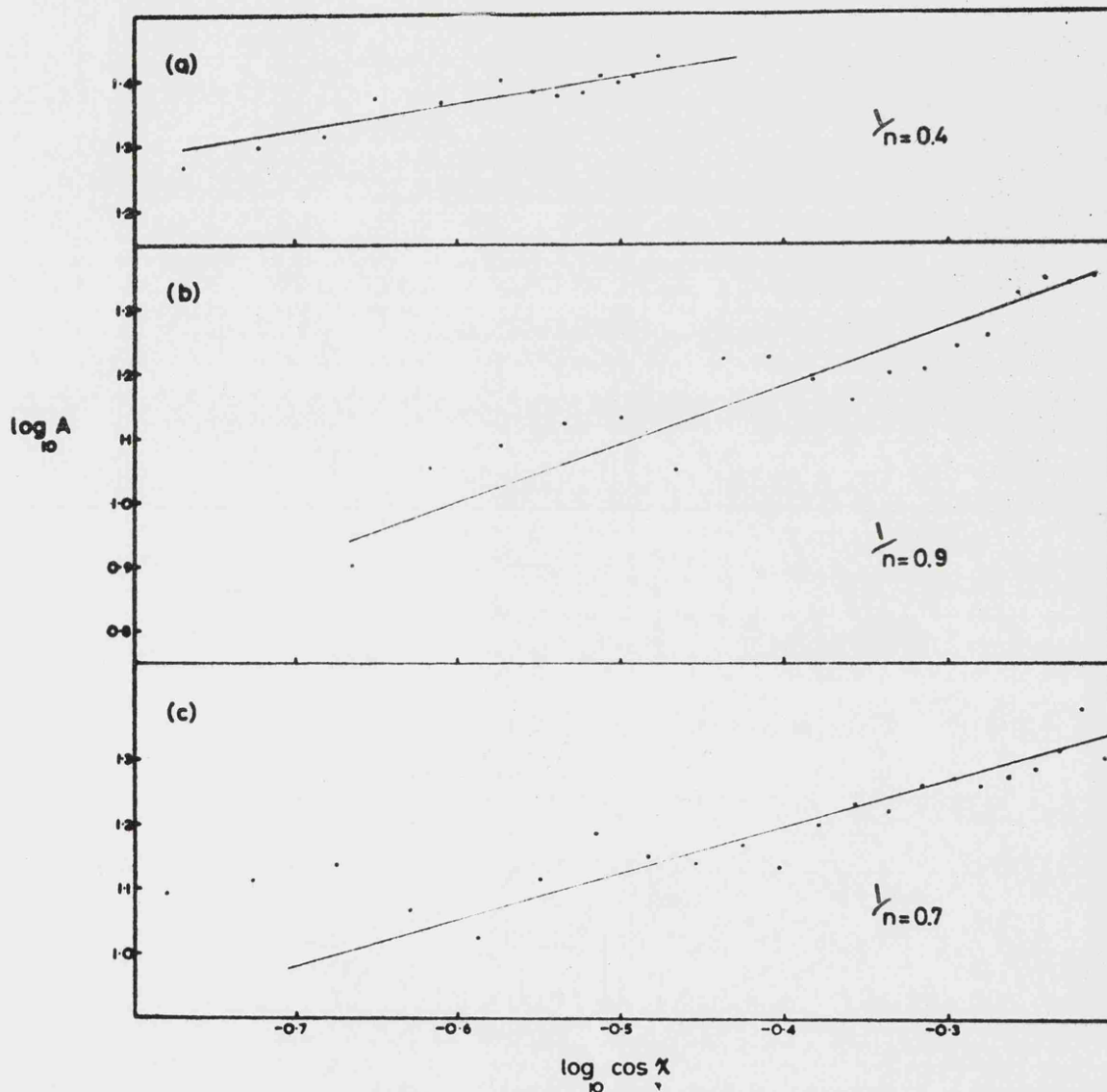


FIG.8.2.7 The logarithm of the absorption of a fixed frequency (in dB) against $\log \cos \lambda$ for 3 selected days
 (a) 5.2.69 frequency 2.05 MHz
 (b) 1.4.69 " " "
 (c) 19.6.69 " 2.266 MHz

effects of localised disturbances spaced in both distance (800 km) and time (Jones and Keenlside(1970)). Figure 8.2.6. presents the same data plotted separately for each station against the time of year and shows clearly the agreement of the two data sources and also the marked rise in winter absorption, the so called 'winter anomaly'.

The absorption curves represented by figure 8.2.1. indicate that on a fixed frequency, the absorption experienced by a pulse reflected from the F layer is higher than would be expected from an E region reflection at the same zenith angle. The absorption curve for the E layer reflection has been extrapolated to higher values of χ using equation 8.2.1. to facilitate this comparison. This difference in absorption is to be expected since $\int N^2 dh$, which governs the extent of the absorption in non-deviative regions (Chapter 3), is greater for the F region reflection.

8.3. Computed Variations of Absorption and virtual height at a fixed frequency

8.3.1. Collisional Frequency in the height range 110-200 km.

In Chapter 3 the dependence of radio wave absorption upon the electron collision frequency of the propagating medium has been discussed theoretically. As a preliminary to the detailed discussion of absorption it is necessary to first consider the details of the collisional frequency models employed in the present analysis.

Theoretical models of the variation of collision frequency in the height range 110-200 km have been discussed

in section 3.2. In figure 8.3.1. the collision frequency-height profile calculated for the parabolic electron density distribution 120 in figure 7.4.11. has been plotted together with the theoretical curves published by Beynon and Rangaswamy (1969) and various experimental observations made below 140 km (Thrane and Piggott, 1966). The tendency of the computed profile to higher values at heights greater than 100 km results from the inclusion of the atomic oxygen and ion collision terms and leads to a closer agreement with the experimental observations. At greater heights the effect of electron ion collisions becomes predominant giving rise to an increase in collision frequency above 140 km. The extent of this increase and its position on the height scale is a function of the electron density distribution and may produce marked changes in the absorption values computed for waves reflected in this region.

The effect of introducing the two additional terms in computing the collision frequency profile has been studied for the Bourne, Setty and Smith profile for 1 hour after sunrise (profile 60 of figure 7.5.2.) and the results have been tabulated in table 8.3.1. A considerable increase in the absorption of frequencies near 2.0 MHz is produced by the inclusion of the additional collision terms at this time of day when reflection of these frequencies occurs at heights greater than 120 km. Also included in the table are the computed virtual heights which are in agreement with the observations of Titheridge (1961b), exhibiting very little dependence upon collision frequency.

The variation of the collision frequency profile during

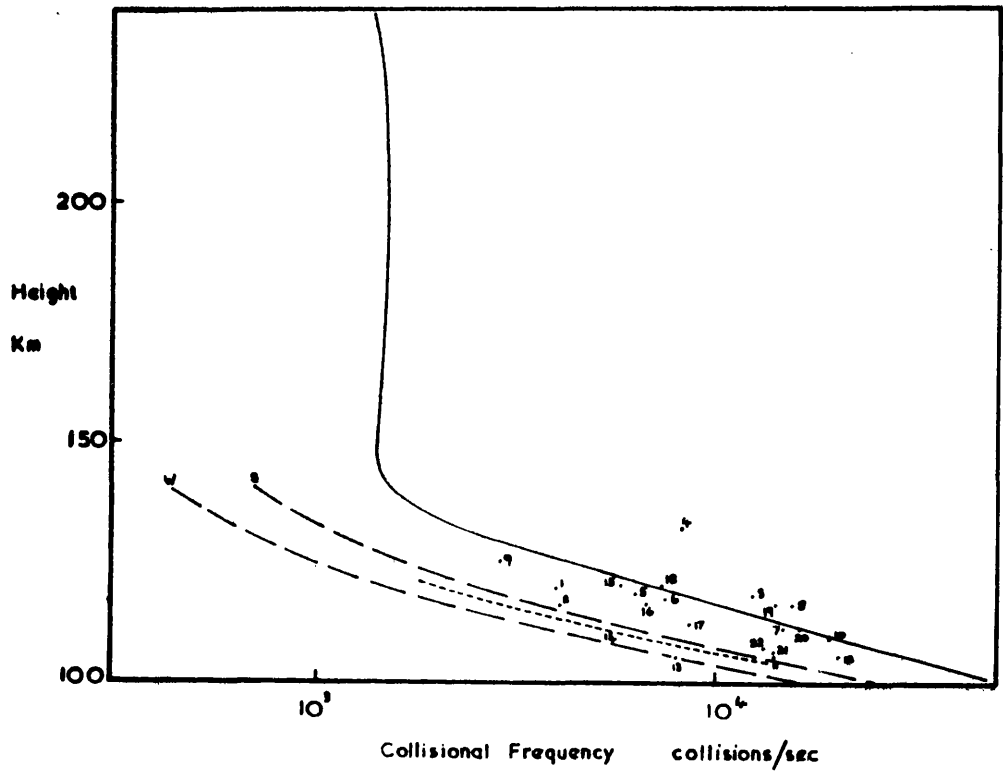


FIG.8.3.1 Collisional frequencies above 100 Km.

- Leicester calculation
 Beynon and Ranfaswamy (1969)
 W Thrane and Piggott (1966) Winter
 S " " " (1966) Summer
1. Appleton 1939
 2. Farmer
 3. Briggs 1950
 4. Briggs 1951
 5. " "
 6. " "
 7. " "
 8. Rawer 1951
 - 9.
 10. Beynon and Davies 1955
 11. Beynon and Brown 1955
 - 12.
 13. Whitehead 1959a
 14. " 1959b
 15. Schlapp 1959
 16. " "
 17. " "
 18. " "
 19. " "
 20. " "
 21. " "
 22. Yasuda 1963

Frequency MHz	Virtual Height km			Absorption nepers		
1.5	141.27283	141.66160	140.91950	0.26641892	0.33874905	0.41688861
1.7	143.34715	143.15602	142.98331	0.20852757	0.27315256	0.35657747
1.9	150.21947	150.10590	150.23079	0.19843151	0.26343739	0.36881411
2.1	419.67284	419.67281	419.73523	0.22635308	0.31882036	0.62652215
2.3	389.80920	389.80974	389.76768	0.12931038	0.18021725	0.35448369
2.5	393.70404	393.70299	393.74555	0.10179384	0.14106456	0.28007248
2.7	401.42805	401.42839	401.42828	0.08592573	0.11848228	0.23660275

Table 8.3.1 Calculated values of Absorption and Virtual Height from the Bourne, Setty and Smith (1964) profile for 60 minutes after sunrise employing Collisional Frequency profiles including various collision terms.

the early morning hours has been illustrated in figure 8.3.1.1 where profiles computed from the Thomson Scatter electron density profiles are presented. This procedure for computing the collision frequency from each electron density distribution in turn (section 3.2.) has been adopted throughout the following theoretical study.

8.3.2. Calculation of absorption and virtual height variations in the early morning.

The absorption and virtual height variations with time following the sunrise have been calculated for the profiles of figures 7.5.2, 7.5.3 and 7.5.4. These results are compared with the experimental observations discussed above. In addition the variation of absorption with frequency has also been computed for the various ionospheric models.

(a) Theoretical Profiles

The variations of absorption and virtual height with time have been computed from the Bourne, Setty and Smith (1964) theoretical models (figure 7.5.2.) and their corresponding collision frequency profiles and these results are presented in figure 8.3.2. for frequencies 1.5, 2.0 and 2.5 MHz. The time definition of these results for each frequency is insufficient to show any fine detail in the time variations but high absorptions and virtual heights close to the penetration frequency have been reproduced by the analysis, suggesting the characteristic cusp type structure consistent with the experimental observations. The predominant effect of the non-deviative component of absorption is clearly marked by the inverse correlation of absorption with frequency in the un-

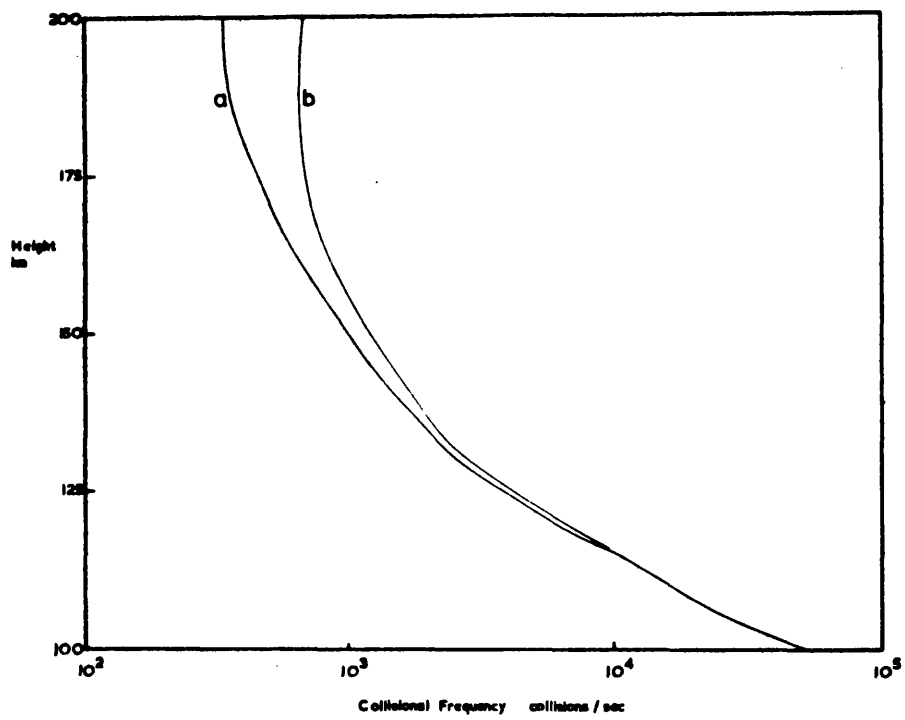


FIG.8.3.1.1 Collisional frequency-height profiles computed from the Thomson Scatter profiles for (a) 0529h and (b)0632h on the 11th April 1969.

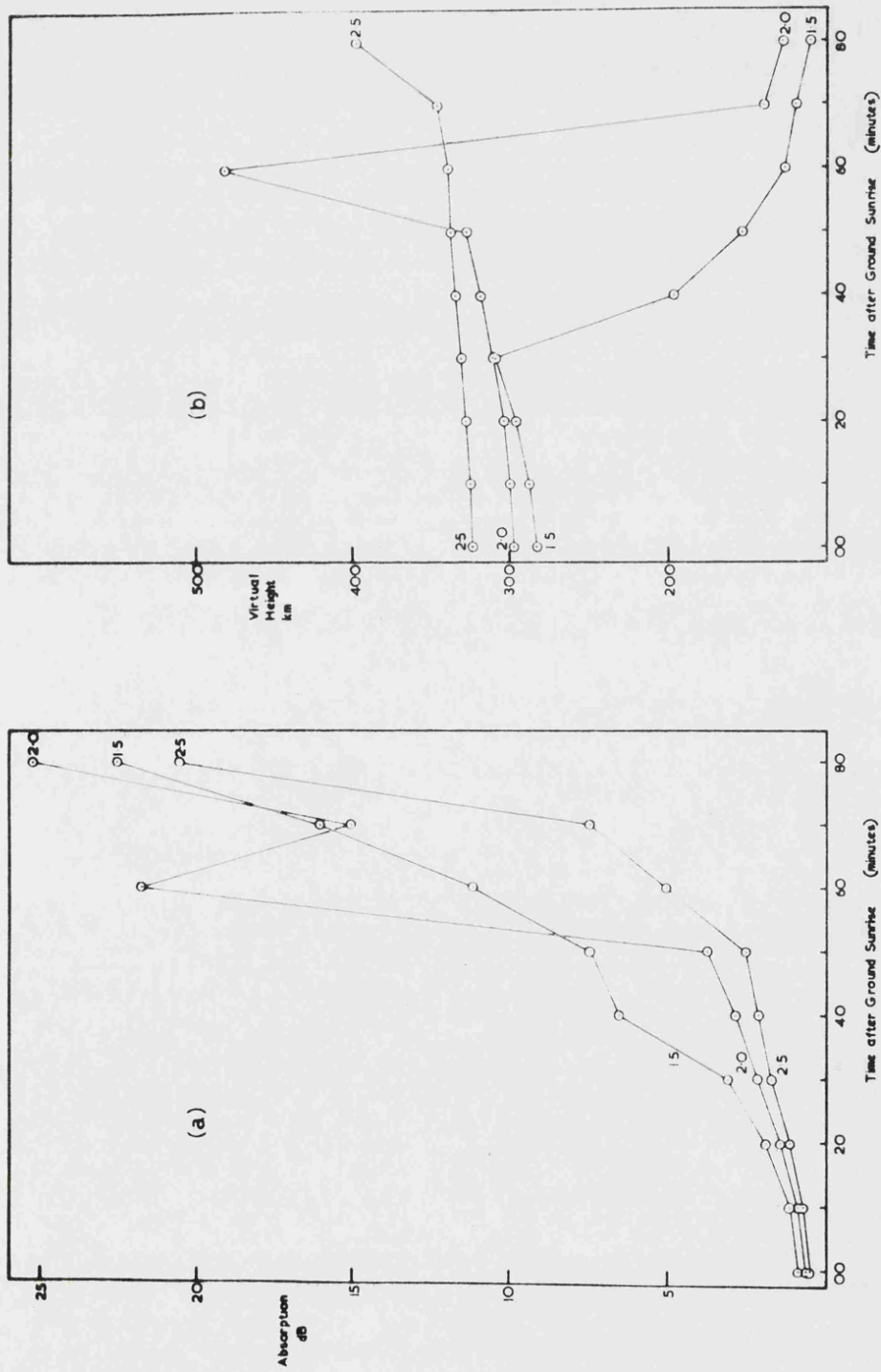


FIG. 8.3.2 Time variation of (a) absorption and (b) virtual height of the frequencies shown (in MHz) computed from the Bourne, Setty and Smith models.

disturbed portions of the trace. This point is further illustrated in figure 8.3.3. where absorption and virtual height have been plotted against frequency for the profile representing conditions 70 minutes after sunrise. Near the cusp structure the marked influence of deviative absorption is evident. However, away from this feature the variation of absorption shows good agreement with the variation of the non-deviative absorption, as predicted by the formula

$$A_{nd} \propto \frac{1}{(\omega \pm |\omega_L|)^2}$$

given by Appleton and Piggott (1954), which has been superimposed in the figure. Furthermore, it is clear from this last figure that absorption is a more sensitive parameter to fluctuations in the electron density distribution than is the virtual height and that the extent of the enhanced deviative absorption produced by the transition region may be far greater than would be expected from inspection of the virtual height records. This observation has been more closely studied by computing the absorption and virtual height of a 3.35 MHz signal reflected from the two variant models based upon the parabolic profile 120 (figure 7.4.11.) and illustrated in figure 8.3.4. The results presented in table 8.3.2. clearly show that for these models the change in absorption expressed as $\Delta A/A$ is more than twice $\Delta h'/h'$. Further confirmation can be obtained from consideration of the simple formula for the absorption

$$A = \frac{\nu^2}{2c} \left\{ h' - P \right\}$$

from which, if ν is considered to remain constant, the expression

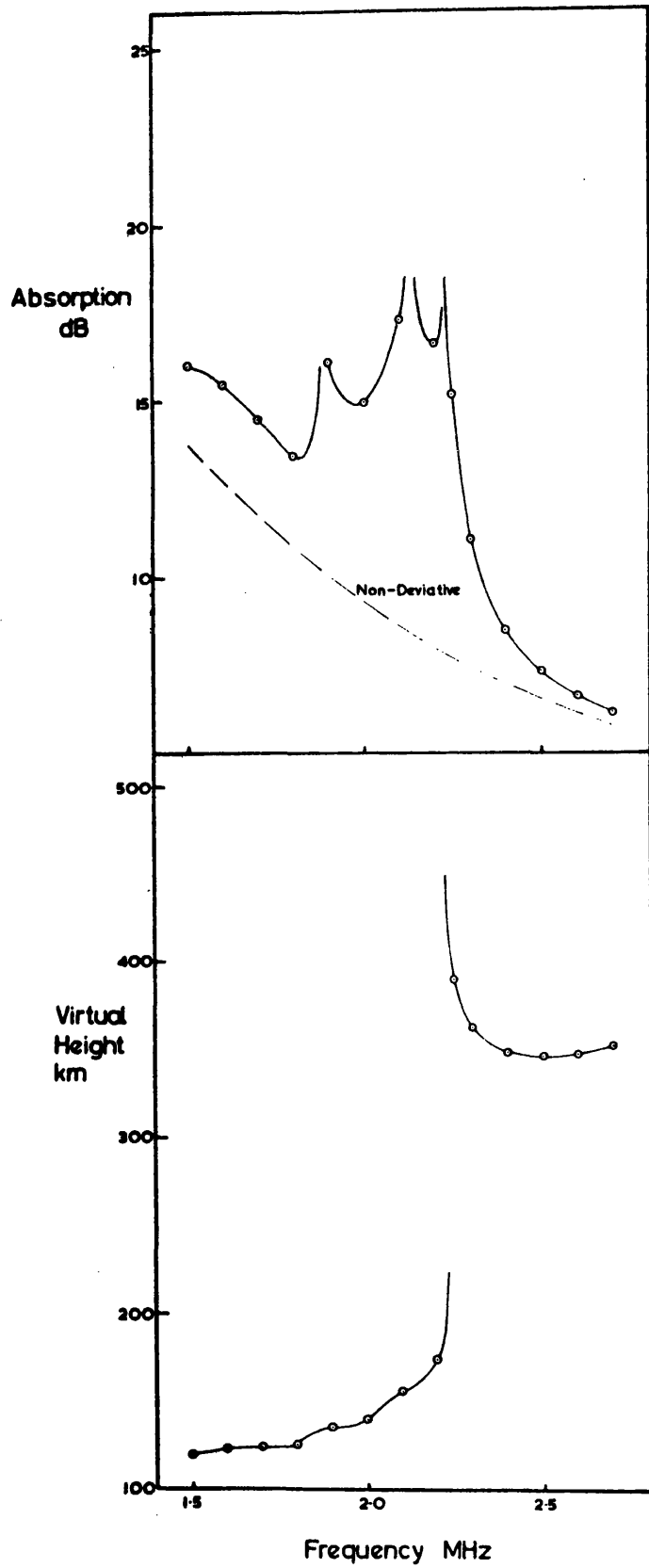


FIG.8.3.3 Variation of absorption and virtual height with frequency computed from the Bourne,Setty and Smith model for 70 minutes after ground sunrise.

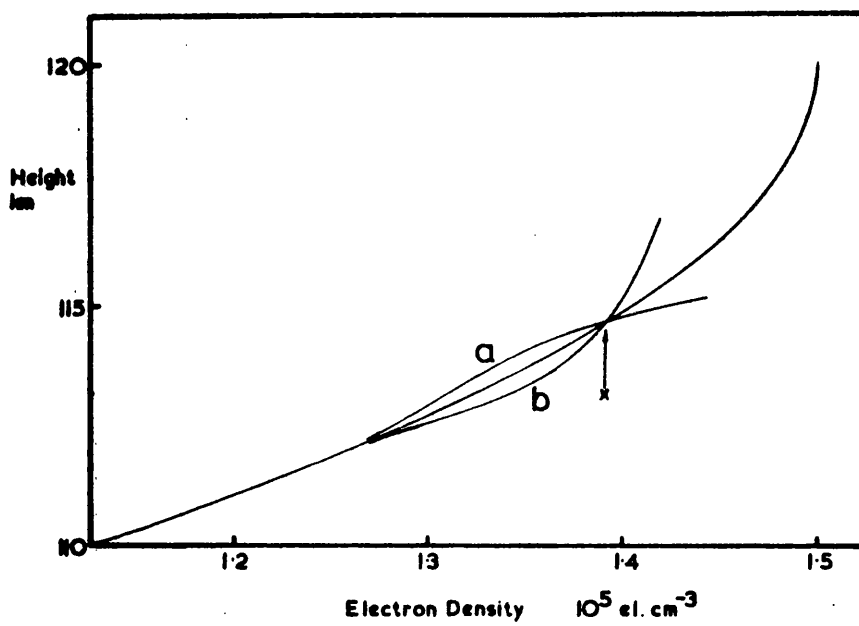


FIG. 8.3.4 Models simulating changes in electron density distribution near the reflection level of 3.35 MHz(x)

Profile	Absorption dB	VirtualHeight km
a	16.006448	140.43471
b	24.350499	166.43785

$$\Delta A/A = 0.413512499 \quad \Delta h'/h' = 0.1694719137$$

Table 8.3.2 Absorption and Virtual Height computed from the profiles of fig.8.3.4 for 3.35 MHz.

Frequencies Compared MHz		$\Delta A/A$	$\Delta h'/h'$
2.225	2.25	1.847	1.05
2.35	2.36	0.2508	0.248
2.05	2.1	0.24	0.07

Table 8.3.3 Comparison of $\Delta A/A$ with $\Delta h'/h'$

$$\left| \frac{\Delta A}{A} \right| = \left| \frac{\Delta h' - \Delta P}{h' - P} \right|$$

may be derived. Thus since the phase path, P, is positive and decreases as virtual height increases

$$\left| \frac{\Delta h' - \Delta P}{h' - P} \right| > \left| \frac{\Delta h'}{h'} \right|$$

and hence

$$\left| \frac{\Delta A}{A} \right| > \left| \frac{\Delta h'}{h'} \right|$$

(b) Thomson Scatter Profiles

The Thomson Scatter profiles, illustrated in figure 7.5.4, have been analysed in the same way as the theoretical distribution discussed above. The results of these calculations are presented in figures 8.3.5. and 8.3.6. The limited number of electron density profiles available has resulted in some loss of time definition as illustrated in figure 8.3.5. However, these computations indicate that the time dependence of absorption and virtual height derived from the Thomson Scatter profiles are far more complex than those predicted by the theoretical models. Consideration of the variations of virtual height and absorption with wave frequency, presented in figure 8.3.5, in which the detailed features are more closely defined by the computation of additional data points, further illustrates the increased complexity derived from the experimental profiles. The frequency variation of non-deviative absorption is included and again shows good agreement with the computed values away from the transition

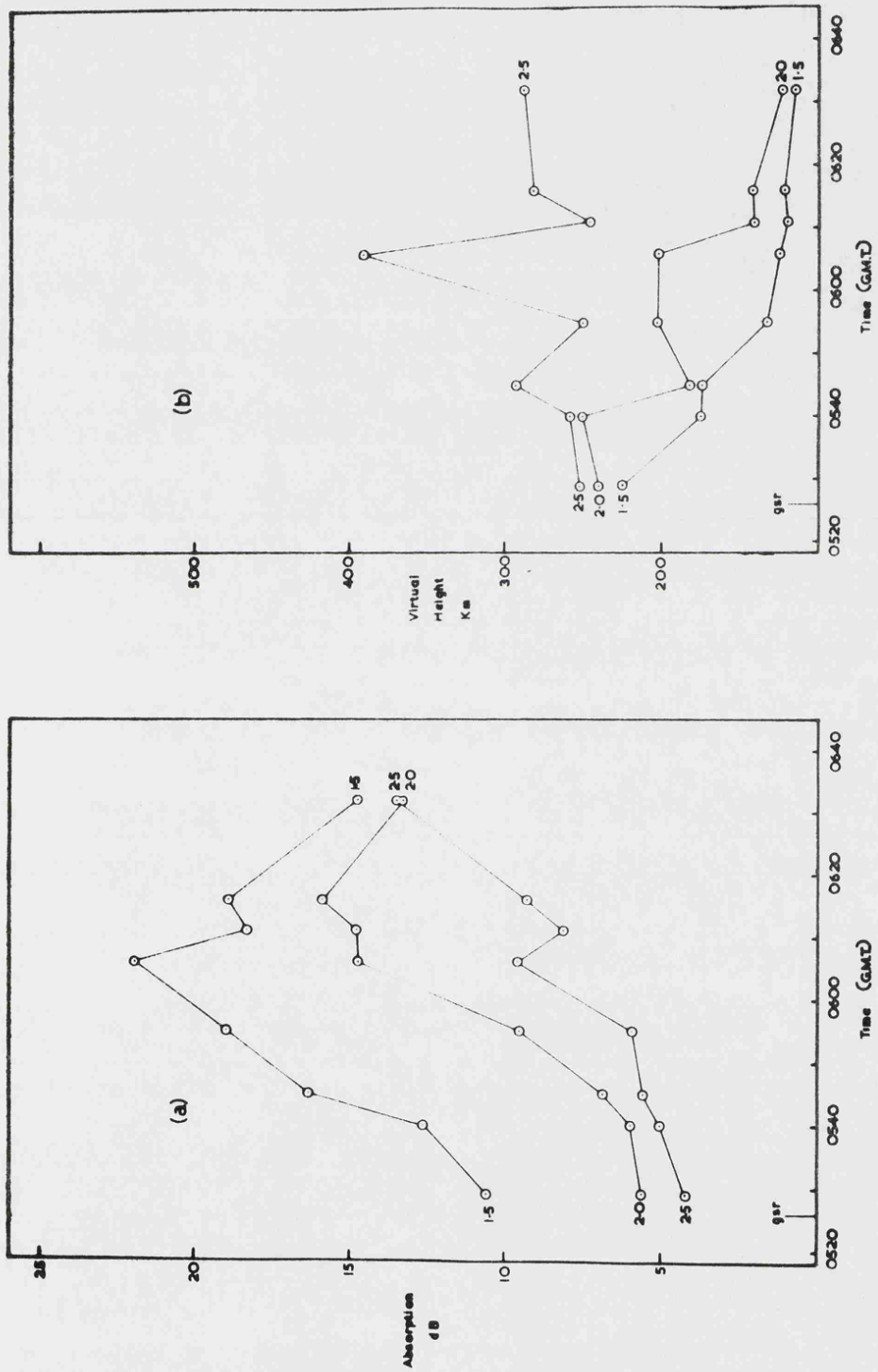


FIG. 8.3.5 Time variation of (a) Absorption (b) Virtual height of the frequencies shown (in MHz) computed from the Thomson Scatter profiles of 11th April 1969.

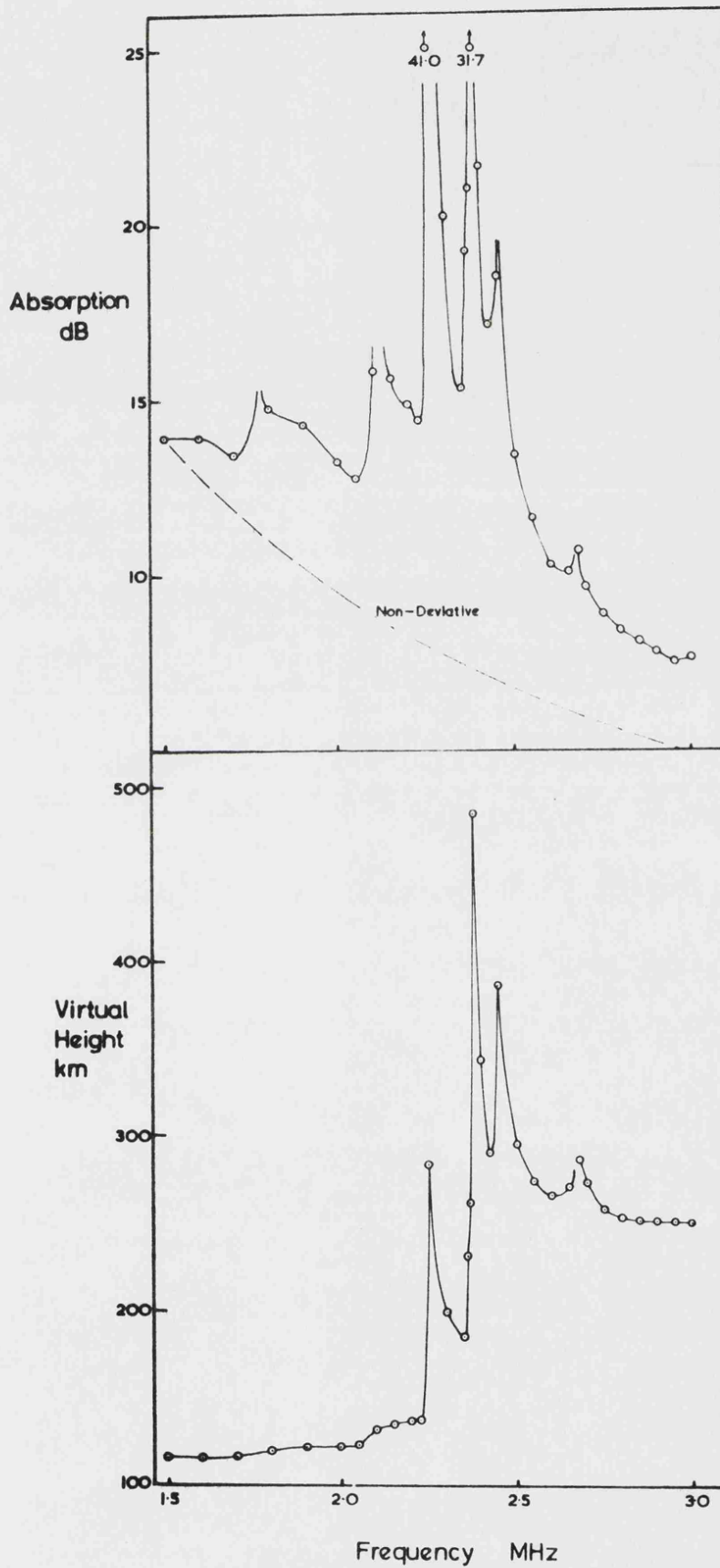


FIG.8.3.6 Variation of absorption and virtual height with frequency computed from the Thomson Scatter profile for 0632 11 April 1969.

disturbance. Furthermore, the increased sensitivity of the absorption in exhibiting fine structure is illustrated, six clear discontinuities being produced compared with four on the virtual height curve. This observation is supported by the values of $\Delta A/A$ and $\Delta h'/h'$ computed for 3 pairs of closely spaced frequencies in figure 8.3.6. and presented in table 8.3.3.

(c) Profiles derived from Leicester Ionograms

The electron density profiles derived from the ionograms recorded at Leicester on the morning of 10th April 1969 (figure 7.5.3.) have been used to compute the time variation of absorption and virtual height of several fixed frequencies and these results are presented in figure 8.3.7. The variations of the computed virtual height and absorption with time for a 2.05 MHz wave have also been computed and are presented in figures 8.5.2. and 8.5.3. Figure 8.3.8. illustrates the variation of these parameters with frequency for the profile obtained from the ionogram for 0630 10th April 1969. The complexity of these variations is again noticeable and the greater sensitivity of the absorption to profile change is further illustrated by a comparison of the curves of figure 8.3.8. below 2.0 MHz.

8.4. The influence of the electron density distribution below 100 km on absorption in the early morning hours

The effect of various models of the electron density distribution below 100 km upon virtual height has been discussed briefly in section 7.5.3. The same models, presented

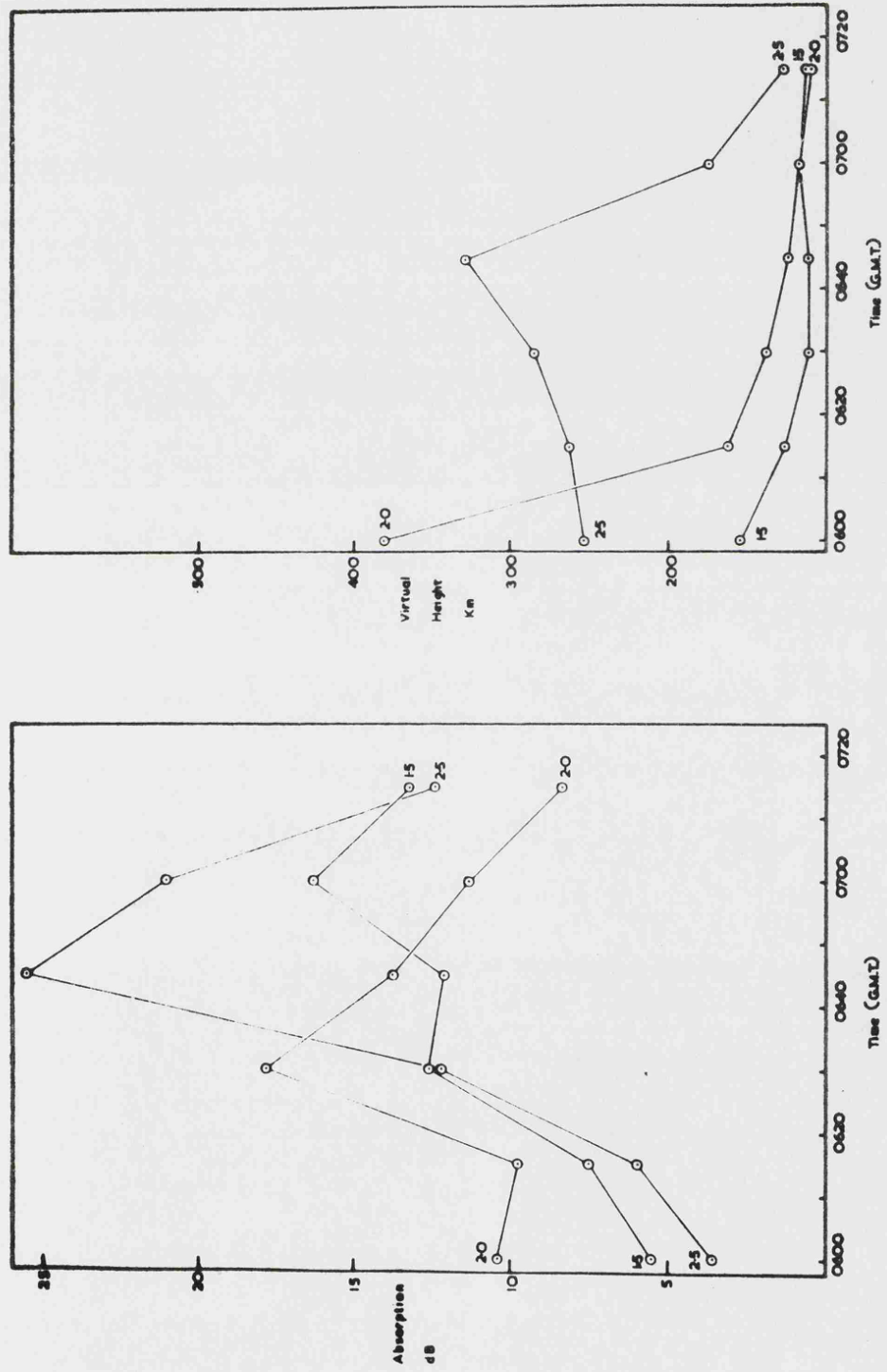


FIG. 8.3.7 Time variation of (a) Absorption (b) Virtual height of the frequencies shown in MHz) computed from Leicester electron density profiles for 10th April 1969

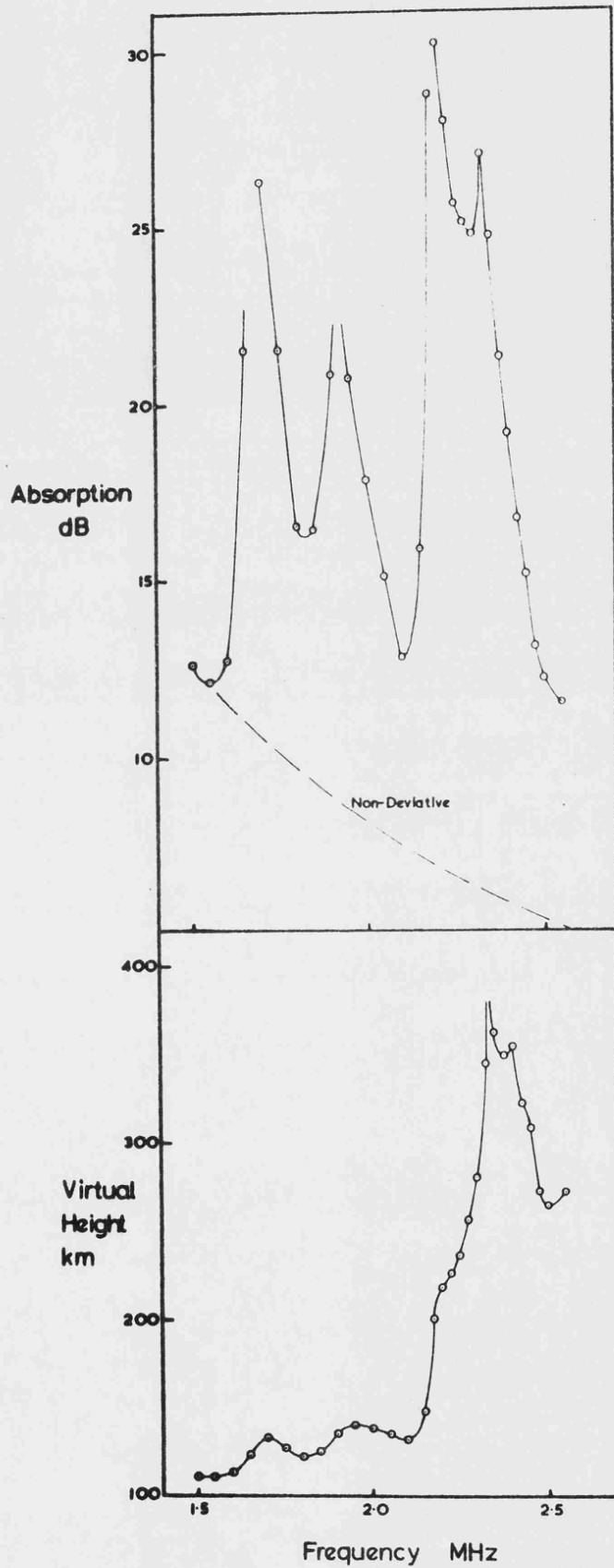


FIG.8.3.8 Variation of absorption and virtual height with frequency computed from the Leicester monotonic profile for 0630 10th April 1969

in figure 7.5.9. are employed here to investigate their effect upon the computed absorption. The variation of absorption with frequency computed from the Thomson Scatter profiles for 0529 h and 0632 h on the 11th April 1969 are presented in figures 8.4.1. and 8.4.2. Conditions shortly after sunrise are illustrated in figure 8.4.1. in which frequencies greater than 1.6 MHz are reflected from the F region. The model 0 (figure 7.5.9.) incorporates the Smith (1966) D region model for $\chi = 87.9^\circ$ and a tangential link with the Thomson Scatter profile for 0529 h. The three further models represent decreasing electron densities between 83 and 95 km. The Deeks (1966) D region model was found to coincide with the Thomson Scatter profile at 92 km and the resulting profile is labelled 4. The greatest difference in the computed absorption, amounting to 0.8 dB, was found between models 3 and 4. This corresponds to a difference of 14% at 2.0 MHz as compared with only 7% between profiles 0 and 3 at this frequency.

The results presented in figure 8.4.2. illustrate conditions more than one hour after sunrise at which time an appreciable section of the frequency range shown in the figure is reflected from the E region. The model 4 (figure 7.5.9.), incorporating the Deeks D region model for sunrise, gives computed absorption values which are again higher than those calculated for the models 0 to 3. The difference between the values computed for models 3 and 4 was approximately 2 dB, 16% at 2 MHz. This deviation increases at lower frequencies as would be expected. The models, 0 to 3, incorporating the Smith D region show greater differences in the computed absorption values in figure 8.4.2. than in figure 8.4.1. which

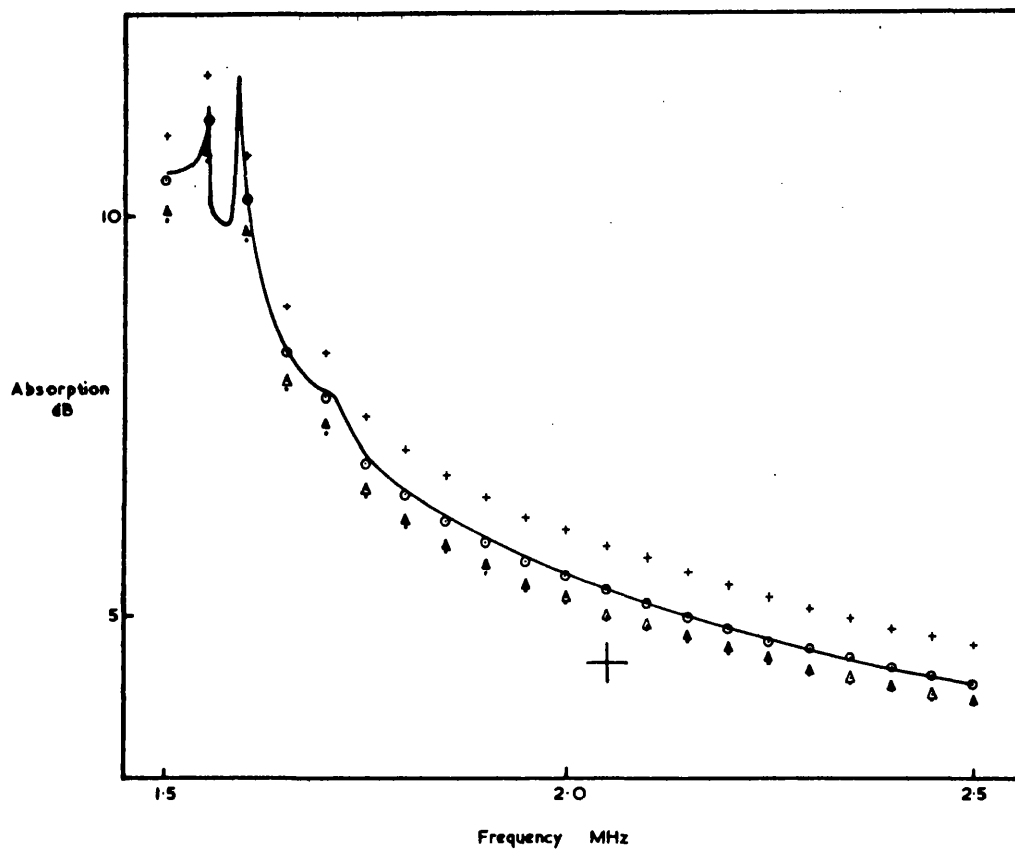


FIG.8.4.1 Variation of absorption with frequency for the various models of fig 7.5.9 for 0529 11th April 1969.

—	model	0
⊙	"	1
△	"	2
×	"	3
▽	"	4
+	mean of experimental observations near 0529 11th April 1969	

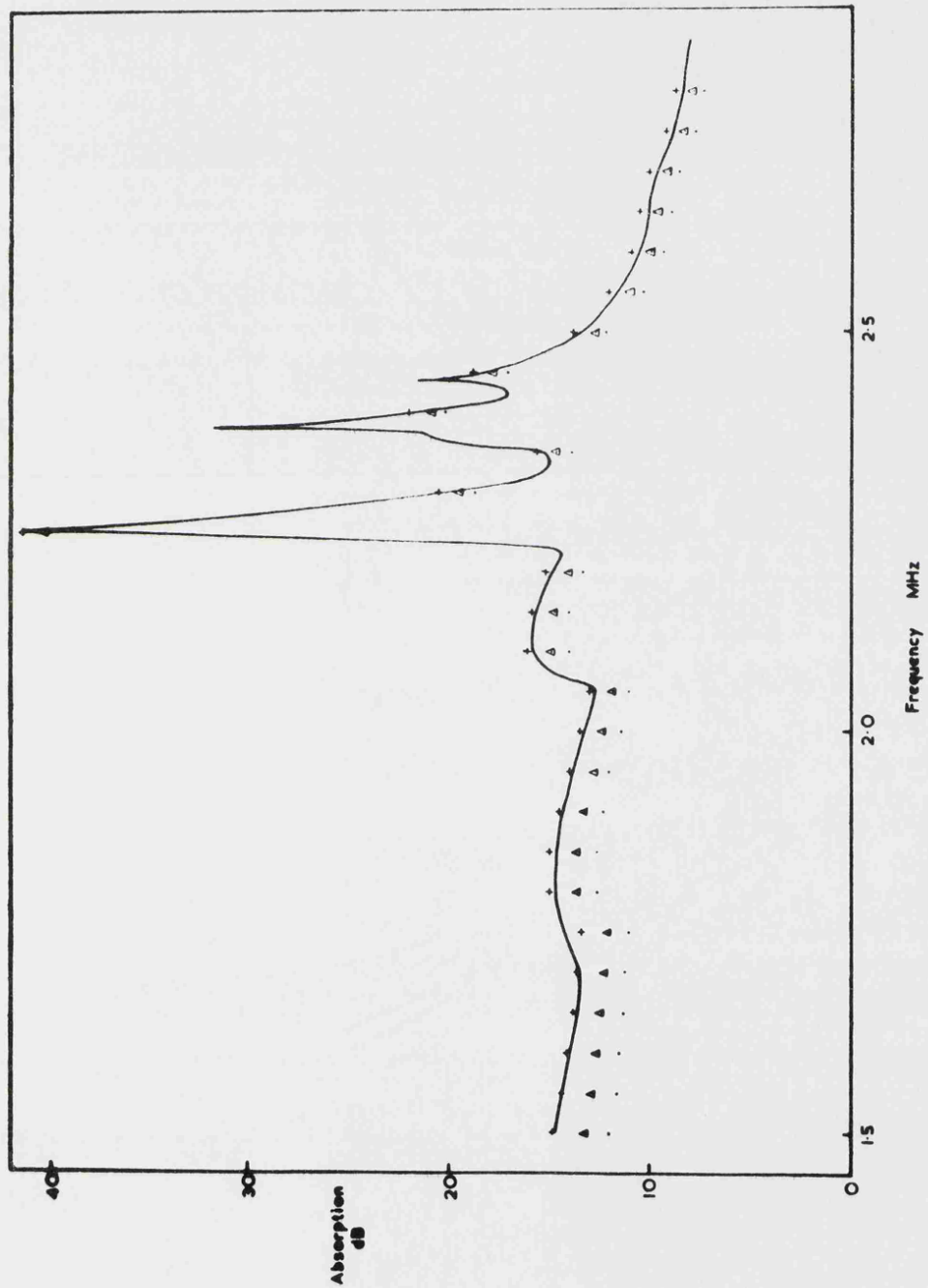


FIG.8.4.2 Variation of absorption with frequency for the various models of fig.7.5.9 for 0632 11th April 1969.

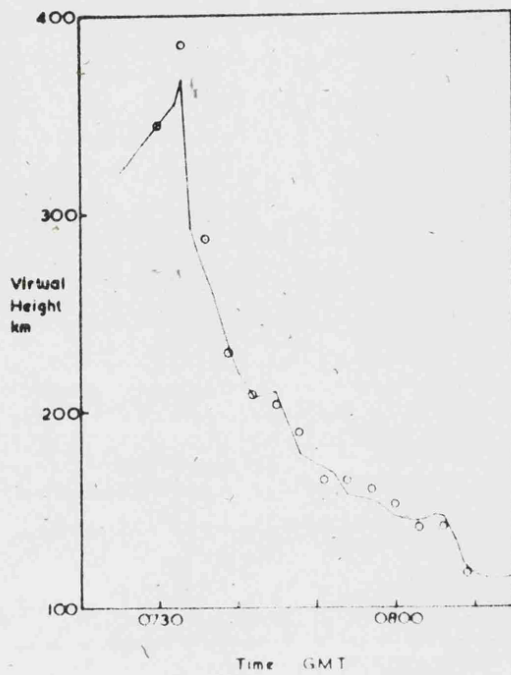
——— model 0 and 1
 Δ model 2
 ○ " 3
 + " 4

may arise directly from the increased height range over which the interpolation between the Smith D region and the Thomson Scatter profile was necessary.

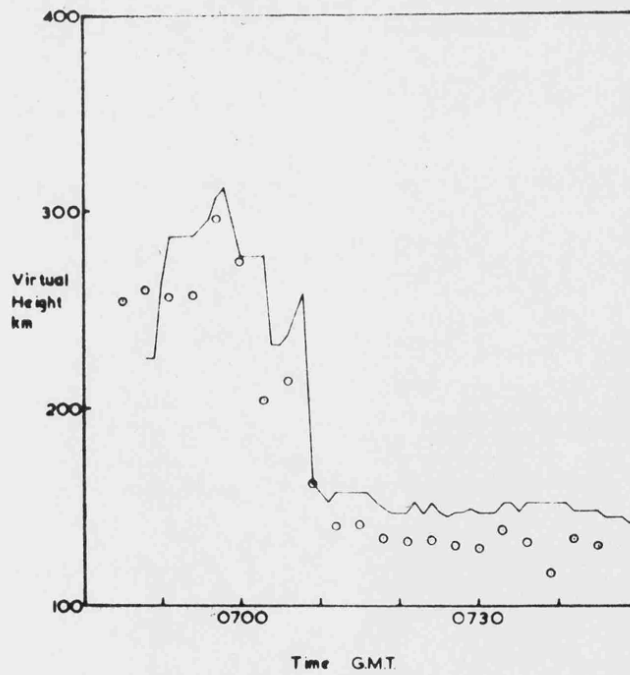
It can be concluded from these results that the form of the D region model for post sunrise conditions has little effect upon the computed attenuation experienced by both E and F region reflections and the small differences are probably due to the form of the interpolation or D-E transition profile, Beynon and Rangaswamy (1969) have recently discussed representative models and emphasise the importance of this region in calculating the noon absorption. However, the 16% difference observed here is considered to be comparable with other errors involved in the computation of the absorption. It is therefore concluded that in the immediate post sunrise period the form of the D and D-E transition regions is not a critical feature in the calculation of absorption of radio pulses reflected in the E and F regions.

8.5. Comparison of computed time variations of virtual height and absorption with observed values

Four days were selected on which virtual height and absorption measurements have been made at a fixed frequency in addition to the continuous recording of ionograms. The electron density profiles computed from these ionograms have been presented in figure 7.5.3. and in figure 8.5.2. the calculated virtual heights for 2.05 MHz are plotted together with the direct observations for the period around the 'change over' time from F to E region reflection. The agreement between the computed and observed values is generally



(a) 26 2 69 frequency 2.05 MHz

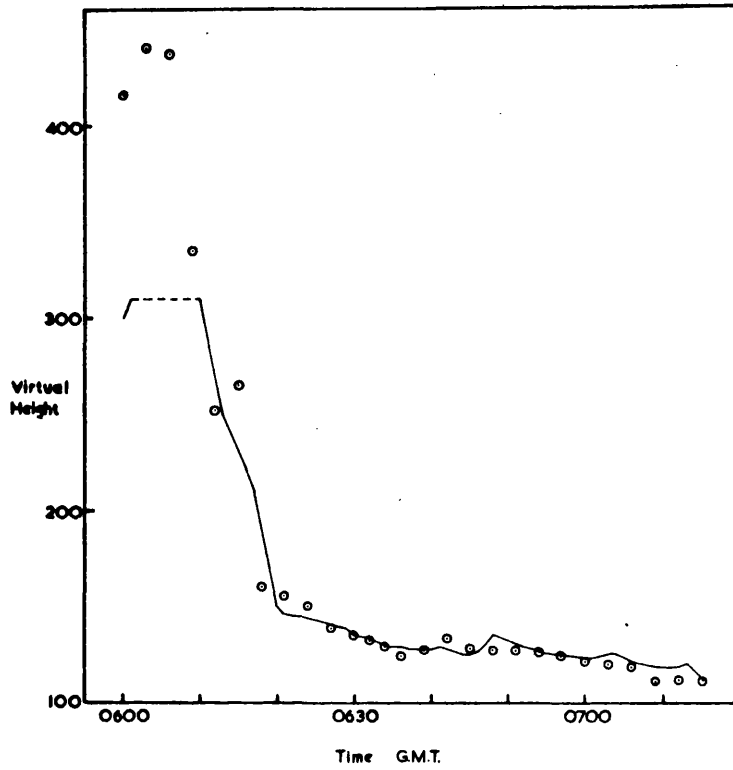


(b) 13 3 69 frequency 2.05 MHz

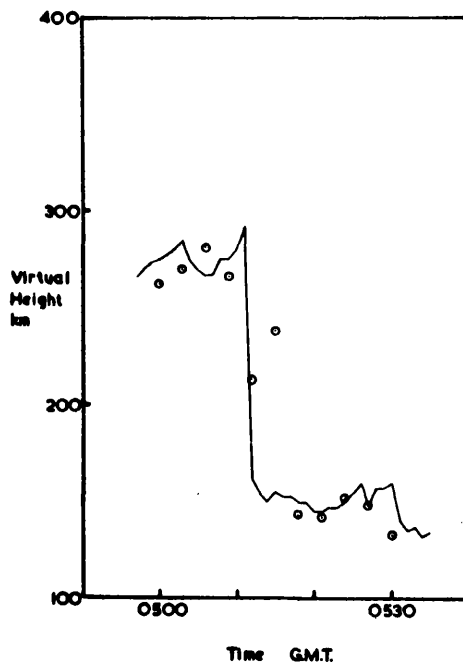
FIG.8.5.2 Variation of virtual height with time on a fixed frequency

— experimental observations

⊙ calculated from Leicester profiles.

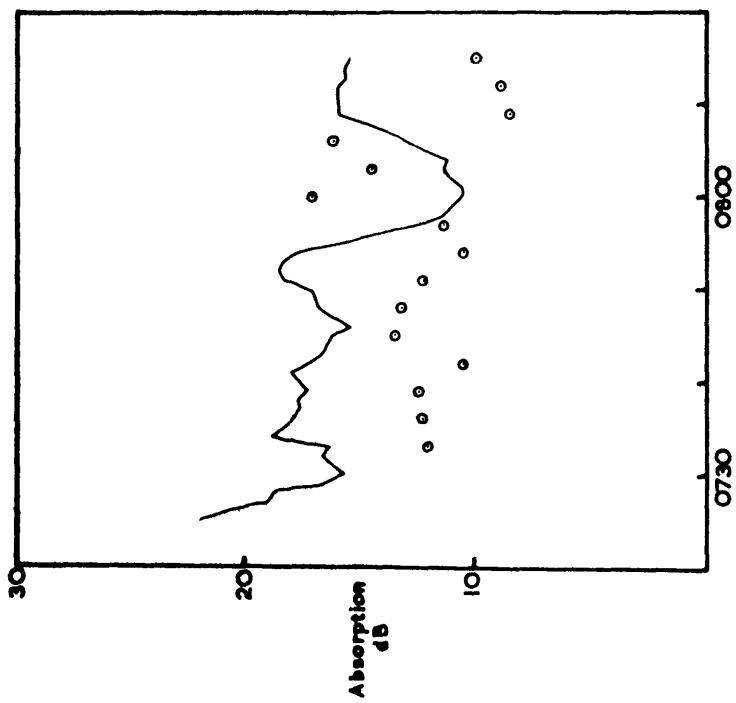


(c) 10.4.69 frequency 2.05 MHz

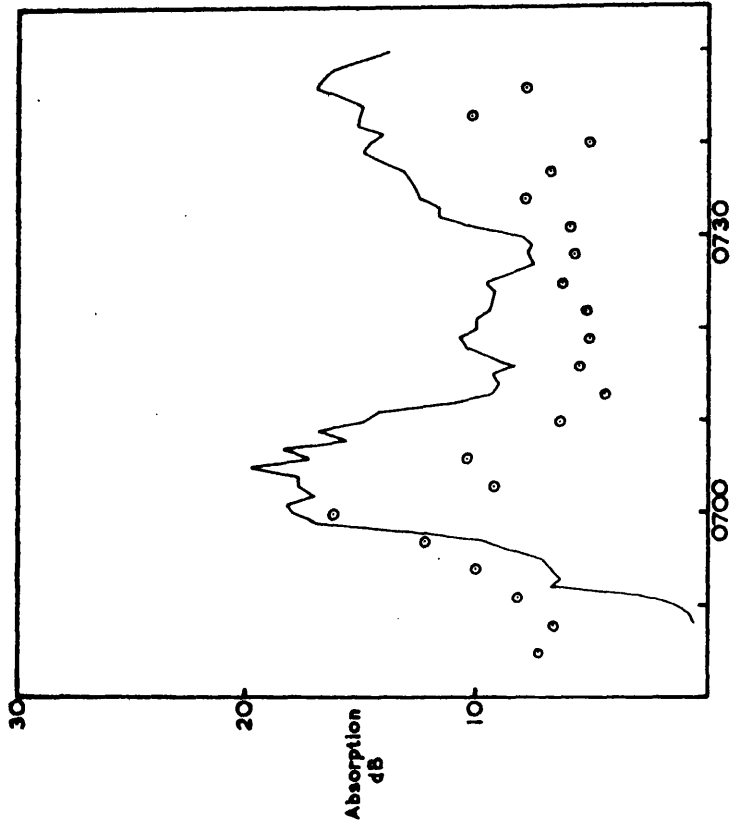


(d) 21.5.69 frequency 2.266 MHz

good and it may again be concluded that the monotonic electron density distribution obtained by the Titheridge reduction method (section 3.4.) is a satisfactory model for the reproduction of virtual heights. However, the discrepancy occurring between the observed and computed absorption values presented in figure 8.5.3. is very marked and only the general trends of the observed results are evident in the computed values. These discrepancies may be the result of the inherent inaccuracies of the monotonic distributions of electron density or low lying ionization existing below the lower limit of the ionogram data. The effect of various D region models and the extrapolations to the computed profiles has again been investigated and the models employed are presented in figure 8.5.4. The profiles 0 to 5 are extrapolations of the Smith (1966) D region model for $\lambda = 79^\circ$ to the E region profile computed from the ionogram for 0630 10th April 1969, while profile 6 includes the Deeks (1966) model for 0630 h March equinox sunspot minimum conditions. The absorption on 2.05 MHz has been calculated for each profile and included in figure 8.5.3. Apart from model 2, in which the 80-100 km region has been greatly enhanced, the various models show once again that this region plays only a minor role in the absorption of a 2.05 MHz wave at this time of day. These results also indicate that adjustment of this extrapolated region cannot account for the observed difference between the computed and observed absorption values. The shape of the layer in the region around the reflection point is known to play a predominant part in determining the computed absorption and hence it may be concluded that although the monotonic profile, produced by ionogram reduction, indicates the gross

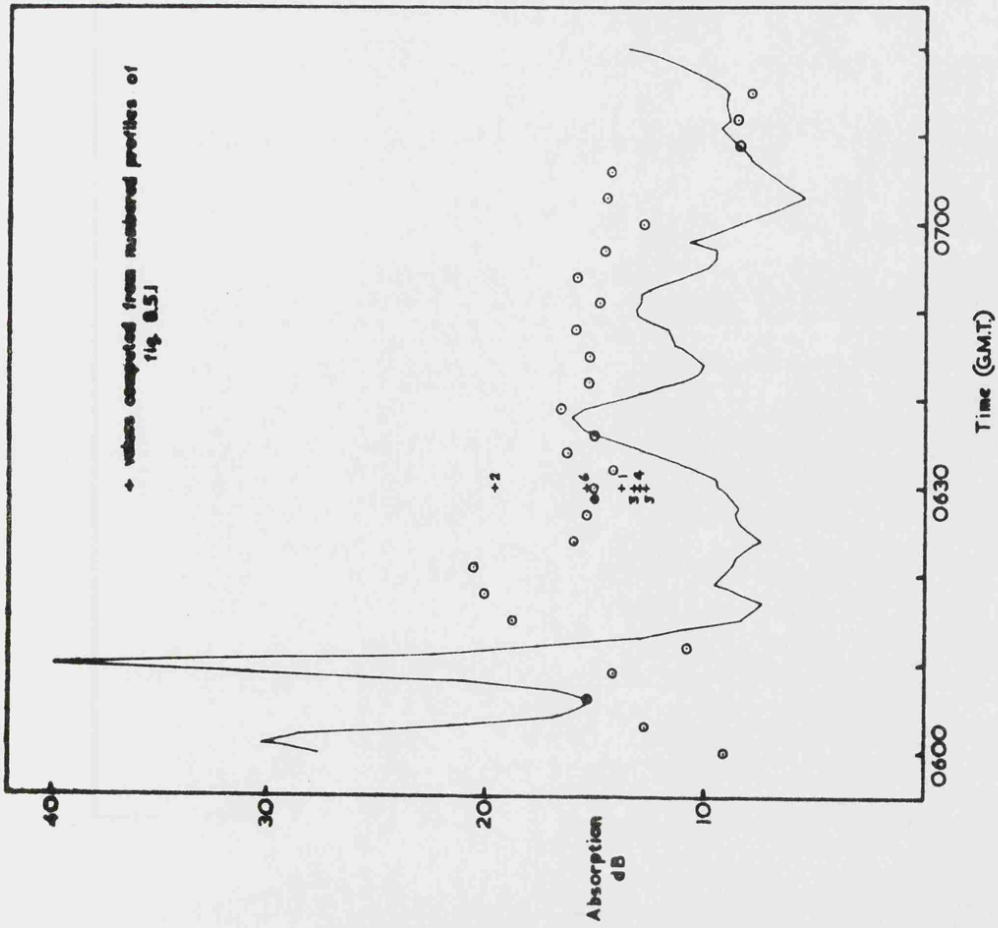


(a) 26.2.69 frequency 26.2.69 MHz
Time (GMT)

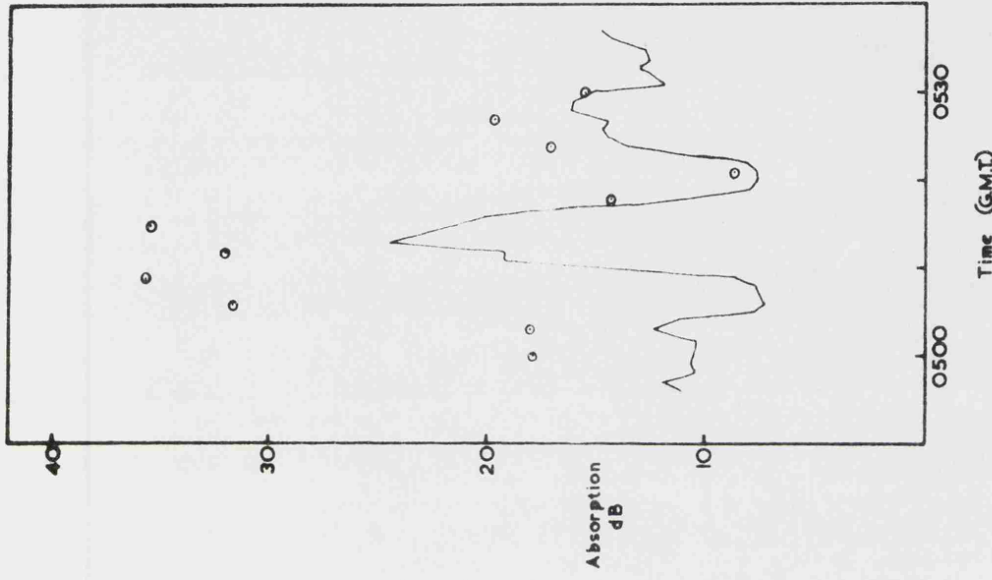


(b) 13.3.69 frequency 13.3.69 MHz
Time (GMT)

FIG.8.5.3 Variation of absorption with time on a fixed frequency, ——— experimental observation, \circ calculated from Leicester profiles



(c) 10 4.69 frequency 2.05 MHz



(d) 21.5.69 frequency 2.266 MHz

features of the true electron density profile, it may be appreciably in error when detailed variations of absorption are considered.

A similar analysis of the Thomson Scatter profiles for the 11th April 1969, and the Bourne, Setty and Smith theoretical models has produced the computed variations of absorption and virtual height presented in figure 8.5.5. In this figure the computed values are superimposed upon the values of the two parameters observed experimentally at Leicester in the early morning hours of 11th April 1969. The absorption and virtual height values computed from the Thomson Scatter profiles display extremely good agreement while the theoretical models of Bourne, Setty and Smith give values differing greatly from the observations. The values of virtual height computed from the Thomson Scatter profiles generally agree with experiment to within 10%, while the absorption values fall within the fluctuations in the measured absorption introduced by fading. In making this comparison several factors are encountered which would account for the discrepancy between the observed and computed values of absorption. Firstly, the single well defined profile employed in the computations cannot represent the conditions encountered by all ray components constituting the observed reflection. Hence the phenomenon of fading will not be represented and a difference comparable to the fading depth may occur between the observed and computed values. Secondly, the distance between the two observing stations Malvern and Leicester may result in minor changes in the electron density profile and hence effect the comparability of the computed absorption. Considering these points in the light of the agreement noted

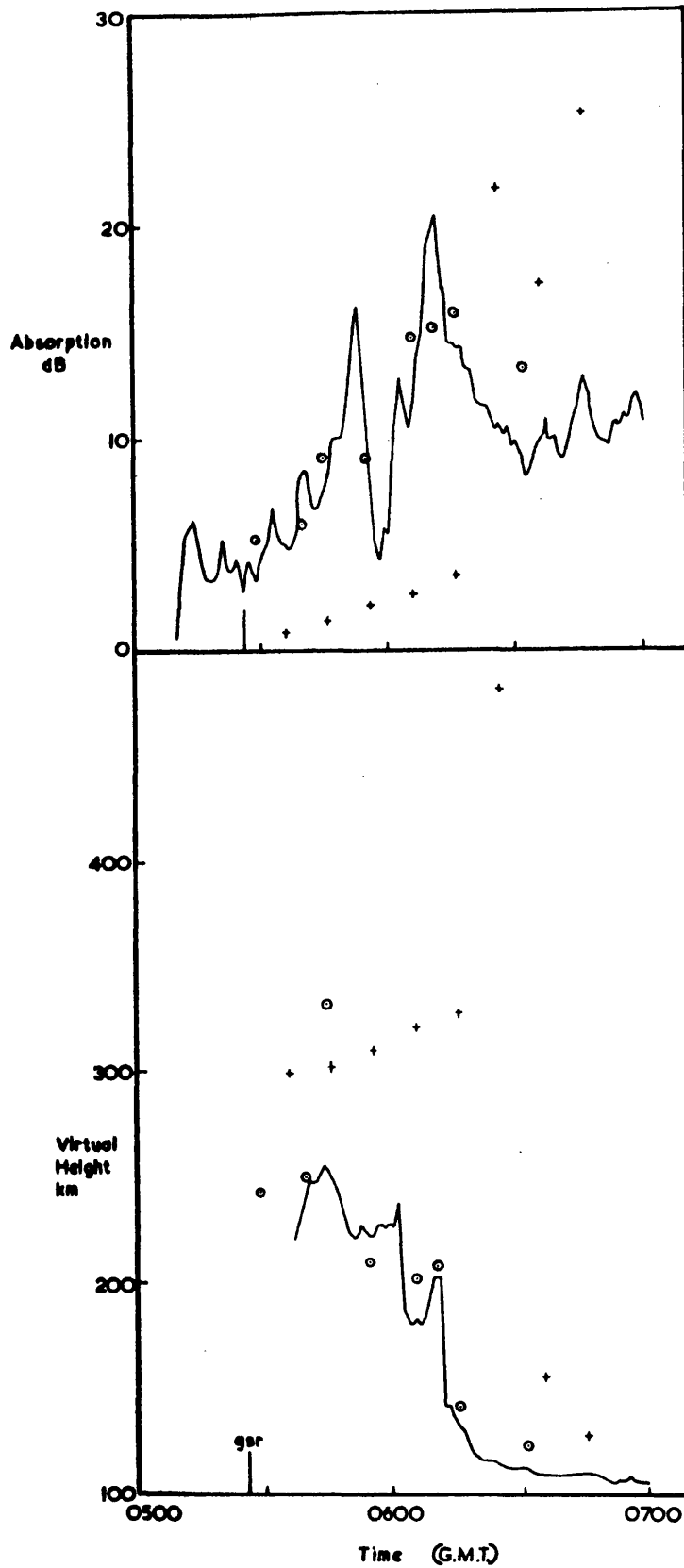


FIG.8.5.5 Comparison of the absorption and virtual height of 2.05 MHz recorded experimentally at Leicester with that calculated from the Thomson Scatter profiles for the same day, 11th April 1969 and from the Bourne Setty and Smith models.

— experimental observations
 ○ Thomson Scatter calculations
 + Bourne et al. calculations.

between the data it may be concluded that the Thomson Scatter profiles give a very good representation of conditions at any particular time and again that the structure of the profile is generally constant over distances up to 87 km. Furthermore, comparing the results obtained from Thomson Scatter profiles with those from monotonic profiles, it is suggested that although these profiles represent conditions sufficiently well to give fairly accurate values of virtual height, they are far from satisfactory for the computation of absorption values. This may result from the distortion of gradients and the omission of re-entrant regions of the electron density distribution to which the absorption is more sensitive than the virtual height.

Chapter 9

Summary and Conclusions

An attempt has been made in this study to investigate the physical properties of the E-F transition region both experimentally and theoretically. In Chapter 3, the details of the polynomial reduction technique for the computation of monotonic electron density profiles from ionogram data were discussed. The calculation of absorption and virtual height of frequencies reflected near the E layer maximum of various electron density models by means of a phase integral analysis has also been described.

During the period of the study ionograms have been recorded on a routine hourly basis and augmented with continuous recordings on selected days between February and June 1969. From these observations a synoptic study of the ionogram fine structure has been made and its frequency of occurrence was discussed in some detail in Chapter 7. Various forms of $h'(f)$ cusp structure were studied and the corresponding perturbations in the electron density profile necessary to produce these features have been described. Finally in Chapter 7, the $h'(f)$ curves computed from electron density profiles observed at R.R.E. Malvern by a Thomson Scatter experiment and from theoretical models constructed by Bourne, Setty and Smith (1964) have been compared with the Leicester ionogram records. From this work and the direct comparison of these electron density profiles with the computed monotonic profiles the

structure and growth of the transition region during the early morning has been investigated.

Experimental observations were made of the absorption and virtual height of reflection of radio pulses at a fixed frequency of 2.05 MHz between 5th February and 15th April 1969, and 2.266 MHz between 16th April and 20th June 1969. Throughout these periods measurements were made at times when the reflection height of these frequencies traversed the transition region. A comparison of the calculated absorption and virtual height variations with the experimental observations was carried out in order to establish the validity of the various profiles and to test the accuracy of the phase integral method. Special attention has been given to the observations made both at Leicester and Malvern on the 11th April 1969 and some conclusions have been drawn as to the extent of perturbations in the electron density profile in space and time. The conclusions drawn from these experimental and theoretical investigations of the E-F transition region will now be summarised.

(1) It has been shown that, in agreement with Becker and Dieminger (1951), the occurrence of fine structure on the ionogram traces recorded at Leicester is a regular feature of the morning and afternoon observations, but a less common occurrence at noon. Furthermore, the development of such structures during the morning is found to follow fairly well that predicted by the formula

$$f_{\text{cusp}} = A \cos^n \chi$$

with the constant A taking various values for the different cusps observed.

(2) The polynomial ionogram reduction technique is capable of rendering a monotonic electron density distribution from which by means of the phase integral analysis virtual height data may be recalculated to a reasonable degree of accuracy. However, such a monotonic distribution can be greatly in error when radio wave absorption is computed.

(3) Movements of a model cusp structure on an $h'(f)$ record^{result} in the movement, on a monotonic profile, of a small percentage of the ionization through a comparatively short range in height near the reflection level. This may be simulated by the postulation of highly localised vertical drift disturbances.

(4) The use of the phase integral analysis in computing radio wave absorption and virtual height in a region of high deviative absorption is seen to be justified. The errors involved in adopting the W.K.B. approximate solutions to the wave equation are therefore considered to be of the same order as those involved in the experimental observations.

(5) The influence of the ionosphere below 100 km on both absorption and virtual height is fairly small during the early morning hours. The errors involved in approximating its detailed features are considered to be small when the propagation parameters for frequencies reflected in the E-F transition region during the early morning are calculated.

(6) The variations of absorption with time and virtual height with time and frequency, calculated from the electron density profiles obtained by the Thomson Scatter technique, agree, to a high degree of accuracy, with the variations observed experimentally. It is therefore concluded that these

profiles represent closely the structure and growth of the upper E and E-F transition regions.

(7) The sensitivity of the radio wave absorption to fluctuations in the detailed structure of the electron density profile is greater than that of the virtual height.

(8) The theory of the production of the E and E-F transition regions, as presented by Bourne, Setty and Smith, does not predict conditions in agreement with the observations made at Leicester or Malvern. The movement of an ionization production maximum downwards through the transition region is in marked contrast to the almost constant growth throughout the height range 110-170 km indicated by the Thomson Scatter observations.

(9) The observations of virtual height and absorption have shown that the detailed structure of the E-F transition region is highly complex and subject to great variability on a localised basis. Such variability of detailed structure has been observed in the nocturnal E layer by Belrose (1963) and others. If the basis of the Bourne, Setty and Smith theory, that production systems may be added to the residual ionization in the region, is adopted, it seems reasonable to expect this variability to be reproduced in the daytime E-F transition region. The observed variation of the time at which the reflection level of a 2.05 MHz pulse moves from the F region to the lower reflecting region and to some extent the variability of tabulated noon f_oE data further illustrate this point. However, marked changes in the form of the electron distribution of the transition region are indicated

by the cusp structure changes during the morning, suggesting that the physical and chemical conditions prevailing in the region may be very complex.

It has been shown that such changes in the $h'(f)$ curve can result from small highly localised disturbances in the electron density profile. The Thomson Scatter profiles lend support to this observation in showing much fine structure superimposed upon an almost constant electron density throughout the transition region. Furthermore it has been suggested that these redistributions of ionization might be the result of localised vertical drifts. Some support for such a conclusion is given by the observations made of ionospheric wind structure by Wright, Murphy and Bull (1967). The day to day variation of the growth of the transition region may also be a result of changes in the chemical composition of the region. Measurements of positive ion composition of the height range 110-150 km (Munro 1970) have shown it to be complex and further complication may arise from the influence of meteoric ions (Lehmann and Wagner 1966). The physical conditions in the transition region are complicated at this latitude, 52° N, (Wakai 1967) since it falls between the region of marked Sq and S_p current influence and higher latitudes where ion precipitation predominates.

General Conclusions

The interplay of many variable parameters suggests that the physical and chemical conditions prevailing in the E-F transition region are complex and subject to rapid changes and unpredictable variations which result in the perturba-

tions of the electron density profile observed in this study. It has been established that the observed variations in ionogram cusp structure are due to small perturbations imposed upon an electron distribution which follows fairly closely the predictions of the Chapman theory and exhibits an almost constant growth rate throughout the transition region giving no noticeable valley structure during the early morning. Furthermore the more marked structures are shown to be fairly long lived and to be features of the ionosphere over distances of the order of 90 km.

Suggestions for future investigation

The results of the present study indicate that the following problems require further investigation:

1. The study of the physical conditions prevailing in the height range 110-170 km with special reference to the detailed structure of vertical drift patterns. The variations of temperature and pressure with height and time should also be investigated.
2. The ion chemistry of the E-F transition region and its reaction to changes in the physical conditions in the region.
3. The variation of collisional frequency above 100 km both with height and time.
4. The growth theory of the transition region as expounded by Bourne, Setty and Smith (1964) is unsatisfactory and requires some modification.
5. A closer examination of the relationship $\frac{\Delta A}{A} > \frac{\Delta h'}{h'}$ should

be made and the feasibility of sweep frequency absorption sounding considered in detail. A preliminary study of A(f) sounding has been made and is presented in Appendix I.

6. This study has shown the electron density profiles obtained by the Thomson Scatter technique to represent the ionospheric conditions to a high degree of accuracy. The technique should therefore be more widely used on a routine basis to enable detailed studies of ionospheric structure and its variations to be made.

Appendix I

Vertical Incidence A(f) sounding

The feasibility of recording the variation of total radio wave absorption with frequency during the sweep of an ionospheric sounder was first investigated by Paul (1962). In this technique the amplitude data was superimposed on the normal photographic ionogram by delaying the observed echo in alternate cycles (i.e. 25 Hz) by an amount proportional to its amplitude. Wakai and Ishizawa (1962) have developed a method by which a record of the shape, amplitude and delay of the echo pulse was obtained by rotation of the 'A scan' display through 45°. The records obtained by both these techniques are difficult to interpret and an attempt has been made to develop equipment to produce a direct pen recorder output proportional to the echo amplitude. This equipment can also measure the amplitudes of several echoes simultaneously giving an independent output for each one.

In order to monitor the amplitude of an ionospheric echo produced by an ionosonde during its sweep it must be borne in mind that the reflection height of an echo changes continuously and, at any given frequency, there will usually be several echoes present from different heights or from multiple reflections. It is imperative, therefore, that any electronic monitoring system should be able to (a) resolve between the various echoes present, and (b) lock onto the selected echo and follow its height changes during the sweep. In addition, the system should have a wide dynamic range to accommodate the

large fluctuations that occur in echo amplitudes.

The equipment, illustrated in the block diagram, figure A.1, was designed to operate in conjunction with a Union Radio Ionosonde Mark II and derives its video input and triggering impulses from it. The transmitter modulation pulse is used to trigger a gating system which switches the receiver output alternately into two amplifier channels. In the first channel the pulses are amplified, squared and passed through a threshold gate set so as to remove any background noise. These pulses are fed into a decade counter from which are derived triggering pulses corresponding to the ground pulse, first echo, second echo etc. The pulses are then delayed by the repetition time of the transmitter pulse (20 ms) and are then used to generate strobes for the gated amplifiers in the individual monitor channels; channel 1, first echo; channel 2, second echo; and so on. The strobes are thus locked to their corresponding echo, apart from any movement which may occur during the 20 ms delay time. The strobe outputs are fed to pulse height monitors, based on the design of Bronzite (1965), from which output voltages are displayed on a multi-track pen recorder.

Preliminary tests with this instrument show that in its original form it was prone to interference from c.w. transmissions and high amplitude noise bursts from electrical installations. The introduction of a simple electronic 'fly wheel' circuit is to be investigated with a view to minimising this interference.

A critical study of the absorption records made by the

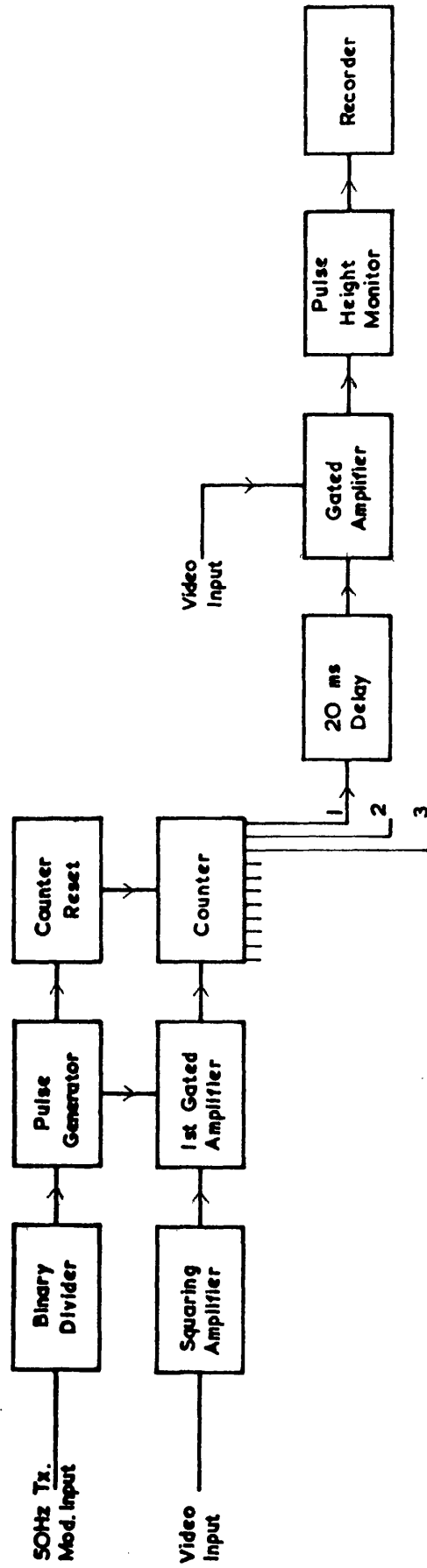


FIG.A.1 Schematic representation of the A(f) sounding system.

sweep frequency technique is necessary in order to assess their value in the light of two phenomena external to the monitoring equipment. These are (i) the efficiency of the sounder tuning control system in keeping the receiver accurately in tune with transmitter throughout the sweep, and (ii) the effects of rapid ionospheric fading and the lack of any extended measurement to overcome sampling and fading errors.

Appendix IICircuit ComponentsDiagram 1 Transmitter Oscillator

R1 = 47 k Ω	R2 = 39 k Ω	R3 = 15 k Ω
R4 = 330 Ω	R5 = 220 k Ω	R6 = 220 k Ω
C1 = 6-65 pF	C2 = .01 μ F	C3 = .01 μ F
C4 = 100 pF	C5 = .01 μ F	C6 = .01 μ F
C7 = 6-65 pF	C8 = .002 μ F	C9 = 120 pF
L1 = L2 = 24 mH	V1 = EF 80	V2 = EL36
T1 = ferrite ring FX1108/B5 80 turns primary 90 turns center taped secondary		

Diagram 2 Pulsed Power Amplifier

R1 = 470 k Ω	R2 = 100 k Ω	R3 = 47 Ω
R4 = 47 Ω	R5 = 47 Ω	R6 = 47 Ω
R7 = 100 k Ω	R8 = 470 k Ω	R9 = 1 k Ω
R10 = 47 Ω	R11 = 47 Ω	R12 = 1 k Ω
R13 = 4.7 k Ω	R14 = 4.7 k Ω	R15 = 250 Ω
R16 = 100 k Ω	R17 = 47 Ω	R18 = 47 Ω
R19 = 47 k Ω	R20 = 47 k Ω	R21 = 11 Ω
R22 = 11 Ω	R23 = 200 k Ω	C1 = .01 μ F
C2 = 6-65 pF	C3 = .02 μ F	C4 = .02 μ F
C5 = 6-65 pF	L1 = 1.5 mH	L2 = 1.5 mH
V3 = EL 36	V4 = EL 36	V5 = $\frac{1}{2}$ QQV07-40A
V6 = $\frac{1}{2}$ QQV07-40A	V7 = V8 = 4B60	
T2 = 2 ferrite rings FX 1108/B5 130 turn primary 120 turn secondary		
T3 = 4 ferrite rings FX 1108/B5 40 turn centre taped primary 20 turn secondary		

Diagram 3 50 Hertz Modulator

R1 = 330 k Ω	R2 = 330 k Ω	R3 = 560 k Ω
R4 = 220 k Ω	R5 = 560 k Ω	R6 = 4.7 M Ω
R7 = 47 k Ω	R8 = 470 k Ω	R9 = 22 k Ω
R10 = 10 M Ω	R11 = 10 k Ω	R12 = 56 k Ω
R13 = 220 k Ω	R14 = 1.5 k Ω	R15 = 180 k Ω
R16 = 100 k Ω	R17 = 47 k Ω	R18 = 1 M Ω
R19 = 22 k Ω	R20 = 2.2 k Ω	R21 = 56 k Ω
R22 = 10 k Ω	R23 = 47 k Ω	R24 = 4.7 k Ω
R25 = 10 k Ω	R26 = 33 k Ω	C1 = 1 μ F
C2 = .02 μ F	C3 = .02 μ F	C4 = .007 μ F
C5 = 350 pF	C7 = .01 μ F	C8 = 2 μ F
C9 = 1.0 μ F	C6 = switched 150-300 pF	
V9 = $\frac{1}{2}$ ECC 82	V10 = $\frac{1}{2}$ ECC 82	V11 = EF 80
V12 = $\frac{1}{2}$ ECC 82	V13 = $\frac{1}{2}$ ECC 82	V14 = EF 80
V15 = BYX 22		

Diagram 4 Modified triggering system

R1 = 330 k Ω	R2 = 330 k Ω	R3 = 560 k Ω
R4 = 560 k Ω	R5 = 220 k Ω	R6 = 43 k Ω
R7 = 470 k Ω	R8 = 22 k Ω	R9 = 10 M Ω
R10 = 10 k Ω	R11 = 56 k Ω	R12 = 4.7 M Ω
R13 = 1 M Ω	R14 = 47 k Ω	R15 = 4.7 k Ω
R16 = 22 k Ω	R17 = 470 k Ω	R18 = 1 M Ω (Var)
R19 = 1 M Ω	R20 = 22 k Ω	R21 = 4.7 k Ω
R22 = 47 k Ω	R23 = 1 M Ω	R24 = 1 M Ω
R25 = 1 M Ω	R26 = 220 k Ω	R27 = 1 M Ω
R28 = 1 M Ω	R29 = 4.7 k Ω	R30 = 100 k Ω
R31 = 8.2 k Ω	R32 = 250 k Ω (Var)	R33 = 150 k Ω
R34 = 22 k Ω	R35 = 1 M Ω	R36 = 330 Ω

R37 = 220 k Ω	R38 = 47 k Ω	R39 = 1 M Ω
R40 = 150 k Ω	R41 = 100 k Ω (Var)	R42 = 4.7 k Ω
R43 = 82 k Ω	R44 = 100 k Ω	R45 = 33 k Ω
R46 = 2.2 M Ω	R47 = 10 k Ω	R48 = 2.2 M Ω
R49 = 1 M Ω	R50 = 47 k Ω	R51 = 4.7 k Ω
R52 = 22 k Ω	R53 = 470 k Ω	R54 = 1 M Ω (Var)
R55 = 1 M Ω	R56 = 22 k Ω	R57 = 4.7 k Ω
R58 = 47 k Ω	R59 = 1 M Ω	R60 = 1 M Ω
R61 = 1 M Ω	R62 = 220 k Ω	R63 = 1 M Ω
R64 = 1 M Ω	R65 = 4.7 k Ω	R66 = 100 k Ω
R67 = 150 k Ω	R68 = 33 k Ω	R69 = 250 k Ω (Var)
C1 = 1 μ F	C2 = .02 μ F	C3 = .01 μ F
C4 = .002 μ F	C5 = 47 pF	C6 = .002 μ F
C7 = .002 μ F	C8 = .05 μ F	C9 = 22 pF
C10 = .047 pF	C11 = 25 μ F	C12 = .1 μ F
C13 = .01 μ F	C14 = 120 pF	C15 = .01 μ F
C16 = .05 μ F	C17 = 470 pF	C18 = .047 μ F
C19 = .005 μ F	C20 = .047 μ F	C21 = 22 pF
C22 = .01 μ F	C23 = 25 μ F	
V1 = $\frac{1}{2}$ ECC 81	V2 = $\frac{1}{2}$ ECC 81	V3 = EF 80
V4 = $\frac{1}{2}$ ECC 81	V5 = $\frac{1}{2}$ ECC 81	V6 = $\frac{1}{2}$ ECC 81
V7 = $\frac{1}{2}$ ECC 81	V8 = $\frac{1}{2}$ ECC 81	V9 = $\frac{1}{2}$ ECC 81
V10 = $\frac{1}{2}$ ECC 81	V11 = $\frac{1}{2}$ ECC 81	V12 = $\frac{1}{2}$ ECC 81
V13 = $\frac{1}{2}$ ECC 81	V14 = $\frac{1}{2}$ ECC 81	V15 = $\frac{1}{2}$ ECC 81
V16 = $\frac{1}{2}$ ECC 81	V17 = $\frac{1}{2}$ ECC 81	V18 = $\frac{1}{2}$ ECC 81
V19 = $\frac{1}{2}$ ECC 81	V20 = $\frac{1}{2}$ ECC 82	V21 = $\frac{1}{2}$ ECC 82
V22 = BYX22/800	V23 = OA 81	V24 = OA 81
V25 = OA 81	V26 = OA 81	V27 = OA 81
V28 = OA 81		

Bibliography

- | | | |
|---------------------------------------|---------|---|
| Altman, C. | 1965 | J. Res. Nat. Bur. Stand.
<u>69D</u> , 511. |
| Anderson, J.M. and
Goldstein, L. | 1955 | Phys. Rev. <u>100</u> , 1037. |
| Appleton, E.V. | 1927 | Nature, <u>120</u> , 330. |
| Appleton, E.V. | 1928 | Proc. Phys. Soc. (Lond.)
<u>41</u> , 43. |
| Appleton, E.V. | 1932 | Proc. Inst. Elect. Engrs.
(Lond.) <u>71</u> , 642. |
| Appleton, E.V. | 1933 | Nature, <u>131</u> , 872. |
| Appleton, E.V. | 1937 | Proc. R. Soc. <u>A162</u> , 451. |
| Appleton, E.V. and
Barnett, M.A.F. | 1925(a) | Electrician, <u>1925</u> , 368. |
| Appleton, E.V. and
Barnett, M.A.F. | 1925(b) | Nature, <u>115</u> , 334. |
| Appleton, E.V. and
Barnett, M.A.F. | 1925(c) | Proc. R. Soc. <u>A109</u> , 621. |
| Appleton, E.V. and
Builder, G. | 1932 | Proc. Phys. Soc. (Lond.) <u>44</u> ,
76. |
| Appleton, E.V. and
Chapman, F.W. | 1932 | Proc. Phys. Soc. (Lond.) <u>44</u> ,
246. |
| Appleton, E.V. and
Lyon, A.J. | 1957 | J. Atmosph. Terr. Phys. <u>10</u> , 1 |
| Appleton, E.V. and
Lyon, A.J. | 1961 | J. Atmosph. Terr. Phys. <u>21</u> ,
73. |
| Appleton, E.V. and
Naismith, R. | 1935 | Proc. R. Soc. <u>A150</u> , 685. |
| Appleton, E.V. and
Piggott, W.R. | 1954 | J. Atmosph. Terr. Phys. <u>5</u> ,
141. |
| Appleton, E.V. and
Ratcliffe, J.A. | 1930 | Proc. R. Soc. <u>A128</u> , 133. |
| Axford, W.J. and
Cunnold, D.M. | 1966 | Radio Sci., <u>1</u> , 191. |
| Bailey, V.A. and
Somerville, J.M. | 1938 | Phil. Mag. <u>26</u> , 888. |

- Baral, S.S. 1955 J. Atmosph. Terr. Phys. 6, 160.
- Bauer, L.H., Spencer, N.W. and Carignon, G.R. 1964 J. Geophys. Res. 68, 5397.
- Becker, W. and Dieminger, W. 1950 URSI Proc. Comm. on the Ionosphere, 2nd meeting, Brussels, p.126.
- Belrose, J.S. 1963 Agardograph 74, Blackband, W.T. (Ed.).
- Belrose, J.S. 1965 "Physics of the Earth's Upper Atmosphere", Prentice Hall, N.J., U.S., 1965, p.46.
- Best, J.E. and Ratcliffe, J.A. 1938 Proc. Phys. Soc. (Lond.), 50, 233, 278.
- Beynon, W.J.G. and Brown, G.M. 1959 J. Atmosph. Terr. Phys. 14, 138.
- Beynon, W.J.G. and Davies, K. 1954 J. Atmosph. Terr. Phys. 5, 273.
- Beynon, W.J.G. and Rangaswamy, S. 1969 J. Atmosph. Terr. Phys. 31, 891.
- Bibl, K. 1951 Ann. Geophys. 7, 208.
- Bibl, K. 1953 Z. Geophys. 19, 136.
- Bibl, K., Paul, R and Rawer, R. 1965 J. Atmosph. Terr. Phys. 27, 145.
- Booker, H.G. 1935 Proc. R. Soc. A150, 267.
- Booker, H.G. and Smith, E.K. 1970 J. Atmosph. Terr. Phys. 32, 467.
- Bourne, J.A., Setty, C.S.G.K. and Smith, R.A. 1964 J. Inst. Telecom. Engrs. 10, 341.
- Breit, G. and Tuve, M.A. 1925 Nature, 116, 357.
- Bronzite, M. 1965 El. Eng., 37, 394.
- Budden, K.G. 1955 "The Physics of the Ionosphere", p.332, The Physical Society.
- Budden, K.G. 1961 "Radio Waves in the Ionosphere", C.U.P.
- Budden, K.G. 1965 J. Res. Nat. Bur. Stand. 69D, 191.

- Budden, K.G. and Cooper, E.A. 1962 J. Atmosph. Terr. Phys., 24, 509.
- Chalmers, J.A. 1962 J. Atmosph. Terr. Phys., 24, 219.
- Chapman, S. 1931 Proc. Phys. Soc., 43, 26 & 484.
- Chapman, S. and Bartels, J. 1940 "Geomagnetism", Clarendon Press, Oxford.
- Chapman, S. and Cowling, T.G. 1939 "The Mathematical Theory of non-uniform gases", C.U.P.
- Clarke, C. and Shearman, E.D.R. 1953 Wireless Engineer, Sept. 1953, p.211.
- Coll, D.C. and Storey, J.R. 1965 J. Res. Nat. Bur. Stand., 69D, 1191.
- Cooper, E.A. 1961 J. Atmosph. Terr. Phys. 22, 122.
- Cooper, E.A. 1964 J. Atmosph. Terr. Phys. 26, 995.
- Cowling, T.G. 1945 Proc. R. Soc., A183, 453.
- Davies, K. 1965 "Ionospheric Radio Propagation" N.B.S. Monograph, 80.
- Davies, K. and Saha, A.K. 1962 "Electron Density Profiles in the Ionosphere and Exosphere", p.162, Maehlum, B., Pergamon Press, N.Y.
- Deeks, D.G. 1966 Proc. R. Soc., A291, 413.
- Dieminger, W. 1962 "Electron Density Profiles in the Ionosphere and Exosphere", p.85, Maehlum, B., Pergamon, London.
- Donahue, T.M. 1966 Planet. Space Sci., 14, 33.
- Donnelly, R.F. 1967 ESSA Technical Report, IER 19-ITSA 19.
- Drude, P. 1902 "The Theory of Optics", Longmans, Green, London.
- Eccles, D. and King, J.W. 1970 J. Atmosph. Terr. Phys. 32, 517.
- Eccles, W.H. 1912 Proc. R. Soc., A87, 79.
- Eckersley, T.L. 1931 Proc. R. Soc., A132, 83.

- Eckersley, T.L. 1932(a) Proc. R. Soc., A136, 499.
- Eckersley, T.L. 1932(b) Proc. R. Soc., A137, 158.
- Faraday, M. 1832 Occ. Not. R. Soc. No. 2, 9.
- Fejer, J A. 1955 J. Atmosph. Terr. Phys. 2, 322.
- Fenwick, R.B. and Barry, G.H. 1967 Proc. Conf. "Ground-Based Radio wave propagation studies of the lower Ionosphere", Vol. 2, p.532, Ottawa, Canada.
- Fitzenreiter, R.J. and Blumle, L.J. 1964 J. Geophys. Res. 69, 407.
- Gardner, F.F. and Pawsey, J.L. 1953 J. Atmosph. Terr. Phys. 3, 321.
- Gauss, C.F. 1839 "General Theory of Terrestrial Magnetism", Scientific Memoirs (Ed. R. Taylor), Vol. 2. p.184, London 1841.
- Gilliland, T.R. 1934 Proc. Instn. Radio Engrs., 22, 236.
- Gilliland, T.R. 1935 Proc. Instn. Radio Engrs., 23, 1076.
- Halliday, E.C. 1936 Proc. Phys. Soc. 48, 421.
- Hartree, D.R. 1929 Proc. Camb. Phil. Soc., 25, 97.
- Hartree, D.R. 1931(a) Proc. Camb. Phil. Soc., 27, 143.
- Hartree, D.R. 1931(b) Proc. R. Soc. A131, 428.
- Heaviside, O. 1902 Encyclopaedia Britannica, (10th Ed.) 33, 213.
- Henry, G.W. 1966 Univ. of Illinois, Aeronomy Report, 13.
- Hibberd, F.H. 1962 J. Atmosph. Terr. Phys. 24, 843.
- Jaeger, J.C. 1947 Proc. Phys. Soc. 59, 87.
- Jenkins, J.B. and Ratcliff, G. 1953 Electr. Engr. 25, 140.
- Jones, R.M. 1966 ESSA Tech. Rep. IER 17-ITSA 17.

- Jones, T.B. and Keenlside, W. 1970 Agard Conf. Proc. No. 49, p.24.
- Kaiser, T.R. 1962 J. Atmosph. Terr. Phys. 24, 865.
- Kelso, J.M. 1952 J. Geophys. Res. 57, 357.
- Lord Kelvin (Thomson, W.) 1860 "Papers on Electrostatics and Magnetism", p.217, Macmillan, London 1884.
- Kennelly, A.E. 1902 Elect. World, N.Y. 39, 473.
- King, G.A.M. 1960 J. Res. Nat. Bur. Stand. 64D, 501.
- Klein, M.M. and Brueckner, K.A. 1958 Phys. Rev. 111, 1115.
- Larmor, J. 1924 Nature 114, 650 and Phil. Mag. 48, 1025.
- Lassen, H. 1927 Elekt. Nachr. Tech. 4, 324.
- Lehmann, H.R. and Wagner, C.V. 1966 J. Atmosph. Terr. Phys. 28, 617.
- Long, A.R. 1962 J. Geophys. Res. 67, 989.
- Lorentz, H.A. 1909 "The Theory of Electrons", Leipzig, B.G. Teubner.
- Lowan, A.N., Davids, N. and Levenson, A. 1942 Bull. Am. Math. Soc. 48, 739.
- Lyon, A.J. and Moorat, A.J.G. 1956 J. Atmosph. Terr. Phys. 8, 309.
- Madden, D.R. 1967 Radio and Space Research Station, Slough, I.M.304.
- Manning, L.A. 1949 Proc. Inst. Radio Engrs. 37, 599.
- Martyn, D.F. 1947 Proc. R. Soc. A190, 273.
- McNicol, R.W.E. 1949 Proc. Instn. Elect. Engrs. 96 III, 517.
- McNicol, R.W.E. and Gipps, G. de V. 1951 J. Geophys. Res. 56, 17.
- Morgan, A.D. 1966 J. Atmosph. Terr. Phys. 28, 1233.
- Munro, G.H. and Heisler, L.H. 1956 Aust. J. Phys. 2, 343.
- Munro, P.E. 1970 J. Atmosph. Terr. Phys. 32, 373.

- Murty, Ramana, Y.V. 1964 Ind. J. Pure. Appl. Phys. 3, 392.
- Naismith, R. 1933 J. Instn. Elect. Engrs. 72, 246.
- Naismith, R. 1936 Nature, 137, 615.
- Naismith, R. and Bailey, R. 1951 Proc. Instn. Elect. Engrs. 98 III, 11.
- Nichols, H.W. and Schellang, J.C. 1925 Science, 61, 288.
- Nicolet, M. 1949 J. Geophys. Res. 54, 373.
1951 J. Atmosph. Terr. Phys. 1, 111
- Nicolet, M. 1953 J. Atmosph. Terr. Phys. 3, 200.
- Nicolet, M. 1959 Phys. of Fluids, 2, 95.
- Nicolet, M. and Aiken, A.C. 1960 J. Geophys. Res. 65, 1469.
- Oya, H. and Aso, T. 1968 Space Res. IX, 290.
- Pack, J.L. and Phelps, A.V. 1961 Phys. Rev. 121, 798.
- Paul, A.K. 1960 Arch. Elek. Übertragung, 14, 468.
- Paul, A.K. 1962 Thesis, Freiburg.
- Paul, A.K. 1966 Radio Sci. 1, 441.
- Paul, A.K. and Wright, J.W. 1963 J. Geophys. Res. 68, 5413.
- Phelps, A.V. 1960 J. Appl. Phys. 31, 1723.
- Phelps, A.V. and Pack, J.K. 1959 Phys. Rev. Lett. 3, 340.
- Phillips, G.J. 1951 Proc. Instn. Elect. Engrs. 98 III, 237.
- Piggott, W.R. 1953 Proc. Instn. Elect. Engrs. 100 III, 61.
- Piggott, W.R., Beynon, W.J.G., Brown, G.M. and Little C.G. 1957 Annals of the I.G.Y. Vol. III, pt. II, Pergamon, London.
- Piggott, W.R. and Rawer, K. 1961 "URSI HANDBOOK of Ionogram Interpretation and reduction", Elsevier Publishing Co.
- Pitteway, M.L.V. 1965 Phil. Trans. R. Soc. 257, 219.

- Rai, R.K. 1969(a) Radio Science, 4, 751.
- Rai, R.K. 1969(b) Radio Science, 4, 757.
- Ratcliffe, J.A. 1951 J. Geophys. Res. 56, 463.
- Ratcliffe, J.A. 1959 "The Magneto-Ionic Theory and its applications to the Ionosphere", C.U.P.
- Robinson, B.J. 1960(a) J. Atmosph. Terr. Phys. 18, 215.
- Robinson, B.J. 1960(b) J. Atmosph. Terr. Phys. 19, 160.
- Sagalyn, R.C. and Smiddy, M. 1964 Space Res. V, 189.
- Saha, A.K. 1964 Ind. J. Pure Appl. Phys. 2, 242.
- Sanatani, S. and Shirke, J.S. 1966 J. Atmosph. Terr. Phys. 28, 185.
- Schmerling, E.R. 1967 Radio Sci. 2, 1233.
- Sen, H.K. and Wyller, A.A. 1960 J. Geophys. Res. 65, 3931.
- Shinn, D.H. 1953 J. Atmosph. Terr. Phys. 4, 240.
- Shkarofsky, I.P. 1961 Proc. Instn. Radio Engrs. 49, 1857.
- Skinner, N.J., Brown, R.A. and Wright, R.W. 1954 J. Atmosph. Terr. Phys. 5, 95.
- Sissenwine, N., Dubin, M. and Wexler, H. 1962 "U.S. Standard Atmosphere", U.S. Gov. Printing Office, Washington, D.C.
- Smith, R.A., Coyne, T. N.R., Loch, R.G. and Bourne, I.A. 1966 "Ground-Based radio wave prop. studies of the lower ionosphere". Conference proceedings, Ottawa, Canada. Vol. I, p.335.
- Smith, E.K. and Matsushita, S. 1962 "Ionospheric Sporadic E", Pergamon, Oxford.
- Smith, L.G. 1966 Radio Sci. 1, 178.
- Spence, N.W. and Brace 1965 J. Geophys. Res. 70, 2665.
- Stewart, B. 1878 Encyclopaedia Britannica, (9th Ed.), Vol. 16, p.181.
- Taylor, N. 1969 (Private Communication)

- Thomas, J.O., Haselgrove, J.
and Robbins, A. 1958 J. Atmosph. Terr. Phys.
12, 46.
- Thomas, J.O. and Vickers,
M.D. 1959 D.S.I.R. Radio Res. Spec.
Rep. 28. (H.M.S.O. London)
- Thomas, J.O. 1968 (Private Communication)
- Thrane, E.V. and
Piggott, W.R. 1966 J. Atmosph. Terr. Phys.
28, 721.
- Titheridge, J.E. 1959(a) J. Atmosph. Terr. Phys. 17,
96.
- Titheridge, J.E. 1959(b) J. Atmosph. Terr. Phys. 17,
110.
- Titheridge, J.E. 1961(a) J. Atmosph. Terr. Phys. 21,
1.
- Titheridge, J.E. 1961(b) J. Atmosph. Terr. Phys. 22,
200.
- Titheridge, J.E. 1967(a) Radio Sci. 2, 133.
- Titheridge, J.E. 1967(b) Radio Sci. 2, 1237.
- Wait, J.R. 1962 "Electromagnetic Waves in
stratified media", Pergamon
Press, N.Y.
- Wakai, N. 1966 "Ground Based radio wave
propagation studies of the
lower ionosphere". Con-
ference Proc. Ottawa, Vol. 2,
p.552.
- Wakai, N. 1967 J. Geophys. Res. 72, 4507.
- Wakai, N. and
Ishizawa, K. 1962 Jap. Radio Res. Labs. 9, 421.
- Watson, G.N. 1919 Proc. R. Soc. A95, 546.
- Watts, J.M. and
Brown, J.N. 1954 J. Geophys. Res. 59, 71.
- Whale, H.A. 1951 J. Atmosph. Terr. Phys. 1,
233.
- White, F.W.G. 1933 Proc. Phys. Soc. (Lond.) 46,
91.
- White, F.W.G. and
Brown, L.W. 1936 Proc. R. Soc. 153A, 639.
- Whitehead, J.D. 1952 J. Atmosph. Terr. Phys. 2,
361.

- | | | |
|--|------|---|
| Whitehead, J.D. | 1956 | J. Atmosph. Terr. Phys. <u>9</u> ,
276. |
| Whitehead, J.D. | 1962 | J. Atmosph. Terr. Phys. <u>24</u> ,
681. |
| Whitehead, J.D. | 1970 | Rev. Geophys. Space Phys. <u>8</u>
65. |
| Wilson, L.D. | 1962 | Aust. J. Appl. Sci. <u>13</u> , 89. |
| Wright, J.W., Knecht,
R.W. and Davies, K. | 1957 | Annals of the I.G.Y. Vol. 3,
Part I, Pergamon, London. |
| Wright, J.W., Murphy,
C.H. and Bull, G.V. | 1967 | J. Geophys. Res. <u>72</u> , 1443. |
| Wright, J.W. and
Smith, G.H. | 1967 | Radio Sci., <u>2</u> , 1119. |